Last change: September 23, 2019

Notes on Biofluid Dynamics

Rodolfo Repetto

Department of Civil, Chemical and Environmental Engineering
University of Genoa, Italy
Email: rodolfo.repetto@unige.it
Phone: +39 010 3532471
http://dicca.unige.it/rrepetto/
skype contact: rodolfo-repetto

Academic year 2019/2020

Table of contents I

Table of contents II

Table of contents III

Table of contents IV

Acknowledgements

Rodolfo Repetto wishes to thank **Jennifer H. Siggers** (Department of Bioengineering, Imperial College London, UK) and **Giovanni Seminara** (DICCA, University of Genoa) for providing some of the material presented in these lectures.

Introduction to biofluid dynamics

Introduction to biofluid dynamics

What is biological fluid mechanics?

Biological fluid mechanics (or *biofluid mechanics*) is the study of the motion of biological fluids in any possible context (e.g. blood flow in arteries, animal flight, fish swimming, ...)

In the present course we will focus on fluid motion in the human body.

There are many organs in the human body whose functioning involves fluid motion. Examples are:

- **blood circulation**
  - hearth pumping;
  - flow in the systemic arteries;
  - flow in the pulmonary arteries;
  - flow in the microcirculation;
  - flow in veins.
- **air flow in the respiratory system**
- **flow in the eye**
  - flow in the tear film on the cornea;
  - flow of the aqueous humour in the anterior chamber;
  - drainage of aqueous humour;
  - flow of the vitreous body due to eye rotations;
  - flow of the axoplasm in the optic nerve axons.
- **flow in the ureter**
- ...

Introduction to biofluid dynamics

What is biological fluid mechanics useful for?

- **Pure physiology:** understanding how animals, and in particular humans, work.
- **Pathophysiology:** understanding why they might go wrong. In other words understanding the origins and development of diseases.
- **Diagnosis:** recognising diseases from possibly non-traumatic measurements.
- **Cure:** providing support to surgery and to the design of prosthetic devices.

Peculiarities of physiological fluid flows

Thomas Young (1808):

The mechanical motions, which take place in animal body, are regulated by the same general laws as the motion of inanimate bodies . . . and it is obvious that the enquiry, in what matter and in what degree, the circulation of the blood depends on the muscular and elastic powers of the heart and of the arteries, . . . , must become simply a question belonging to the most refined departments of the theory of hydraulics.

There are some key features which characterise physiological flows.

- **Pulsatility.** In most cases physiological flows are highly unsteady and are often pulsatile (e.g. flow in the systemic arteries or in the respiratory system . . .).
- **Complex geometries.** Typically physiological flows take place in very complex geometries. In order to study the problems by analytical means it is therefore necessary to idealise the geometry in a suitable manner. It is a research challenge of recent years to perform numerical simulations on real geometries.
- **Deformability.** Not only the geometry of the flow domain might be complex but it also often varies in time. This typically induces great complication in the mathematical analysis. Often the problem to be solved is effectively a solid-fluid interaction.
- **Low Reynolds number flows.** In many cases of physiological interest (but by no means always) the Reynolds number of the flow is fairly low and this allows simplifying the equations.

Some textbooks in biofluid dynamics

The following are a few reference books on fluid mechanics:

- Acheson (1990);
- Aris (1962);
- Batchelor (1967);
- Ockendon and Ockendon (1995);
- Pozrikidis (2010).

The following textbooks consider various aspects of physiological flows in the human body:

- Caro et al. (1978);
- Ethier and Simmons (2007);
- Pedley (1980);
- Pedley (2000);
- Ottesen et al. (2004);
- White and Fine (2007);
- Keener and Sneyd (1998).

Basic notions of fluid mechanics

The Continuum Approach

Fluids (liquids, gases, ...) are composed of particles (molecules). Each molecule is composed of a central nucleus surrounded by a cloud of electrons. Some typical dimensions are given in the following table

Diameter of	
an atomic nucleus	$2 \cdot 10^{-15}$ m
a gas molecule	$6 \cdot 10^{-10}$ m
Spacing of gas molecules	$3 \cdot 10^{-9}$ m
Diameter of	
a red blood cell	$8 \cdot 10^{-6}$ m
a capillary	$4 - 10 \cdot 10^{-6}$ m
an artery	$\approx 10^{-2}$ m

In most applications of fluid mechanics, the typical spatial scale under consideration, L, is much larger than the spacing between molecules, l. In this case we suppose the material to be composed of elements whose size is small compared to L but large compared to l. We then assume each fluid element occupies a point in space.

We assume each property, F, of the fluid (e.g. density, pressure, velocity, ...), to be a continuous function of space $\mathbf{x}$ and time t

$$F = F(\mathbf{x}, t).$$

Forces on a continuum I

Two kind of forces can act on a continuum body

- **body forces;**
- **surface forces.**

Body forces

These forces are slowly varying in space. If we consider a small volume, δV, the force is approximately constant over it. Therefore the force on the volume is

$$\delta \mathbf{F} = \tilde{\mathbf{f}} \delta V,$$

where $\mathbf{f}$ is the force per unit volume. In most cases of interest for this course $\delta \mathbf{F}$ is proportional to the mass of the element. Therefore we may write

$$\delta \mathbf{F} = \rho \mathbf{f} \delta V,$$

where ρ denotes the fluid density, i.e. mass per unit volume ($[\rho] = ML^{-3}$), and $\mathbf{f}(\mathbf{x}, t)$ is independent of the density.
The vector field $\mathbf{f}$ is termed the **body force field**, and has the dimensions of acceleration or force per unit mass

$$[\mathbf{f}] = LT^{-2}.$$

In general $\mathbf{f}$ and $\tilde{\mathbf{f}}$ depend on space and time: $\mathbf{f} = \mathbf{f}(\mathbf{x}, t)$ and $\tilde{\mathbf{f}} = \tilde{\mathbf{f}}(\mathbf{x}, t)$. If we want to compute the total force $\mathbf{F}$ on a finite volume V we need to integrate $\mathbf{f}$ over V

$$\mathbf{F} = \iiint_V \tilde{\mathbf{f}} dV = \iiint_V \rho \mathbf{f} dV.$$

Forces on a continuum II

Surface forces

The force is approximately constant over a small surface δS, and therefore the force on the surface is

$$\delta \mathbf{\Sigma} = \mathbf{t} \delta S,$$

where $\mathbf{t}$ is the force per unit area or **tension**, and has dimensions given by

$$[\mathbf{t}] = ML^{-1}T^{-2}.$$

As well as depending on position $\mathbf{x}$ and time t, the vector $\mathbf{t}$ also depends on the orientation of the surface. The orientation is uniquely specified by the unit vector $\mathbf{n}$ normal to the surface, meaning that $\mathbf{t} = \mathbf{t}(\mathbf{x}, t, \mathbf{n})$.
To compute the force $\mathbf{\Sigma}$ on a surface S we must integrate

$$\mathbf{\Sigma} = \iint_S \mathbf{t} dS.$$

Cauchy's principle and the stress tensor

Cauchy's stress principle asserts that

"When a continuum body is acted on by forces, i.e. surface forces and body forces, there are internal reactions throughout the body acting between the material points."

Based on this principle, Cauchy demonstrated that the state of stress at a point in a continuum body is completely defined by the nine components σ_{ij} of a **second-order tensor** called the **Cauchy stress tensor**.
The stress vector $\mathbf{t}(\mathbf{n})$ at any point P, acting on a plane of normal vector $\mathbf{n}$, can be expressed in terms of the stress tensor

$$\text{in component form as} \quad t_i(\mathbf{n}) = \sigma_{ij} n_j, \quad \text{or in vector form as} \quad \mathbf{t}(\mathbf{n}) = \boldsymbol{\sigma} \cdot \mathbf{n},$$

where σ_{ij} represents the ith component of the stress on the plane with normal $\mathbf{e}_j$.

Properties of the stress tensor

- **The stress tensor is symmetric**, i.e. $\sigma_{ij} = \sigma_{ji}$.
- The terms on the principal diagonal of the stress tensor matrix are termed the **normal stresses**. The other six (not on the principal diagonal) are **shear stresses.**
- In a fluid at rest we have

$$\text{in component form as} \quad \sigma_{ij} = -p\delta_{ij}, \quad \text{or in vector form as} \quad \boldsymbol{\sigma}(\mathbf{n}) = -p\mathbf{I},$$

where $p(\mathbf{x}, t)$ is the **pressure** and δ_{ij} is the Kronecker delta. In this case the stress tensor is **a multiple of the identity.**

Statics of fluids I

Equation of statics in integral form

Given a volume V with surface S, the equilibrium of forces acting on the body can be written as

$$\iiint_V \rho \mathbf{f} dV + \iint_S \mathbf{t} dS = 0.$$

For a fluid at rest, since $\mathbf{t} = -p\mathbf{n}$, we can write

$$\iiint_V \rho \mathbf{f} dV + \iint_S -p\mathbf{n} dS = 0, \tag{1}$$

and applying Gauss' theorem

$$\iiint_V (\rho \mathbf{f} - \nabla p)\, dV = 0.$$

It can be shown that there are no resultant moments acting on the volume, and therefore equation (1) provides necessary and sufficient conditions for equilibrium.

Equation of statics in differential form

Since the volume V is arbitrary, the integrand must be zero everywhere

$$\rho \mathbf{f} - \nabla p = 0. \tag{2}$$

Statics of fluids II

Incompressible fluids in a gravitational field

For many problems of practical relevance we can assume

- $\rho =$constant;
- $\mathbf{f} = (0, 0, -g)$, with respect to a system of coordinates (x_1, x_2, x_3) with x_1 and x_2 horizontal and x_3 pointing vertically upward, and with g being the acceleration of gravity ($g \approx 9.81$ m s^{-2}).

In this case equation (2) can be easily solved, leading to the following result, known as **Stevin's law**

$$h = x_3 + \frac{p}{\gamma} = \text{const.},$$

where $\gamma = \rho g$ is the specific weight (force per unit volume) of the fluid ($[\gamma] = ML^{-2}T^{-2}$).

This implies that the **pressure increases linearly as we move vertically downwards, and the rate of increase is equal to the specific weight of the fluid**.

Basic notions of kinematics of fluids I

Kinematics is the study of fluid motion.
Two main approaches are adopted in fluid mechanics

- **Eulerian reference frame (spatial approach);**
- **Lagrangian reference frame (material approach).**

Eulerian approach

We define a system of coordinates fixed in space, $\mathbf{x} = (x_1, x_2, x_3)$. This means that any vector $\mathbf{x}$ denotes a particular point in space (note that this point will, in general, be occupied by different fluid particles at different times).

When a fluid property (say F) is described as $F(\mathbf{x}, t)$, it tells us how F varies in time at a fixed point in space. We can also define $\partial F(\mathbf{x}, t)/\partial t$, which is the rate of change in time of F in $\mathbf{x}$. In most cases this approach is very convenient.

Important note on derivatives:
Consider the velocity field, i.e. we take $F = \mathbf{u}$. If we take the partial derivative of $\mathbf{u}$ with respect to time, i.e. $\partial \mathbf{u}(\mathbf{x}, t)/\partial t$, we **do not get the acceleration of the fluid!** This is because the point $\mathbf{x}$ is, in general, occupied by different fluid particles at different times. The quantity $\partial \mathbf{u}(\mathbf{x}, t)/\partial t$ is the rate of change of the velocity at a single point rather than the rate of change of the velocity of fluid particles (which we usually term the acceleration). We will return to this point shortly.

Basic notions of kinematics of fluids II

Lagrangian approach

We define $\mathbf{X} = (X_1, X_2, X_3)$ as a system of coordinates fixed with material particles. This means that any value of $\mathbf{X}$ is always associated with a particular fluid particle.

Any fluid property F can then be described as $F(\mathbf{X}, t)$. This tells us how the value of F associated with a material fluid particle varies in time. We can define $\partial F(\mathbf{X}, t)/\partial t$, which is the rate of change in time of F associated with the particle $\mathbf{X}$.

As the meaning of this time derivative is different from that taken with the Eulerian approach, different notations are often adopted

$$\frac{\partial F(\mathbf{x}, t)}{\partial t} = \frac{\partial F}{\partial t},$$
$$\frac{\partial F(\mathbf{X}, t)}{\partial t} = \frac{DF}{Dt}.$$

In some cases the Lagrangian approach is more convenient (e.g. it is often used for studying fluid mixing).

Important note on derivatives:
In this case the partial derivative of $\mathbf{u}$ with respect to t does give the acceleration $\mathbf{a}$

$$\frac{\partial \mathbf{u}(\mathbf{X}, t)}{\partial t} = \frac{D\mathbf{u}}{Dt} = \mathbf{a}.$$

Basic notions of kinematics of fluids III

Material derivative with respect to spatial coordinates

We can establish a relationship between the Eulerian and Lagrangian approaches if we know the function

$$\mathbf{x} = \mathbf{x}(\mathbf{X}, t), \tag{3}$$

which is well defined since a point in space cannot be occupied by two particles. The above equation represents the position $\mathbf{x}$ of a material particle, identified by $\mathbf{X}$, in time. This is called **particle trajectory**.

Since a particle cannot occupy two different points in space, equation (3) is invertible. Therefore we can write

$$\mathbf{X} = \mathbf{X}(\mathbf{x}, t).$$

Let us now consider a material derivative of any fluid property F

$$\frac{DF}{Dt} = \left.\frac{\partial F(\mathbf{X}, t)}{\partial t}\right|_{\mathbf{X}} = \left.\frac{\partial F(\mathbf{x}(\mathbf{X}, t), t)}{\partial t}\right|_{\mathbf{X}} = \left(\frac{\partial F}{\partial t}\right)_{\mathbf{x}} + \left(\frac{\partial F}{\partial x_i}\right)_t \left(\frac{\partial x_i}{\partial t}\right)_{\mathbf{X}} = \frac{\partial F}{\partial t} + u_i \frac{\partial F}{\partial x_i}. \tag{4}$$

We can use this formula to compute the material derivative of F at each point in space and time.

In particular, we can define the particle acceleration in terms of spatial coordinates as

$$\mathbf{a} = \frac{D\mathbf{u}}{\partial t} = \frac{\partial \mathbf{u}}{\partial t} + (\mathbf{u} \cdot \boldsymbol{\nabla})\mathbf{u} \quad \text{or} \quad a_i = \frac{\partial u_i}{\partial t} + u_j \frac{\partial u_i}{\partial x_j}.$$

Basic notions of kinematics of fluids IV

Flow field

- **Steady flow**
  If the spatial velocity does not depend on time in the Eulerian reference frame, the flow field is said to be steady
  $$\mathbf{u} = \mathbf{u}(\mathbf{x}).$$
- **Uniform flow**
  If the spatial velocity does not depend on space the flow is said to be uniform
  $$\mathbf{u} = \mathbf{u}(t).$$
- **Streamlines**
  We define a streamline as a line which is everywhere tangent to the velocity vectors. Streamlines are defined by the solution of the equation
  $$d\mathbf{x} \times \mathbf{u}(\mathbf{x}, t) = 0,$$
  at a fixed time t. Alternatively
  $$\frac{dx_1}{u_1} = \frac{dx_2}{u_2} = \frac{dx_3}{u_3}.$$
  In steady flows streamlines and particle trajectories are coincident.

Principle of conservation of mass

"The mass of a material body[1] within a continuum remains constant in time."

The above principle can be expressed mathematically in differential form as

$$\frac{\partial \rho}{\partial t} + \nabla \cdot (\rho \mathbf{u}) = 0. \tag{5}$$

Incompressible fluids

An **incompressible fluid** is one whose density $\rho(\mathbf{x}, t)$ is constant.

- **To a good approximation, many liquids are incompressible.**
- **The assumption of incompressibility is good for most internal fluid flows in mathematical biology.**

For an incompressible fluid, the principle of mass conservation is equivalent to

$$\nabla \cdot \mathbf{u} = 0. \tag{6}$$

[1] A material body is a body that is always composed of the same fluid particles.

Principle of conservation of momentum

"The time derivative of the momentum of a material body of continuum equals the resultant of all the external forces acting on it."

In differential form this can be expressed as

$$\rho\left(\frac{\partial}{\partial t}\mathbf{u} + (\mathbf{u}\cdot\nabla\mathbf{u}) - \mathbf{f}\right) = \nabla\cdot\boldsymbol{\sigma}, \tag{7}$$

where $\boldsymbol{\sigma}$ is the stress tensor.

"The time derivative of the angular momentum of a material body of continuum equals the resultant of all external moments acting on it."

Using this principle it can be shown that the stress tensor $\boldsymbol{\sigma}$ is symmetric.

Definition of pressure in a moving fluid I

We have seen that, **in a fluid at rest,** the stress tensor takes the simple form

$$\sigma_{ij} = -p\delta_{ij},$$

where the scalar p is the static pressure.
In the case of a moving fluid, the situation is more complicated. In particular:

- the tangential stresses are not necessarily equal to zero;
- the normal stresses can depend on the orientation of the surface they act on.

Therefore the notion that the normal stress is the pressure, which acts equally in all directions is lost. We can define the pressure in a moving fluid as

$$p = -\frac{1}{3}\sigma_{ii}, \qquad \text{or,} \qquad p = -\frac{1}{3}\,\mathrm{tr}(\boldsymbol{\sigma}).$$

Important note

- **Compressible fluids**
  From classical thermodynamics it is known that we can define the pressure of the fluid as a **parameter of state**, making use of an **equation of state**. Thermodynamical relations refer to equilibrium conditions, so we can denote the thermodynamic pressure as p_e.
- **Incompressible fluids**
  For an incompressible fluid the pressure p is an independent, purely dynamical, variable.

Definition of pressure in a moving fluid II

In the following we will consider **incompressible fluids** only.
It is usually convenient to split to the stress tensor σ_{ij} into an **isotropic part**, $-p\delta_{ij}$, and a **deviatoric part**, d_{ij}, which is entirely due to fluid motion. Thus we write

$$\sigma_{ij} = -p\delta_{ij} + d_{ij}.$$

The tensor d_{ij} accounts for tangential stresses and also normal stresses, whose components sum to zero.

Constitutive relationship for Newtonian fluids I

A **constitutive law** links the stress tensor to the kinematic state of the fluid.

- **This law provides a third relationship, which, together with the equations of mass and momentum conservation, closes the problem for the velocity and pressure fields.**

The constitutive law for **Newtonian fluids** can be obtained by assuming the following:

1. The deviatoric part of the stress tensor, $\mathbf{d}$, is a continuous function of the **rate-of-strain** tensor $\mathbf{e}$, defined as

$$\text{in component form,} \quad e_{ij} = \frac{1}{2}\left(\frac{\partial u_i}{\partial x_j} + \frac{\partial u_j}{\partial x_i}\right) \quad \text{or, in vector form,} \quad \mathbf{e} = \frac{1}{2}\left(\boldsymbol{\nabla}\mathbf{u} + (\boldsymbol{\nabla}\mathbf{u})^T\right).$$

2. If $\mathbf{e} = \mathbf{0}$ (i.e. the flow is **uniform**) then $\mathbf{d} = \mathbf{0}$. This means that $\boldsymbol{\sigma} = -p\mathbf{I}$, i.e. the stress reduces to the stress in static conditions.
3. The fluid is homogeneous, i.e. $\boldsymbol{\sigma}$ does not depend explicitly on $\mathbf{x}$.
4. The fluid is isotropic, i.e. there is no preferred direction.
5. The relationship between $\mathbf{d}$ and $\mathbf{e}$ is linear.
6. The fluid is incompressible.

These assumptions imply that

$$\text{in component form,} \quad \sigma_{ij} = -p\delta_{ij} + 2\mu e_{ij}, \quad \text{or, in vector form,} \quad \boldsymbol{\sigma} = -p\mathbf{I} + 2\mu\mathbf{e}, \tag{8}$$

where μ is the **dynamic viscosity**.

Constitutive relationship for Newtonian fluids II

Definitions

- The **dynamic viscosity** μ has dimensions $[\mu] = ML^{-1}T^{-1}$.
- It is often convenient to define the **kinematic viscosity** as

$$\nu = \frac{\mu}{\rho}.$$

The kinematic viscosity has dimensions $[\nu] = L^2T^{-1}$.

Inviscid fluids

A fluid is said to be **inviscid** or **ideal** if $\mu = 0$. For an inviscid fluid the constitutive law (8) becomes

$$\text{in component form,} \quad \sigma_{ij} = -p\delta_{ij}, \quad \text{or, in vector form,} \quad \boldsymbol{\sigma} = -p\mathbf{I}. \tag{9}$$

Thus the motion of the fluid does not affect the stress. Note that there are no truly inviscid fluids in nature. However, the inviscid approximation is good in certain cases, such as fast flows of a low-viscosity fluid.

The Navier-Stokes equations

Substituting the constitutive law (8) into the equation for conservation of motion (7), we obtain

$$\frac{\partial u_i}{\partial t}+u_j\frac{\partial u_i}{\partial x_j}-f_i+\frac{1}{\rho}\frac{\partial p}{\partial x_i}-\nu\frac{\partial^2 u_i}{\partial x_j\partial x_j}=0, \quad \text{or, in vector form,} \quad \frac{\partial \mathbf{u}}{\partial t}+(\mathbf{u}\cdot\nabla)\mathbf{u}-\mathbf{f}+\frac{1}{\rho}\nabla p-\nu\nabla^2\mathbf{u}=0, \tag{10}$$

where $\mathbf{f}=f_i\mathbf{e}_i$ is the resultant external body force acting on the fluid. Recalling the definition of material derivative (4) the above equation can also be written as

$$\frac{Du_i}{Dt}-f_i+\frac{1}{\rho}\frac{\partial p}{\partial x_i}-\nu\frac{\partial^2 u_i}{\partial x_j^2}=0, \quad \text{or, in vector form,} \quad \frac{D\mathbf{u}}{Dt}-\mathbf{f}+\frac{1}{\rho}\nabla p-\nu\nabla^2\mathbf{u}=0.$$

This equation is called the **Navier-Stokes equation**, and it is of fundamental importance in fluid mechanics. It is actually three equations, one for each spatial component. The equations govern the motion of a Newtonian incompressible fluid and should to be solved together with the continuity equation (6).

Buckingham's Π theorem I

In fluid dynamics problems one often wishes to find a physical quantity in terms of other variables in the problem, that is

$$a = f(a_1, \ldots, a_k),$$

where a is the quantity of interest and a_i $(i = 1, 2, \ldots, k)$ are other variables and parameters in the problem.
The Buckingham Π theorem states that equation (30) is equivalent to

$$\Pi = \mathcal{F}(\Pi_1, \ldots, \Pi_m),$$

where $m \leq k$ and the quantities Π, Π_1, Π_2, $\ldots$, Π_m are all dimensionless. The number of variables that have been removed, $k - m$, equals the number of **independent dimensions** in the variables a_i.

- In fluid dynamics problems, we often have $k - m = 3$, since all variables have dimensions that are combinations of **length, time and mass**, leading to three independent dimensions.
- **Rescaling** or **nondimensionalising** is a powerful tool in fluid mechanics, as, through simplifying a problem, it enables us to obtain a great deal of insight.

Dimensionless Navier-Stokes equations I

When dealing with theoretical modelling of physical phenomena, it is convenient to work with dimensionless equations. The main reasons are:

- the number of parameters in the problem decreases if one passes from a dimensional to a dimensionless formulation;
- if proper scalings are adopted, it is much easier to evaluate the relative importance of different terms appearing in one equation.

Let us consider the Navier-Stokes equation and assume that the body force is gravity. Equations (10) can then be written as

$$\underbrace{\frac{\partial \mathbf{u}}{\partial t} + (\mathbf{u}\cdot\nabla)\mathbf{u}}_{①} = \underbrace{\mathbf{g}}_{②} \underbrace{-\frac{1}{\rho}\nabla p}_{③} + \underbrace{\nu\nabla^2\mathbf{u}}_{④} = 0, \tag{11}$$

where the vector $\mathbf{g}$, representing the gravitational field, has magnitude g and is directed vertically downwards. We recall the physical meaning of all terms:

- ①: convective terms;
- ②: gravity;
- ③: pressure gradient;
- ④: viscous term.

Dimensionless Navier-Stokes equations II

We will now scale the Navier–Stokes equation. Suppose that L is a characteristic length scale of the domain under consideration and U a characteristic velocity. We can introduce the following dimensionless coordinates and variables

$$\mathbf{x}^* = \frac{\mathbf{x}}{L}, \qquad \mathbf{u}^* = \frac{\mathbf{u}}{U}, \qquad t^* = \frac{t}{L/U},$$

where superscript stars indicate dimensionless quantities.
In scaling the pressure there are two commonly used possibilities:

1. The pressure gradient, ③, balances with the viscous forces, ④, leading to

$$p^* = \frac{p}{\rho \nu U/L}.$$

   This is the most relevant case for studying physiological flows, for reasons that will be made clear in the following.

2. The pressure gradient, ③, balances with the convective terms, ①, giving

$$p^* = \frac{p}{\rho U^2}.$$

Dimensionless Navier-Stokes equations III

Low-Reynolds-number flows

Let us consider the first case $p = (\mu U/L)p^*$. Equation (11) becomes

$$Re\left[\frac{\partial \mathbf{u}^*}{\partial t^*} + (\mathbf{u}^* \cdot \nabla^*)\mathbf{u}^*\right] + \frac{Re}{Fr^2}\hat{\mathbf{z}} + \nabla^* p^* - \nabla^{*2}\mathbf{u}^* = 0, \tag{12}$$

where $\hat{\mathbf{z}}$ is the upward directed vertical unit vector.
In the above equation we have introduced two dimensionless parameters.

- $Re = \dfrac{UL}{\nu}$: **Reynolds number**. This represents the ratio between the magnitude of inertial (convective) terms and viscous terms. It plays a fundamental role in fluid mechanics.
- $Fr = \dfrac{U}{\sqrt{gL}}$: **Froude number**. This represents the square root of the ratio between the magnitude of inertial (convective) terms and gravitational terms. It plays a fundamental role when gravity is important, e.g. in free surface flows.

If we now consider the limit $Re \to 0$ the dimensionless Navier-Stokes equation (12) reduces to the so called **Stokes equation**, i.e.

$$\nabla^* p^* - \nabla^{*2}\mathbf{u}^* = 0.$$

This equation is much simpler to solve than the Navier-Stokes equation, primarily because it is linear.

Dimensionless Navier-Stokes equations IV

High-Reynolds-number flows

We now consider the case in which the pressure gradient balances the convective terms. The dimensionless Navier-Stokes equation takes the form

$$\frac{\partial \mathbf{u}^*}{\partial t^*} + (\mathbf{u}^* \cdot \nabla^*)\mathbf{u}^* + \frac{1}{Fr^2}\mathbf{z} + \nabla^* p^* - \frac{1}{Re}\nabla^{*2}\mathbf{u}^* = 0. \tag{13}$$

In the limit $Re \to \infty$ the viscous term in equation (13) tends to zero. Thus at large values of Re the fluid behaves as an **ideal** or **inviscid fluid**.
However, this limit leads to a qualitative change in the Navier–Stokes equation (13). The viscous term contains the highest order derivatives in equation (13), and therefore, if it is neglected, it is not possible to impose the usual number of boundary conditions. To resolve this, we assume that thin **boundary layers** form at the boundaries, and within these the viscous terms in the Navier-Stokes equations have the same magnitude as the convective terms.
If we are only interested in the flow away from the boundaries, we may compute this by solving equation (13) in the limit $Re \to \infty$ and applying no-penetration boundary conditions (no fluid flow through the boundary, rather than the full no-slip conditions).

The dynamic pressure

We now assume that the body force acting on the fluid is gravity, therefore we set in the Navier-Stokes equation (10) $\mathbf{f} = \mathbf{g}$. When ρ is constant the pressure p in a point $\mathbf{x}$ of the fluid can be written as

$$p = p_0 + \rho \mathbf{g} \cdot \mathbf{x} + P, \tag{14}$$

where p_0 is a constant and $p_0 + \rho \mathbf{g} \cdot \mathbf{x}$ is the pressure that would exist in the fluid if it was at rest. Finally, P is the part of the pressure which is associated to fluid motion and can be named **dynamic pressure**. This is in fact the departure of pressure from the hydrostatic distribution. Therefore, in the Navier-Stokes equations, the term $\rho \mathbf{g} - \nabla p$ can be replaced with $-\nabla P$. Thus we have:

$$\begin{aligned} &\nabla \cdot \mathbf{u} = 0, \\ &\frac{\partial \mathbf{u}}{\partial t} + (\mathbf{u} \cdot \nabla)\mathbf{u} + \frac{1}{\rho}\nabla P - \nu \nabla^2 \mathbf{u} = 0. \end{aligned} \tag{15}$$

If the Navier-Stokes equations are written in terms of the dynamic pressure gravity does not explicitly appear in the equations.
In the following whenever gravity will not be included in the Navier-Stokes this will be done with the understanding that the pressure is the dynamic pressure (even if p will sometimes be used instead of P).

Lubrication theory I

This technique provides a good approximation to the real solution as long as **the domain of the fluid is long and thin**. It is used because it results in a **considerable simplification** of the Navier–Stokes equations. An example where lubrication theory has been successfully used to analyse a problem is in blood flow in a capillary, specifically in the small gap between a red blood cell and the wall of the capillary.

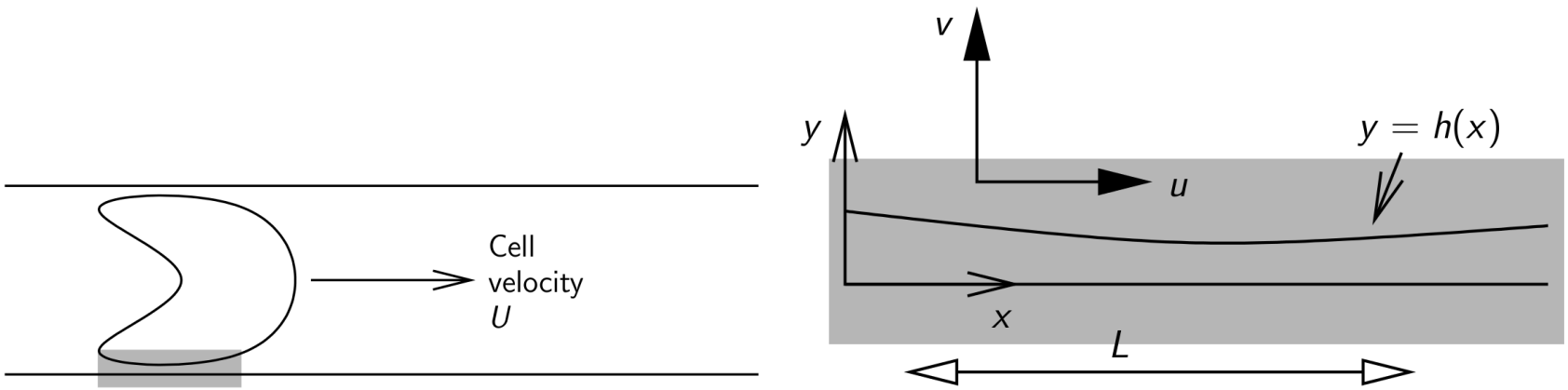

Example of a scenario where lubrication theory may be applied. A cell moves steadily with speed U along a vessel with a narrow gap at the walls (Secomb, 2003).

Lubrication theory applies if one dimension of the space occupied by the fluid is much smaller than the other(s).

Lubrication theory II

Mathematical formulation

For simplicity let us assume that the flow is two dimensional (all derivatives with respect to the third coordinate, say z, may be neglected) and that the height of the domain is $h(x)$ and a typical streamwise length is L.

The fluid velocity at the vessel walls is zero (no-slip condition) but the fluid velocity at the surface of the cell equals the cell velocity (U). Therefore changes in the x-velocity u are on the order of U, that is $|\Delta u| \sim U$, and $|\partial u/\partial y| \sim |\Delta u/\Delta y| \sim U/h_0$, where h_0 is a characteristic value of $h(x)$.

The change in fluid velocity as we move through a distance L in the x-direction is likely to be at most U, and therefore $|\partial u/\partial x| \sim U/L$. The continuity equation,

$$\frac{\partial u}{\partial x} + \frac{\partial v}{\partial y} = 0,$$

implies that $|\partial v/\partial y| \sim U/L$; hence $|\Delta v| \sim h_0 U/L$.

Scaling

We nondimensionalise

$$x = Lx^*, \quad y = h_0 y^*, \quad h(x) = h_0 h^*(x^*), \quad u = Uu^*, \quad v = h_0 U v^*/L, \quad p = p_0 p^*,$$

where p_0 is an appropriate scale for the pressure (to be chosen). Note that x^*, y^*, u^*, v^* and p^* are all order 1.

Lubrication theory III

Assuming a steady solution, the nondimensional governing equations are

$$\epsilon^2 Re\left(u^*\frac{\partial u^*}{\partial x^*}+v^*\frac{\partial u^*}{\partial y^*}\right)=-\frac{h_0^2 p_0}{\mu UL}\frac{\partial p^*}{\partial x^*}+\epsilon^2\frac{\partial^2 u^*}{\partial x^{*2}}+\frac{\partial^2 u^*}{\partial y^{*2}}, \tag{16}$$

$$\epsilon^3 Re\left(u^*\frac{\partial v^*}{\partial x^*}+v^*\frac{\partial v^*}{\partial y^*}\right)=-\frac{h_0^2 p_0}{\epsilon\mu UL}\frac{\partial p^*}{\partial y^*}+\epsilon^3\frac{\partial^2 v^*}{\partial x^{*2}}+\epsilon\frac{\partial^2 v^*}{\partial y^{*2}}, \tag{17}$$

$$\frac{\partial u^*}{\partial x^*}+\frac{\partial v^*}{\partial y^*}=0, \tag{18}$$

where $\epsilon = h_0/L \ll 1$ and $Re = UL/\nu$.
We may immediately cancel the viscous terms that have a repeated x^*-derivative since they are much smaller than the viscous terms with a repeated y^*-derivative. Balancing the pressure derivative and viscous terms in the x-component equation (16) leads to the scaling $p_0 = \mu UL/h_0^2$. Multiplying equation (17) by ϵ and simplifying, equations (16) and (17) can be written as

$$\epsilon^2 Re\left(u^*\frac{\partial u^*}{\partial x^*}+v^*\frac{\partial u^*}{\partial y^*}\right)=-\frac{\partial p^*}{\partial x^*}+\frac{\partial^2 u^*}{\partial y^{*2}}, \tag{19}$$

$$0=-\frac{\partial p^*}{\partial y^*}, \tag{20}$$

where **we have neglected terms of order ϵ^2 and terms of order $\epsilon^3 Re$ relative to the leading-order terms.**

Lubrication theory IV

Solution procedure

- The quantity $\epsilon^2 Re$ is called the **reduced Reynolds number**. We assume it is not too large, which places an upper bound on the possible flux.
- We may immediately solve (20) to find that the pressure is a function of x^* only, that is, **the pressure is constant over the height of the gap**.
- The governing equations are thus (19) and (18), where p^* is a function of x^* only and these must be solved subject to no-slip boundary conditions for u^* at the walls.

Lubrication theory V

Series expansion for small reduced Reynolds number

In the case that the reduced Reynolds number is small, $\epsilon^2 Re \ll 1$ we can use a **series expansion** method to find the velocity, by setting

$$\begin{aligned} u^* &= u_0^* + \epsilon^2 Re\, u_1^* + \left(\epsilon^2 Re\right)^2 u_2^* + \ldots, \\ v^* &= v_0^* + \epsilon^2 Re\, v_1^* + \left(\epsilon^2 Re\right)^2 v_2^* + \ldots, \\ p^* &= p_0^* + \epsilon^2 Re\, p_1^* + \left(\epsilon^2 Re\right)^2 p_2^* + \ldots. \end{aligned}$$

noting that all the p_i^*'s are independent of y, and then solving for u_0^* (from equation (19)), v_0^* (from equation (18)), u_1^* (from equation (19)), v_1^* (from equation (18)), *etc* in that order. An equation for the pressure can be obtained by integrating the continuity equation over the gap height.

In many cases it is sufficiently accurate to find just the first terms u_0^* and v_0^* (or even just u_0^*).

Generalisation

Note that we could generalise this approach to include:

- dependence upon the third spatial dimension;
- time-dependence of the solution;
- gravity;
- ....

Lubrication theory VI

Example of solution

We consider the domain shown in the figure. For simplicity, we assume two-dimensional flow. We wish to solve the flow in the gap $0 \leq y \leq h(x)$, with $0 \leq x \leq L$.
The flow
is subject to the following boundary conditions:

- no-slip at $y = 0$ and $y = h(x)$;
- given
  flux per unit length $F = \int_0^{h_0} u dy$ at $x = 0$;
- given pressure $p = 0$ at $x = L$.

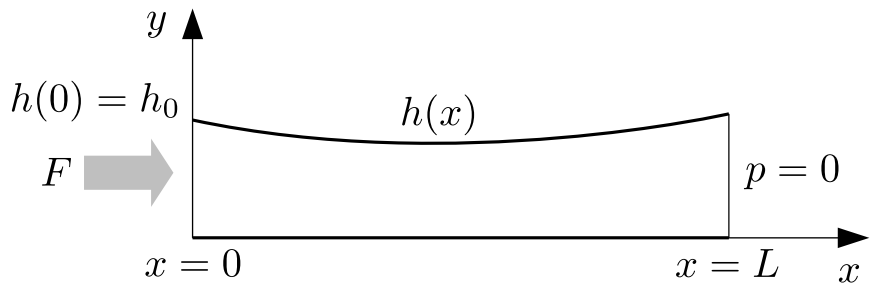

We assume that $h_0 = h(0)$ is a typical value of
the thickness of the domain in the y-direction and
assume that $\epsilon = h_0/L \ll 1$. We can, therefore, apply the lubrication theory.
We scale the variables as follows

$$x^* = \frac{x}{L}, \qquad y^* = \frac{y}{h_0}, \qquad u^* = \frac{u}{U}, \qquad v^* = \frac{v}{\epsilon U},$$

with $U = F/h_0$.

Lubrication theory VII

Assuming that $\epsilon^2 Re \ll 1$, we need to solve the following dimensionless equations (see equations (19), (20) and (18))

$$\frac{\partial^2 u^*}{\partial y^{*2}} - \frac{\partial p^*}{\partial x^*} = 0, \tag{21}$$

$$\frac{\partial p^*}{\partial y^*} = 0, \tag{22}$$

$$\frac{\partial u^*}{\partial x^*} + \frac{\partial v^*}{\partial y^*} = 0, \tag{23}$$

subject to the boundary conditions

$$u^* = v^* = 0 \qquad (y^* = 0), \tag{24}$$

$$u^* = v^* = 0 \qquad [y^* = h^*(x^*)], \tag{25}$$

$$\int_0^1 u^* dy^* = 1 \qquad (x^* = 0), \tag{26}$$

$$p^* = 0 \qquad (x^* = 1). \tag{27}$$

Lubrication theory VIII

Equation (22) imposes that p^* cannot depend on y^*. As a consequence equation (21) can be integrated with respect to y^* and, also using the boundary conditions (24) and (25), we obtain

$$u^*(x^*, y^*) = \frac{1}{2}\frac{dp^*}{dx^*}\left(y^{*2} - h^* y^*\right). \tag{28}$$

In the above expression the term dp^*/dx^* is still an unknown function of x^*.
Using the boundary condition (26) and (28) we find that

$$\left.\frac{dp^*}{dx^*}\right|_{x^*=0} = -12. \tag{29}$$

We now integrate the continuity equation (23) with respect to y^*

$$\int_o^{h^*} \frac{\partial u^*}{\partial x^*} + \frac{\partial v^*}{\partial y^*} dy^* = \cancel{v^*(h^*)} - \cancel{v^*(0)} + \int_o^{h^*} \frac{\partial u^*}{\partial x^*} dy^* = 0,$$

where we have used the no-slip boundary conditions (24) and (25).
Using Leibniz rule[2] and, again, the no-slip boundary conditions (24) and (25) we obtain the following second order equation for the pressure

$$\frac{d}{dx^*}\left(h^{*3}\frac{dp^*}{dx^*}\right) = 0.$$

Lubrication theory IX

From the above equation and using (29) we obtain

$$\frac{dp^*}{dx^*} = -\frac{12}{h^{*3}},$$

which we can plug into equation (28) to obtain the following expression for the velocity in the x^*-direction

$$u^*(x^*, y^*) = -\frac{6}{h^{*3}}\left(y^{*2} - h^* y^*\right).$$

The y^*-component of the velocity can be obtained from the continuity equation (23) and reads

$$v^*(x^*, y^*) = -6\left(-\frac{y^{*3}}{h^{*4}} + \frac{y^{*2}}{h^{*3}}\right)\frac{dh^*}{dx^*}.$$

Finally, the pressure distribution can be obtained by integrating (36) and using the boundary condition (27).
We note that we managed to obtain an analytical expression for the velocity without having to specify the shape of the domain $h^*(x^*)$.

2

$$\int_{a(z)}^{b(z)} \frac{\partial f(x,z)}{\partial z}\,dx = \frac{\partial}{\partial z}\int_{a(z)}^{b(z)} f(x,z)dx - f(b,z)\frac{\partial b(z)}{\partial z} + f(a,z)\frac{\partial a(z)}{\partial z}.$$

The Boussinesq approximation for thermally driven flows I

Justification of the Boussinesq approximation

Let us consider a fluid with a weakly variable density and viscosity, so that we can write

$$\rho = \rho_0 \left(1 + \frac{\rho'}{\rho_0}\right), \qquad \nu = \nu_0 \left(1 + \frac{\nu'}{\nu_0}\right), \tag{30}$$

with $\rho'/\rho_o \ll 1$ and $\nu'/\nu_o \ll 1$.
We assume that **fluid flow is generated by buoyant effects.** We fist consider the continuity equation (5), which we write here in index notation

$$\frac{\partial \rho}{\partial t} + \frac{\partial}{\partial x_i}(\rho u_i) = 0. \tag{31}$$

Substituting (30) into (31) we obtain

$$\frac{\partial \rho'}{\partial t} + \left(\rho_0 + \rho'\right) \frac{\partial u_i}{\partial x_i} + u_i \frac{\partial \rho'}{\partial x_i} = 0. \tag{32}$$

We now introduce nondimensional variables as follows

$$x_i^* = \frac{x_i}{L}, \qquad t^* = \frac{tU}{L}, \qquad u_i^* = \frac{u_i}{U}, \tag{33}$$

The Boussinesq approximation for thermally driven flows II

where L is a typical length scale of the problem and U a proper scale for the velocity. Substituting the dimensionless variables (33) into (32) we obtain

$$\frac{\partial}{\partial t^*}\left(\frac{\rho'}{\rho_0}\right) + \left(1+\frac{\rho'}{\rho_0}\right)\frac{\partial u_i^*}{\partial x_i^*} + u_i^*\frac{\partial}{\partial x_i^*}\left(\frac{\rho'}{\rho_0}\right) = 0,$$

which shows that, since $\rho'/\rho_0 \ll 1$, at leading order the continuity equation is the same as for an incompressible fluid

$$\frac{\partial u_i^*}{\partial x_i^*} = 0.$$

Let us now consider the momentum equation (7), which we again write in index notation, and in which we substitute the expression (30) for the density

$$\rho_0\left(1+\frac{\rho'}{\rho_0}\right)\left(\frac{\partial u_i}{\partial t} + u_j\frac{\partial u_i}{\partial x_j}\right) + \frac{\partial p}{\partial x_i} - \rho_0\nu_0\left(1+\frac{\rho'}{\rho_0}\right)\left(1+\frac{\nu'}{\nu_0}\right)\frac{\partial^2 u_i}{\partial x_j^2} + \rho_0\left(1+\frac{\rho'}{\rho_0}\right)g\hat{z}_i = 0, \tag{34}$$

where $\hat{\mathbf{z}}$ is the upward directed vertical unit vector. It is convenient to decompose the pressure as $p_o + p'$, so that

$$\frac{\partial p_0}{\partial x_i} + \rho_0 g\hat{z}_i = 0. \tag{35}$$

The Boussinesq approximation for thermally driven flows III

Substituting (35) into (34) we obtain

$$\rho_0 \left(1+\frac{\rho'}{\rho_0}\right)\left(\frac{\partial u_i}{\partial t}+u_j\frac{\partial u_i}{\partial x_j}\right)+\frac{\partial p'}{\partial x_i}-\rho_0\nu_0\left(1+\frac{\rho'}{\rho_0}\right)\left(1+\frac{\nu'}{\nu_0}\right)\frac{\partial^2 u_i}{\partial x_j^2}+\rho' g\hat{z}_i=0, \qquad (36)$$

We now scale the momentum equation using the following scales for the pressure: $p'^{*}=\dfrac{p'}{\rho_0 U^2}$.

With the above assumption the dimensionless version of equation (36) reads

$$\left(1+\frac{\rho'}{\rho_0}\right)\left(\frac{\partial u_i^*}{\partial t^*}+u_j^*\frac{\partial u_i^*}{\partial x_j^*}\right)+\frac{\partial p'^*}{\partial x_i}-\frac{1}{Re}\left(1+\frac{\rho'}{\rho_0}\right)\left(1+\frac{\nu'}{\nu_0}\right)\frac{\partial^2 u_i^*}{\partial x_j^{*2}}+\frac{\rho'}{\rho_0}\frac{1}{F^2}\hat{z}_i=0, \qquad (37)$$

Since we assumed that flow is generated by buoyancy effects, the leading order terms in the equation have to balance with the gravitational term. Thus we need to have

$$\frac{\rho'}{\rho_0}\frac{1}{F^2}\approx 1 \qquad \text{if } Re\gg 1,$$

$$\frac{\rho'}{\rho_0}\frac{Re}{F^2}\approx 1 \qquad \text{if } Re\ll 1.$$

The Boussinesq approximation for thermally driven flows IV

If we now neglect in (37) terms of order ρ'/ρ_0 and ν/ν_0 with respect to terms of order 1 we obtain

$$\frac{\partial u_i^*}{\partial t^*} + u_j^* \frac{\partial u_i^*}{\partial x_j^*} + \frac{\partial p'^*}{\partial x_i} - \frac{1}{Re} \frac{\partial^2 u_i^*}{\partial x_j^{*2}} + \frac{\rho'}{\rho_0} \frac{1}{F^2} \hat{z}_i = 0,$$

Writing the continuity and momentum equation back in dimensional form still neglecting small terms, we obtain

$$\frac{\partial u_j}{\partial x_j} = 0, \tag{38a}$$

$$\left(\frac{\partial u_i}{\partial t} + u_j \frac{\partial u_i}{\partial x_j} \right) + \frac{1}{\rho_0} \frac{\partial p}{\partial x_i} - \nu_0 \frac{\partial^2 u_i}{\partial x_j^2} + \left(1 + \frac{\rho'}{\rho_0} \right) g \hat{z}_i = 0. \tag{38b}$$

In other words, at leading order, the only term in which the perturbation of density appears is gravity. This is what is called the **Boussinesq approximation** of the equations of motion.

The Boussinesq approximation for thermally driven flows V

Heat transport equation

When density changes are due to temperature variations, for liquids we can write

$$\rho = \rho_0 \left[1 - \alpha(T - T_0)\right], \tag{39}$$

where α is the **coefficient of thermal expansion.**
In this case the equations of motion have to be coupled with the heat transport equation, which reads

$$\frac{\partial T}{\partial t} + u_j \frac{\partial T}{\partial x_j} - D \frac{\partial^2 T}{\partial x_j^2} = 0,$$

or, in vector form,

$$\frac{\partial T}{\partial t} + \mathbf{u} \cdot \nabla T = D \nabla^2 T,$$

where T denotes temperature and D is the **thermal diffusion coefficient** ($[D] = L^2 T^{-1}$).

Irrotational flows I

Potential function of the velocity

We define the **vorticity** as

$$\boldsymbol{\omega} = \nabla \times \mathbf{u}. \tag{40}$$

In the absence of viscous effects (and introduction of vorticity at the boundaries), it can be shown that vorticity cannot be generated in a moving fluid.
As mentioned, for large values of the Reynolds number, the flow away from the boundaries behaves as if it were inviscid. Therefore, if the vorticity is initially zero, it will remain so at all times (provided there is no mechanism of introduction at the boundaries). In this case the flow is said to be **irrotational**.
We assume

- **incompressible fluid,** and
- **irrotational flow,**

i.e.

$$\nabla \cdot \mathbf{u} = 0, \qquad \nabla \times \mathbf{u} = 0. \tag{41}$$

Note that the conditions (41) are purely kinematic in nature (although they do, of course, affect the dynamic behaviour of the fluid).

Irrotational flows II

Let us consider a closed curve C in an irrotational flow. By Stokes' theorem,

$$\oint_C \mathbf{u} \cdot d\mathbf{x} = \iint_S (\nabla \times \mathbf{u}) \cdot \mathbf{n} dS = \iint_S \boldsymbol{\omega} \cdot \mathbf{n} dS = 0,$$

and thus the **circulation** is zero.
Now consider any two points, say O and P, and any two paths, C_1 and C_2 from O to P through the irrotational flow. Since travelling along C_1 and then back along C_2, is a closed curve through the flow, we must have

$$\oint_{C_1} \mathbf{u} \cdot d\mathbf{x} - \oint_{C_2} \mathbf{u} \cdot d\mathbf{x} = 0 \quad \Rightarrow \quad \oint_{C_1} \mathbf{u} \cdot d\mathbf{x} = \oint_{C_2} \mathbf{u} \cdot d\mathbf{x}.$$

Thus the integral between O and P does not depend on the path of integration, but only on the starting and ending points. This means we can define a function, $\Phi(\mathbf{x})$, which we call the **potential** of the velocity field, such that

$$\Phi(\mathbf{x}) = \Phi_0 + \int_O^P \mathbf{u} \cdot d\mathbf{x}, \tag{42}$$

where Φ_0 is the velocity potential at the point O. In a simply connected region the velocity potential is unique up to the constant Φ_0. Equation (42) implies that we can write

$$\mathbf{u} = \nabla \Phi. \tag{43}$$

Irrotational flows III

The continuity equation for an incompressible fluid, i.e. $\nabla \cdot \mathbf{u} = 0$, together with (43) implies

$$\nabla^2 \Phi = 0. \tag{44}$$

This means **the potential function Φ is harmonic**, that is, it satisfies the Laplace equation. If we solve the problem for the function Φ we can find the velocity $\mathbf{u}$ using equation (43).
The mathematical problem to find an irrotational flow is much easier than that for a rotational flow, for the following main reasons:

- equation (44) is linear, whereas the Navier–Stokes equations are nonlinear;
- the problem is solved for a single scalar function (the potential) rather than multiple functions (the velocity and pressure – four components altogether, which much be solved simultaneously);

From Equation (44), the velocity distribution has the following properties.

- Equation (44) is elliptic, so Φ is smooth, except possibly on the boundary.
- The function Φ is single-valued (as long as the domain is simply connected).

Bernoulli equation for irrotational flows I

If

- **the flow is incompressible,**
- **the flow is irrotational**, and
- **the body force field is conservative**, i.e. $\boldsymbol{\nabla} \times \mathbf{f} = 0$,

then it may be shown that

$$\mathcal{H} = \frac{\partial \Phi}{\partial t} + \frac{|\mathbf{u}|^2}{2} + \frac{p}{\rho} + \Psi = c, \tag{45}$$

where Ψ is the potential of the body force field $\mathbf{f}$, defined as $\mathbf{f} = -\nabla\Psi$, and c is constant. This is the **Bernoulli theorem for irrotational flows**.

Once the velocity field is known, we can use this theorem to find the pressure.

Rheological models for non-Newtonian fluids I

Newtonian incompressible fluids

We recall that for an incompressible Newtonian fluid we can express the stress tensor $\boldsymbol{\sigma}$ as a function of the rate of deformation tensor $\mathbf{e}$ as

$$\boldsymbol{\sigma} = -p\mathbf{I} + 2\mu\mathbf{e}, \tag{46}$$

where p is pressure, $\mathbf{I}$ is the identity tensor, μ is the dynamic viscosity of the fluid and $\mathbf{e}$ is defined as the symmetric part of the velocity gradient tensor $\nabla\mathbf{u}$.

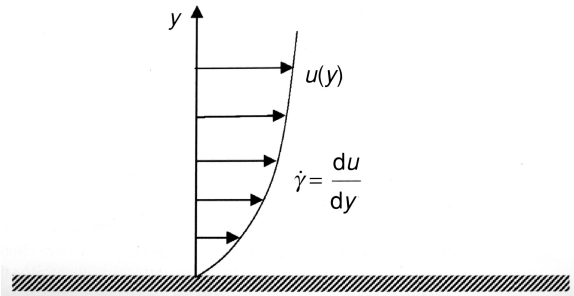

If we refer to a **one-dimensional shear flow** like that reported on the left, with velocity components $[u(y), 0, 0]$ in the directions x the shear stress at any point is given by

$$\sigma_{xy} = \tau = \mu\frac{du(y)}{dy} = \mu\dot{\gamma},$$

where $\dot{\gamma}$ is referred to as **rate of shear strain**.

Rheological models for non-Newtonian fluids II

Newtonian incompressible fluids

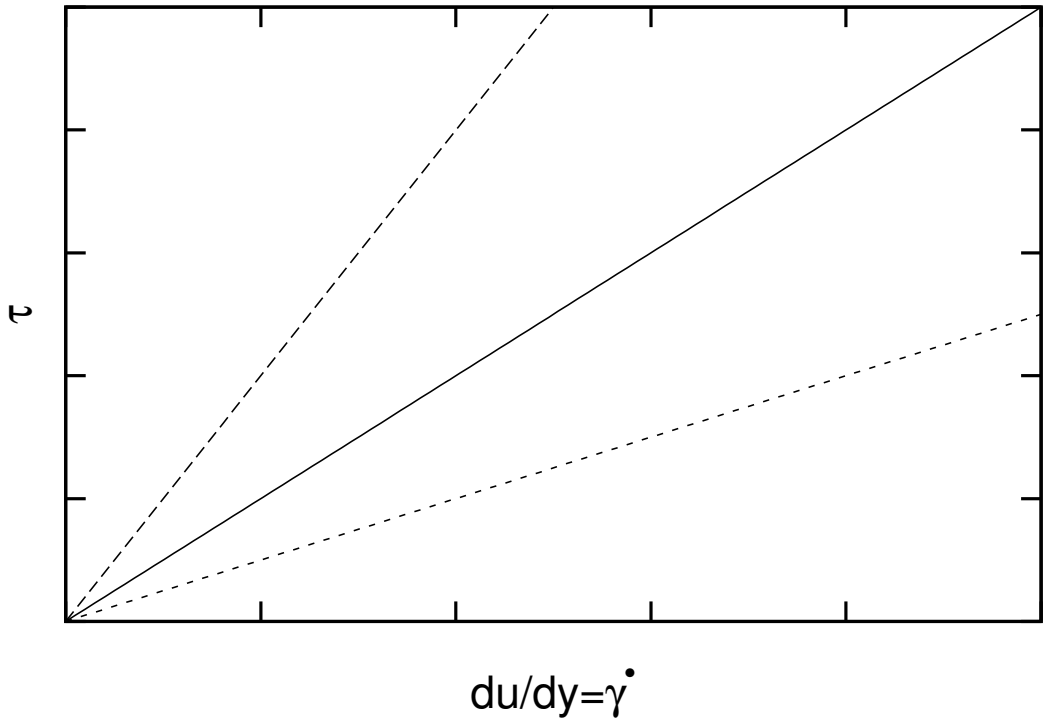

Qualitative dependence of the shear stress τ on the rate of shear strain $\dot{\gamma}$ for three Newtonian fluids with different viscosity.

Time-independent non-Newtonian fluids I

We now consider more complicated behaviours by referring first to the one-dimensional shear flow and then presenting the three-dimensional formulation of the constitutive relationship.
A good reference for non-Newtoninan fluid flow is the book by Tanner (2000).

For **inelastic, non-Newtonian fluids** a possible model for shear behaviour is

$$\dot{\gamma} = f(\tau).$$

The **shear rate** $\dot{\gamma}$ at any point in the fluid is a function of the **shear stress** τ at that point. Fluid behaving in this way are named **non-Newtoninan viscous fluids** or **generalised Newtonian fluids**. They can be distinguished in the following categories:

- **Bingham-Green;**
- **shear thinning** or pseudo-plastic;
- **shear-thickening fluids** or dilatant.

Time-independent non-Newtonian fluids II

Bingham-Green fluids

One-dimensional formulation

In Bingham-Green fluids if the shear stress is below a certain threshold value τ_c no-flow occurs. As the shear stress exceeds such a value the fluid behaves in analogy to a Newtonian fluid.
In one-dimensions we can thus write

$$\tau = \tau_c + \mu\dot{\gamma}.$$

Three-dimensional generalisation

The above constitutive behaviour can be generalised to the three-dimensional case as follows

$$\boldsymbol{\sigma} = -p\mathbf{I} + \left(2\mu + \frac{\tau_c}{\sqrt{-I_{II}}}\right)\mathbf{e}, \tag{47}$$

where I_{II} is the second invariant of the rate of deformation tensor, defined as

$$I_{II} = \frac{1}{2}\left[(tr\mathbf{e})^2 - \left(tr\mathbf{e}^2\right)\right],$$

and, for an incompressible fluid can be written as

$$|I_{II}| = \frac{1}{2}\mathbf{e} : \mathbf{e}.$$

Time-independent non-Newtonian fluids III

Bingham-Green fluids

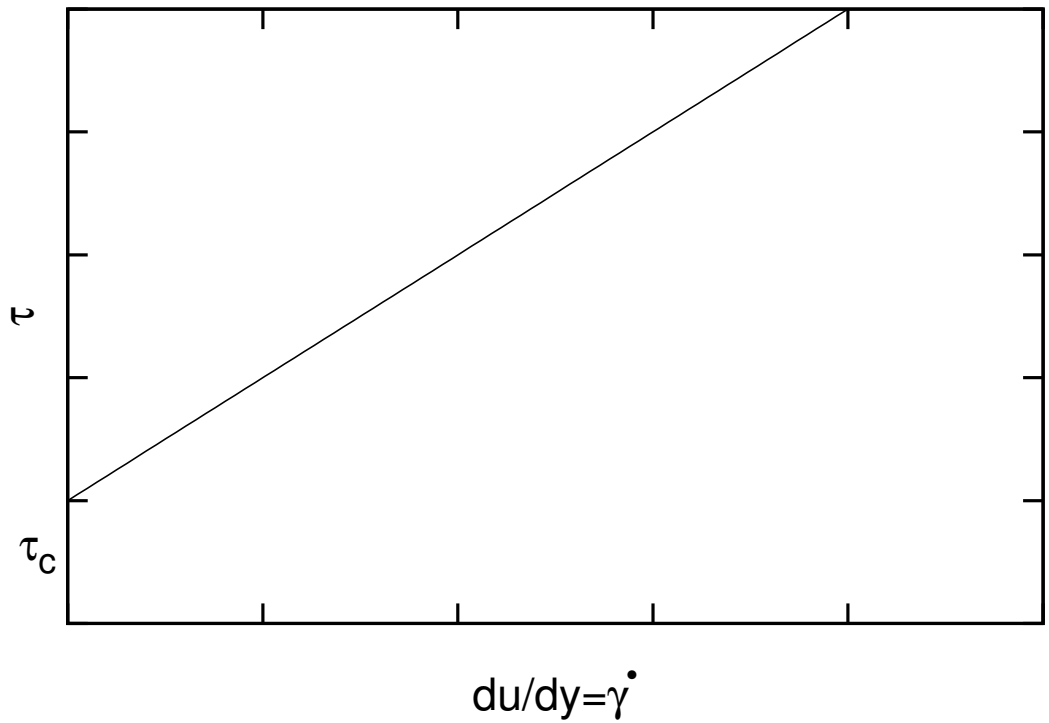

Qualitative dependence of the shear stress τ on the rate of shear strain $\dot{\gamma}$ for a Bingham-Green fluid.

Time-independent non-Newtonian fluids IV

Shear thinning/thickening fluids

One-dimensional formulation

The behaviour of many real fluid is approximately Newtonian in small intervals of the rate of strain but with a viscosity that changes with $\dot{\gamma}$.
This behaviour can often be expressed with good approximation with the following one-dimensional law

$$\tau = \mu_n \left|\dot{\gamma}\right|^n \operatorname{sgn}\left(\dot{\gamma}\right),$$

where the quantity μ_n has the following dimensions: $[\mu_n] = ML^{-1}T^{-2+n}$ and, therefore, is not a viscosity in general. However, it is possible to define an **effective viscosity** μ_{eff}, so that we have

$$\tau = \mu_{eff}\left(\dot{\gamma}\right)\dot{\gamma}.$$

Comparing the above two equations yields the following definition

$$\mu_{eff} = \mu_n \left|\dot{\gamma}\right|^{n-1}.$$

- If the effective viscosity μ_{eff} grows with $\dot{\gamma}$ the fluid is said to be **shear thickening**;
- if the effective viscosity μ_{eff} decreases with $\dot{\gamma}$ the fluid is said to be **shear thinning**.

Three-dimensional generalisation

The above constitutive behaviour can be generalised to the three-dimensional case as follows:

$$\boldsymbol{\sigma} = -p\mathbf{I} + \left(\frac{2^n \mu_n}{\sqrt{-I_{II}}^{1-n}}\right)\mathbf{e}. \tag{48}$$

Time-independent non-Newtonian fluids V

Shear thinning/thickening fluids

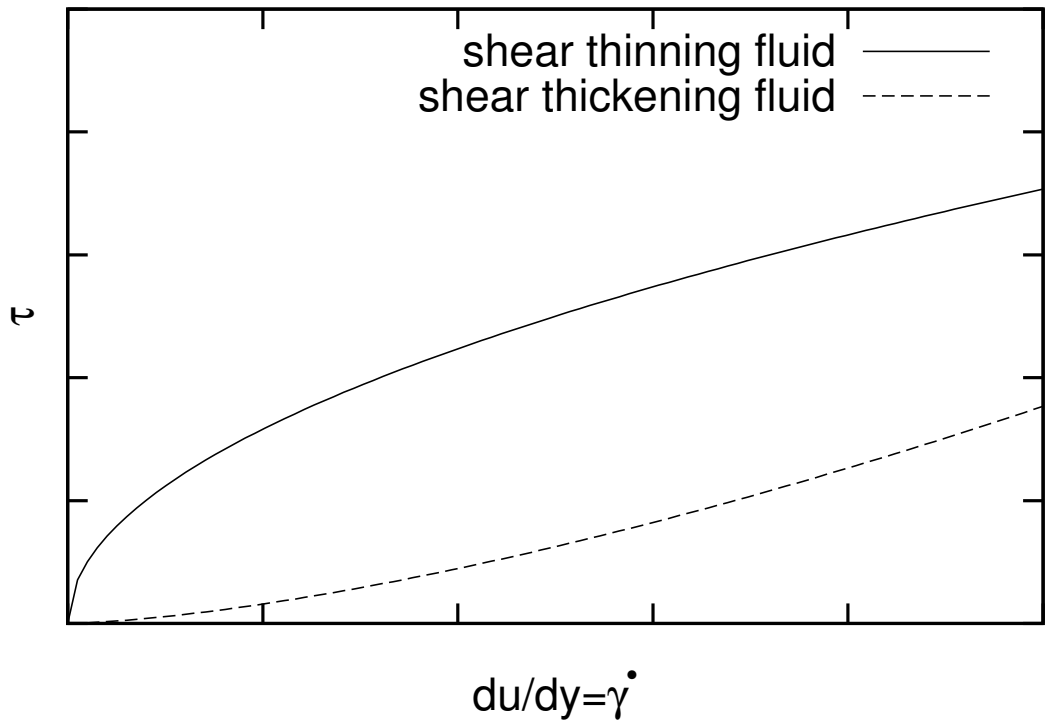

Qualitative dependence of the shear stress τ on the rate of shear strain $\dot{\gamma}$ for a shear thinning and a shear thickening fluid.

Time-independent non-Newtonian fluids VI

Herschel-Bulkley fluids

One-dimensional formulation

The behaviour of fluids carrying particles in suspension can often be expressed superimposing the characteristics of a Bingham-Green fluid with those of a shear thinning/thickening fluid, in the following form:

$$\tau = \left[\tau_c + \mu_n \left|\dot{\gamma}\right|^n\right] \operatorname{sgn}\left(\dot{\gamma}\right).$$

Three-dimensional generalisation

The above constitutive behaviour can be generalised to the three-dimensional case as follows:

$$\boldsymbol{\sigma} = -p\mathbf{I} + \left(\frac{\tau_c}{\sqrt{I_{II}}} + \frac{2^n \mu_n}{\sqrt{-I_{II}}^{1-n}}\right)\mathbf{e}. \tag{49}$$

This is known as a Herschel-Bulkley fluid.

Note that:

- for $\tau_c = 0$ (49) reduces to (47);
- for $n = 1$ (49) reduces to (48);
- for $\tau_c = 0$ and $n = 1$ (49) reduces to (46).

Time-independent non-Newtonian fluids VII

Herschel-Bulkley fluid

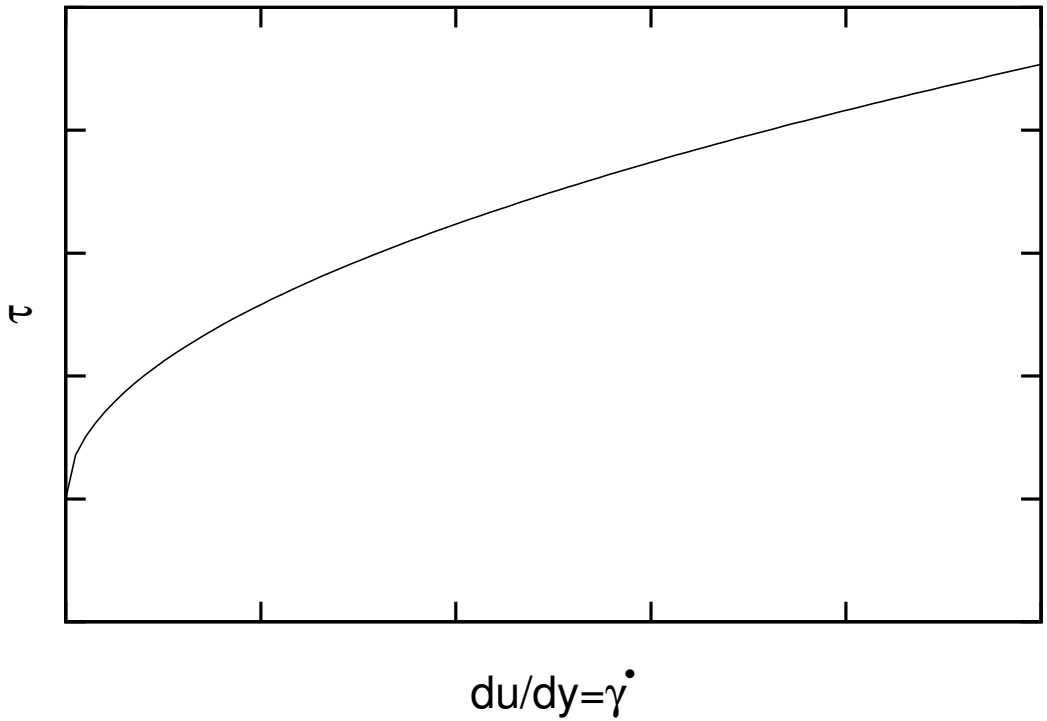

Qualitative dependence of the shear stress τ on the rate of shear strain $\dot{\gamma}$ for a Herschel-Bulkley fluid.

Viscoelastic materials I

In many cases materials display both an **elastic** and **viscous behaviour**.

- In the theory of **linear elasticity** the stress τ in a sheared body is taken proportional to the amount of shear γ;
- in a **Newtonian fluid** shearing stress is proportional to the rate of shear $\dot{\gamma}$.

Stress relaxation

We consider the behaviour of a material in a simple shearing motion, assuming inertia can be neglected.
Suppose the sample is homogeneously deformed, with the amount of shear $\gamma(t)$ variable in time. Let $\tau(t)$ be the corresponding shearing stress.
We consider the **single-step shear history** $\gamma(t) = \gamma_0 H(t)$, with $H(t)$ being the **Heaviside unit step function** ($H(t) = 0$ for $t < 0$, $H = 1$ for $t \geq 0$).

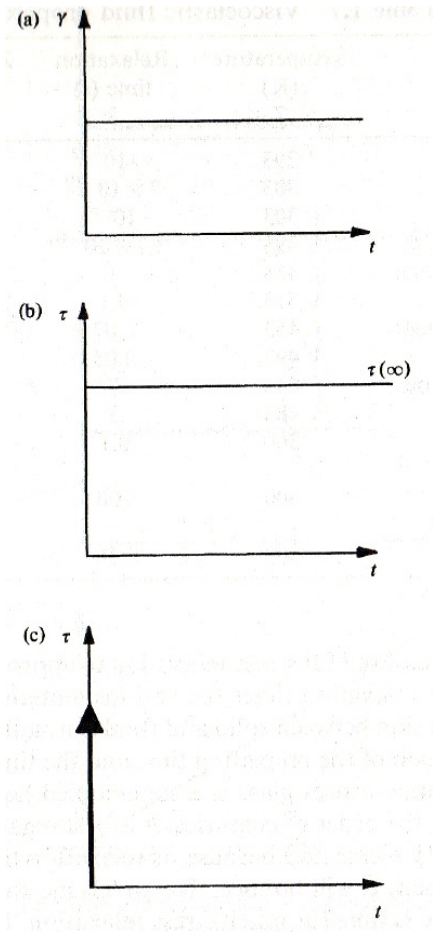

- **Elastic solid:** $\tau(t) = \tau_0 H(t)$, with $\tau_0 = \text{const}$.
- **Newtonian fluid:** since $\tau = \mu\dot{\gamma}$, it would be instantaneously infinite at $t = 0$ and zero for $t > 0$. Then, since

$$\gamma(t) = \frac{1}{\mu}\int_{-\infty}^{t} \tau dt = \gamma_0, \quad (t \geq 0),$$
$$\gamma = 0, \quad (t < 0),$$

τ is a **delta-function with strength** $\mu\gamma_0$.

Viscoelastic materials II

Observations on real materials show that the above idealised models are always inaccurate. The stress τ decreases from its initial value to a limiting value τ_∞. The decrease is rapid first and then slows down. This process is called **relaxation**.

- If the limiting value is not zero we say that the material is a **solid;**
- If the limiting value is zero we say that the material is a **fluid.**

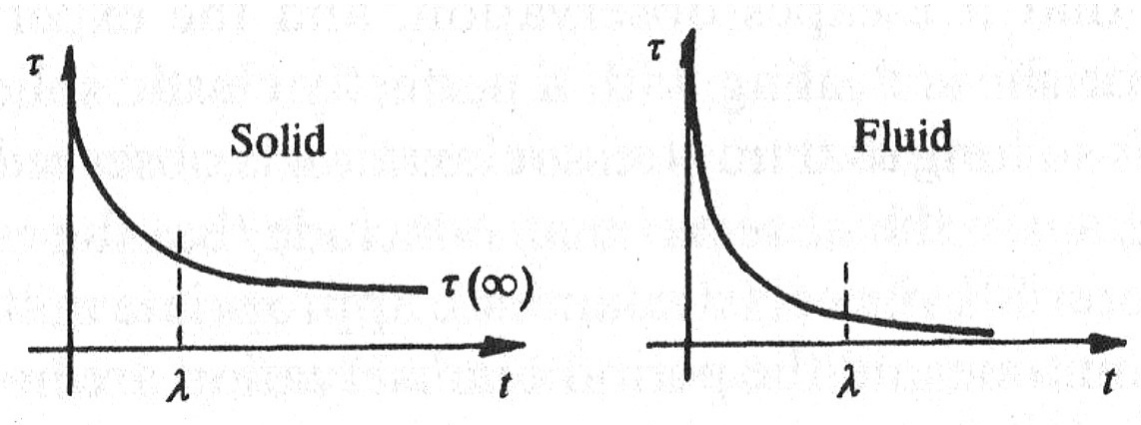

We can define a **relaxation time** λ. This time has to be compared with the **period of observation** T_{obs}.

- If $\lambda/T_{\text{obs}} \ll 1$ one can conclude that the material is a perfectly elastic solid or a viscous fluid, depending on the value of τ_∞;
- if $\lambda/T_{\text{obs}} \gg 1$ one can conclude that the material is a solid;
- if $\lambda/T_{\text{obs}} \approx \mathcal{O}(1)$ we call the material **viscoelastic**.

Viscoelastic materials III

Creep

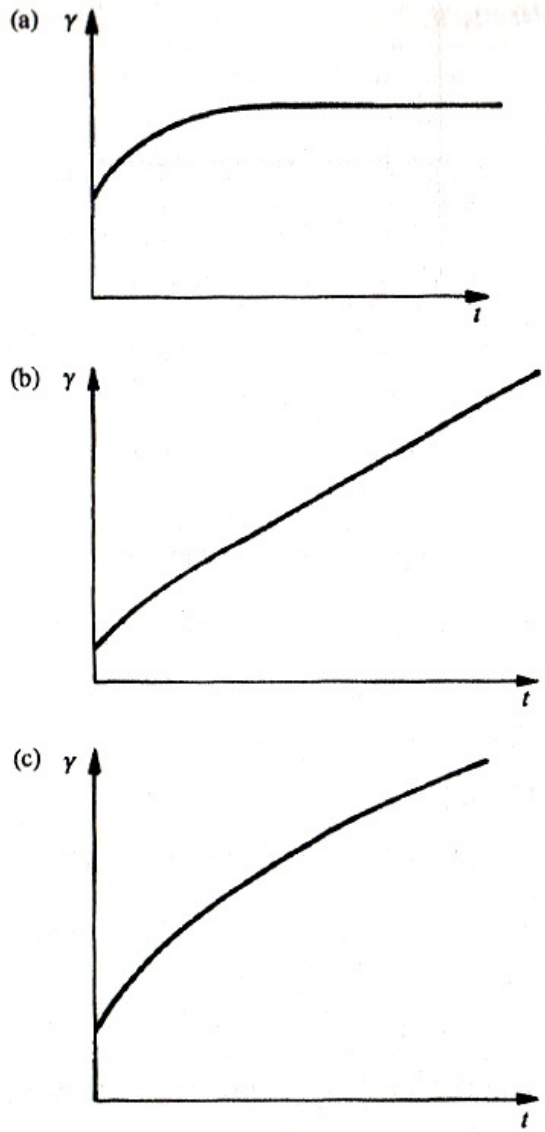

We now consider a **single-step stress history** $\tau(t) = \tau_0 H(t)$.

- **Elastic solid:** $\gamma(t) = \gamma_0 H(t)$, with $\gamma_0 = \text{const}$.
- **Newtonian fluid:** the shear grows at a constant rate, thus $\gamma(t) = \tau_0 t/\mu$, with μ being the dynamic viscosity.

Again, the behaviour of real materials shows departures from these idealised cases. The shear, after an initial possible jump, continues to increase over time.

- If the shear approaches a limiting value γ_∞ the material is said to be a **solid;**
- if the shear grows linearly after a long time the material is said to be a **viscous fluid.**

Viscoelastic materials IV

Response functions

We introduce

- **stress relaxation function** $R(\gamma, t)$: the stress at a time t after the application of a shear step of size γ;
- **creep function** $C(\tau, t)$: the shear at a time t after the application of a stress step of size τ.

The functions R and C are supposed to be zero for $t < 0$.
If the material is isotropic R has to be an odd function of γ and C an odd function of τ.
Assuming that

- R and C are smooth functions,
- γ and τ are small,

we can write

$$R(\gamma, t) = G(t)\gamma + \mathcal{O}(\gamma^3), \qquad C(\tau, t) = J(t)\tau + \mathcal{O}(\tau^3),$$

where we have defined

- $G(t)$ **linear stress relaxation modulus;**
- $J(t)$ **linear creep compliance.**

Viscoelastic materials V

Moreover we define

$$G(0+) = G_g, \qquad J(0+) = J_g, \qquad G(\infty) = G_e \qquad J(\infty) = J_e.$$

Immediately after application of a step in stress/strain ($t = 0+$) we have

$$\tau = G_g \gamma, \qquad \gamma = J_g \tau,$$

therefore we have

$$G_g J_g = 1.$$

Viscoelastic materials VI

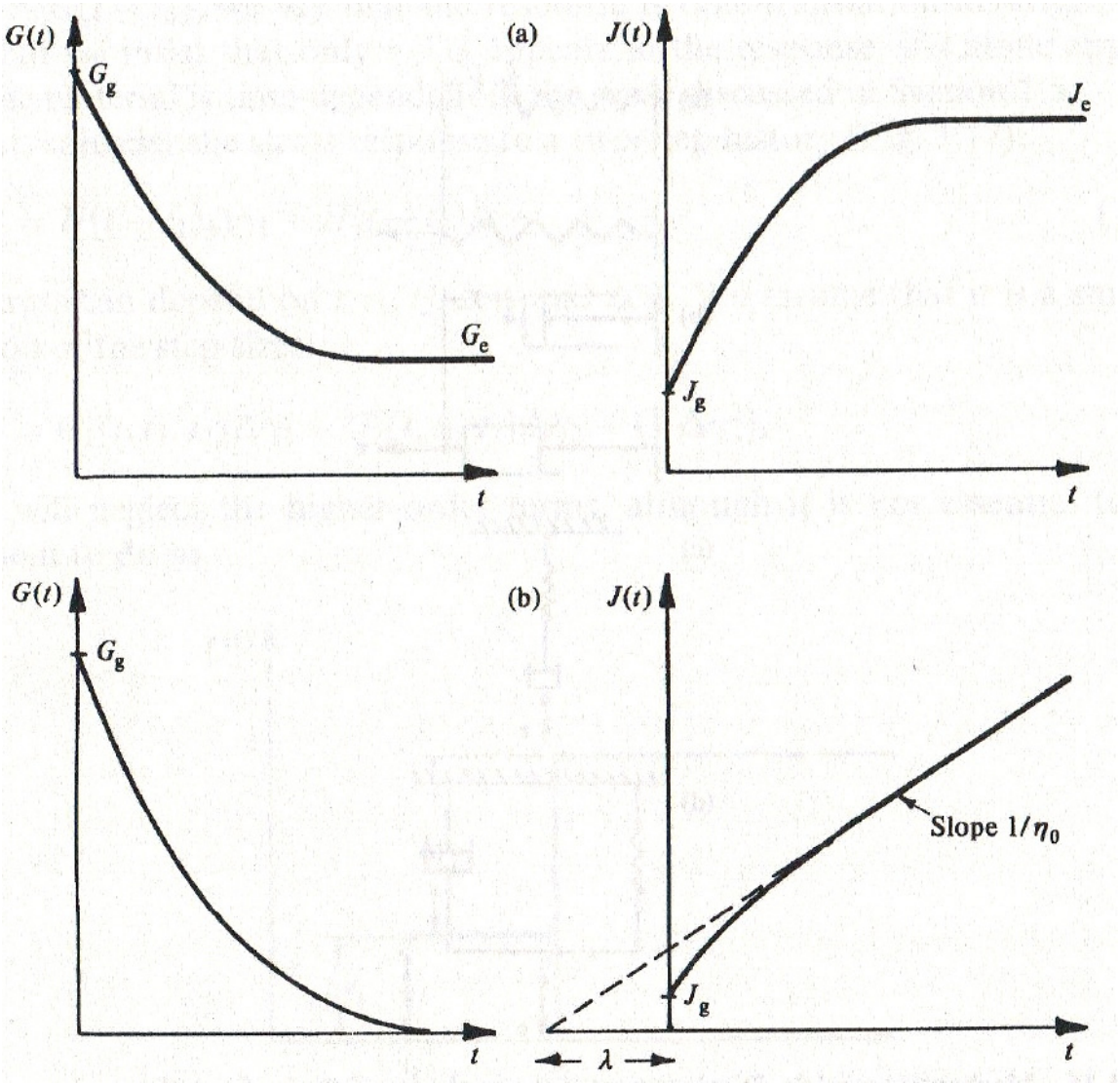

Relaxation modulus G and creep compliance J for (a) solids and (b) fluids.

Viscoelastic materials VII

Spring-dashpot models

It is useful to consider idealised models consisting of combinations of **springs** and **dashpots** to interpret the behaviour of complex viscoelastic materials.

- **Spring.** The spring obeys the simple relationship $\tau = k\gamma$. For the spring we have

$$G(t) = kH(t), \qquad J(t) = \frac{1}{k}H(t).$$

- **Dashpot**. This is a viscous element so that $\dot{\gamma} = \tau/\mu$. For the dashpot the following relationships hold

$$G(t) = \mu\delta(t), \qquad J(t) = t\frac{H(t)}{\mu}.$$

Dashpots and springs can be combined with the following rules

- when two elements are **combined in series their compliances are additive;**
- when two elements are **combined in parallel their moduli are additive.**

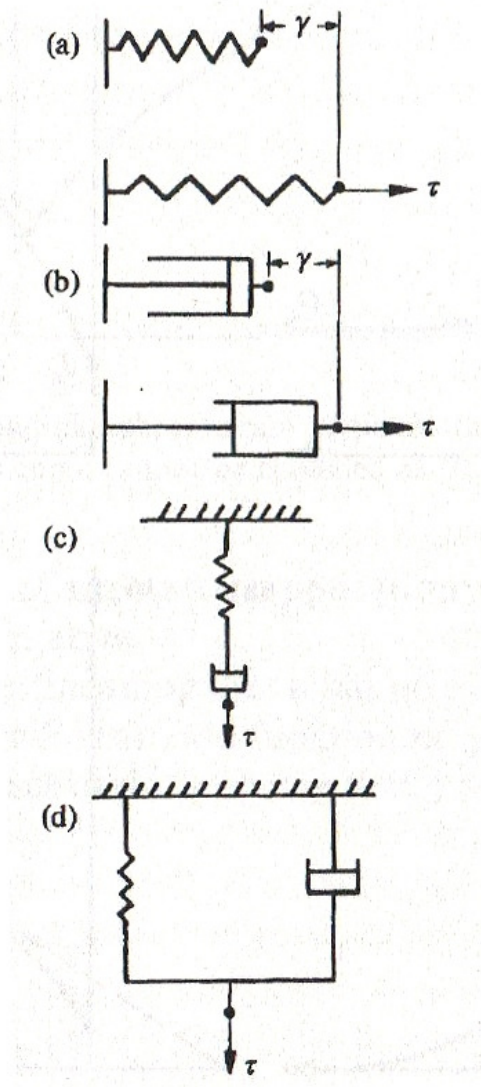

Viscoelastic materials VIII

Examples

Maxwell element

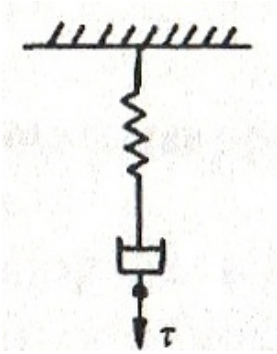

A Maxwell element consists of a spring and a dashpot in series. The creep compliance is therefore

$$J(t) = \left(\frac{1}{k} + \frac{t}{\mu} \right) H(t).$$

Kelvin-Meyer element

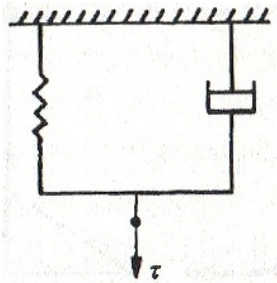

A Kelvin-Meyer element consists of a spring and a dashpot in parallel. The relaxation modulus is therefore

$$G(t) = kH(t) + \mu\delta(t).$$

Viscoelastic materials IX

Superposition of multiple steps

Knowledge of the single-step response functions $G(t)$ and $J(t)$ allows one to predict the **response to any input** within the linear range, i.e. when stresses proportional to γ^3 and strains proportional to τ^3 can be neglected.

We first note that the response is **invariant to time translations**, so that

$$\gamma(t) = \gamma_0 H(t - t_0) \quad \Rightarrow \quad \tau(t) = \gamma_0 G(t - t_0).$$

We now consider a 2-step shear history

$$\gamma(t) = H(t - t_1)\Delta\gamma_1 + H(t - t_2)\Delta\gamma_2.$$

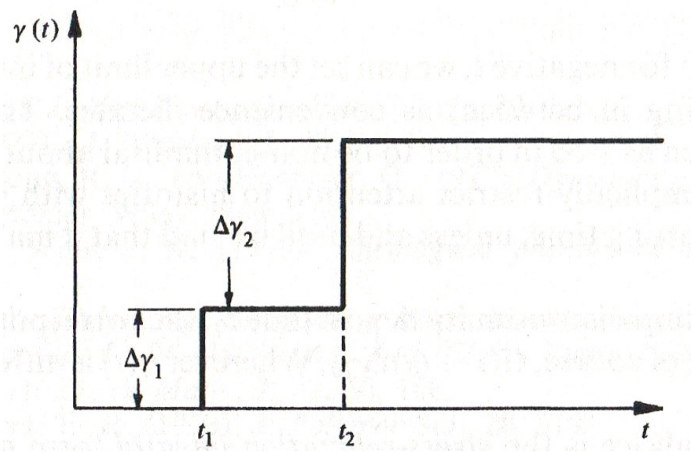

In general the corresponding stress can depend on t, t_1, t_2, $\Delta\gamma_1$ and $\Delta\gamma_2$. We assume that it is a smooth function of the step sizes and expand it as follows

$$\tau(t) = G_1(t, t_1, t_2)\Delta\gamma_1 + G_2(t, t_1, t_2)\Delta\gamma_2 + \mathcal{O}(\Delta\gamma^3).$$

Since the above expression also has to hold for $\Delta\gamma_1 = 0$ and $\Delta\gamma_2 = 0$ it follows that $G_i = G(t - t_i)$, with $i = 1, 2$. Generalising ot N steps at the times t_n we obtain

$$\gamma(t) = \sum_{n=1}^{N} H(t - t_n)\Delta\gamma_n \quad \Rightarrow \quad \tau(t) = \sum_{n=1}^{N} G(t - t_n)\Delta\gamma_n.$$

Viscoelastic materials X

Passing to the limit in the above sums we obtain that the shear history can be written as

$$\gamma(t) = \int_0^t H(t-t')d\gamma(t'),$$

and the stress in time as

$$\tau(t) = \int_{-\infty}^t G(t-t')d\gamma(t'). \tag{50}$$

This is called the **stress relaxation integral**.

Important notes

- Since $G(t) = 0$ for $t < 0$ the upper limit in the integral can be arbitrarily chosen in the range $[t, \infty)$.
- Assuming $\gamma(t)$ is differentiable, we have $d\gamma(t) = \dot{\gamma}(t)dt$.

Following analogous steps we could consider the following stress history

$$\tau(t) = \int_0^t H(t-t')d\tau(t'),$$

and obtain the **creep integral** as

$$\gamma(t) = \int_{-\infty}^t J(t-t')d\tau(t').$$

Viscoelastic materials XI

Linear viscoelastic behaviour

A suitable three-dimensional extension of equation (50) is given by

$$\sigma_{ij} + p\delta_{ij} = d_{ij} = \int_{-\infty}^{t} 2G(t - t')e_{ij}(t')dt', \tag{51}$$

where d_{ij} is the deviatoric part of the stress tensor and e_{ij} is the rate of strain tensor.

Note: for a Newtonian fluid we have $G(t - t') = \mu\delta(t - t')$ and therefore

$$\sigma_{ij} + p\delta_{ij} = d_{ij} = \int_{-\infty}^{t} 2\mu\delta(t - t')e_{ij}(t')dt' = 2\mu e_{ij}(t),$$

which agrees with equation (46).

Viscoelastic materials XII

Sinusoidal viscoelastic response

A commonly used procedure to test rheological properties of viscoelastic fluids consists of applying to the material a time-sinusoidal strain of small amplitude, so that

$$\gamma = \hat{\gamma} e^{i\omega t} + c.c., \qquad \dot{\gamma} = i\omega\hat{\gamma} e^{i\omega t} + c.c. \tag{52}$$

with $\hat{\gamma} \ll \pi$. Under the assumption of linear behaviour of the system, following from the assumption $\hat{\gamma} \ll \pi$, the shear modulus can be written as

$$\tau = \hat{\tau} e^{i\omega t} + c.c.$$

Substituting (52) into (50) (and omitting the complex conjugates) we obtain

$$\hat{\tau} e^{i\omega t} = i\omega\hat{\gamma} \int_{-\infty}^{t} G(t - t') e^{i\omega t'} dt'.$$

We define the **complex modulus** G^* as $\hat{\tau}/\hat{\gamma}$. From the above equation, setting $s = t - t'$, we obtain

$$G^* = G' + iG'' = i\omega \int_0^{\infty} G(s) e^{-i\omega s} ds. \tag{53}$$

Separating in (53) the real and imaginary parts we find

$$G^* = G' + iG'' = \int_0^{\infty} \omega G(s) \sin(\omega s) ds + i \int_0^{\infty} \omega G(s) \cos(\omega s) ds.$$

with

Viscoelastic materials XIII

- $G'(\omega)$ is the **storage modulus;**
- $G''(\omega)$ is the **loss modulus.**

It is also possible to define the **complex viscosity** as

$$\mu^* = \frac{\hat{\tau}}{\hat{\dot{\gamma}}} = \mu' - i\mu'' = \frac{G^*}{i\omega} = \frac{G''}{\omega} - i\frac{G'}{\omega}. \tag{54}$$

Note that $\mu' = G''/\omega$ is the equivalent of the dynamic viscosity for a Newtonian fluid.

If we record with and an experiment $\gamma(t)$ and $\tau(t)$ we have a phase shift δ between the two signals. If $G'' = 0$ the phase shift is zero ($\delta = 0$). In particular we have

$$\tan\delta = \frac{G''}{G'}.$$

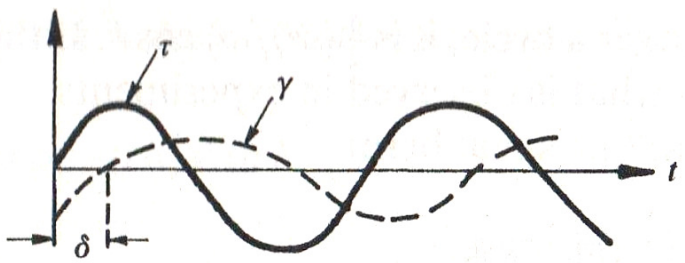

Viscoelastic materials XIV

Solution of sinusoidally oscillating linear flows of a viscoelastic fluid

The equation of motion is given by the Cauchy equation (7) and the continuity equation (6)

$$\rho\left(\frac{\partial \mathbf{u}}{\partial t}+(\mathbf{u}\cdot\nabla\mathbf{u})\right)=\nabla\cdot\boldsymbol{\sigma}, \tag{55}$$

$$\nabla\cdot\mathbf{u}=0, \tag{56}$$

Substituting (51) into (55) and **neglecting quadratic terms in the velocity**, we obtain

$$\rho\frac{\partial \mathbf{u}}{\partial t}=-\nabla p+\int_{-\infty}^{t} G\left(t-t'\right)\nabla^2\mathbf{u}\,dt'. \tag{57}$$

Assuming a sinusoidally oscillating flow we can set $\mathbf{u}(\mathbf{x},t)=\hat{\mathbf{u}}(\mathbf{x})e^{i\omega t}+c.c.$ and $p(\mathbf{x},t)=\hat{p}(\mathbf{x})e^{i\omega t}+c.c.$, and substituting into (57), also making use of (53) and (54), we obtain

$$\rho i\omega\hat{\mathbf{u}}=-\nabla\hat{p}+\mu^*\nabla^2\hat{\mathbf{u}}, \tag{58}$$

$$\nabla\cdot\hat{\mathbf{u}}=0. \tag{59}$$

In other words the problem to solve is the same as that for a Newtonian fluid under the same conditions, provided the fluid viscosity μ is replaced with the complex viscosity μ^*.

Flow in porous media I

A porous medium is a solid that has **many interconnected holes (pores)** within it. Flows in porous media are described in great detail in the book by Bear (1988).
We do not consider the complicated details of the fluid flow in each individual pore, but rather we are interested in phenomena that occur on **lengthscales that are much larger than typical inter-pore distances.**

Applications:

- flow in soil and fractured rocks;
- **flow in capillary beds;**
- flow in soft tissues (e.g. the brain tissue)
- ...

Assumptions and definitions

- We assume that the porous medium consists of a **rigid solid with many small pores** saturated with a fluid.
- We assume that the porous medium is **homogeneous** and **isotropic**.
- We define the **porosity** ϕ of the porous medium by considering a sample of the solid whose lengthscale is large compared to the individual pore size but small compared to the lengthscale of interest in the experiment. The porosity is defined to be **the total volume of the pores in the sample divided by the total volume of the sample**.

Flow in porous media II

The Darcy equation

On scales that are large compared to that of an individual pore, the flow of a Newtonian fluid in the porous medium is governed by the Darcy equation:

$$\mathbf{q} = -\frac{k}{\mu}\nabla p. \tag{60}$$

- $\mathbf{q}$ is the **volume flux per unit area in the medium**. Sometimes $\mathbf{q}$ is referred to as **apparent or Darcy velocity.** For a flat cross-section of the solid of area A with unit normal $\mathbf{n}$ (A contains many pores), the flux through A is $\mathbf{q} \cdot \mathbf{n}A$.
  $\mathbf{q}$ has the dimensions of a velocity
  $$[q] = LT^{-1}.$$
  Note: $\mathbf{q}$ is not an actual physical velocity; the average velocity within the pores is $\overline{\mathbf{u}} = \mathbf{q}/\phi$.
- k is the **permeability of the medium** ($[k] = L^2$). It quantifies how much **"resistance"** the solid provides to fluids flowing through it (a larger resistance corresponds to a lower value of k). k depends on
  - the porosity ϕ;
  - the geometry of the pores, in particular the **tortuosity of the pores** and the **degree to which they are interconnected**.

  It does not depend on the rheology of the fluid filling the pores.
- μ is the dynamic viscosity of the fluid.
- p is the fluid pressure.

Flow in porous media III

Continuity equation

To find the fluid velocity and pressure we need a further equation, which is provided by **mass conservation**. For an incompressible fluid flowing though an incompressible solid the continuity equation becomes

$$\nabla \cdot \mathbf{q} = 0.$$

Taking the divergence of Darcy's equation (60), we obtain the **Laplace equation for the pressure**

$$\nabla^2 p = 0. \tag{61}$$

This means that the velocity field of an incompressible fluid in a porous medium is a **harmonic function.**

Flow in porous media IV

Informal justification of the Darcy equation

We assume the pores of the porous medium are tubes of radius a oriented in random directions (since the medium is isotropic).
A straight tube of radius a containing Poiseuille flow driven by a pressure gradient ∇p has flux

$$Q = \frac{\pi a^4}{8\mu} |\nabla p| . \tag{62}$$

Thus in a pore of the medium that is oriented in the direction of the unit vector $\mathbf{m}$, we estimate the flux as

$$Q = \frac{\pi a^4}{8\mu\chi} \nabla p \cdot \mathbf{m}. \tag{63}$$

The factor $\chi \geq 1$ has been inserted to represent the **extra resistance arising from the tortuosity** of the pore.

Observations

- Pores aligned in the same direction as ∇p have the largest fluxes, whilst those perpendicular to ∇p have zero flux.
- Since the directions of the pores are distributed **isotropically**, the components of the fluxes that are perpendicular to ∇p tend to cancel, and **the average flux through many nearby pores is parallel to ∇p.**

Flow in porous media V

- The formula (63) suggests that the magnitude of the flux per unit area $\mathbf{q}$ is proportional to the magnitude of ∇p.
- The formula (63) shows that $\mathbf{q}$ is inversely proportional to the viscosity μ.

The above points **justify the form of the Darcy equation.**

Darcy equation can also be derived in a more formal way, adopting homogenisation techniques (Mei and Vernescu, 2010).

The permeability k

The value of the permeability for a given porous medium must be determined empirically.
A formula that works quite well in the case of flow between pseudo-spherical grains (such as grains of sand) is the Carman–Kozeny formula, which is

$$k \approx \frac{\phi^3 d^2}{180(1-\phi)^2},$$

where d is the typical diameter of a grain.

The cardiovascular system: blood rheology

Main functions of blood

In large animals, transport of material from different parts of the body involves fluid flowing along and across the walls of systems of tubes. The most studied tube system in biomechanics is the mammalian **cardiovascular system**. The fluid flowing in such a system is **blood**.

Blood

- carries oxygen and nutrients to metabolically active tissues;
- returns carbon dioxide to the lungs;
- delivers metabolic end-products to the kidneys;
- ...

Blood does more than simply delivering substances to tissues. In particular:

- provides a buffering reservoir to control the pH of bodily fluids;
- serves as an important locus for the immune system;
- transports heat, contributing to maintain a constant temperature throughout the body.

In the present section we will be concerned with **blood rheology**, i.e. the way in which tensions are generated in the blood as a response to a given kinematic state.

Blood composition

In order to understand the rheological behaviour of blood we need to know its composition.

There are approximately 5 l of blood in an average human being. Blood volume is regulated by the kidneys.

Blood consists of a suspension of particles (**formed elements**) floating in a fluid medium (**plasma**).

As shown in the figure below the formed elements constitute approximately 46% of the total blood volume.

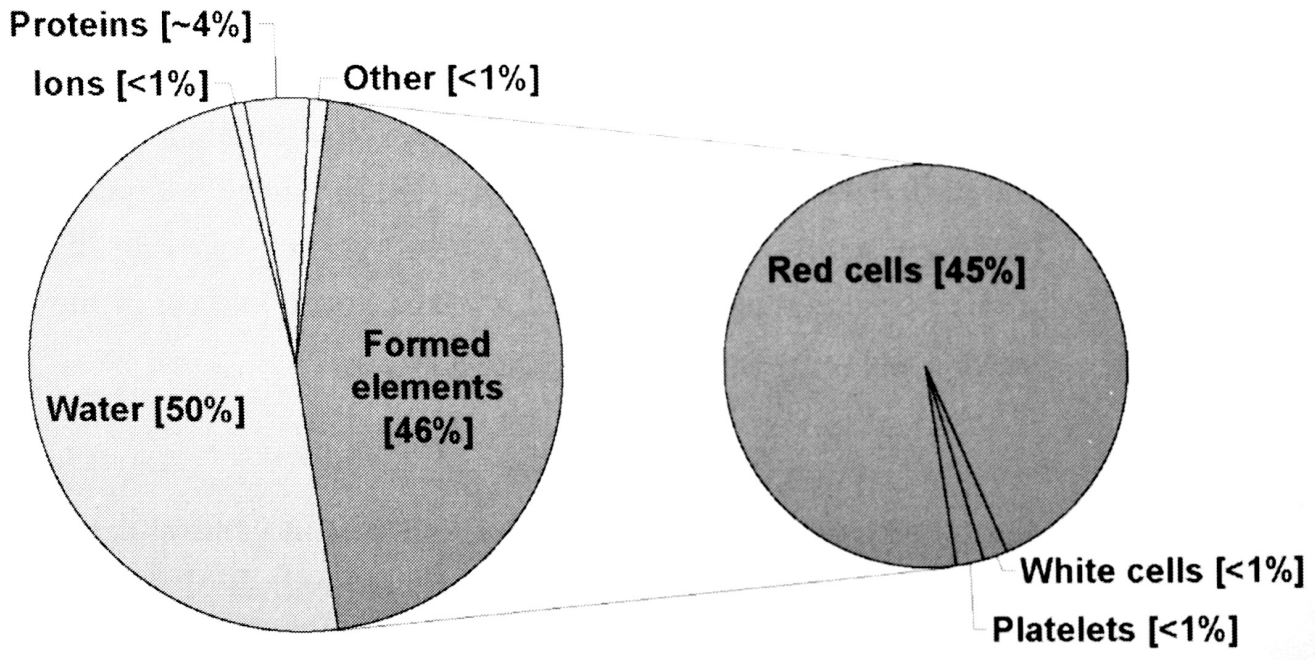

Blood composition (from Ethier and Simmons, 2007).

Plasma I

Composition

Material	Concentration (g per 100 ml)	Molecular weight $\times 10^{-3}$	Molecular dimensions (nm)
Water	90–92		
Proteins			
Serum albumin	3·3–4·0	69	15 × 4
α_1 globulins (including lipoproteins)	0·31–0·32	44–200	
α_2 globulins (including glycoproteins)	0·48–0·52	150–300	
β globulins (including lipoproteins)	0·78–0·81	90–1300	20–50
γ globulins	0·66–0·74	160–320	23 × 4
Fibrinogen	0·34–0·43	400	50–60 × 3–8
Inorganic constituents			
Cations			
Sodium	0·31–0·34		
Potassium	0·016–0·021		
Calcium	0·009–0·011		
Magnesium	0·002–0·003		
Anions			
Chloride	0·36–0·39		
Bicarbonate	0·20–0·24		
Phosphate	0·003–0·004		

Composition of plasma (from Caro et al., 1978).

Plasma II

Viscosity

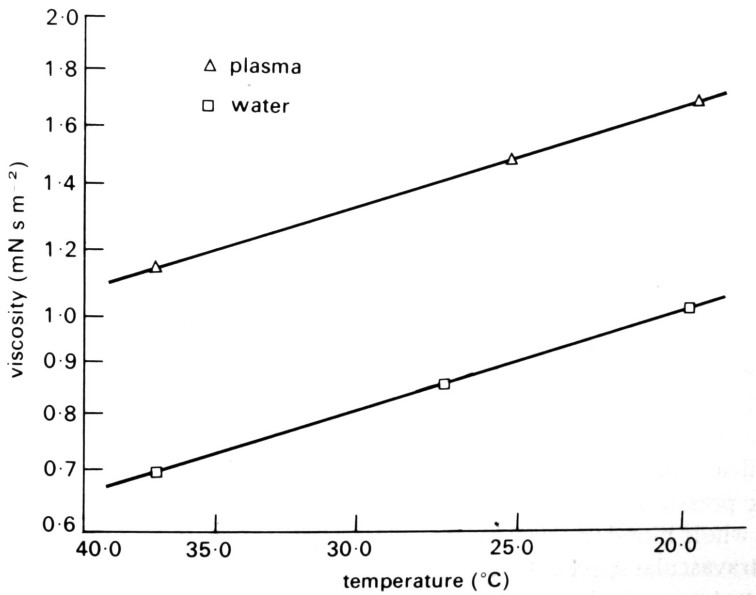

Dependence on temperature of plasma and water (from Cokelet, 1972).

From the mechanical point of view the **plasma behaves as a Newtonian fluid**.

Its dynamic viscosity is $1.2 \cdot 10^{-3}$ Pa s at $37°$. Thus the viscosity of plasma slightly exceeds that of water.

The osmotic pressure I

Osmotic pressure is a thermodynamically generated force on a solvent that requires

- a **solvent**;
- one (or more) **solutes**;
- a **semipermeable membrane**, i.e. a barrier that allows solvent molecules to pass freely and prevents the passage of solute molecules.

Let us consider a container with two chambers containing two solutions of one (or more) solute(s). The chambers are separated by a membrane that is permeable to the solvent but not to the solute.
Let us consider the flux of solvent Q_{12} form chamber 1 to chamber 2. This flux can be written as

$$Q_{12} = C[(p_1 - \pi_1) - (p_2 - \pi_2)],$$

where we define π as the **osmotic pressure** and C is a constant.
According to **van't Hoff's law** we can write

$$\pi = RT \sum_{j=1}^{N} c_j,$$

where

- R: universal gas constant (8.314 J/mol K);
- T: absolute temperature;

The osmotic pressure II

- c_j: molar concentration of the species j in solution.

This law holds for sufficiently diluted solutions.
Note that the above equations imply that if $\pi_1 \neq \pi_2$ (i.e. the solutions in the two chambers are at different concentrations) the pressures on the two sides of the membrane are not the same at equilibrium ($p_1 \neq p_2$).

The plasma osmotic pressure

The osmotic pressure in the plasma is mainly due to the presence of **albumin**. The plasma osmotic pressure has important effects on the mechanics of circulation.

- Variations of the osmotic pressure π in the plasma might induce a osmotic pressure variation across red blood cell membranes. This leads to a flux of water across the cell membrane that produces a modification of the shape of the cell as discussed later.
- Variations of π in the plasma might induce variations of the volumetric concentration of red blood cells. This, in turn, significantly affects the rheological properties of blood.

Formed elements in blood I

The formed elements mainly consist of the following bodies.

- **Red cells (erythrocytes)**

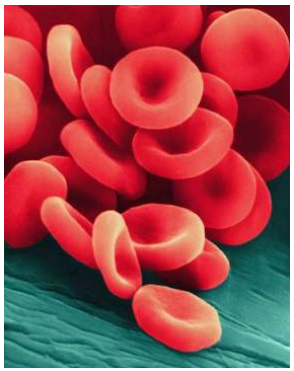

Red blood cells are the means of delivering oxygen to the body tissues via the blood flow. They take up oxygen in the lungs or gills and release it in the microcirculation. Red blood cells have no nucleus.

- **White cells (leukocytes)**

They play an important role in the immune response as they defend the body against both infectious disease and foreign materials. There are various different types of leukocytes.

- **Platelets**

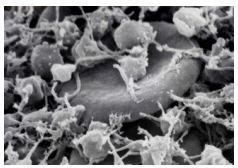

Platelets are small cytoplasmic bodies derived from cells in the bone marrow, and that circulate in the blood and are involved in blood clotting. Like red blood cells, platelets have no nucleus. If the number of platelets is too low, excessive bleeding can occur, however if the number of platelets is too high, blood clots can form.

Formed elements in blood II

The following table shows the percentage of blood cells present in normal blood.

Cell	Number per mm^3	Unstressed shape and dimensions (μm)	Volume concentration (%) in blood
Erythrocyte	$4–6\times10^6$	Biconcave disc $8\times1–3$	45
Leucocytes			
Total	$4–11\times10^3$		
Granulocytes			
Neutrophils	$1{\cdot}5–7{\cdot}5\times10^3$	Roughly spherical 7–22	1
Eosinophil	$0–4\times10^2$		
Basophil	$0–2\times10^2$		
Lymphocytes	$1–4{\cdot}5\times10^3$		
Monocytes	$0–8\times10^2$		
Platelets	$250–500\times10^3$	Rounded or oval 2–4	

Formed elements in blood (from Caro et al., 1978).

It appears that there are few white blood cells and platelets compared to red blood cells. This implies that **the mechanical behaviour of the formed elements is dominated by red cells**.

The volume fraction of red blood cells is extremely important for blood rheology and also for physiological characteristics of blood. It is known as **haematocrit** H and is defined as

$$H = \frac{\text{volume of red blood cells}}{\text{total blood volume}}.$$

Red blood cells I

Individual red blood cells are shaped like **biconcave disks** as shown in the picture below.

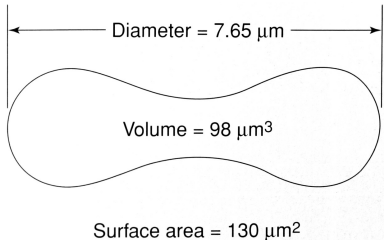

Sketch of the shape of a red blood cell.

The table gives some geometrical properties of red cells.

Diameter $[\mu]$	Thickness $[\mu]$	Volume $[\mu^3]$	$\frac{\text{Diameter}}{\text{Thickness}}$
7.8	1.84	88	4.2

The cytoplasm of red cells has a viscosity which is higher than that of plasma.

The cytoplasm contains a large amount of a protein called **haemoglobin** that is very efficient at binding oxygen. For this reason the oxygen-carrying capacity of whole blood is ≈ 65 times larger than that of plasma alone:

- **whole blood:** ≈ 21 ml O_2 per 100 ml of blood;
- **plasma:** ≈ 0.3 ml O_2 per 100 ml of plasma.

Red blood cells are **highly deformable**. This is important since, in the microcirculation, they have to pass through very narrow openings.

Red blood cells II

If the rate of shear is very small red blood cells tend to aggregate forming stacks known as **roleaux**. The presence of roleaux in the blood affects significantly its viscosity.

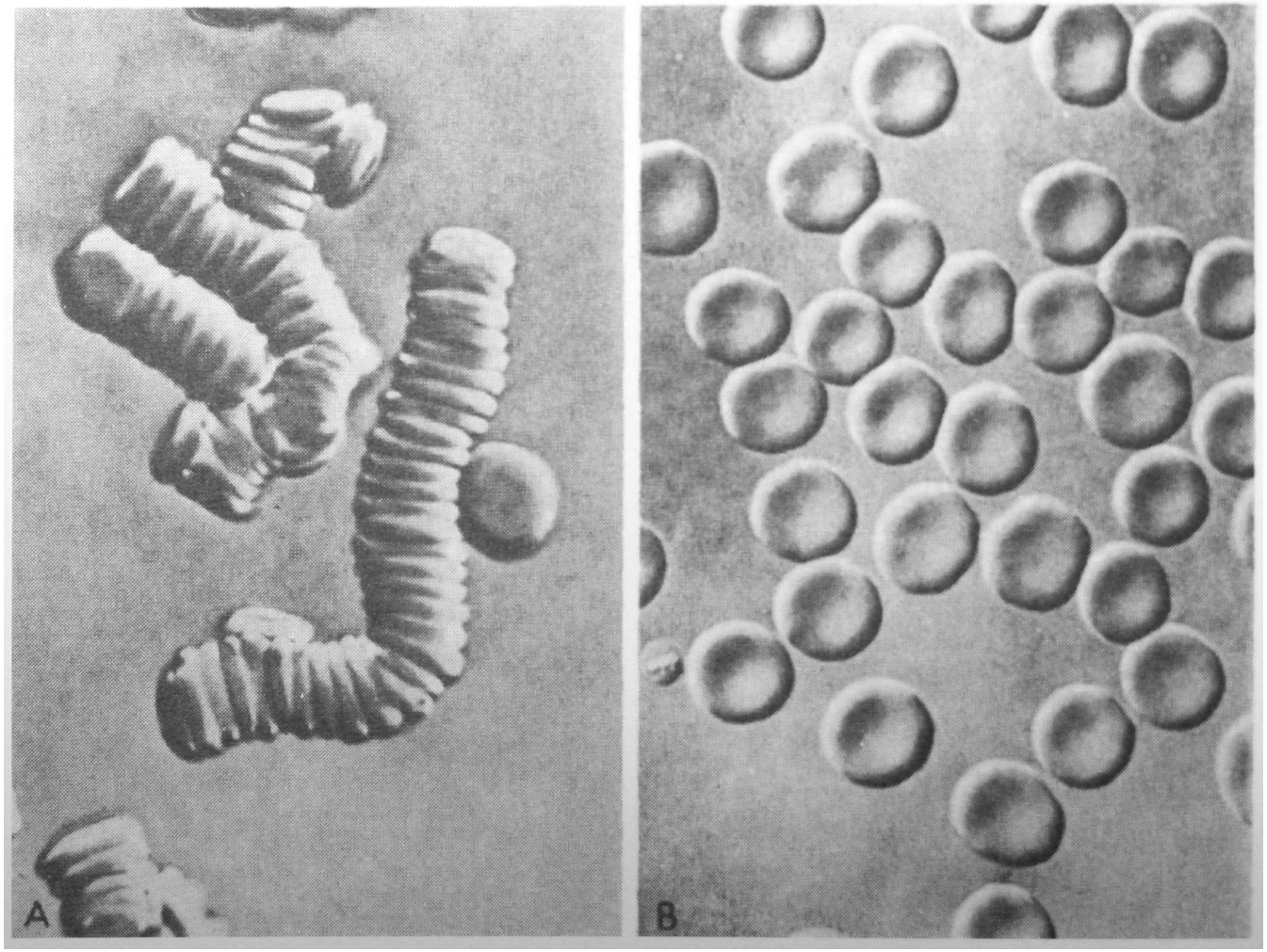

(a) Roleaux, (b) normal red cells (from Ethier and Simmons (2007).

Red blood cells III

The effect of the osmotic pressure

Red blood cells are normally in osmotic equilibrium with the plasma.

- If they are immersed in solutions with smaller osmotic pressure erythrocytes swell, assuming an approximately spherical shape (**hypotonic red blood cells**).
  Red blood cells can blow (**haemolysis**), releasing **haemoglobin** into the plasma.
- The opposite process can also occur. In that case red blood cells loose water (**hypertonic red blood cells**).

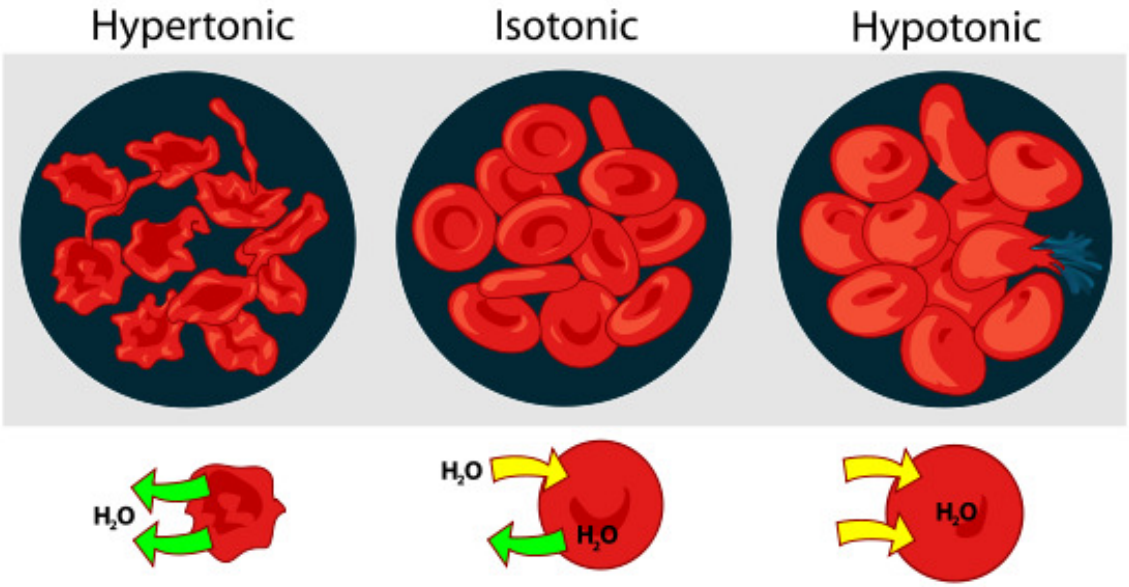

Effect of the osmotic pressure on red blood cells.

Mechanics of suspensions I

Settling velocity of a particle

Let us first consider the sedimentation of a single spherical particle in a Newtonian incompressible fluid otherwise at rest.
The **settling velocity** u_s of a single particle in a suspension can be determined by equating the weight of the particle W to the drag force D it experiences while settling. In general no analytical expression is available for D.
An analytical solution is available for the case of low Reynolds number $Re = u_s d/\nu$, with d particle diameter and ν kinematic viscosity of the fluid. In this case we have

Stokes formula: $D = 3\pi d \mu u_s.$

Stokes formula is known to be valid for $Re \lessapprox 0.5$.

Thus in this case we have

$$(\rho_s - \rho) g \pi \frac{d^3}{6} = 3\pi d \mu u_s,$$

from which we get

$$u_s = \frac{g d^2}{18\nu} \left(\frac{\rho_s}{\rho} - 1 \right). \tag{64}$$

Mechanics of suspensions II

Example

Let us consider the settling of a red blood cell in the plasma. We have

$$\rho_s \approx 1.05\rho, \quad d \approx 10^{-5}\ \text{m}, \quad \nu \approx 1.2 \times 10^{-6}\ \text{m}^2\text{s}^{-1},$$

and we obtain $u_s \approx 2.3 \times 10^{-6}$ m/s.

Mechanics of suspensions III

Transient motion

If the particle starts from rest, there will be a transient motion ($u(t)$) before reaching the settling velocity (u_s). If we assume that, even during such a transient motion, Stokes drag resistance is dominant with respect to other forces, we may write the following equation of motion for the particle:

$$\rho_s \pi \frac{d^3}{6} \dot{u} = (\rho_s - \rho) g \pi \frac{d^3}{6} - 3\pi d \mu u.$$

This equation can be solved to get

$$u(t) = u_s \left(1 - e^{-t/T}\right),$$

with T characteristic time scale for the transient flow, defined as

$$T = \frac{\rho_s d^2}{18 \rho \nu}.$$

Example

Let us consider the settling of a red blood cell in the plasma and evaluate T. Using $\rho_s \approx 1.05\rho$, $d \approx 10^{-5}$ m, $\nu \approx 1.2 \times 10^{-6}$ m^{2}s^{-1}, we obtain $T \approx 5 \times 10^{-6}$ s, which is a very small time compared to the time scale we are typically interested in studying blood flow.

Mechanics of suspensions IV

Settling velocity of a suspension of particles

When a suspension of particles settles in a fluid at rest the velocity of sedimentation of each particle will not be that predicted by equation (64). This is because particles interact to each other.
A complete theory for the settling of a suspension of particles is not available yet.
The effect of the interactions is such to decrease the settling velocity.

Important note

In the case of a suspension of settling red blood cells the problem is even more complicated due to the fact that particles tend to aggregate, forming roleaux. The settling velocity of roleaux is larger than that of single cells.

Mechanics of suspensions V

Viscosity of suspensions

If the particles are sufficiently small compared to the domain of the flow the mixture fluid/particles can still be thought of as a continuum fluid.
The viscosity of the whole fluid is affected by the presence of particles. Analysing the behaviour of a suspension of particles in a Newtonian fluid helps understanding what determines the overall viscosity and if the mixture is still expected to behave in a Newtonian way.

Spherical rigid particles

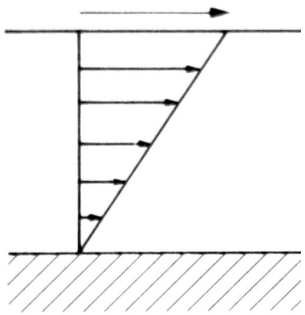

Let us consider the simple shear flow as that is reported in the figure. The flow may be induced in a gap by the motion of the upper solid surface while the lower surface is kept fixed. It can be shown that the velocity distribution is linear.
Suppose that particles are **rigid, spherical and non-settling**.

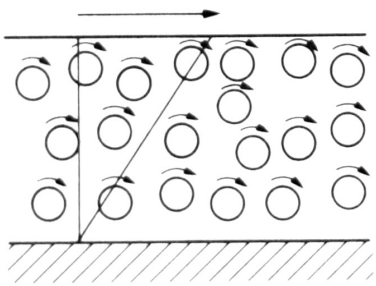

- If the concentration c of particles is small ($c \lessapprox 0.3$) the effective viscosity of the whole mixture μ_{eff} is independent of the shear rate $\dot{\gamma}$.
- However, if $c \gtrapprox 0.1$, μ_{eff} depends on the method of measurement, i.e. on the flow field in the viscometer.
- The mixture is Newtonian in the sense that μ_{eff} is independent of $\dot{\gamma}$ with a particular measurement technique.
- The effective viscosity is always larger than the viscosity of the suspending fluid because the deformations in the fluid are greater for the same motion of boundaries and the average shear-rate increases.

Mechanics of suspensions VI

Deformable particles

Let us now consider a **suspension of deformable non-settling particles**.

- Also in this case the effective viscosity increases with increasing values of the concentration c.
- The growth rate is typically smaller than in the case of rigid particles. This is because particles can reshape to adapt to flow conditions and therefore the additional rate of strain imposed on the suspending fluid is less.

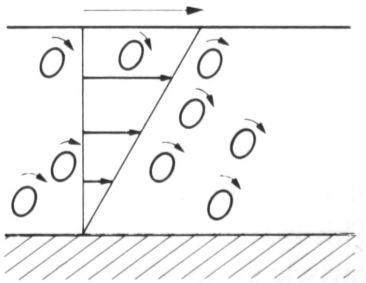

- As the shear rate increases particles tend to align with the flow. This means the the shear stress does not increase linearly with the shear rate.
- The suspension is not Newtonian but **shear thinning.**

Asymmetric particles

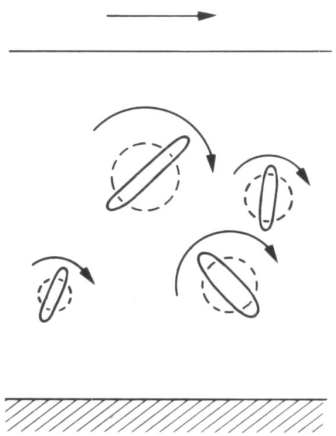

- As spherical particles also asymmetric particles rotate when immersed in a shearing fluid. However, the angular velocity is not constant, being highest when the particle long axis is at right angle with the flow.
- Therefore particles spend more time, on average, aligned with the flow.
- The effect of this lining-up of the particles is to decrease the effective viscosity of the suspension.
- The effective viscosity of a suspension of randomly oriented asymmetric particles exceeds that of a suspension of spheres in the same concentration.

Mechanics of suspensions VII

Theoretical formulae

In 1906 Albert Einstein obtained an analytical expression for the viscosity of a suspension of rigid non-settling particles in a Newtonian fluid. The formula is valid for concentration $c \ll 1$ and reads:

$$\mu_r = \frac{\mu_{eff}}{\mu_0} = 1 + \frac{5}{2}c,$$

where μ_r is the **relative viscosity** and μ_0 the viscosity of the suspending fluid. The formula works well for $c \lessapprox 0.1$.

In 1932 G. I. Taylor extended Einstein's formula to the case of liquid droplets in suspension, which are forced to remain spherical due to surface tension. His formula reads:

$$\mu_r = \frac{\mu_{eff}}{\mu_0} = 1 + c\left(\frac{\mu_0 + 5/2\overline{\mu}}{\mu_0 + \overline{\mu}}\right),$$

where $\overline{\mu}$ is the viscosity of the liquid within the drop.

Mechanics of suspensions VIII

Red blood cells

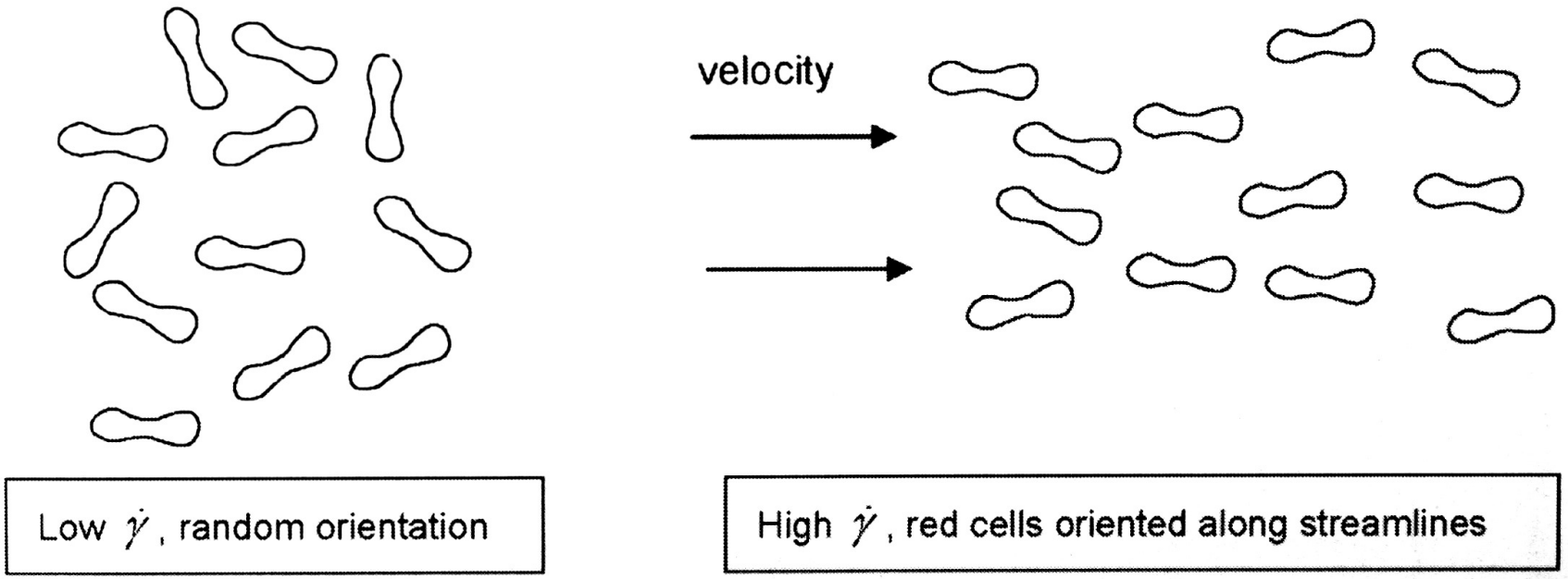

Red blood cells subject to low rate of strain (left) and high rate of strain (right).

Characteristic	Low shear stress	High shear stress
Roleaux behaviour	Roleaux formation enhanced; μ_{eff} is increased	Roleaux break up; μ_{eff} is decreased
Individual red cell orientation	Red cells are randomly oriented; μ_{eff} is increased	Red cells are aligned with streamlines; μ_{eff} is decreased

Mechanics of suspensions IX

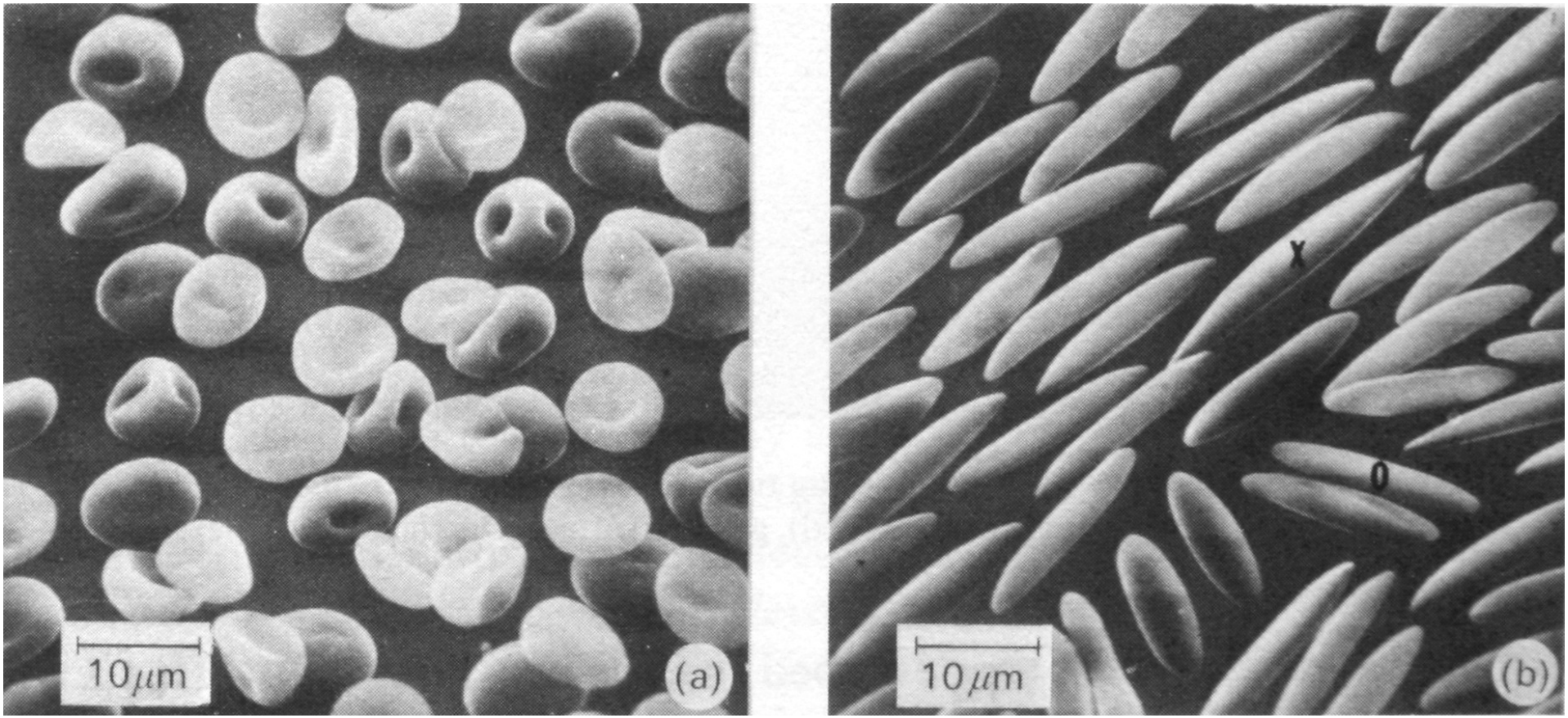

Red blood cells subject to low rate of strain (a) and high rate of strain (from Caro et al. (1978)).

Mechanics of suspensions X

The presence of red cells in the blood affects significantly blood viscosity.

As the rate of strain $\dot{\gamma}$ increases

- roleaux tend to disappear;
- blood cells deform and the to spend more time aligned with the flow.

For the above reasons we expect that the effective viscosity of blood might change with the rate of strain, in particular decreasing. Therefore, **we expect the blood to have a shear thinning behaviour.**

Rheology of the whole blood

Effective viscosity of blood

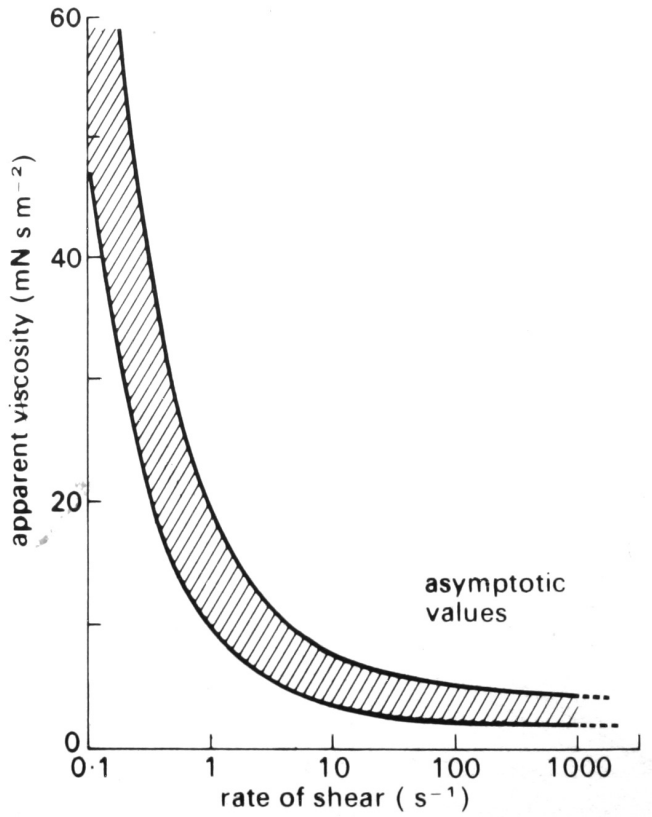

Effective viscosity of normal blood as a function of the rate of shear (from Whitmore, 1968).

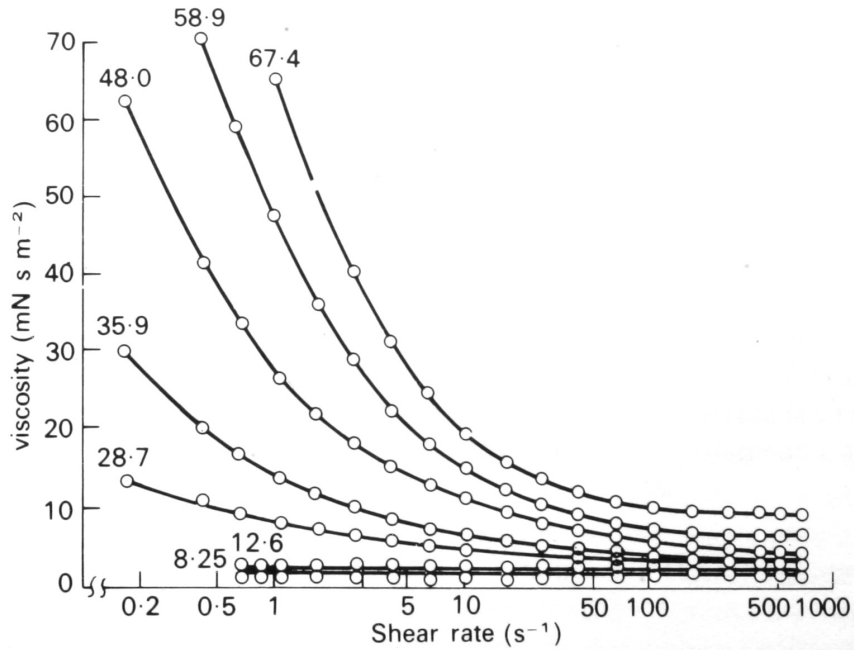

Effective viscosity of blood as a function of the rate of shear for different values of the haematocrite (from Brooks et al., 1970).

Conclusions

- **The whole blood does not have a Newtonian behaviour.**
- It has a **shear thinning behaviour** as the apparent viscosity decreases with the rate of shear. This behaviour is due to the presence of particulate material and can be qualitatively explained by the following observations:
  - red blood cells tend to orientate in the direction of motion as the shear rate increases;
  - roleaux are destroyed at large values of the shear rate.
- **For large values of the shear rate ($\dot{\gamma} \gtrapprox 100\ \mathrm{s}^{-1}$) blood behaves approximately as a Newtonian fluid.**

The cardiovascular system: the heart

General description of the cardiovascular system I

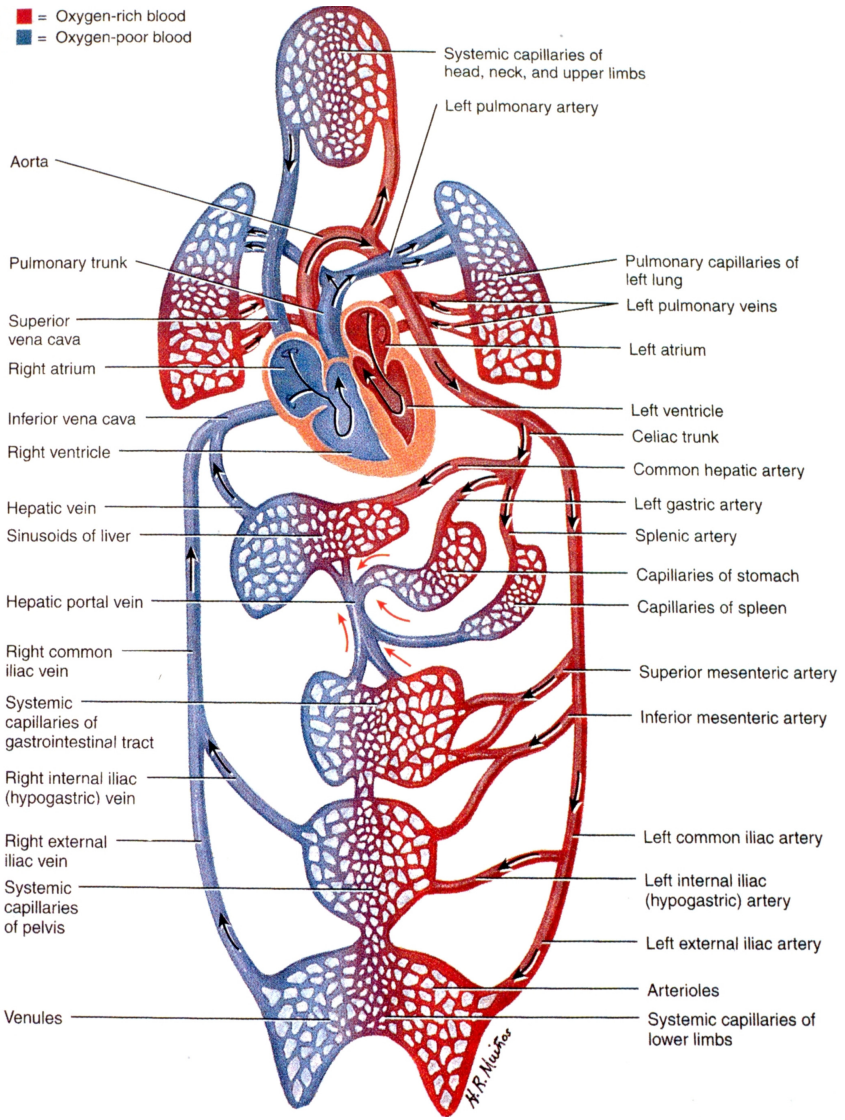

Sketch of the cardiovascular system (from Ottesen et al., 2004).

The human cardiovascular system is primarily a transport system in which oxygen, carbon dioxide and nutrients are carried by the blood to and from different parts of the body.

It consists of two separate parts: the **systemic circulation** and the **pulmonary circulation**. These two parts are in series to each other.

The two circulations are connected by the **heart**.

- From the **left ventricle** blood is pumped, through the **aortic valve** into the systemic circulation to the **aorta** (which is the largest artery in the body).
- The **systemic arteries** transport oxygen and nutrients to the various muscles and organs.
- In the **capillaries** oxygen and nutrients diffuse from the vessels into the target tissues.
- In the muscles and organs **oxygen is exchanged with carbon dioxide** and the blood becomes deoxigenated.
- From the capillaries blood flows into **venules** and then into **veins**.

General description of the cardiovascular system II

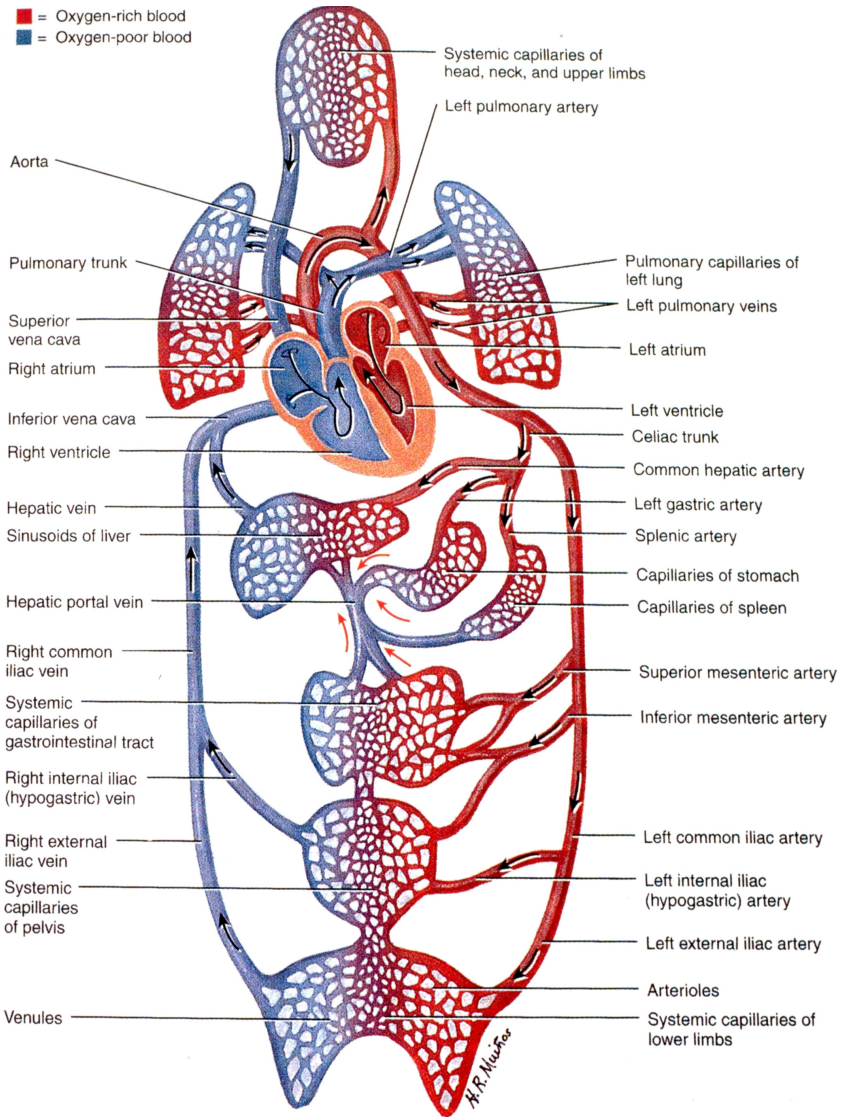

Sketch of the cardiovascular system (from Ottesen et al., 2004).

- Through a network of joining channels the blood reaches the **superior vena cava** and **inferior vena cava** and from there it enters the **right atrium** of the heart.
- From the right atrium, through the **tricuspid valve**, blood enters the **right ventricle**.
- Heart contraction ejects blood from the right ventricle through the **pulmonary valve** into the **pulmonary arteries**.
- The deoxygenated blood is carried to the **lungs**, where carbon dioxide is exchanged for oxygen in the **alveoli**.
- Reoxigenated blood is carried back to the **left atrium** through the **pulmonary veins**.
- From there the blood re-enters the left ventricle through the **mitral valve**.

Pressure distribution in the cardiovascular system

The pressure (cleared from the hydrostatic pressure) in each portion of the circulation changes significantly. It is highest in the ventricles during ejection and the progressively decreases towards the atria.

The maximum pressure in the left ventricle is significantly higher than that in the right ventricle.

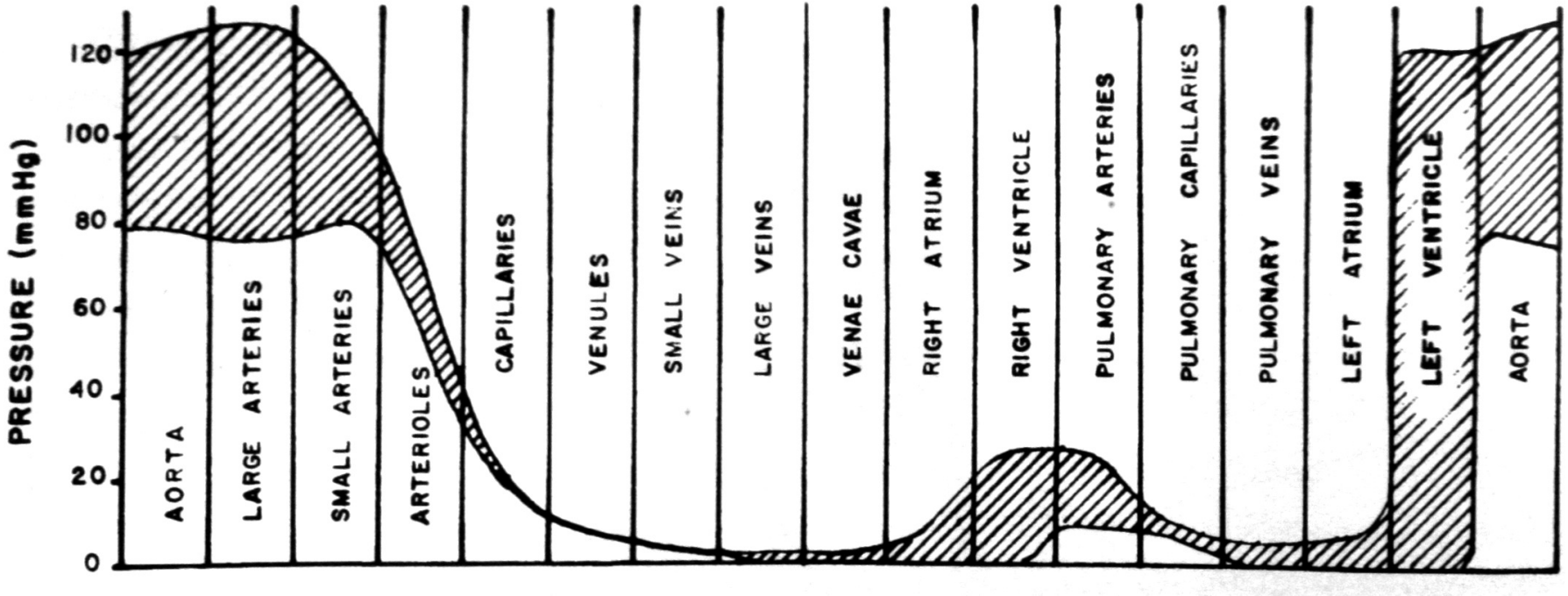

Pressure distribution in the human cardiovascular system (from Ottesen et al., 2004).

Maximum and minimum pressures in the aorta are approximately **120 mmHg and 80 mmHg** ($\approx 16000 - 10665$ Pa).

Blood volume distribution

Approximately 74% of blood volume is contained in the systemic circulation, 14% is in the pulmonary circulation and 12% is in the heart.
In particular

Location	Volume
Systemic arteries	$\approx 20\%$
Systemic veins	$\approx 54\%$
Pulmonary circulation	$\approx 14\%$
Heart	$\approx 12\%$

Volume distribution in the cardiovascular system relative to the total volume.

Cardiac output in man may increase from a resting level of about 5 l min^{-1} to 25 l min^{-1} in strenuous exertion. In all cases the output of the two pumps (left and right ventricles) is the same, being the two systems in series.

The response of the heart involves an increase in rate of contraction and output per beat (**stroke volume**). This implies that cardiac muscle fibres are capable of varying both the duration and amplitude of their contraction.

Anatomy of the heart I

The heart is the pump of the circulatory system, i.e. it is the source of energy that makes the blood flow.

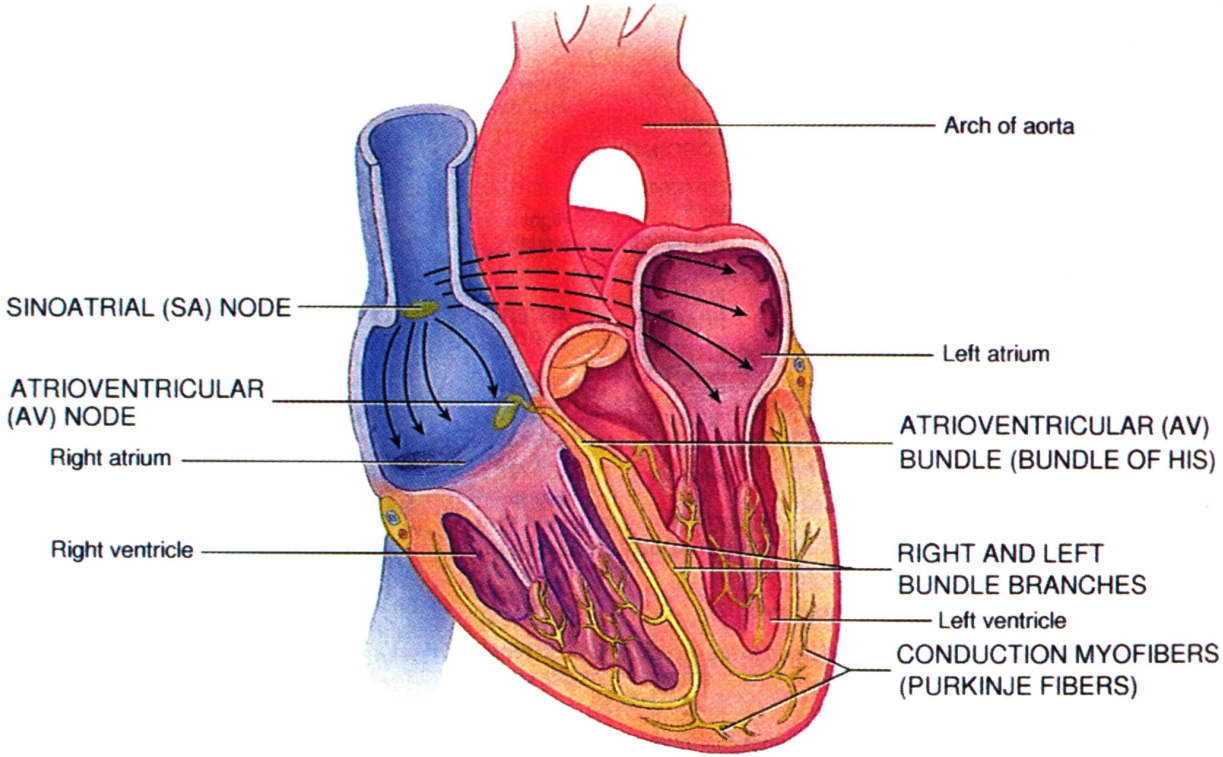

Sketch of the heart (from Ottesen et al., 2004).

The heart may be thought of as a couple of pumps in series. Each of the cardiac pumps consists of a low-pressure chamber (**atrium**), which is filled by the venous system, and a high-pressure chamber (**ventricle**).

The two chambers are separated by a **non-return valve**. From the ventricle the blood exits to an artery through another non-return valve.

Anatomy of the heart II

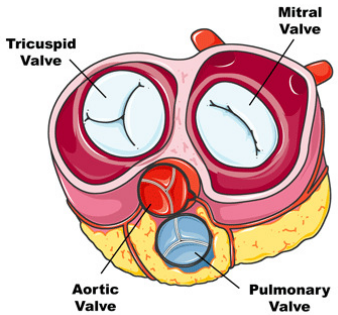

Sketch of a section of the atria.

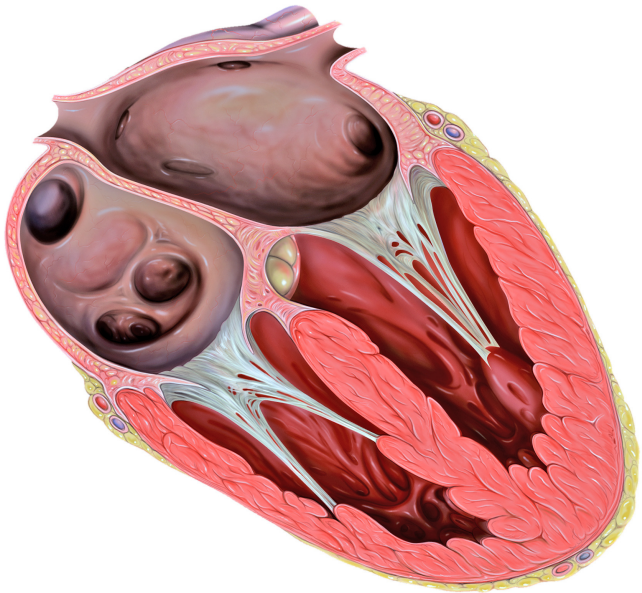

Sketch of a section of the heart.

Atria

The two atria have comparable structure. They have thin, relatively compliant walls and are separated by a common wall, the **interatrial septum**.

Veins are in communication with the atria without valves.

The two **atrioventricular** valves have different structure:

- the one on the right side (**tricuspid valve**) has three cusps;
- the one on the left side (**mitral valve**) has two cusps.

The valve cusps consist of flaps attached along one edge to a **fibrous ring** in the heart wall and with free edges projecting into the ventricles. They are very thin (≈ 0.1 mm). The free edges are attached ('tethered') to the ventricle walls through fibrous bands (**chordae tendinae**) which prevent the valve turning inside out when the pressure in the ventricle rises.

Heart valves open more than 30 million times a year!

The valves are made up of a meshwork of **collagen** and **elastic fibres**, covered by **endothelium** (the cell layer which also covers the walls of the heart chambers and blood-vessels).

Anatomy of the heart III

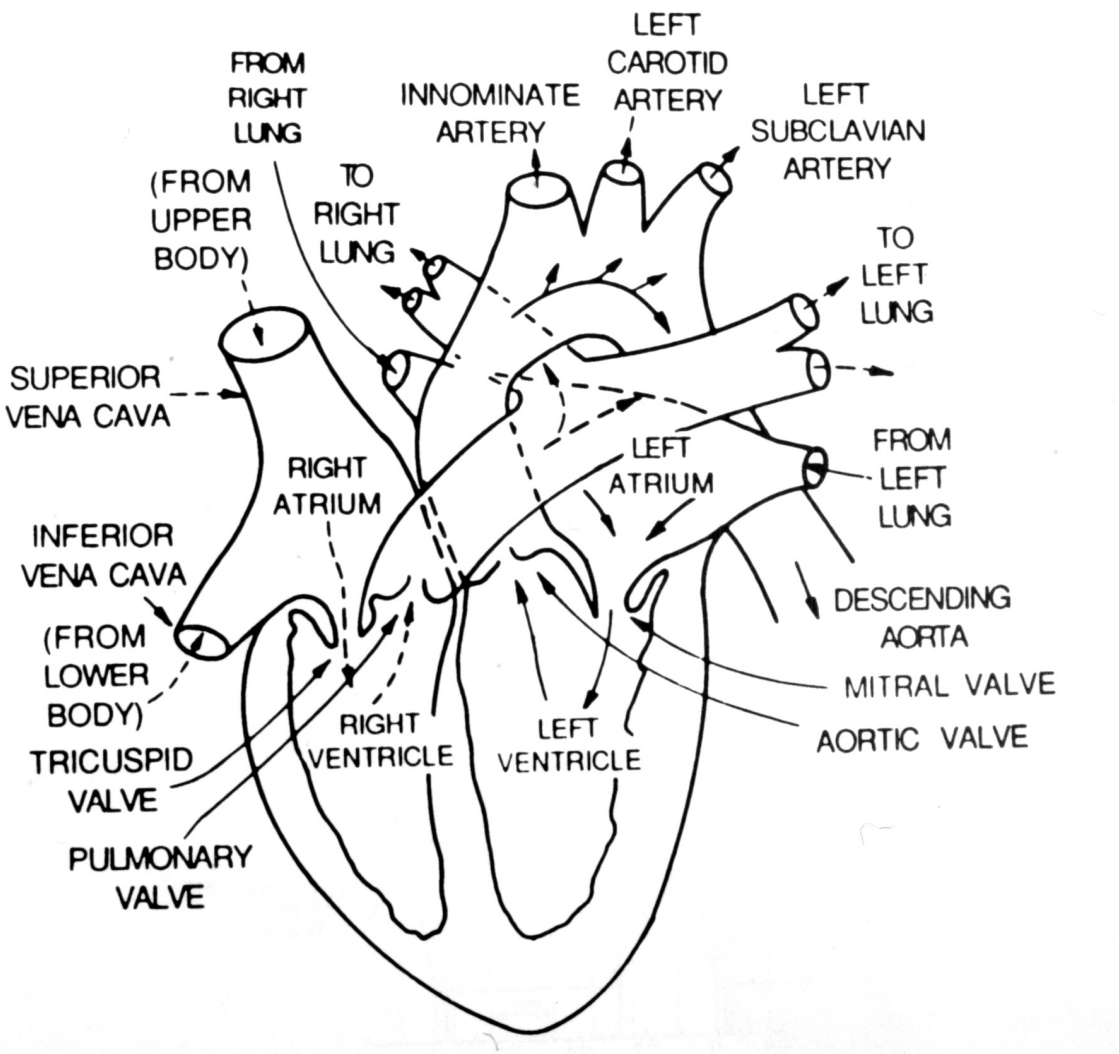

Sketch of a section of the heart.

Pulmonary and aortic valves

The exit valves from the ventricles, the **pulmonary** and **aortic valves**, are very similar to each other and consist of three cusps with free margins. These cusps are not tethered but can nonetheless support considerable pressure differences between the arteries and the ventricles (in the aortic valve ≈ 100 mmHg).

The four valve orifices are approximately aligned in a plane.

Anatomy of the heart IV

The cardiac muscle structure

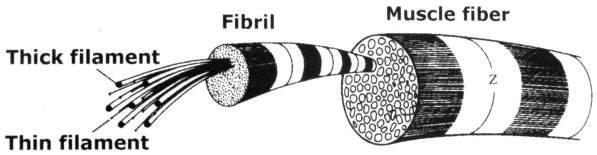

Muscle fibre (from Caro et al., 1978).

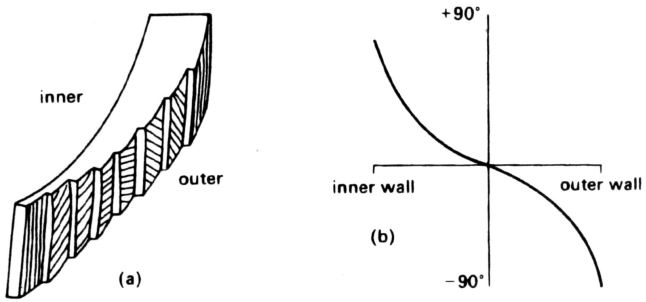

Muscle fibre orientation in wall of the left ventricle (from Caro et al., 1978).

The **myocardium**, the cardiac muscle, is made up of elongated muscle cells running in columns. Blood is supplied to the myocardium by the **coronary arteries** which branch from the aorta, just downstream of the aortic valve.
The wall structure of the left ventricle has been studied in great detail.

- The innermost layer (**subendocardial**) consists of fibres running predominantly in the longitudinal direction (from the fibrous region around the valves (**base**) to the end of the approximately elliptical chamber (**apex**).
- Moving outwards fibre orientation slightly changes. This angulation increases in successively outer fibres.
- Half-way through the wall thickness fibres run parallel to the shorter axis of the chamber, i.e. circumferentially.
- Further outwards the angle of orientation continues to increase and at the outer surface of the ventricle wall (**epicardial**) fibres run again predominantly in the longitudinal direction.

Anatomy of the heart V

The cardiac muscle structure

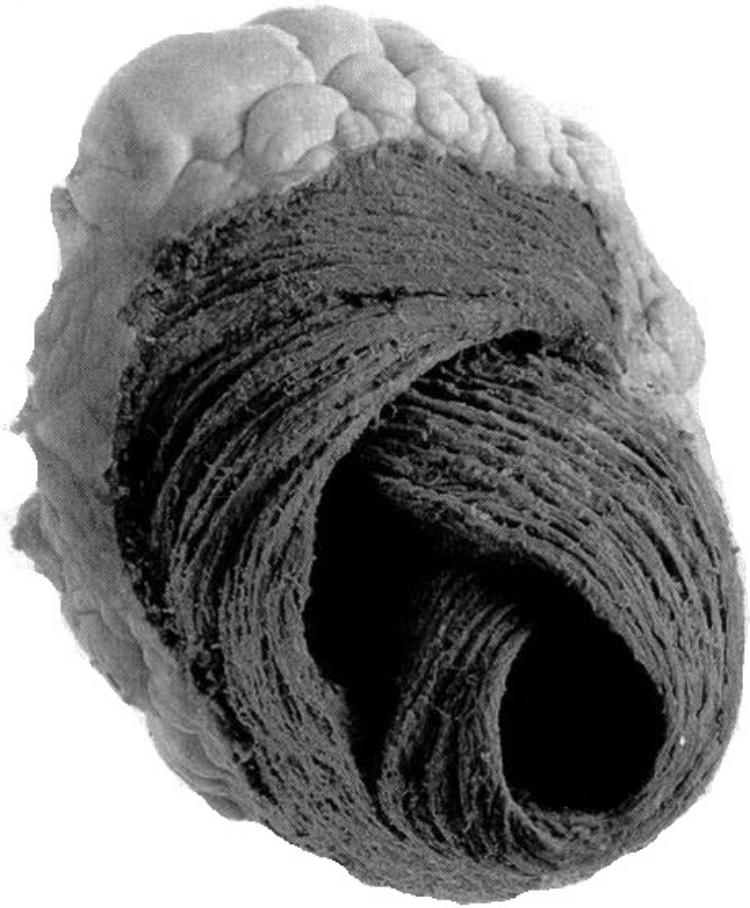

Arrangement of the muscle fibres in wall of the left ventricle.

- Fibres running in the longitudinal direction do not necessarily terminate at the apex but they can turn and spiral back towards the base.

This arrangement of muscle fibres gives the ventricle wall a great **strength in every direction**, even if single fibres can only withstand tension in the axial direction.

Anatomy of the heart VI

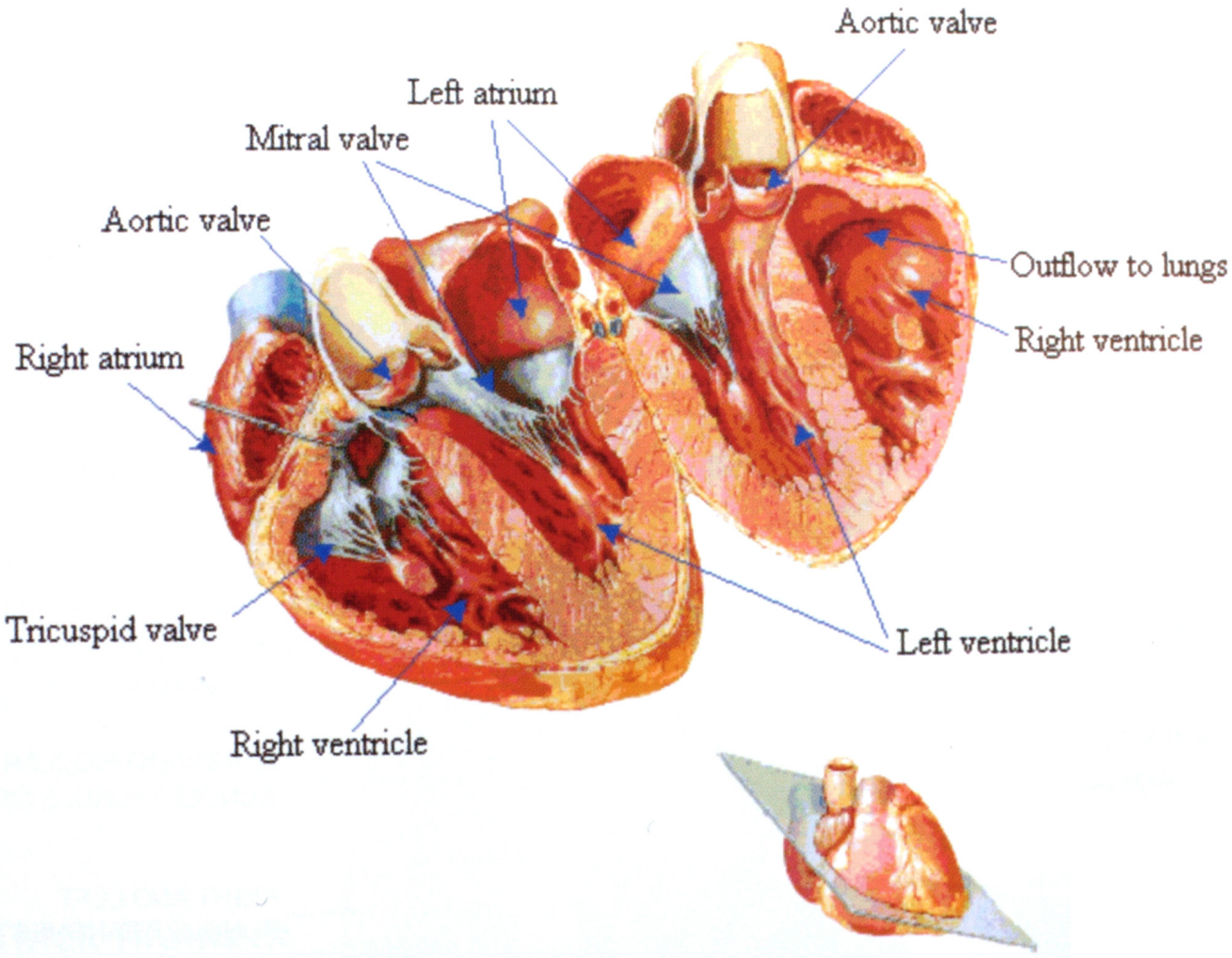

Drawing of the section of a heart (from Ottesen et al., 2004).

The cardiac cycle I

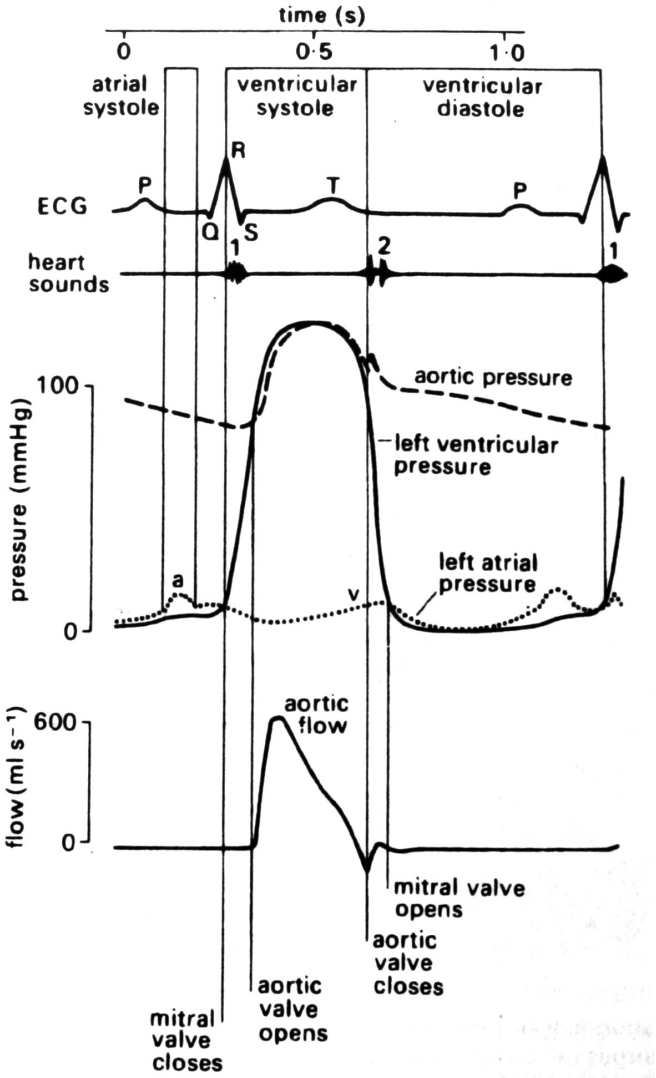

Sequence of events in the left heart during the cardiac cycle (from Caro et al., 1978).

Electrical events - The ECG

The contraction cycle of the heart is governed by **electrical impulses**. It is initiated in a localised area of the nervous tissue in the wall of the right atrium, known as **pacemaker** or **sino-atrial node**.

The cycles of **depolarisation** and **repolarisation** in the cardiac muscle can be recorded as the **electrocardiogram (ECG)**

- When depolarisation occurs in the pacemaker it spreads quickly into the muscle of the right and left atrial walls and causes **atrial contraction**. This produces a small deflection in the ECG known as **'P' wave**.
- The 'P' wave is followed, after about 0.2 s, by a larger deflection of the ECG, known as the **'QRS' complex**. This corresponds to depolarisation of the ventricles and the consequent ventricle contraction.
- Finally, there is the **'T' wave**, which is generated during repolarisation of the ventricles.

The cardiac cycle II

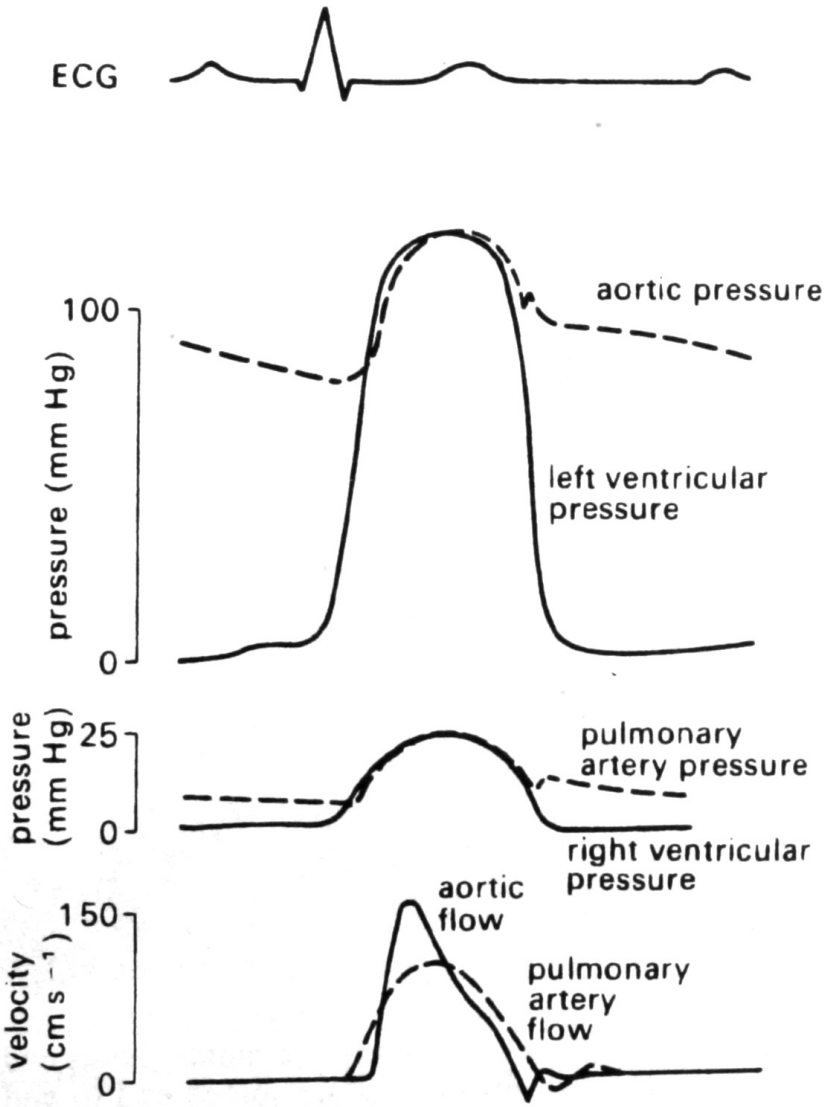

Sequence of events in the **left heart** during the cardiac cycle (from Caro et al., 1978).

Mechanical events

We consider the mechanical events taking place during the cardiac cycle in the left heart.

- In correspondence of the QRS complex in the ECG, ventricles contract. As the transmission of the electrical signal in the ventricular wall muscles is very fast (≈ 5 m/s) the contraction of the two ventricles is almost synchronous.
- As contraction starts in the ventricle, the blood pressure there grows rapidly. At this stage the aortic valve is still closed because the pressure in the aorta exceeds that in the ventricle.
- As the pressure in the ventricle grows larger than that in the atrium and, after a very short period of backward flow into the atrium, the mitral valve closes.
  The valve closure is accompanied by a sound which is audible at the chest. It is known clinically as the **first heart sound**.
  This sound marks the start of the **systole**, which is the period of ventricular contraction.

The cardiac cycle III

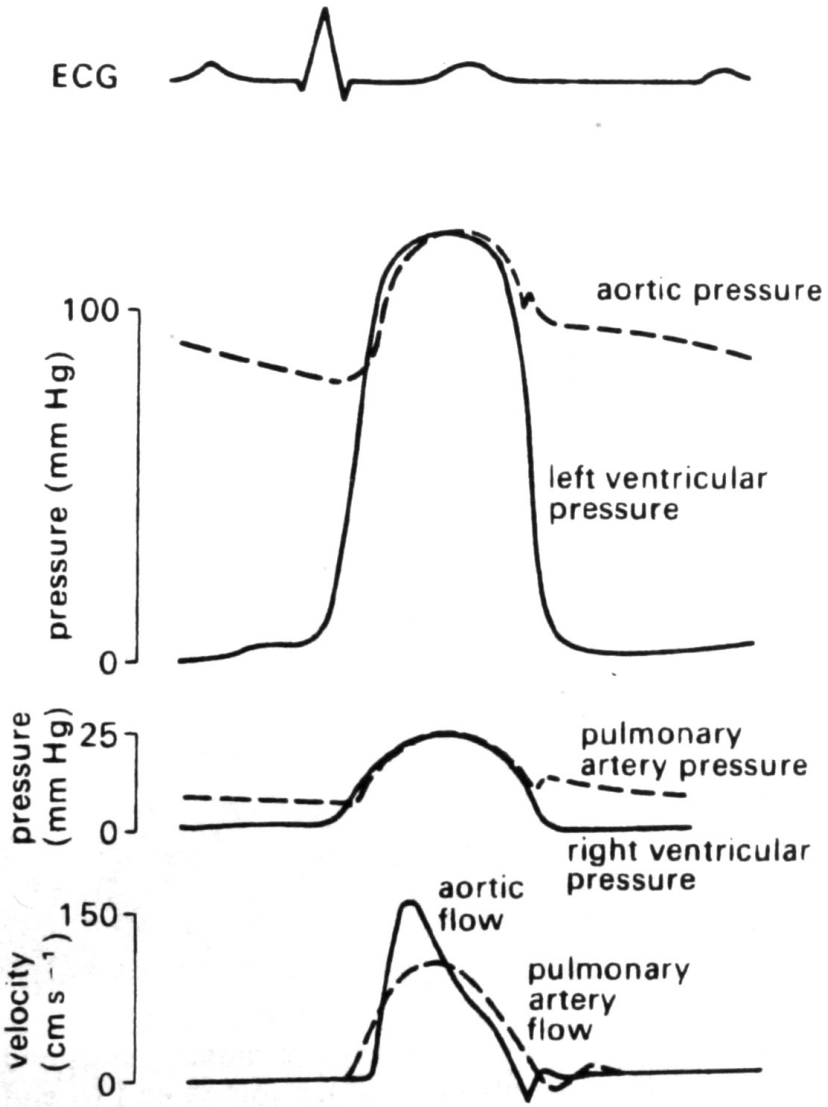

Sequence of events in the **left heart** during the cardiac cycle (from Caro et al., 1978).

Mechanical events

- The pressure in the ventricle keeps rising until it exceeds that in the aorta. During this phase there is no change of ventricular volume as there is no flux through the valves and the blood is effectively incompressible. This phase is known as **isovolumetric period**.
- When the pressure in the ventricle exceeds that in the aorta the aortic valve opens. At this moment the blood ejection into the systemic circulation starts.
- As the tension in the ventricle wall falls, the ventricular pressure starts to decrease. The pressure gradient between the ventricle and the aorta is reversed and flow starts to decelerate.
- After a short period of backflow into the ventricle the aortic valve closes again. This generates the **second heart sound**, which marks the onset of the **diastole**.

The cardiac cycle IV

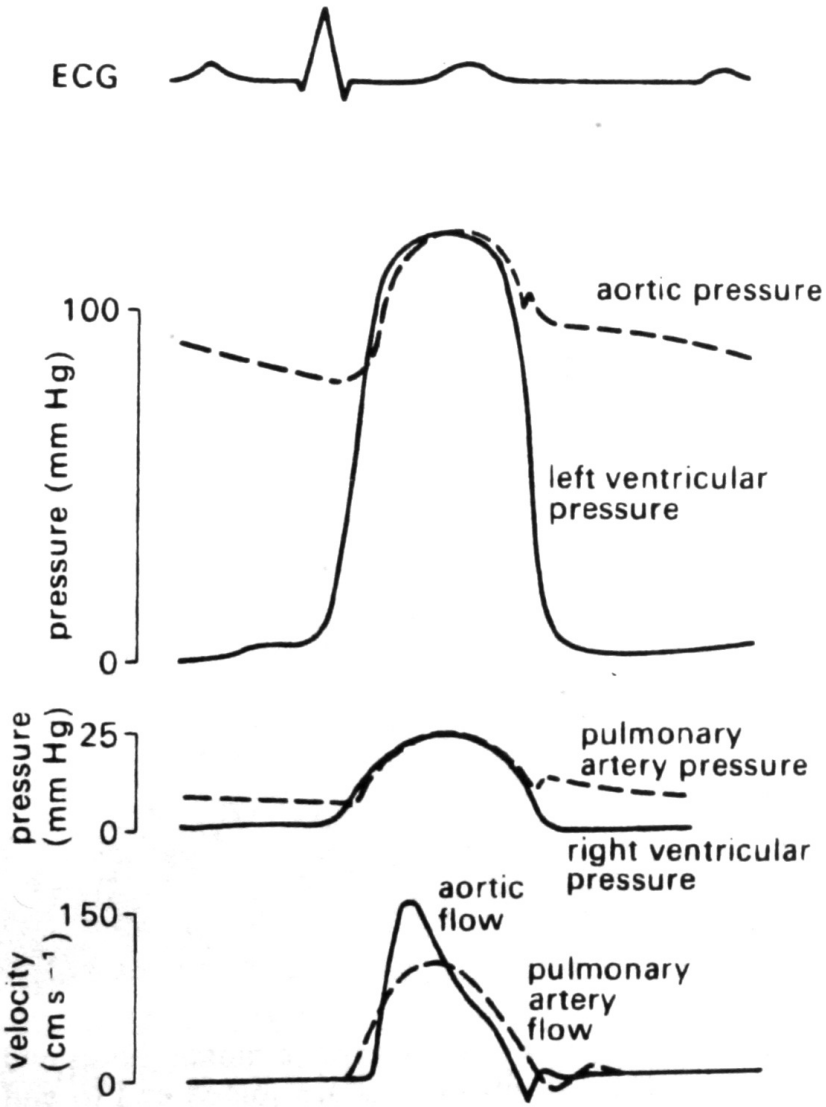

Sequence of events in the **left heart** during the cardiac cycle (from Caro et al., 1978).

Mechanical events

- At this stage all valves are closed again and a second **isovolumetric period** occurs during which the ventricular muscle relaxes and the pressure in the ventricle decrease.
- At the same time the pressure in the atrium rises again as the left atrium is filled from the pulmonary venous system.
- When the pressure in the atrium exceeds that of the ventricle the mitral valve reopens. At this stage flow occurs that refills the ventricle. This process is initially passive, driven by a pressure difference between the atrium and the ventricle. Then, after the P wave in the ECG, it becomes active as the atrium contracts (**atrial systole**).
- Shortly after that the ventricle contracts again (QRS wave) and the cycle starts again.

The cardiac cycle V

Mechanical events in the left ventricle

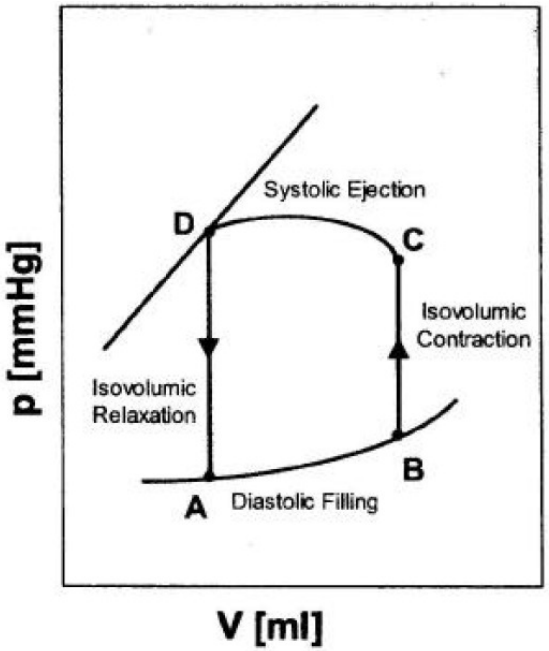

Cardiac cycle of the left ventricle in the plane p (pressure in the ventricle) - V (volume of the ventricle).

The cardiac cycle VI

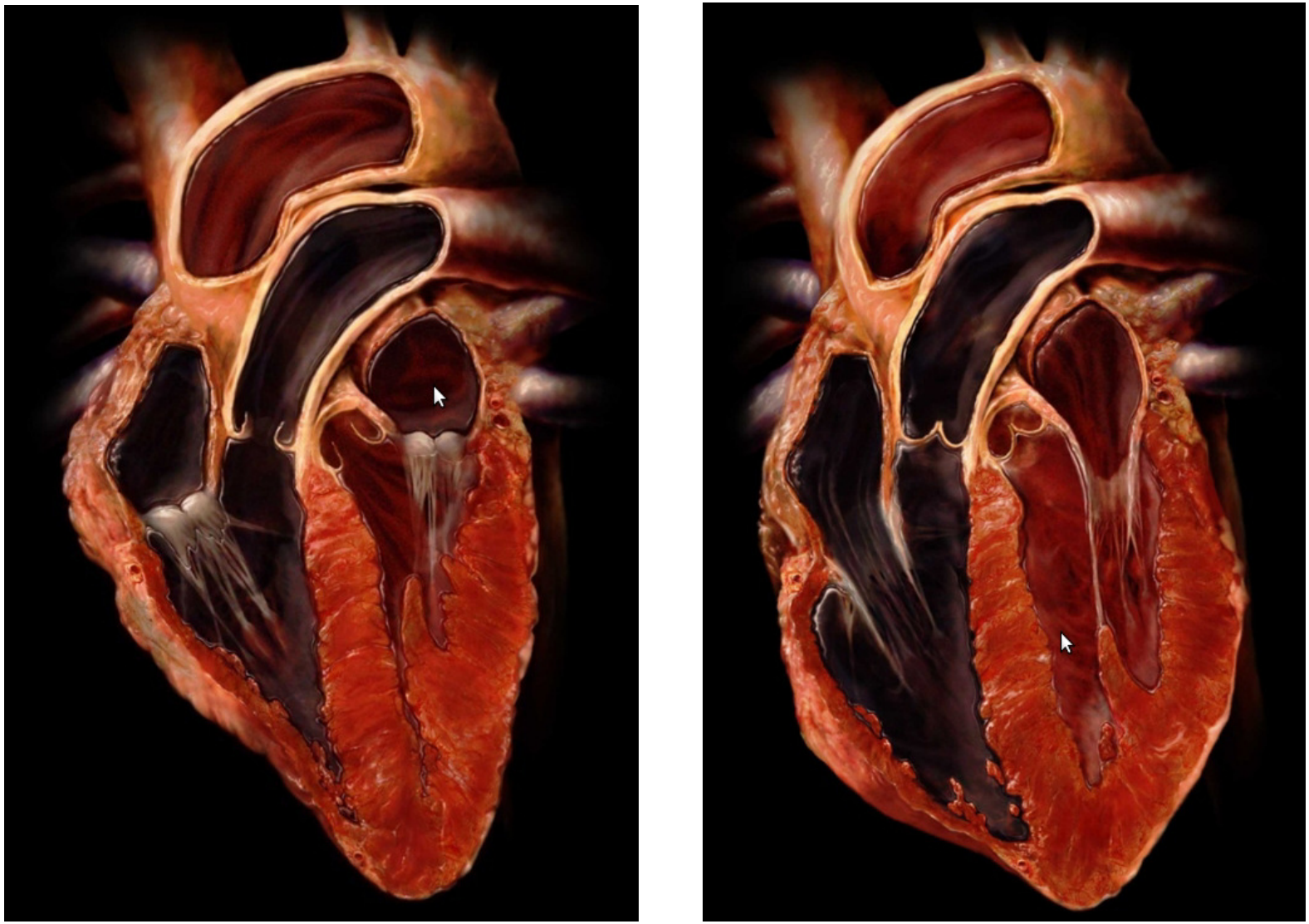

Drawing of a heart section during systole (left) and diastole (right).

Fluid dynamics of the right heart

Flow characteristics in the heart are very complex and not suitable for analytical treatment.

Here we describe the main features of flow in the **right heart**. Flow in the right heart has been far less studied than flow in the left heart.

- The pulsation which characterises the arterial flow is largely smoothed out in the micro circulation. The average pressure is also significantly lower in veins than in arteries, but it is still large enough to induce flow towards the right atrium. This implies that the driving force inducing flow in veins is essentially steady.
- However, unsteadiness arises from various peripheral effects, in particular:
  - contractions of the muscles (**muscle pump**) induce flow pulsation;
  - pressure variations in time are induced by breathing;
  - contractions of the atrium also induce pressure oscillations. These contractions generate pressure waves which propagate backwards into veins.
- For the above reasons **flow entering the right atrium is unsteady and fluctuates during the cardiac cycle**.
- **Functioning of the valves in the right heart is quite similar to that of valves in the left heart**.
- The mechanics of the right ventricle, however, is significantly different.
  - At the beginning of systole pressure rises more slowly in the right ventricle than in the left. However, the pressure in the pulmonary artery ($\approx$ 10 mmHg) is much lower than in the aorta ($\approx$ 100 mmHg) and the pulmonary valve opens before the aortic valve.
  - Both acceleration and deceleration of blood in the pulmonary arteries are lower than in the aorta, thus the waveform there is smoother and ejection takes longer.
  - The peak Reynolds number in the pulmonary artery $Re = Ud/\nu$ (calculated with the peak systolic velocity U , artery diameter d and blood viscosity ν) is lower than in the aorta. It ranges between 2500 and 7000.

Fluid dynamics of the left heart

- Pressure and flow in the pulmonary veins are fairly steady and, therefore, the pulmonary veins essentially act as a reservoir inducing atrium filling during ventricular systole.
- The velocity of flow through the mitral valve rises rapidly in diastole and may exceed 1 m/s.
- The corresponding peak Reynolds number is about 8000.
- The velocity falls during diastole until a final acceleration due to left atrial contraction. Then it falls very rapidly before the mitral valve closure.
- The flow in the left ventricle and the mechanics of ejection from the ventricle will be analysed in detail in the following making use of a numerical model.

The mechanics of mitral valve closure Bellhouse (1972) I

Experimental works have shown that there is very little back flow through the mitral valve during systole. In fact the mitral valve starts closing when flow is still directed to the ventricle and the atrium is contracting.

We present a simple model of the closure of the mitral valve originally proposed by Bellhouse (1972).
We consider the idealised two-dimensional geometry shown in the figure. Let us denote with x the direction of the jet, with $x = 0$ being the apex of the valve cusp and with $x = -l$ the attachment point of the apex on the ventricular wall. Moreover, U is the velocity of the jet in the x direction. We assume that:

- the valve is open, with the two cusps parallel to each other;
- the velocity is constant within the jet thickness, does not depend on x and is variable in time; thus $U = U(t)$.

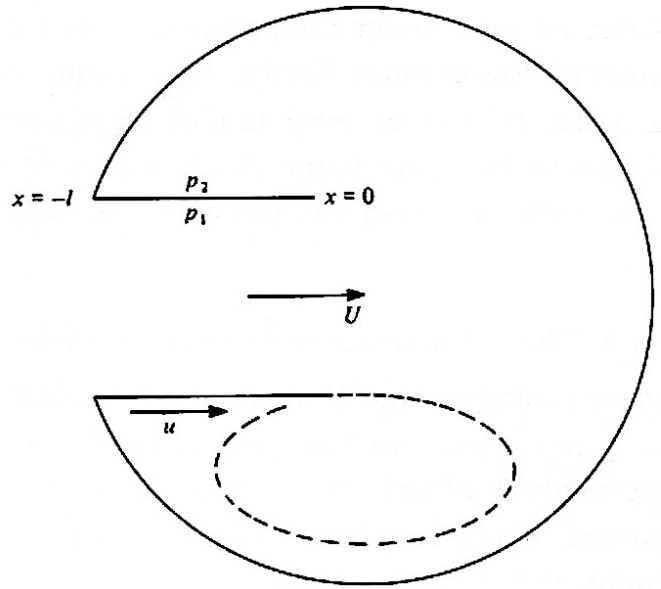

Thus we neglect the presence of the boundary layer that forms at the cusps wall. This boundary layer has thickness $\delta \approx \sqrt{\nu T}$, with T a characteristic time scale of the flow that can be estimated as l/U, with l length of the valve cusp. Since $\nu = 3 \times 10^{-6}$ m^2/s, $l \approx 1$ cm and $U \approx 1$ m/s, we find $T \approx 10^{-2}$ s, and the order of magnitude of $\delta \approx 0.17$ mm and thus significantly smaller than the thickness of the jet, which is ≈ 1 cm.

The mechanics of mitral valve closure Bellhouse (1972) II

Evaluation of the average pressure on the atrial side

We aim at predicting when the valve starts to close. We assume that this happens when the average pressure on the ventricular side of the cusp, $\overline{p}_v$, exceeds that on the atrial side, $\overline{p}_a$. Under the assumptions listed above the Navier-Stokes equation in the jet reduces to

$$\frac{dU}{dt} + \frac{1}{\rho}\frac{\partial p}{\partial x} = 0,$$

with p the dynamic pressure. The above equation can be readily integrated to obtain

$$p = p_0 - \rho \dot{U} x,$$

where p_0 denotes the pressure in section $x = 0$ and $\dot{U} = dU/dt$.
The average pressure $\overline{p}_a$ on the atrial face of the cusp can be obtain as

$$\overline{p}_a = \frac{1}{l}\int_{-l}^{0} \left(p_0 - \rho \dot{U} x\right) dx = p_0 + \frac{1}{2}\rho l \dot{U}.$$

The mechanics of mitral valve closure Bellhouse (1972) III

Evaluation of the average pressure on the ventricular side

The pressure on the ventricular side is strongly influenced by the presence of the circulation produced by vortex emission from the apex of the cusps.

The case of a strong vortex

We assume that the velocity along the cusp wall on the ventricular side is

$$u(x,t) = U(t)\left(1+\frac{x}{l}\right). \tag{65}$$

Thus the equation of motion on the ventricular side reads

$$\frac{\partial u}{\partial t} + u\frac{\partial u}{\partial x} + \frac{1}{\rho}\frac{\partial p}{\partial x} = 0. \tag{66}$$

Substituting (65) into (66) we obtain

$$\frac{\partial p}{\partial x} = -\rho\left(\dot{U}+\frac{U^2}{l}\right)\left(1+\frac{x}{l}\right),$$

and integrating with respect to x

$$p = -\frac{\rho l}{2}\left(\dot{U}+\frac{U^2}{l}\right)\left[\left(\frac{x}{l}\right)^2 + 2\frac{x}{l}\right] + p_0.$$

The mechanics of mitral valve closure Bellhouse (1972) IV

The average pressure p_v on the ventricular side of the cusp can be obtained as

$$\overline{p}_v = \frac{1}{l}\int_{-l}^{0}\left\{-\frac{\rho l}{2}\left(\dot{U}+\frac{U^2}{l}\right)\left[\left(\frac{x}{l}\right)^2+2\frac{x}{l}\right]+p_0\right\}dx = p_0+\frac{1}{3}\rho l\left(\dot{U}+\frac{U^2}{l}\right).$$

We can now compute the difference between the average pressures on the two sides of the cusp as

$$\overline{p}_v-\overline{p}_a=\frac{1}{3}\rho\left(U^2-\frac{1}{2}l\dot{U}\right). \tag{67}$$

The case of a weak vortex

In order to understand the role of the vortex in the mechanics of the valve closure we now consider the case of a very large ventricle. In this case we may assume that the pressure on the ventricular side of the cusp is always equal to p_0. With this assumption we can obtain

$$\overline{p}_v-\overline{p}_a=-\frac{1}{2}\rho l\dot{U}. \tag{68}$$

The mechanics of mitral valve closure Bellhouse (1972) V

Results

We consider the time law assumed by Bellhouse (1972) for the jet velocity:
$U = U_0(1 - \cos 2\pi ft)$, with f frequency of the cardiac cycle (f =0.83 Hz and $U_0 = 0.6$ m/s).
The results obtained from equations (67) and (68) are shown in the figure below.

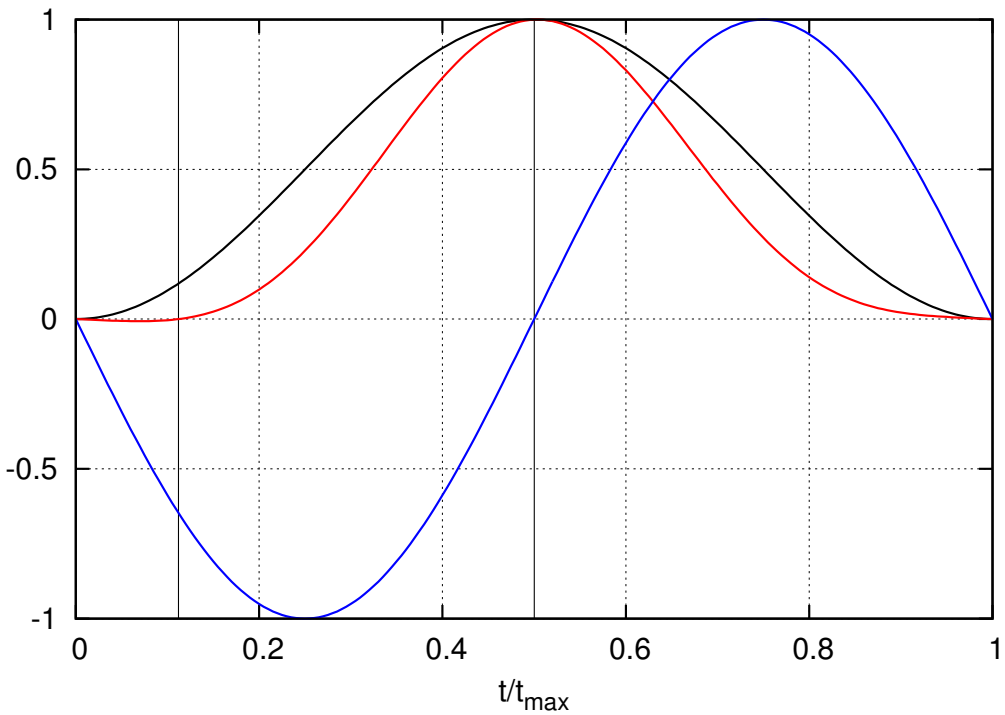

Normalised time on the x-axis. Black curve: normalised velocity of the jet. Red curve: normalised $(\overline{p}_v - \overline{p}_a)$ for the case of a strong vortex. Blue curve: normalised $(\overline{p}_v - \overline{p}_a)$ for the case of a weak vortex. The vertical black lines indicate the times at which the red and blue curves change sign. $l = 0.02$ m.

The mechanics of mitral valve closure Bellhouse (1972) VI

From the figure in the previous page it appears that in the case of "strong vortex" (red curve) the average pressure the ventricular side of the cusp exceeds that on the atrial side from $t \gtrapprox 0.15$ s, and thus this is the time at which the valve starts closing. In the absence of vortex (blue curve) the closure phase is significantly delayed ($t \approx 0.6$).
The above predictions are in quite good agreement with experimental results obtained in–vitro by Bellhouse (1972).

The mechanics of the aortic valve

The aortic valve has three cusps attached to a circular ring of fibrous tissue at the base of the ventricle. The valve can open to expose the full cross-section of the ascending aorta.

Immediately behind each cusp there is a rounded pouch in the aortic wall known as **sinus of Valsalva**. From two of these sinuses branch the left and right coronary arteries.

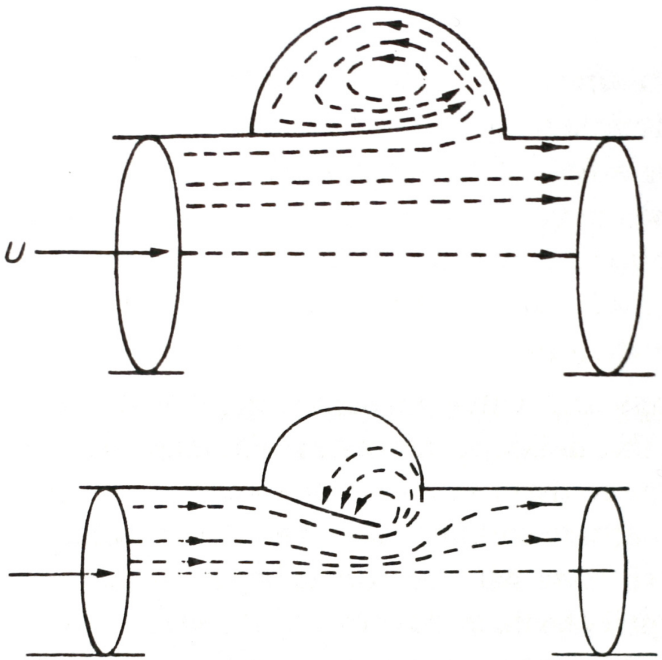

Sketch of streamlines in the aortic root at peak systole (upper plot) and during valve closure (lower plot) (from Caro et al., 1978).

- As for the mitral valve, backflow into the ventricle after aortic valve closure is very limited.
- Measurements have shown the existence of a circulation in the sinuses of Valsalva. It is not clear however, how much this circulation contributes to valve functioning.
- It is known from experimental and numerical work that a **vortex** is generated behind each cusp during systole.
- The entire mechanics of functioning of the aortic valve is far from being understood even if there is increasing numerical and experimental effort in this direction.

Flow in the left ventricle I

The fluid dynamics in the human left ventricle can be synthesised as follows.

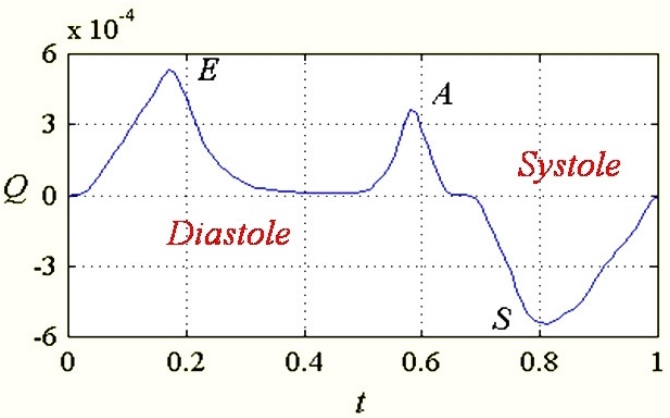

Flow entering the left ventricle versus time.

- The flow is primarily characterised by a strong compact jet that enters the chamber through the mitral orifice during the ventricular filling (diastolic phase).
- The jet has two distinct pulses: the early-filling wave (**E wave**), during ventricular relaxation, followed by the **A wave** produced by the atrial contraction.
- At the end of the diastole, the ventricle begins to contract (systole), the mitral valve closes and the aortic valve opens.

- The diastolic entering jet has an almost irrotational core, surrounded by a shear layer.
- This shear layer rolls up soon and arranges into a ring-shaped vortex structure that enters the cavity.
- As the orifice is displaced with respect to the axis of the cavity the jet is directed towards one wall.
- Flow visualisations on a plane cutting the ventricle, show the development of a persisting **recirculation structure**. This forms due to the asymmetry of the flow.

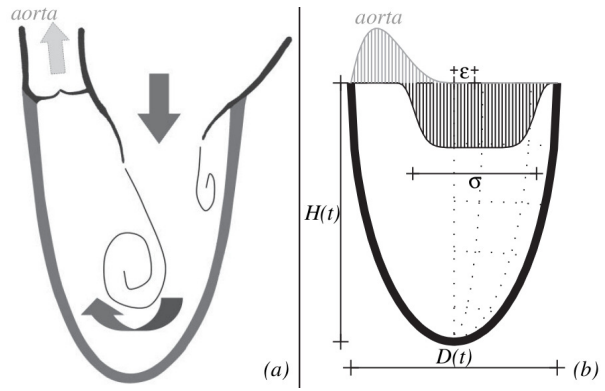

Sketch of the physical problem (from Pedrizzetti and Domenichini, 2005).

Flow in the left ventricle II

- The recirculation cells are thought to act as a reservoir that stores kinetic energy and facilitates blood ejection during systole.
- This suggests that flow asymmetry plays a role in reducing energy dissipation in the ventricle, thus also reducing the work that the myocardial muscle has to do during the ejection phase.

Pedrizzetti and Domenichini (2005) developed a numerical model to verify the above arguments.

Working assumptions made by Pedrizzetti and Domenichini (2005)

- The model is based on the direct numerical solution (DNS) on the Navier Stokes equations.
- The left ventricle is modelled as a half prolate spheroid with moving walls. The geometry is then parametrised by the time dependent functions
  - $D(t)$ equatorial diameter;
  - $H(t)$ major semiaxis.

  These functions specify the ventricle volume $V(t)$.
- The valves are assumed to be circular and are either fully open or closed depending on the sign of $dV(t)/dt$.
- A given velocity profile is given on the equatorial plane in the filling phase ($dV(t)/dt > 0$).

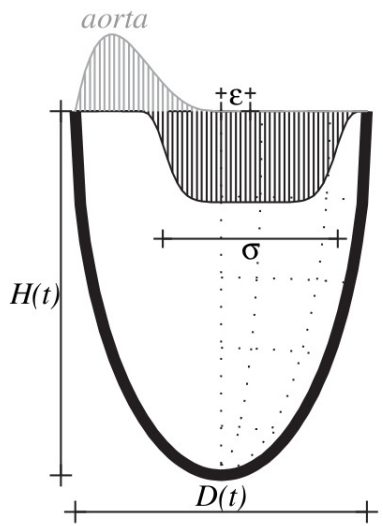

Geometry considered.

- The parameter ε defines the displacement of the inflow jet with respect to the central axis.
- The parameter σ defines the radius of the inflow jet.

Flow in the left ventricle III

- The exit profile (through the aorta) is also specified but has little influence on the solution.

Controlling dimensionless parameters

The flow is governed by the following dimensionless parameters:

- $\beta = D_0^2/(\nu T)$ **Stokes number**,
- $St = D_0/(U_0 T)$ **Strouhal number**,
- ε/D_0,
- σ/D_0,

where $\nu = 3 \times 10^{-6}$ m^2/s is the viscosity of blood (modelled as a Newtonian fluid), T is the heart beat period, D_0 is a reference length scale representative of the diameter of the mitral valve and U_0 is the peak inflow velocity.

Pedrizzetti and Domenichini (2005) made a study on the healthy early-born child of ≈ 1 Kg of weight. This choice limits the numerical requirements. In this case, $D_0 = 9.2$ mm and $T = 480$ ms. The dimensionless numbers assume the following values:

- $\beta = 54$,
- $St = 0.07$,
- $\varepsilon/D_0 = 0.125$.
- $\sigma/D_0 = 0.65$ during the E wave and 0.45 during the A wave.

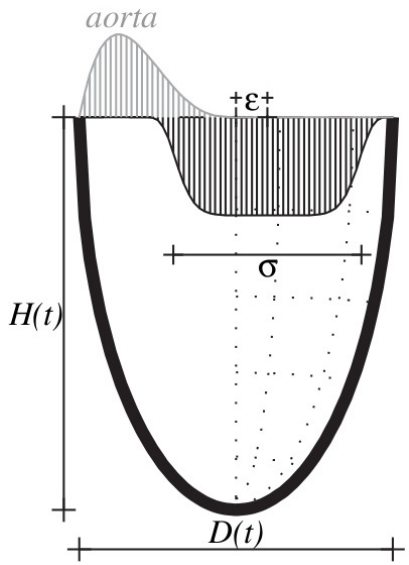

Geometry considered.

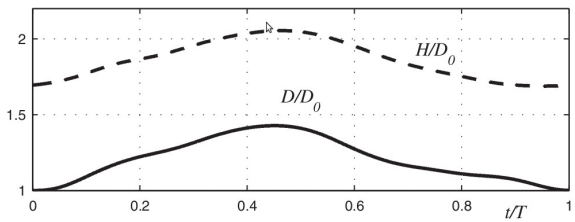

Time variation of H/D_0 and D/D_0.

Flow in the left ventricle IV

Numerical results

The plots on the right are relative to the end of the filling phase (diastole).

- The jet head, initially a vortex ring, is partly dissipated on the side closer to the wall.
- On the opposite side the vortex occupies the centre of the cavity.
- Essentially the asymmetry of the position of the inlet flow with respect to the central axis (ε) induces the formation of a large ventral vortex which dominates the entire flow field.
- The circulating flow at the end of diastole naturally invites the flow towards the opening of the aortic valve.
- This suggests that the natural asymmetry of flow arrangement facilitates the ejection phase.

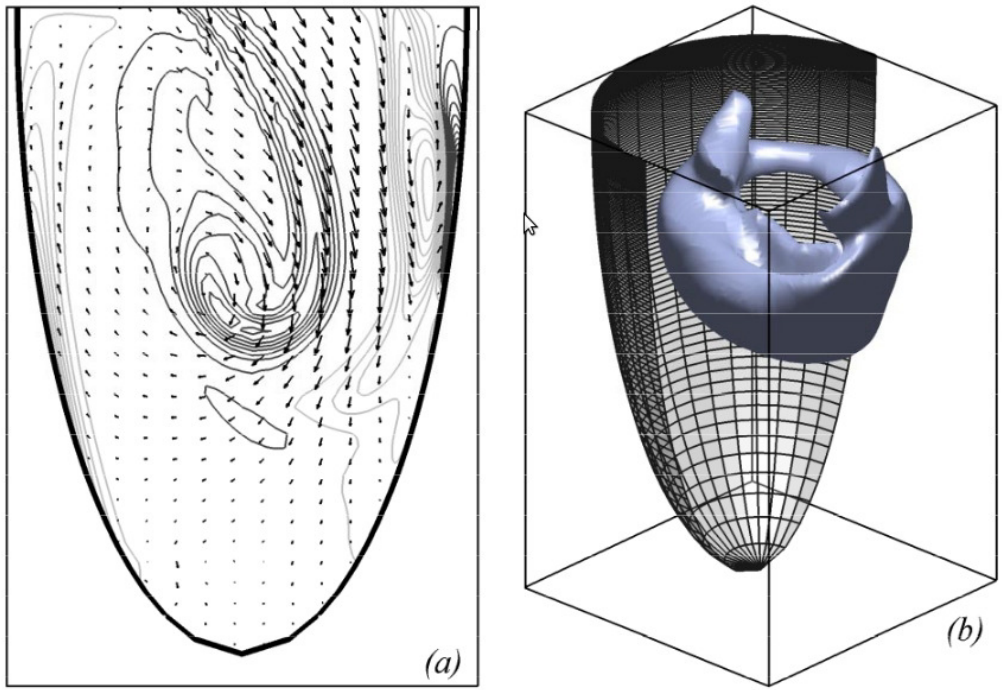

(a) Velocity vectors and contour lines of vorticity on the vertical symmetry plane. In the vorticity contour lines black is clockwise rotation, grey counter-clockwise rotation. (b) Iso surface of the scalar indicator λ_2, whose negative extremes correspond to the trace of coherent vortexes.

Flow in the left ventricle V

Numerical results

The importance of the eccentricity of the jet can be tested by displacing artificially its position.

- If the value of ε/D_0 is very small (a) the vortex ring survives and, on a vertical cross-section, an approximately symmetrical vortex pair is still clearly visible at the end of the filling phase.
- This flow arrangement induces a weak backflow towards the aortic valve.
- If the value of ε/D_0 is larger than normal (b) the jet is strongly redirected towards the lateral wall, and the vortex head on that side closely interacts with the wall boundary layer. This effect is expected to increase energy dissipation.
- In this case backflow toward the aorta also appears to be weaker than in the physiological case.

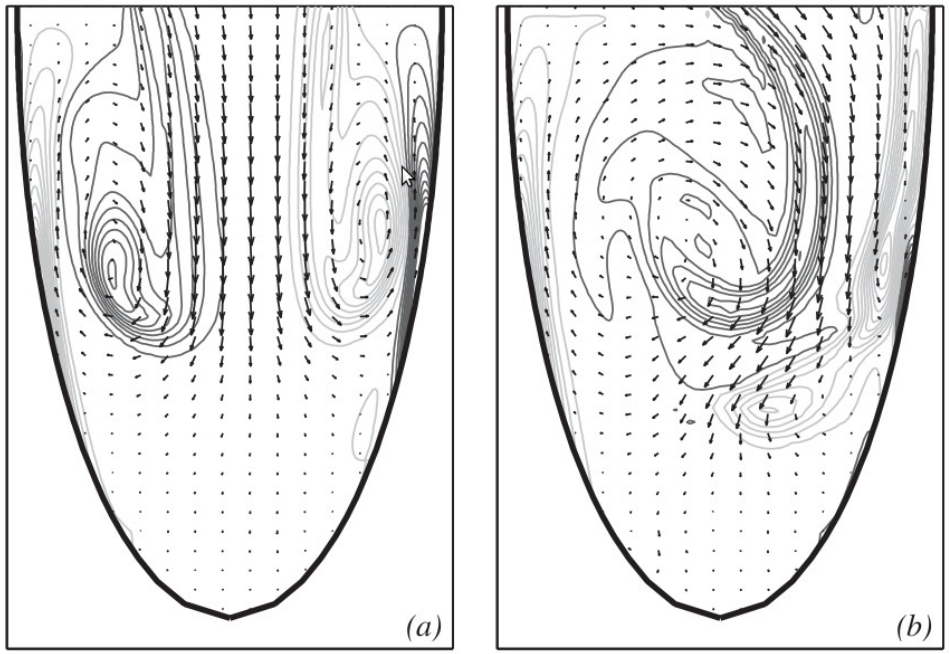

Velocity vectors and contour lines of vorticity on the vertical symmetry plane at the end of diastole. (a) $\varepsilon/D_0 = 0.02$, (b) $\varepsilon/D_0 = 0.25$.

Flow in the left ventricle VI

Calculation of the energy dissipation during diastole

The time evolution of the total dimensionless power dissipated by viscous effects can be computed as

$$\mathcal{P}(t^*) = \frac{T^3}{\rho D_0^5} \int_{V(t^*)} \boldsymbol{\sigma} : \mathbf{e} dV,$$

with $t^* = t/T$ dimensionless time, $\boldsymbol{\sigma}$ stress tensor and $\mathbf{e}$ rate of deformation tensor. The function $\mathcal{P}(t^*)$ is shown for different values of ε/D_0 in the figure.

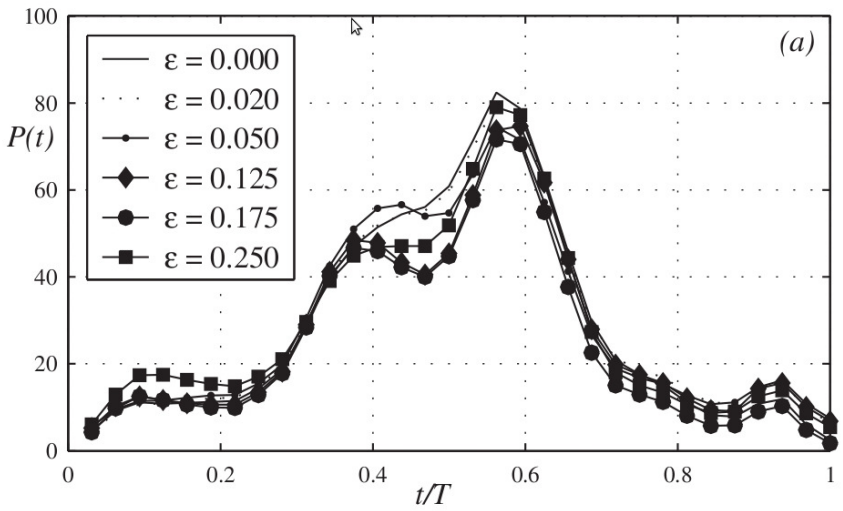

Dimensionless power dissipated by viscous effects $\mathcal{P}$ as a function of t/T, for different values of ε/D_0.

- During the initial stage of the diastolic filling ($t/T \lessapprox 0.35$) all curves are very close to each other. There is only a slightly higher dissipation for $\varepsilon/D_0 = 0.25$ due to early interaction of the vortex ring with the wall.
- In the interval ($0.35 \lessapprox t/T \lessapprox 0.5$), before ejection starts, differences are more evident.
- The physiological case $\varepsilon/D_0 = 0.125$ shows low values of energy dissipation.

Flow in the left ventricle VII

Calculation of the energy dissipation during diastole

The total energy dissipation during filling and until the peak of ejection, which occurs at time $t^*_{sys} = t_{sys}/T = 0.57$, can be computed as

$$\mathcal{I}(t^*) = \int_0^{t^*_{sys}} \mathcal{P}(t^*)dt^*.$$

The figure shows that the lowest value of energy dissipation corresponds to physiological conditions.

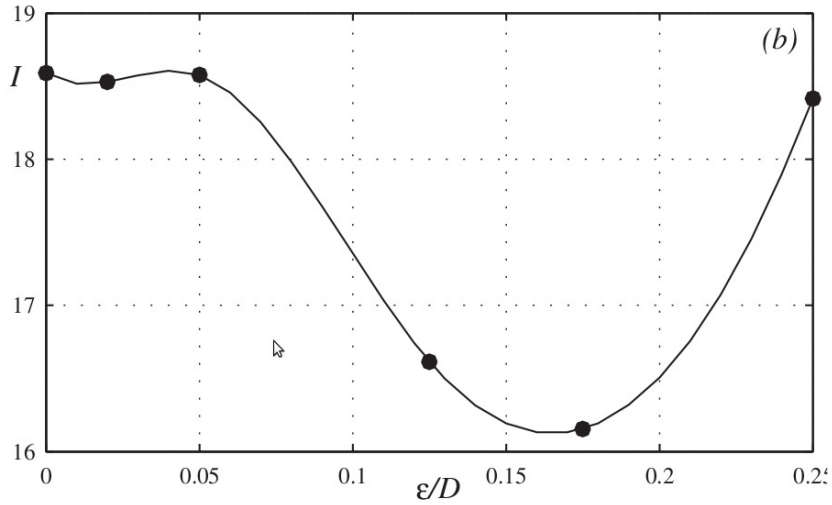

Dimensionless energy dissipation $\mathcal{I}$ for different values of ε/D_0.

Conclusions

- The flow pattern in the left ventricle in physiological conditions is such as to minimise energy dissipation.
- This reduces the work of the heart muscle at every cardiac cycle.

Some films I

All films are courtesy of Gianni Pedrizzetti (University of Trieste) and Federico Domenichini (University of Florence).

- Swirling flow in the heart (ultrasound scan)
- Beating heart (live)
- Longitudinal cross-section (ultrasound scan)
- Transverse cross-section (ultrasound scan)
- Reconstruction of the wall movement - longitudinal cross-section
- Reconstruction of the wall movement - transverse cross-section
- Axisymmetric numerical simulation
- Three-dimensional numerical simulation ($\varepsilon = 0.02$)
- Three-dimensional numerical simulation ($\varepsilon = 0.125$)
- Three-dimensional numerical simulation - λ_2 ($\varepsilon = 0$)
- Three-dimensional numerical simulation - λ_2 ($\varepsilon = 0.125$)
- Three-dimensional numerical simulation, full cycle ($\varepsilon = 0.125$)
- Three-dimensional numerical simulation, full cycle - λ_2 ($\varepsilon = 0.125$)
- Motion of the left ventricle wall in a healthy heart
- Motion of the left ventricle wall in a infarcted heart
- Numerical simulation of the flow in a healthy left ventricle

Some films II

- Numerical simulation of the flow in a infarcted left ventricle
- Numerical simulation of the flow in a healthy left ventricle - λ_2
- Numerical simulation of the flow in a infarcted left ventricle - λ_2
- PIV measurements in the left ventricle
- PIV measurements in the left ventricle of an infarcted heart
- Vortex shedding during the opening of a single leaflet valve
- Vortex shedding during the opening of a double leaflet valve (leaflets with very different length)
- Vortex shedding during the opening of a double leaflet valve (leaflets with similar length): suppression of shedding from the longer leaflet

The cardiovascular system: the systemic arteries

Anatomical introduction I

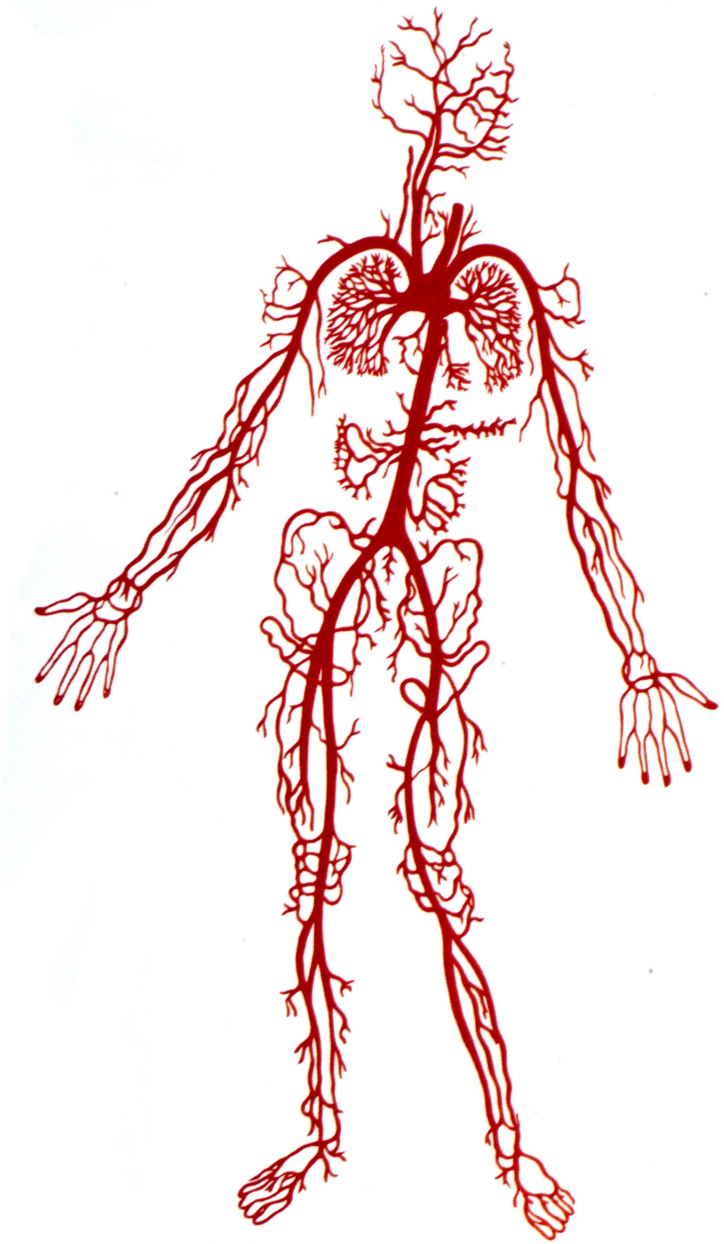

In this chapter we study flow characteristics in the **systemic arteries**, focusing our attention on **large vessels**. We therefore do not consider here neither **pulmonary arteries** nor the **microcirculation.**

More specifically, from the fluid dynamic point of view, we may distinguish in the systemic arterial system, vessels in which

- **flow is dominated by inertia**, i.e. $Re = Ud/\nu$ is quite large (with U characteristic velocity, d vessel diameter and ν blood kinematic viscosity);
- **flow in which inertia is negligible and viscous effects dominate**, i.e. $Re \ll 1$.

We will focus our attention to the first case, in which viscous effects are not very important.

Anatomical introduction II

Structure of the arterial walls

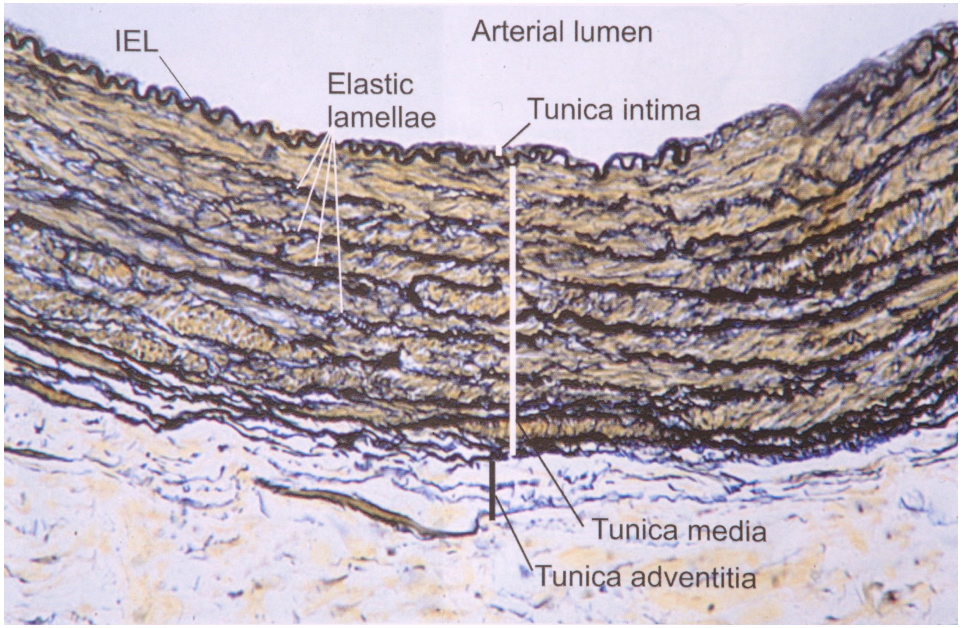

Histological section of an arterial wall (from Ethier and Simmons, 2007).

- **smooth muscle cells;**
- **elastin;**
- **collagen;**
- **proteoglycans.**

The artery wall is a **three-layered structure**.

- **Tunica intima.** The innermost layer is called tunica intima and in a healthy artery is just a few micrometres thick. It consists of **endothelial cells** and their **basal lamina.** Endothelial cells act as a barrier between blood and the artery wall.
- **Tunica media.** The middle layer is known as tunica media and is separated from the intima by a thin elastic surface, called **internal elastic lamina**. From the biomechanics point of view the media is the most important layer as it determines the elastic properties of the arterial wall. It mainly contains:

Anatomical introduction III

Structure of the arterial walls

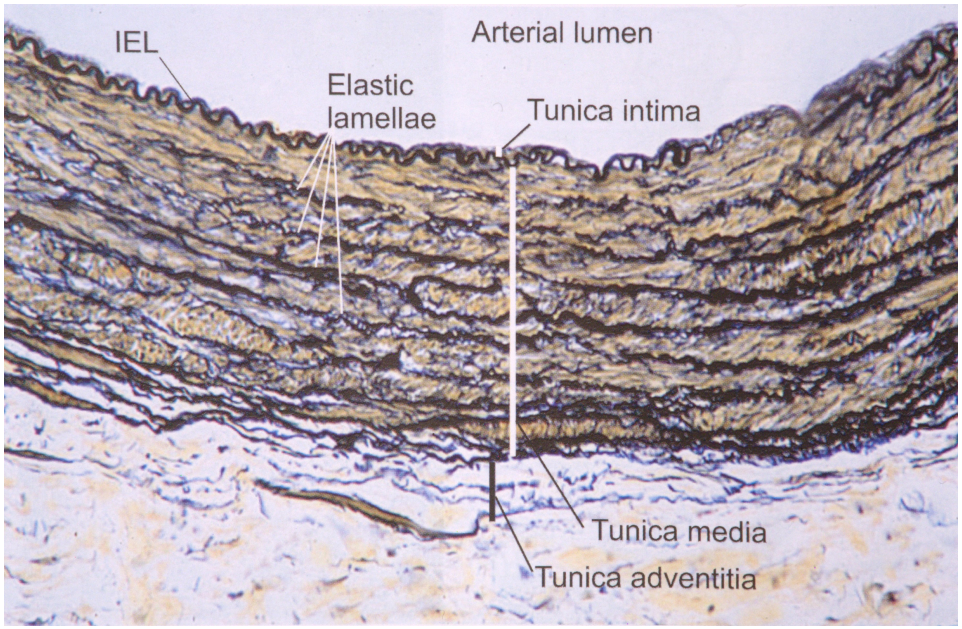

Histological section of an arterial wall (from Ethier and Simmons, 2007).

In the tunica media **smooth muscle cells** are oriented circumferentially and have strong influence on arterial stiffness.

Collagen is also oriented largely circumferentially with a slight helical pattern.

The **relative proportion of elastin to collagen** changes with position in the vascular tree and decreases moving away from the heart.

Anatomical introduction IV

Structure of the arterial walls

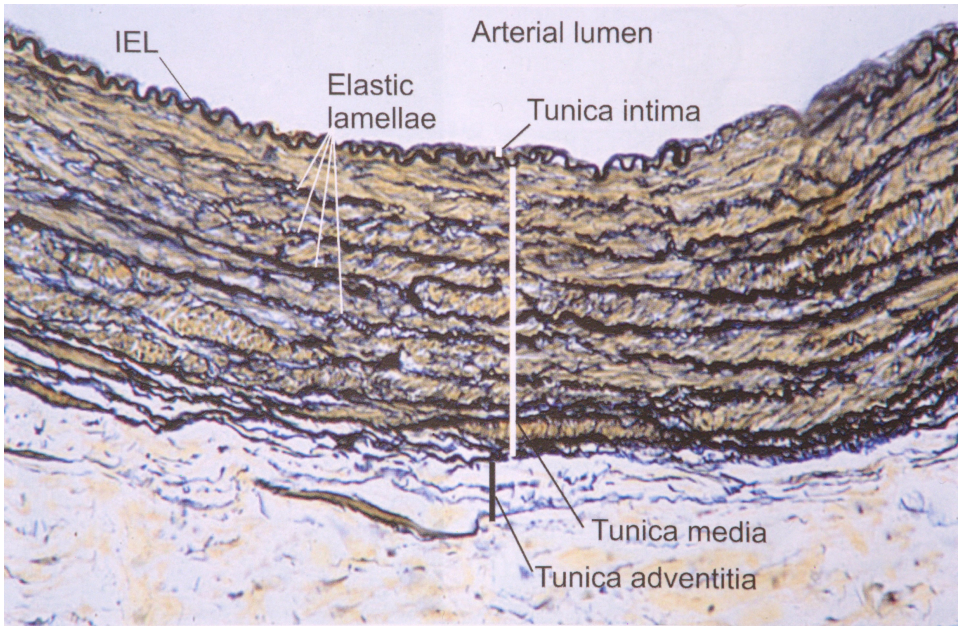

Histological section of an arterial wall (from Ethier and Simmons, 2007).

- **Tunica adventitia.** This layer is separated by the media by the **outer elastic lamina**. The adventitia is a loose connective tissue that contains
  - **collagen;**
  - **nerves;**
  - **fibroblasts;**
  - some **elastic fibres.**

  In some arteries it also contains a vascular network, known as **vasa vasorum**, which provides nutrition to the outer regions of the artery wall.

Anatomical introduction V

The branching network

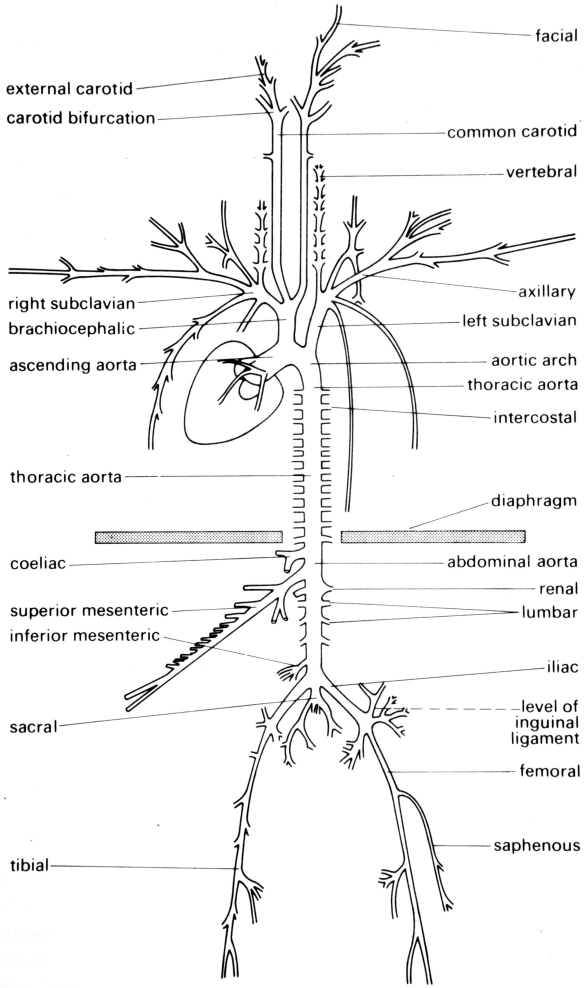

Diagrammatic representation of the major branches in the dog (from Caro et al., 1978).

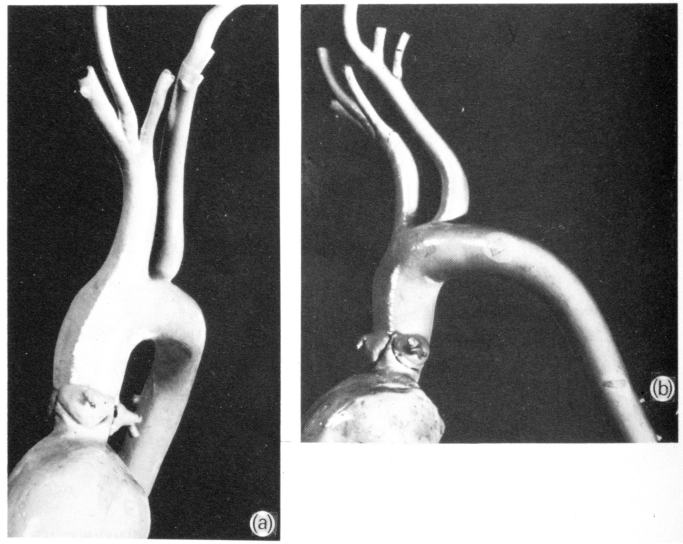

Cast of the dog aorta (from Caro et al., 1978).

The **aorta** originates from the left ventricle. The very first part, for a length of a few centimetres, after the Valsalva sinuses, is almost straight and ascending (**ascending aorta**).
A complicated three-dimensionally curved reach follows (**aortic arch**), characterised by a $\approx 180^\circ$ angle. In correspondence of the aortic arch the **brachiocephalic**, **left common carotid**, and **left subclavian** arteries branch off the aorta, carrying blood to the head and upper limbs.

Anatomical introduction VI

The branching network

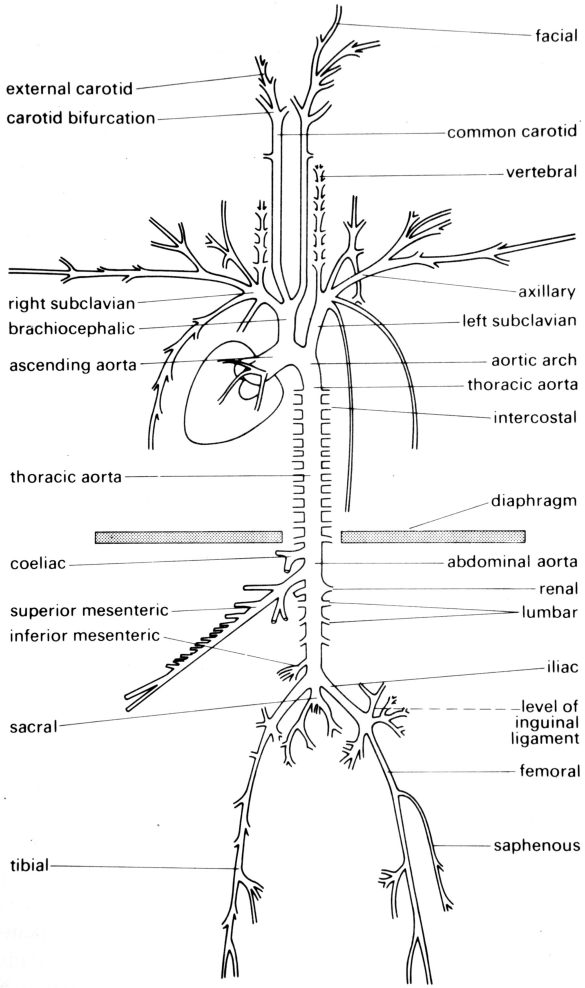

Diagrammatic representation of the major branches in the dog (from Caro et al., 1978).

The aorta then follows a fairly straight and long course down to the abdomen (**descending aorta**). Along this reach several arteries branch off the aorta.

Low down in the abdomen the aorta terminates by dividing into the **iliac arteries** which supply the inferior limbs.

Along its length the aorta tapers. The decrease of the aorta diameter can be described quite accurately with the following law

$$A = A_0 \exp\left(-\frac{Bx}{R_0}\right),$$

where A is the vessel cross-section area, A_0 and R_0 are the area and radius at the upstream site, x is the distance from that upstream site and B is the **taper factor**. Typical values for B range between 0.02 and 0.05.

Anatomical introduction VII

Tapering of the aorta

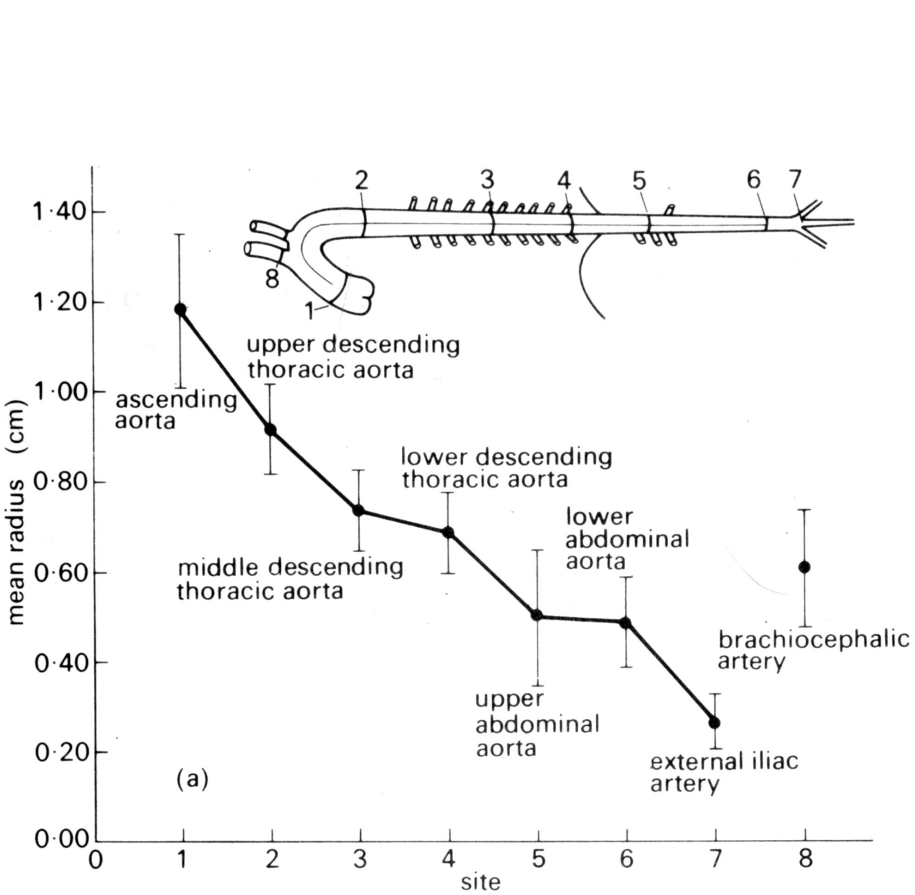

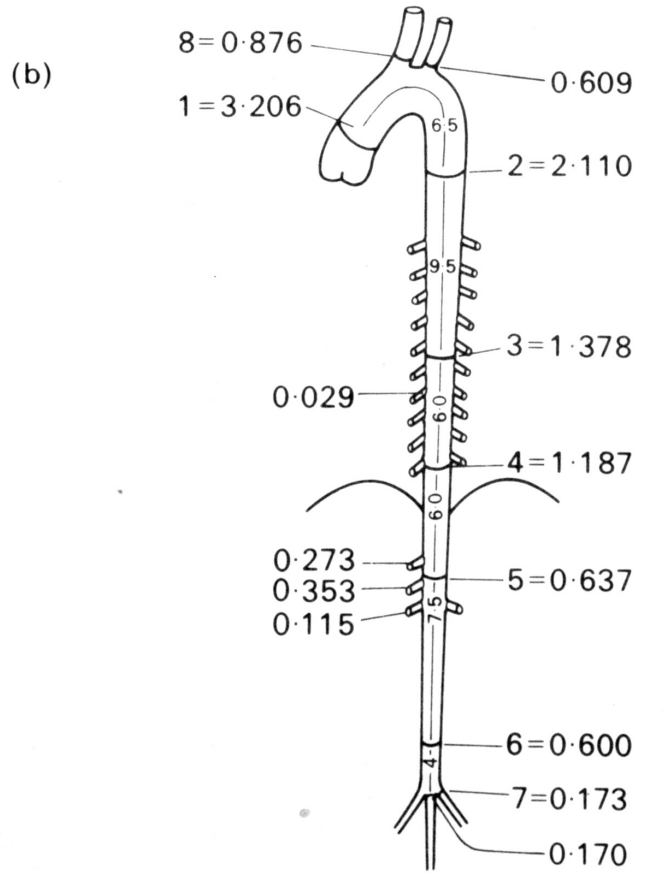

Change in diameter and cross-section area of the canine aorta (from Caro et al., 1978).

Anatomical introduction VIII

Total cross-sectional area of the arterial bed

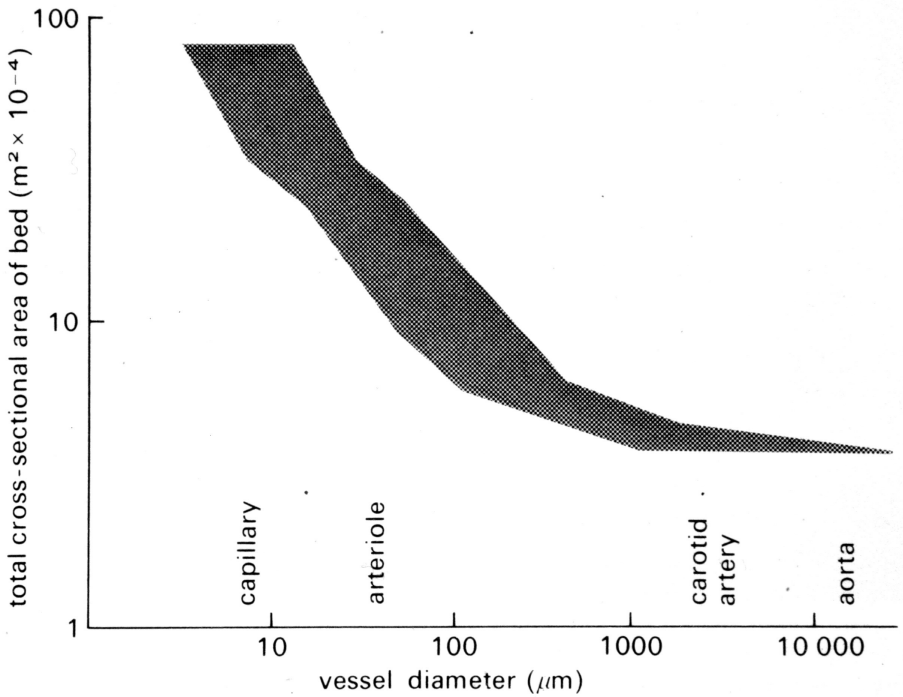

Diagram showing that the cross-section area of the vascular bed grows peripherally (from Caro et al., 1978).

Individual arteries typically taper, however, the total cross-sectional area of the arterial bed increases with distance from the heart.

If we define the **branching ratio** as $(A_2 + A_3)/A_1$, with subscripts 2 and 3 indicating the two daughter vessels and 1 the parent one we find strong variations within the human body, with values ranging between 0.79 to 1.29. We will see that this ratio influences the reflection properties of waves reaching a bifurcation point.

Anatomical introduction IX

The branching network

Artery	No.[a]	R_0 (cm)[b]	Pressure (mmHg) (mmHg)	Radial pulsation (%)[c]	E_p (dyn/cm^2)[d]	Source
Aortic root[e]	1	1.6	–	±4.7	–	Jin *et al.* [23]
Ascending aorta	10	1.42	79–111	±2.9	0.76×10^6	Patel and Fry [24]
Thoracic aorta	12	1.17	98–174	±2.6	1.26×10^6	Luchsinger *et al.* [25]
Femoral	6	0.31	85–113	±0.6	4.33×10^6	Patel *et al.* [24]
Carotid	11	0.44	126–138	±0.5	6.08×10^6	Patel *et al.* [24]
Carotid	16	0.40	96	±7.4	0.49×10^6	Arndt [26]
Carotid	109	–	–	–	0.63×10^6	Riley *et al.* [27]
Pulmonary (main)	8	1.35	16	±5.6	0.16×10^6	Greenfield and Griggs [28]
Pulmonary (left)	5	1.07	25	±6.2	0.17×10^6	Luchsinger *et al.* [25]
Pulmonary (right)	13	1.13	27	±5.8	0.16×10^6	Luchsinger *et al.* [25]
Pulmonary (main)	8	1.43	18–22	±5.4	0.16×10^6	Patel *et al.* [24]

Geometric characteristics of the main vessels in the human body (from Ethier and Simmons, 2007).

The transmural pressure I

The pressure in the systemic arteries fluctuates in time due to the pumping action of the heart. A typical example is reported on the left.

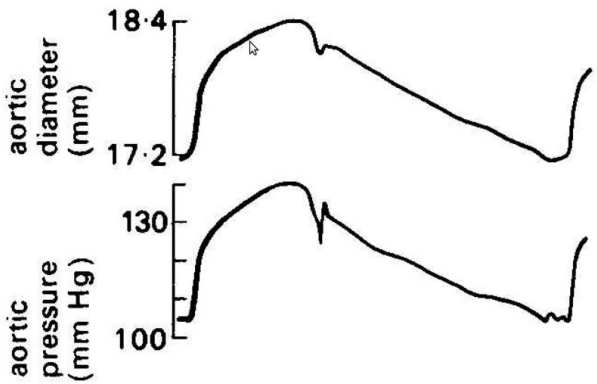

Simultaneous record of pressure and diameter of the aorta during a cardiac cycle (from Caro et al., 1978).

The pressure is clinically measured using a device named **sphygmomanometer**.
Some conventions are customary in measuring arterial blood pressure.

- Pressure is measured in mm Hg. Even if this is not the SI unit for the pressure we will make use of it.
- Blood pressure is always referred to the atmospheric pressure. It is normally considered that out of the arterial wall, i.e. in all tissues of the body, the pressure is equal to the atmospheric one.

The **transmural pressure** p (relative to the atmospheric pressure p_{atm}) is defined as

$$p - p_{atm} = p_i - p_o,$$

with p_i pressure inside the vessel and p_o pressure outside of it. If $p_o = p_{atm}$ as assumed above we simply have

$$p = p_i.$$

The transmural pressure is of great importance in the study of stress in arterial walls.

The transmural pressure II

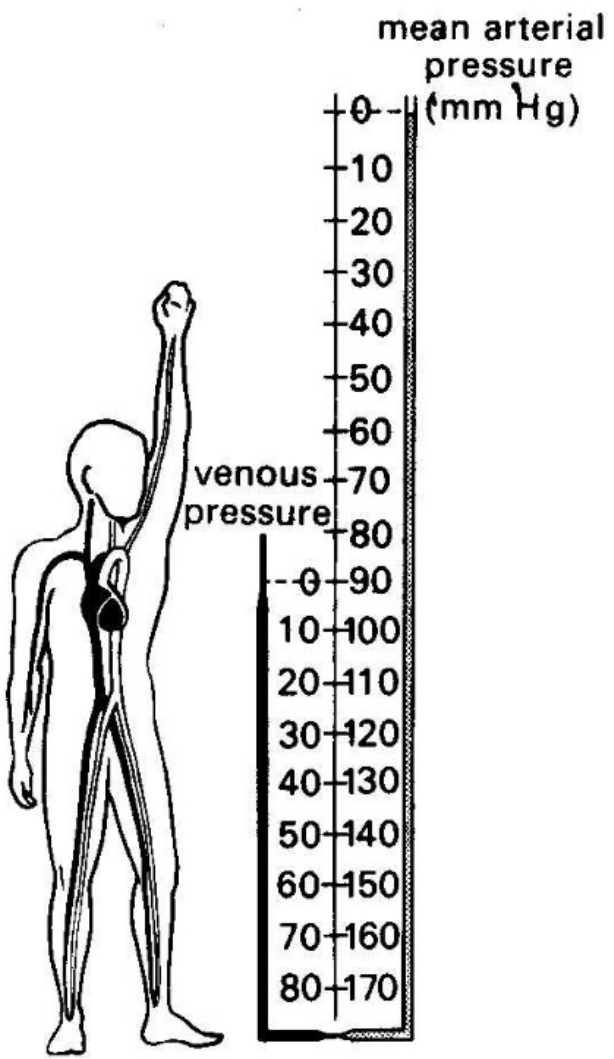

Mean arterial and venous pressure in the human body (from Caro et al., 1978).

Gravity influences significantly the transmural pressure. In fact we can distinguish two different contributions to the transmural pressure:

- **hydrostatic pressure** $-\gamma z$, with z vertically directed coordinate with origin at the level of the right atrium (where the pressure is approximately equal to the atmospheric one);
- **dynamic pressure** P (sometimes referred to as **excess pressure**), which is due the pumping action of the heart.

We can thus write

$$p = P - \gamma z,$$

The hydrostatic contribution can be negative (for instance if we raise our hand above the heart level). The dynamic contribution is obviously always positive.

- In arteries the transmural pressure p is always positive (**arteries cannot collapse**).
- In veins the transmural pressure p can be negative because P is quite small. **Veins can therefore collapse**.

Relationship between transmural pressure and cross-sectional area I

Tension on the wall

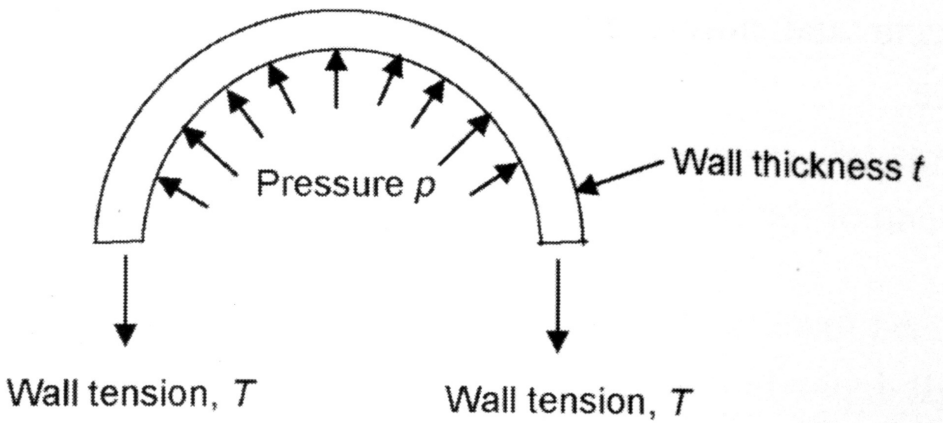

The transmural pressure p can be easily related to the tension T on the wall if we assume:

- circular cross-section;
- infinitely long tube (we neglect side effects);
- constant diameter.
- homogeneous, isotropic and thin wall.

In this case we get

$$T = \frac{pR}{t},$$

where R is the radius of the section and t the wall thickness. This is known as **law of Laplace**.

Relationship between transmural pressure and cross-sectional area II

Pressure-radius relationship in real arteries

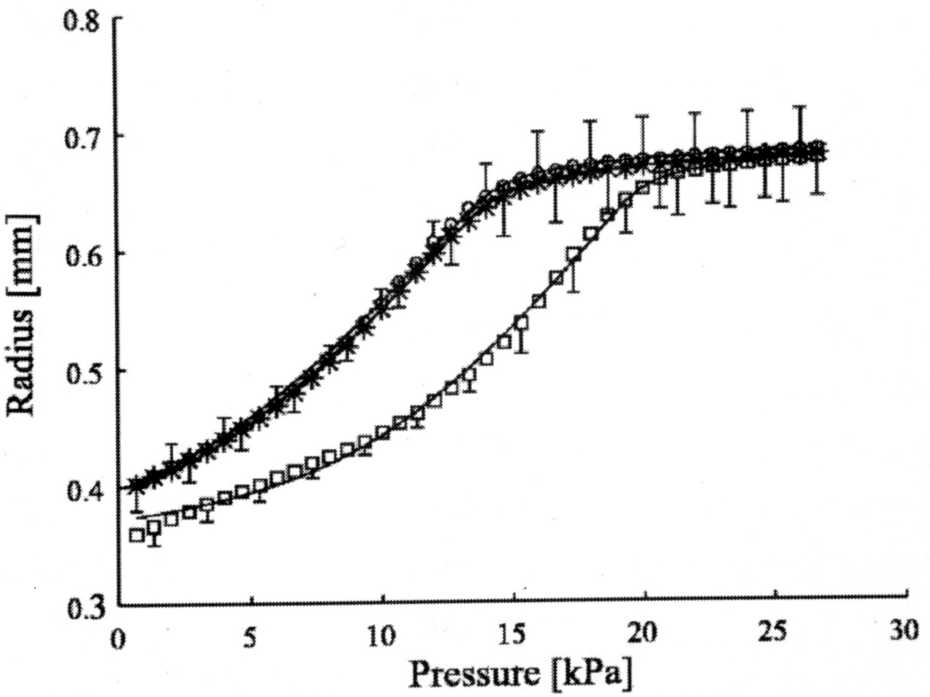

Pressure-radius relationship for the carotid artery of the rat. Each curve refers to a different condition of the vascular smooth muscle (VSM). ($\circ$) fully relaxed VSM, ($*$) normal VSM, ($\square$) maximally contracted VSM (from Ethier and Simmons, 2007).

The arterial wall demonstrates a highly non-linear stress-strain behaviour.

In the figure on the left results from a static inflation test on an excised artery are shown. For a linearly elastic, thin-walled vessel undergoing small deformations a linear pressure-radius relationship is expected.

The figure shows that real arteries experience significant **stiffening** as the lumenal pressure grows.

This reflects the strain-stiffening behaviour of the collagen and elastin contained in the arterial wall.

Relationship between transmural pressure and cross-sectional area III

Pressure-area relationship for negative and positive transmural pressure

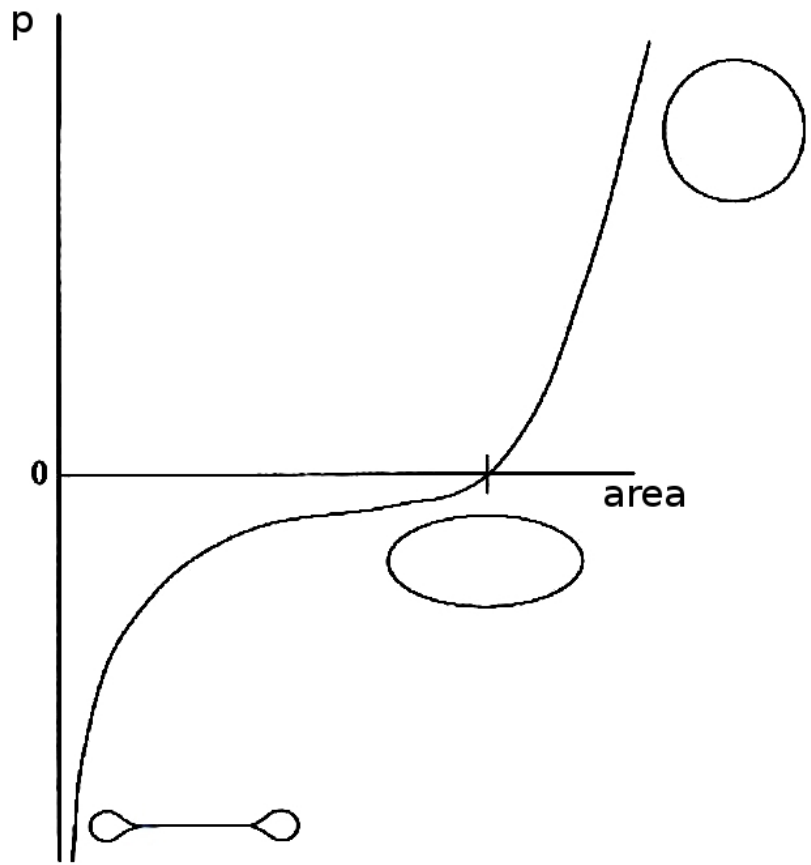

Behaviour of an elastic tube for changing values of the transmural pressure.

Wave propagation in arteries I

Blood dynamics in vessels is not controlled by the transmural pressure but by spatial variations of the dynamic (or excess) pressure P. It is indeed the gradient of the dynamics pressure which drives the flow (see discussion at page 35).

Therefore, **P is often simply referred to as blood pressure**. A scheme of the distribution of P in the systemic circulation is shown below.

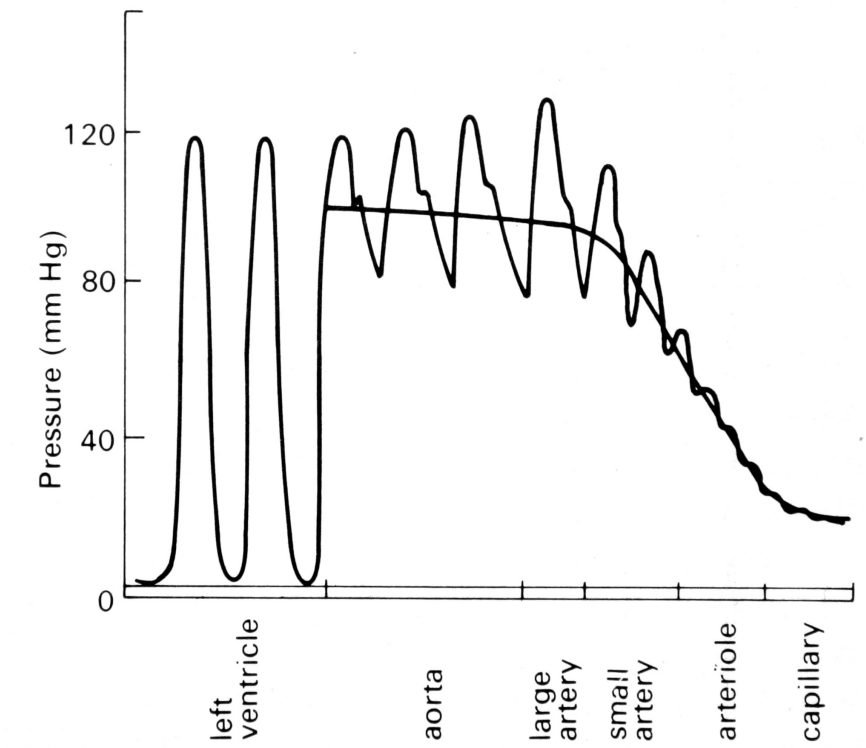

Dynamic pressure and its mean level in the arterial circulation (from Caro et al., 1978).

The time-averaged pressure decreases moving away from the heart due to viscous dissipation. Pressure drop mainly occurs in small vessels.

The pressure unsteadiness progressively decreases as the vessel size decreases.

Here we are mainly concerned with what happens in large arteries, where the pressure and the flow still fluctuate in time.

Note the **growth of the amplitude of fluctuations** along the aorta. This is inherently related to the characteristics of wave propagation that will be dealt with in the following.

Wave propagation in arteries II

Pressure wave

We first examine the **pressure wave**.

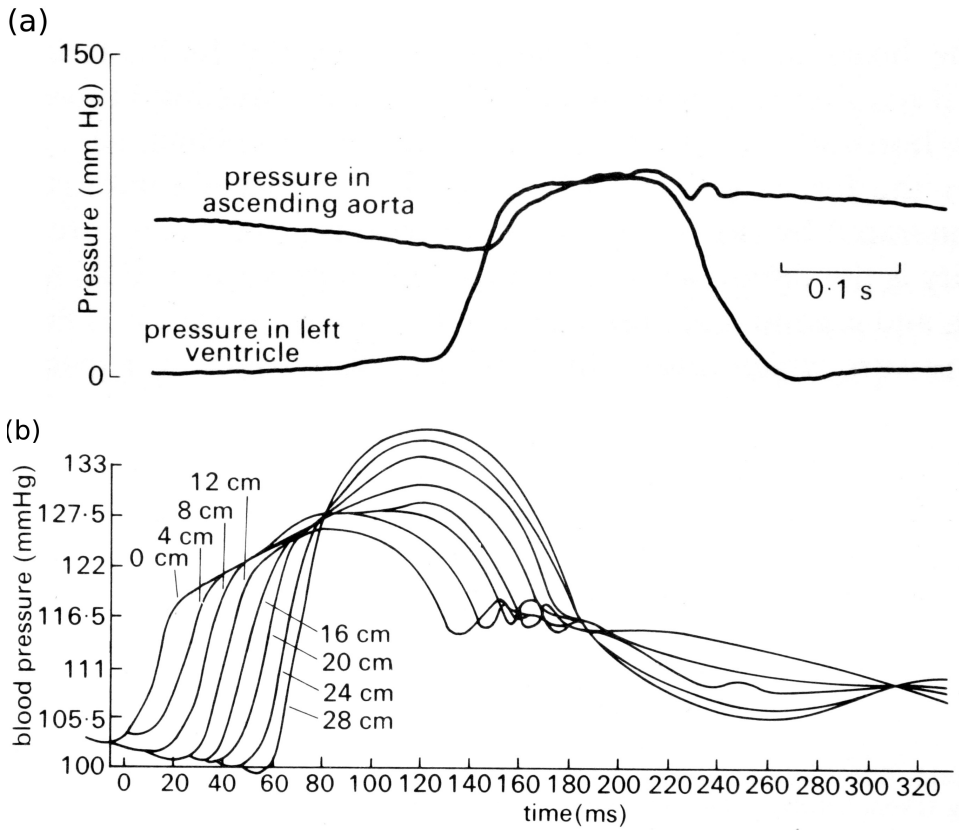

Pressure versus time in (a) the left ventricle and the aorta and (b) at different sites along the aorta (from Caro et al., 1978).

Wave propagation in arteries III

Pressure wave form

We now analyse in detail the different wave forms at different sites along the aorta.

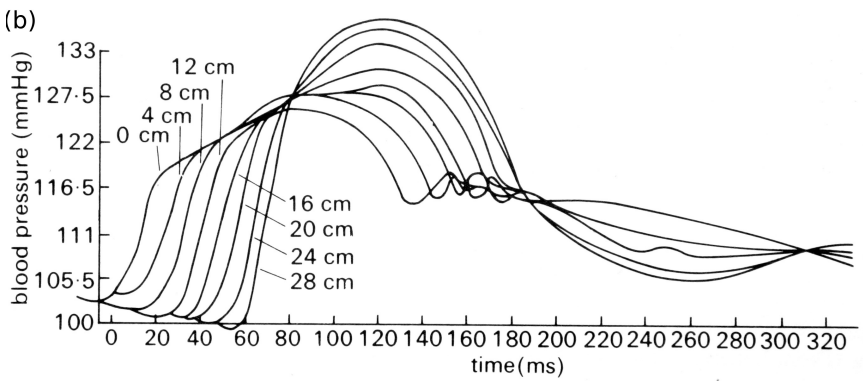

Pressure versus time at different sites in along the aorta (from Caro et al., 1978).

- The wave changes form.
- It steepens and increases its amplitude. Thus **the systolic pressure increases with distance from the heart**.
- The amplification process continues (in the dog) up to the third generation of branches (with a diameter of approximately 1-2 mm).
- Thereafter, both the oscillation and the mean pressure decrease.

- The mean pressure steadily decreases with distance from the heart even if this is hard to see from the above figure.

Wave propagation in arteries IV

Changes of the cross-sectional area

As the pressure wave passes through a cross-section **the cross-sectional area also changes due to the compliance of the vessel wall**.

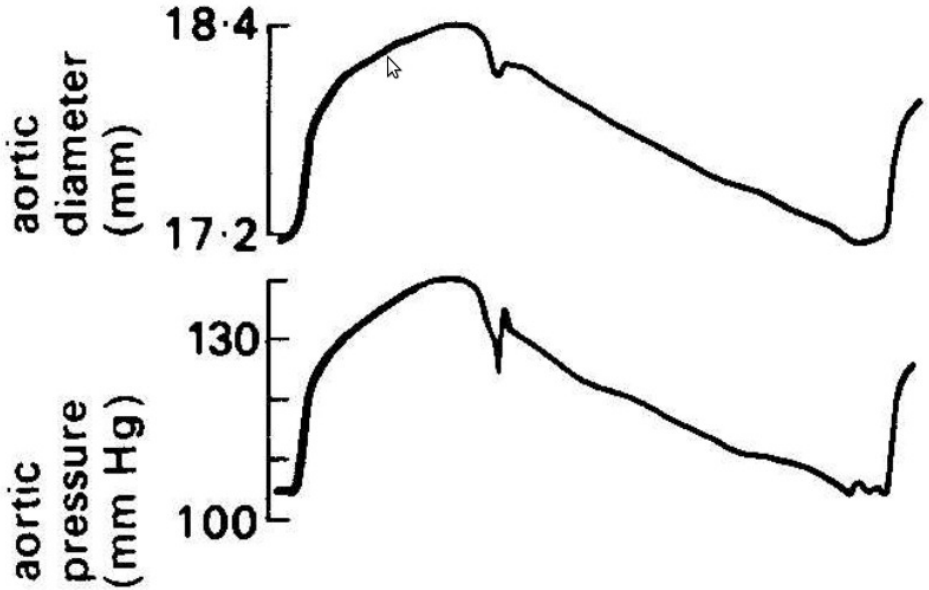

Simultaneous records of pressure and diameter of the aorta during a cardiac cycle (from Caro et al., 1978).

Wave propagation in arteries V

Flow wave

As the pressure and its gradient fluctuate in time the flow also does. Therefore the flow in large arteries is **unsteady**.

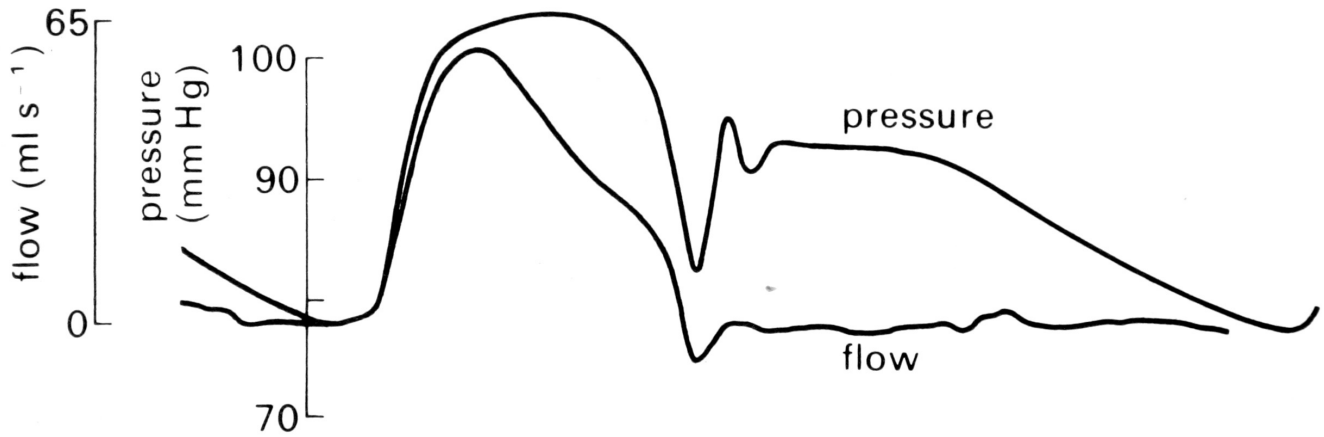

Simultaneous records of pressure and flow in the ascending aorta (from Caro et al., 1978).

- Forward motion in the ascending aorta starts after the aortic valve opens;
- the velocity rises very rapidly to a peak;
- then it falls off more slowly;
- there is a short phase of backward flow before the complete closure of the aortic valve.
- Pressure and flow waveforms are similar in the systolic phase and are clearly different during diastole.

Wave propagation in arteries VI

Pressure and flow waves

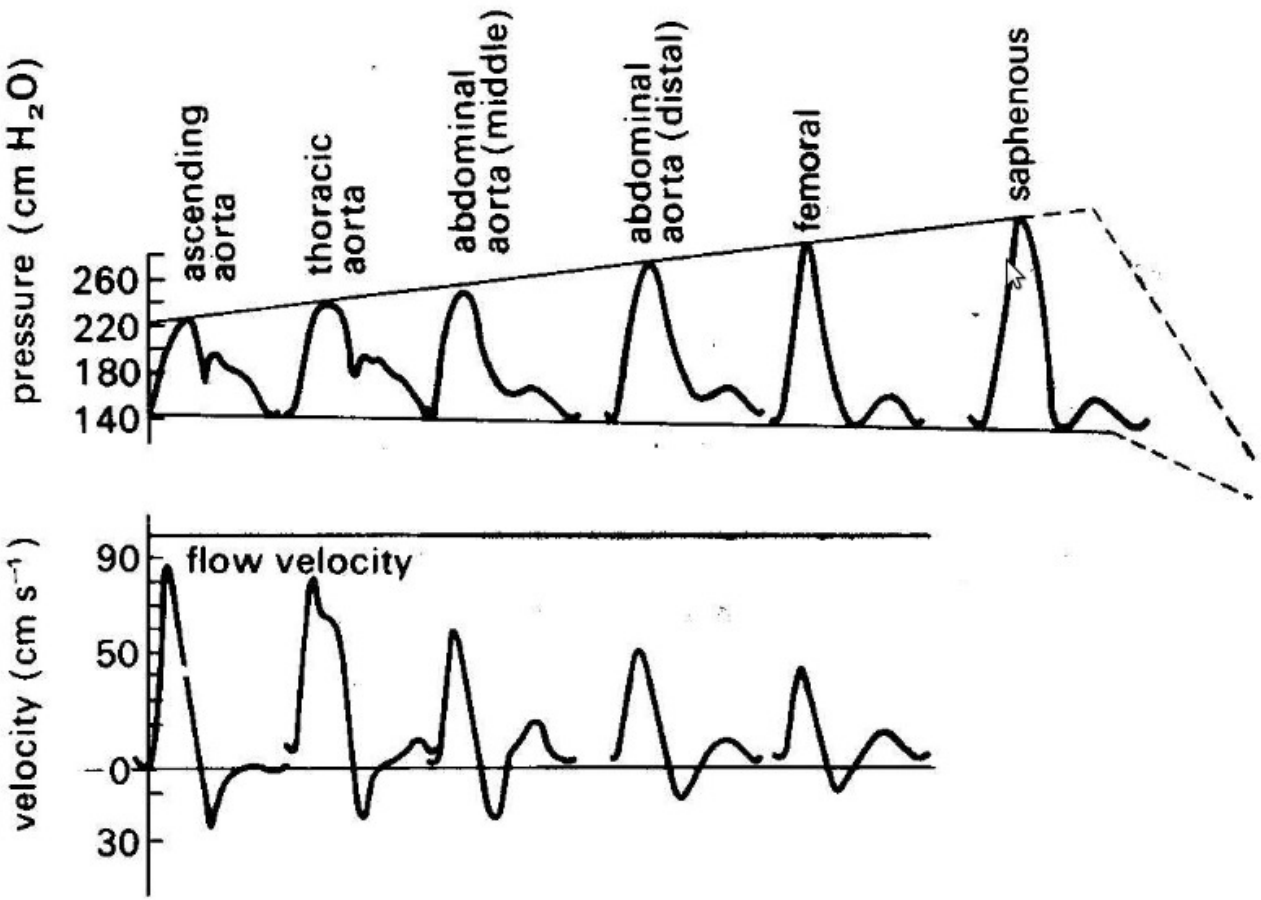

Records of pressure and velocity at different sites of the arterial system (from Caro et al., 1978).

Wave propagation in arteries VII

Pressure and flow waves

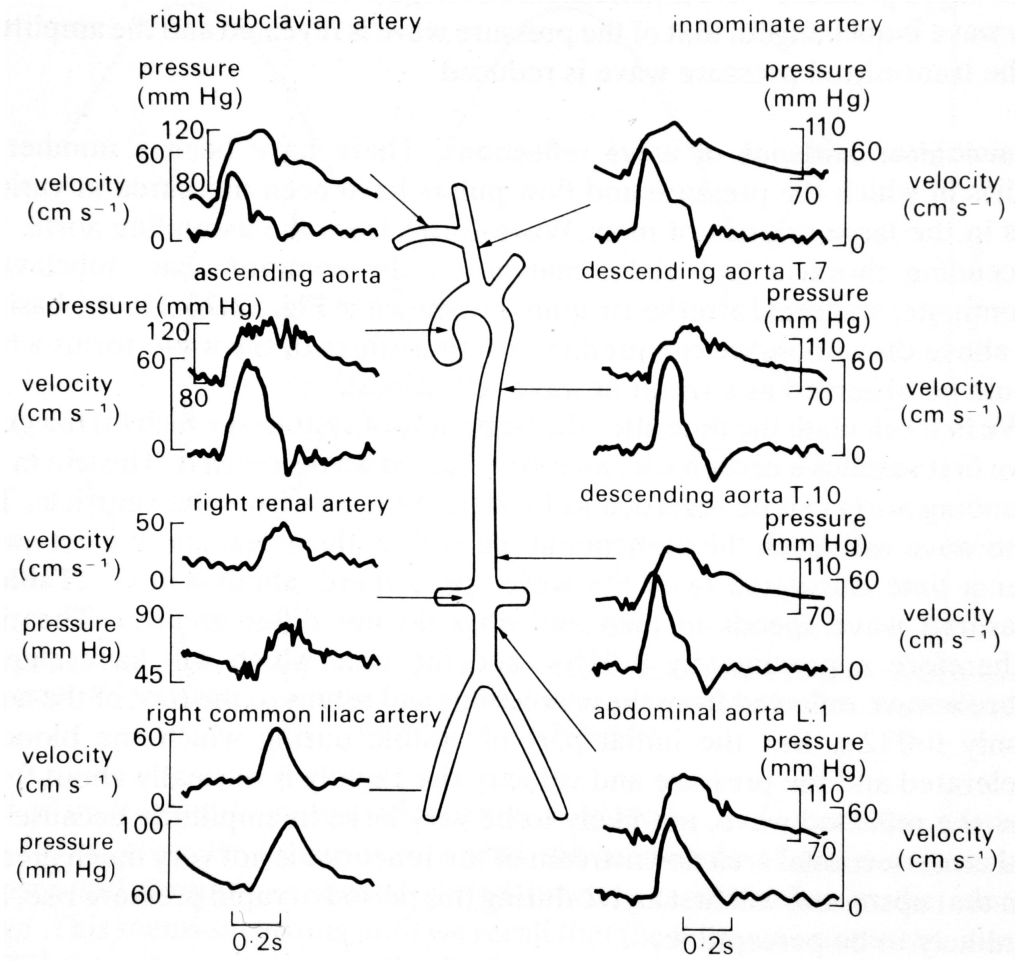

Simultaneous records of pressure and velocity at different sites in the human arterial system (from Ethier and Simmons, 2007).

The Windkessel model I

Formulation of the problem

The simplest possible model of the arterial flow is based on a **0-dimensional** schematisation of the system. The arterial system is described as a compliant reservoir in which a blood flux Q_h enters from the heart and from which a blood flux Q exits to the venous system.
In 0-dimensional models there is not spatial description of the arterial network. This implies that **wave propagation can not be described**. The model was originally proposed by Otto Frank in 1899 and it is known as **windkessel model** (in German windkessel means air chamber).

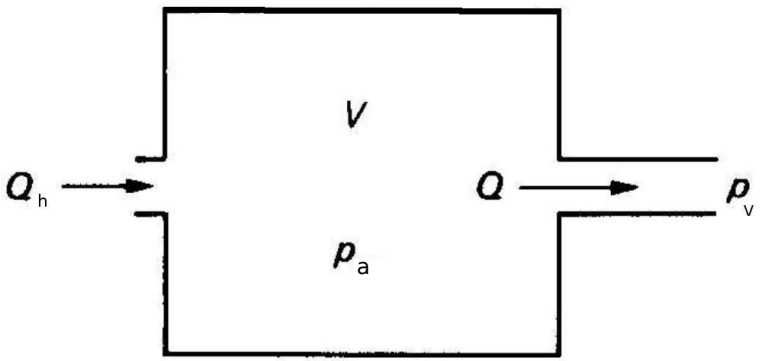

Scheme of the windkessel model.

If the arterial system consisted of a single long, straight tube the volume flux Q through it ($= Q_a$) could be expressed, according to Poiseuille law (62), as

$$Q = \frac{P_a - P_v}{R},$$

with P_a pressure in the arterial system (just downstream of the heart) and P_v pressure in veins, and with R a constant **resistance** ($[R] = \mathrm{L}^{-4}\ \mathrm{T}^{-1}\ \mathrm{M}$).

In the windkessel model this approach is adopted, and since $P_v \approx 0$, we may write

$$P_a \approx RQ. \tag{69}$$

The Windkessel model II

The arterial system is considered compliant and its volume V is related to the arterial pressure by the following relationship

$$P_a = V/C, \tag{70}$$

where C is a **constant compliance** ($[C] = L^4 T^2 M^{-1}$).
In 0-dimensional models there is no equation of motion and only the conservation of mass is imposed. In this case the continuity equation can be written as

$$\frac{dV}{dt} = Q_h - Q, \tag{71}$$

where Q_h denotes the flux ejected by the heart into the arterial system and Q is the flux from the arterial system to veins. Note that Q does not need be equal to Q_h because of the compliance of the arterial system (which implies that $V(t)$ depends on time). Substituting (69) and (70) into (71) we obtain

$$\frac{dV}{dt} = Q_h - \frac{V}{RC}. \tag{72}$$

The Windkessel model III

Solution

Equation (72) is easily solved once Q_h is known.

- **Diastolic phase**

  During diastole $Q_h = 0$ and we get

$$V(t) = c \exp\left(-\frac{t}{RC}\right) \quad \Rightarrow \quad P_a(t) = \frac{c}{C} \exp\left(-\frac{t}{RC}\right),$$

  with c constant. This predicts an exponential decay in time of the arterial pressure. Such behaviour is quite closely satisfied in practise.

- **Systolic phase**

  The general solution of equation (72) is

$$V(t) = \left[\int Q_h(t) \exp\left(\frac{t}{RC}\right) dt + c\right] \exp\left(-\frac{t}{RC}\right).$$

  Note, however that during systole $Q = V/RC$ is very small ($\ll Q_h$) and, at leading order, equation (72) implies

$$\frac{dV(t)}{dt} \propto Q_h \quad \Rightarrow \quad \frac{dP_a(t)}{dt} \propto Q_h.$$

  Experimental observations show, however, that it is P_a to be approximately proportional to Q_h.

The Windkessel model IV

In conclusion, **the Windkessel model reproduces fairly well the pressure decay during diastole but is unable to correctly model the systolic phase.**

Analytical solutions of the flow in a straight pipe I

We now consider various analytical solutions of unidirectional pipe flows relevant for the flow in arteries.

Axisymmetric Poiseuille flow

Let us now consider a steady, fully developed flow in a straight pipe with circular cross-section of radius R. Let the pipe axis be in the z direction and let the flow be axisymmetric. In cylindrical coordinates (z, r, φ) the velocity vector takes the form $\mathbf{u} = [u(r), 0, 0]$, with u velocity component in the z direction. The flow is generated by a constant pressure gradient in the z direction, which we denote by $dp/dz = -\chi$, with $\chi > 0$.

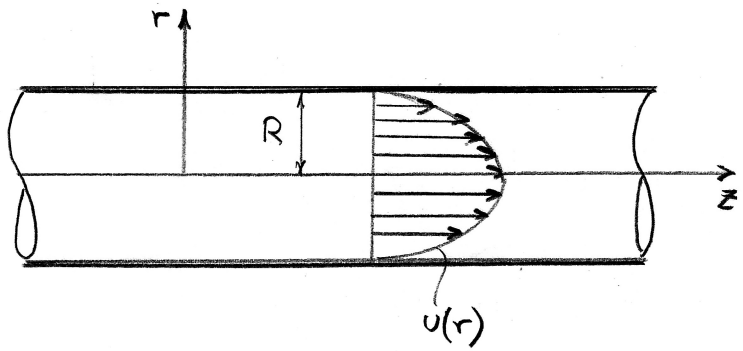

The Navier-Stokes equation in the r direction reads

$$\frac{d^2u}{dr^2} + \frac{1}{r}\frac{du}{dr} = -\frac{\chi}{\mu}, \quad \Rightarrow \quad \frac{1}{r}\frac{d}{dr}\left(r\frac{du}{dr}\right) = -\frac{\chi}{\mu}. \tag{73}$$

The above equation has to be solved subjected to the no-slip boundary condition at $r = R$ and a regularity condition in $r = 0$.
We then have

$$r\frac{du}{dr} = -\frac{\chi}{2\mu}r^2 + c_1, \quad \Rightarrow \quad u = -\frac{\chi}{4\mu}r^2 + c_1 \log r + c_2.$$

Analytical solutions of the flow in a straight pipe II

Regularity at $r = 0$ imposes $c_1 = 0$. Moreover, enforcing the no-slip boundary condition yields $c_2 = \frac{\chi}{4\mu} R^2$. The solution is

$$u = \frac{\chi}{4\mu} \left(R^2 - r^2 \right). \tag{74}$$

This is known as **Poiseuille flow**. The velocity profile is a paraboloid. The volume flux Q is given by

$$Q = \int_0^R \int_0^{2\pi} u r d\varphi dr = \frac{\chi \pi}{8\mu} R^4. \tag{75}$$

Written in cylindrical coordinates (z, r, φ) the stress tensor $\boldsymbol{\sigma}$ for this flow field takes the form

$$\boldsymbol{\sigma} = \begin{pmatrix} 0 & \mu \frac{du}{dr} & 0 \\ \mu \frac{du}{dr} & 0 & 0 \\ 0 & 0 & 0 \end{pmatrix} - p\mathbf{I}.$$

Then, noting that the unit vector normal to the wall is $\mathbf{n} = (0, 1, 0)^T$, we easily compute the tangential stress τ on the wall, which reads

$$\tau = -\frac{\chi R}{2}.$$

Analytical solutions of the flow in a straight pipe III

Transient flow in a pipe

We now consider the transient flow generated in a pipe by a sudden imposition on a constant pressure gradient $\partial p/\partial z = -\chi$ at the time $t = 0$. We assume that the fluid is at rest for $t < 0$. Thus we now need to solve

$$\frac{\partial u}{\partial t} - \frac{\chi}{\rho} - \nu\left(\frac{\partial^2 u}{\partial r^2} + \frac{1}{r}\frac{\partial u}{\partial r}\right) = 0, \tag{76}$$

subject to the conditions

$$\begin{aligned} u &= 0 && (r = R), \\ \text{regularity} && (r = 0), \\ u &= 0 && (t < 0) \end{aligned}$$

For long times the solution should tend to the steady Poiseuille solution, which satisfies equation (73).
To compute the solution, taking advantage of the linearity of the governing equation, we decompose it into a the Poiseuille flow profile u_s and a transient profiles u_t that decays at long times:

$$u(r, t) = u_s(r) + u_t(r, t), \tag{77}$$

where

$$u_s = \frac{\chi}{4\mu}\left(R^2 - r^2\right).$$

Analytical solutions of the flow in a straight pipe IV

Substituting (77) into (76) we find the following homogeneous equation for u_t

$$\frac{\partial u_t}{\partial t} - \nu \left(\frac{\partial^2 u_t}{\partial r^2} + \frac{1}{r} \frac{\partial u_t}{\partial r} \right) = 0. \tag{78}$$

We seek a separate variable solution in the form

$$u_t(r,t) = \sum_{n=1}^{\infty} c_n \phi_n(r) \psi_n(t), \tag{79}$$

where c_n are constant coefficients. Substituting into (78) we obtain

$$\sum_{n=1}^{\infty} c_n \phi_n(r) \psi_n(t) \left[\frac{1}{\psi_n(t)} \frac{d\psi_n(t)}{dt} - \frac{\nu}{\phi_n(r)} \left(\frac{d^2 \phi_n(r)}{dr^2} + \frac{1}{r} \frac{d\phi_n(r)}{dr} \right) \right] = 0.$$

Since the first term within the square brackets is only a function of time and the second only of space, for the above equation to be satisfied for each values of t and r it must be

$$\frac{1}{\psi_n} \frac{d\psi_n}{dt} = \frac{\nu}{\phi_n} \left(\frac{d^2 \phi_n}{dr^2} + \frac{1}{r} \frac{d\phi_n}{dr} \right) = -\nu b_n^2,$$

Analytical solutions of the flow in a straight pipe V

where on the right hand side of the second equality b_n^2 are positive constants, ν has been introduced for convenience of the following calculations and the minus sing is needed for u_t to be a decaying function in time.
We thus need to solve the two following ordinary differential equations

$$\frac{d\psi_n}{dt} + \nu b_n^2 \psi_n = 0, \tag{80}$$

$$\frac{d^2\phi_n}{dr^2} + \frac{1}{r}\frac{d\phi_n}{dr} + b_n^2 \phi_n = 0. \tag{81}$$

- Equation (80) is easily solved and the solution reads

$$\psi_n(t) = \exp(-\nu b_n^2 t), \tag{82}$$

which shows that the transient component of the velocity decays exponentially in time. Note that we do not include in the above expression the constant of integration as is would be absorbed in the u_s component of the velocity.

Analytical solutions of the flow in a straight pipe VI

- Equation (81) can be conducted to the Bessel equation, discussed in Appendix 8. Substituting into equation (142) $b_n r$ to x we obtain the solution

$$\phi_n(r) = J_0(b_n r). \tag{83}$$

We note that we have discarded the solution $Y_o(b_n r)$ since it does not satisfied the regularity condition at the origin.
In order to impose the boundary condition at the wall ($r = R$) we need to impose

$$\phi_n(R) = J_0(b_n R) = 0.$$

In other words $b_n R = \alpha_n$ has to be a root of the Bessel function J_0. These roots are easily determined numerically and the first 6 are reported below

$\alpha_1 = 2.4048$	$\alpha_2 = 5.5201$	$\alpha_3 = 8.6537$
$\alpha_4 = 11.7915$	$\alpha_5 = 14.9309$	$\alpha_6 = 18.0711$

Substituting (82) and (83) into (79) we obtain

$$u_t(r,t) = \sum_{n=1}^{\infty} c_n J_0\left(\frac{\alpha_n r}{R}\right) \exp\left(-\frac{\alpha_n^2 \nu t}{R^2}\right).$$

An estimate of the time T required for the transient flow is given by $T \approx R^2/[\min(\alpha_n^2)\nu]$.

Analytical solutions of the flow in a straight pipe VII

Example

- Let us consider a large artery, so that $R = 0.01$ m. Assuming, $\nu = 3 \times 10^{-6}$ m^2/s, $\min(\alpha_n) = \alpha_1 = 2.4048$.
  In this case we obtain $T \approx 5.8$ s, which is much larger that the time scale of the cardiac beat.
- Let us consider a small artery, so that $R = 5 \times 10^{-4}$ m. In this case we obtain $T \approx 0.01$ s, which is small compared to the time scale of the cardiac beat.

Analytical solutions of the flow in a straight pipe VIII

We finally need to compute the coefficients c_n by imposing the initial condition, i.e.

$$\sum_{n=1}^{\infty} c_n J_0\left(\frac{\alpha_n r}{R}\right) = -\frac{\chi}{4\mu}\left(R^2 - r^2\right). \tag{84}$$

To this end we make use of the orthogonality properties of Bessel functions, i.e. equation (143). Substituting x with r/R in (143) we obtain

$$\int_0^R r J_n\left(\frac{\alpha_i}{R} r\right) J_n\left(\frac{\alpha_j}{R} r\right) dr = \begin{cases} \frac{R^2}{2} J_{n+1}^2(\alpha_i) & \text{if } (i = j), \\ 0 & \text{if } (i \neq j). \end{cases}$$

Multiplying (84) by $rJ_o(\frac{\alpha_m}{R} r)$ on both sides and integrating with respect to r from 0 to R we obtain

$$c_m = -\frac{\chi}{2\mu R^2 J_1^2(\alpha_m)} \int_0^R \left(R^2 - r^2\right) r J_0\left(\frac{\alpha_m}{R} r\right) dr = -\frac{2R^2\chi}{\mu \alpha_m^3 J_1(\alpha_m)}.$$

Thus the solution for u reads

$$u = \frac{\chi}{4\mu}\left[R^2 - r^2 - 8R^2 \sum_{n=1}^{\infty} \frac{1}{\alpha_n^3} \frac{J_0\left(\frac{\alpha_n r}{R}\right)}{J_1(\alpha_n)} \exp\left(-\frac{\alpha_n^2 \nu t}{R^2}\right)\right]. \tag{85}$$

Analytical solutions of the flow in a straight pipe IX

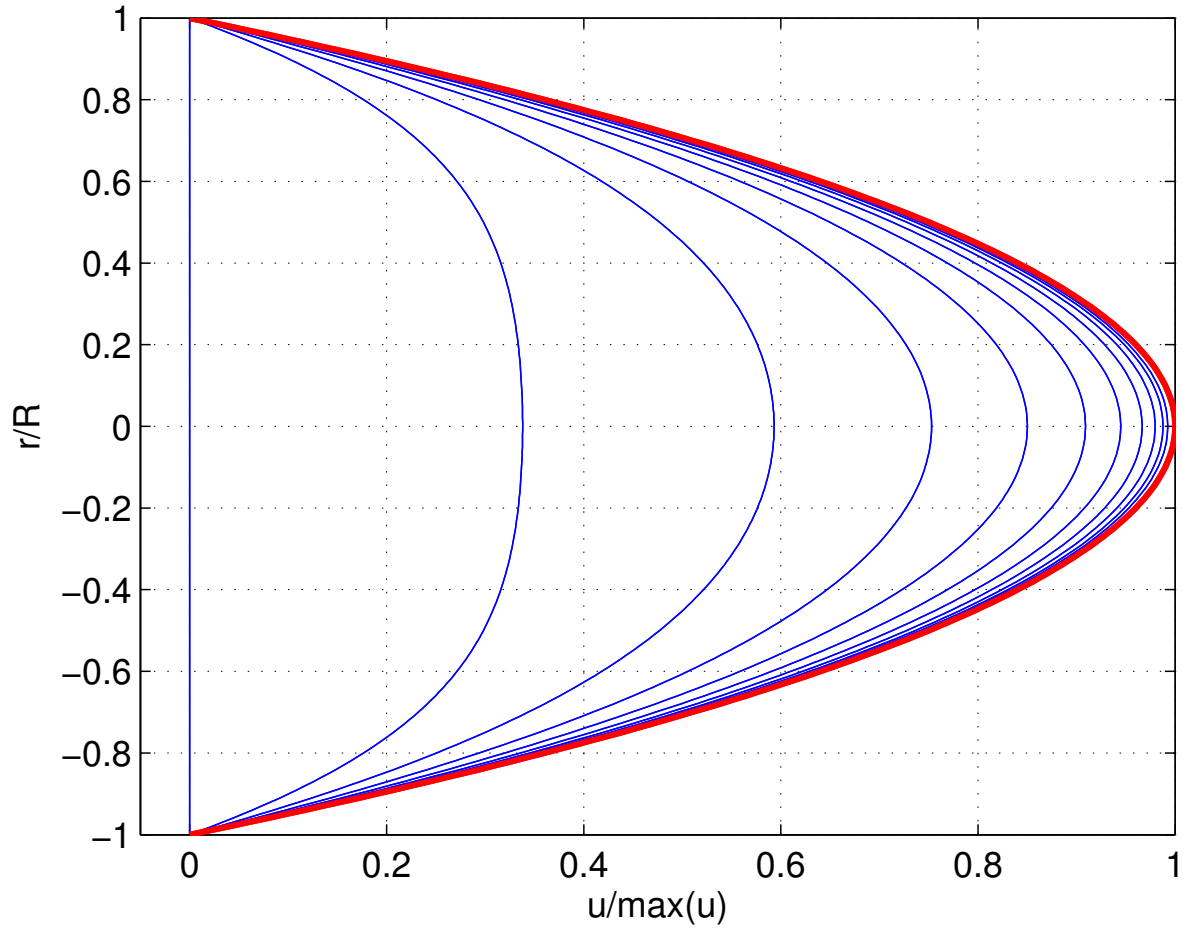

The solution (85) is reported in dimensionless form in the figure above at various times. Poiseuille solution is also reported, in red.

Analytical solutions of the flow in a straight pipe X

Womersley flow

We now consider the so called **Womersley flow**, i.e. the flow induced in a straight pipe by an oscillatory pressure gradient.
We assume

$$\chi(t) = \hat{\chi} e^{i\omega t} + c.c.$$

where $\hat{\chi}$ is a constant.
We thus need to solve the following problem

$$\frac{\partial u}{\partial t} - \frac{1}{\rho}\left(\hat{\chi} e^{i\omega t} + c.c.\right) - \nu\left(\frac{\partial^2 u}{\partial r^2} + \frac{1}{r}\frac{\partial u}{\partial r}\right) = 0, \tag{86}$$

subject to the conditions

$$\begin{aligned} u &= 0 && (r = R), \\ &\text{regularity} && (r = 0). \end{aligned}$$

We seek a solution in the form

$$u(r,t) = \hat{u}(r) e^{i\omega t} + c.c. \tag{87}$$

Substituting (87) into (86) and deviding throughout by $e^{i\omega t}$ we obtain the following ODE

$$i\omega\hat{u} - \frac{\hat{\chi}}{\rho} - \nu\left(\frac{d^2\hat{u}}{dr^2} + \frac{1}{r}\frac{d\hat{u}}{dr}\right) = 0.$$

Analytical solutions of the flow in a straight pipe XI

Introducing the new variable $s = \sqrt{-i\omega/\nu}r$ the above equation can be written as

$$s^2 \frac{d^2\hat{u}}{ds^2} + s\frac{d\hat{u}}{ds} + s^2\hat{u} + s^2\frac{i\hat{\chi}}{\omega\rho} = 0. \tag{88}$$

This is a linear non–homogeneous ODE, thus we can write the solution as

$$\hat{u} = \hat{u}_h + \hat{u}_p,$$

where u_h is the solution of the associated homogeneous problem and u_p is a particular solution. The associated homogeneous equation is Bessel equation (142) (with $\alpha = 0$), therefore

$$\hat{u}_h = c_1 J_0(s) + c_2 Y_0(s).$$

Upon substitution into (88) it is easily verified that the particular solution is

$$\hat{u}_p = -\frac{i\hat{\chi}}{\omega\rho}.$$

Hence, moving back to the variable r, we have

$$\hat{u}(r) = c_1 J_0\left(\sqrt{\frac{-i\omega}{\nu}}r\right) + c_2 Y_0\left(\sqrt{\frac{-i\omega}{\nu}}r\right) - \frac{i\hat{\chi}}{\omega\rho},$$

Analytical solutions of the flow in a straight pipe XII

In order for the solution to be bounded in $r = 0$ it must be $c_2 = 0$. The other constant, c_1, is determined imposing the no slip condition at the wall. We define the **Womersley number** as

$$\alpha = \sqrt{\frac{\omega}{\nu}} R,$$

and find

$$c_1 = \frac{i\hat{\chi}}{\rho\omega} \frac{1}{J_o\left(\sqrt{-i}\alpha\right)}.$$

Therefore, the final expression for the solution is

$$u = \frac{i\hat{\chi}}{\rho\omega} \left(\frac{J_o\left(\sqrt{-i}\alpha r/R\right)}{J_o\left(\sqrt{-i}\alpha\right)} - 1 \right) e^{i\omega t} + c.c.$$

In dimensionless form the above expression reads

$$u^* = i \left(\frac{J_o\left(\sqrt{-i}\alpha r^*\right)}{J_o\left(\sqrt{-i}\alpha\right)} - 1 \right) e^{it^*} + c.c., \tag{89}$$

where $u^* = u/[\hat{\chi}/(\rho\omega)]$, $R^* = r/R$, $t^* = \omega t$.

Analytical solutions of the flow in a straight pipe XIII

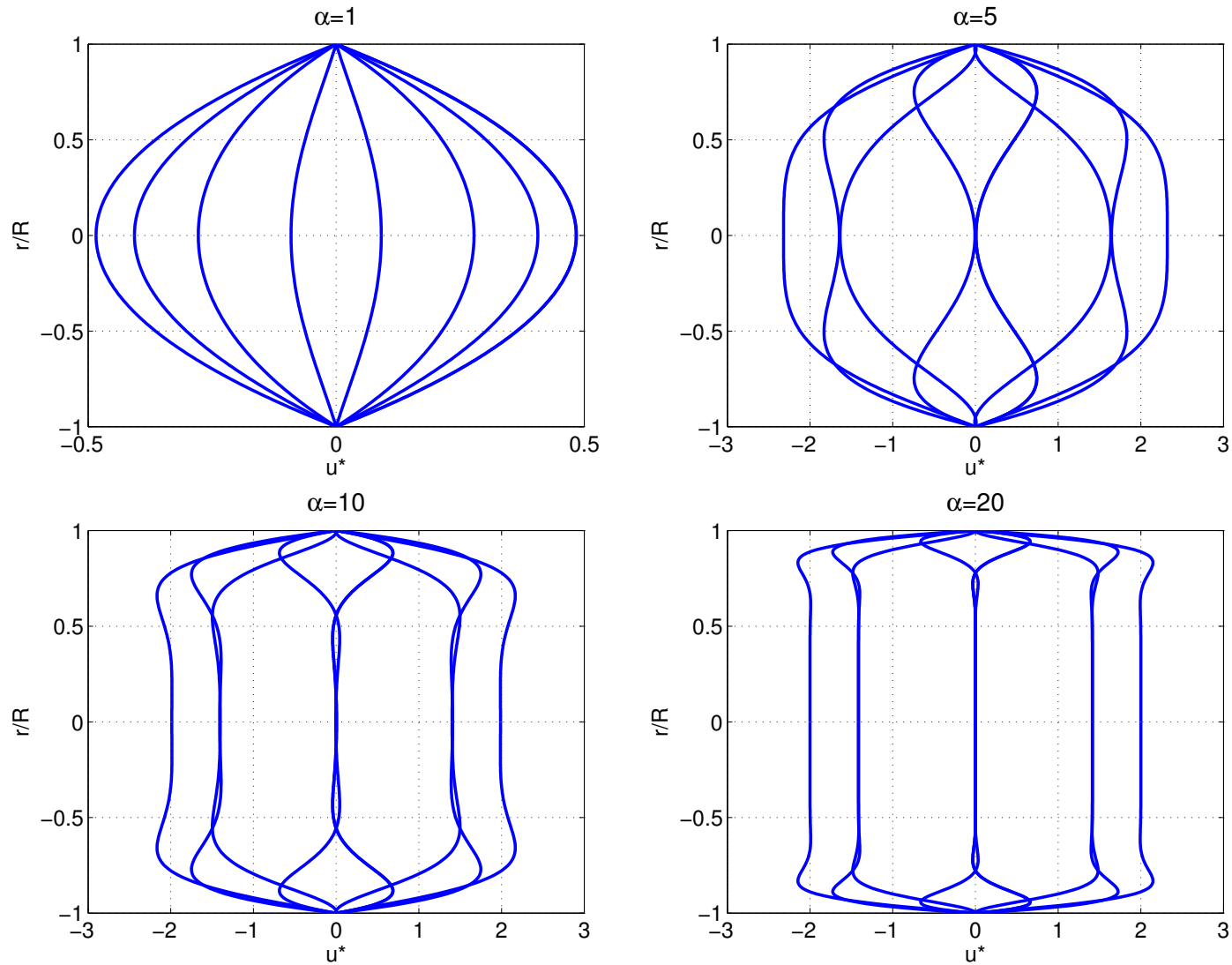

The solution (89) is shown for different values of α.

Characteristics of the flow in a curved pipe I

Arteries are seldom straight. In particular a lot of attention has been devoted to study flow characteristics in the aortic arch. We now briefly describe the characteristics of a flow in a curved pipe.

- We assume that the flow is driven by a constant pressure gradient χ in the longitudinal direction.
- The flow is steady.
- We assume for simplicity that the mean radius of curvature of the pipe $\overline{\mathcal{R}}$ is constant.
- In order for a fluid particle to travel along a curved trajectory with radius of curvature $\overline{\mathcal{R}}$ with a constant velocity u it must be acted on by a lateral force to give it a transverse acceleration equal to $u^2/\overline{\mathcal{R}}$.
- This lateral force has to provided by a transverse pressure gradient.
- The pressure gradient acting on all particles on a cross–section of the flow (a plane orthogonal to the axis of the pipe) is approximately constant.
- The velocity of fluid particles on the cross–section is not constant, owing to the no slip condition at the pipe wall.
- Therefore, particles in the centre of the cross-section will be drifted towards the outer wall of the pipe and, similarly, particles close to the wall will be drifted towards the inner wall.
- The result of this is the formation of two counter rotating vortices, known as **Dean vortices.** Their formation was first explained theoretically by Dean (1928).
- The streamlines on a cross–section associated with Dean vortices are shown in the figure in the next page.

Characteristics of the flow in a curved pipe II

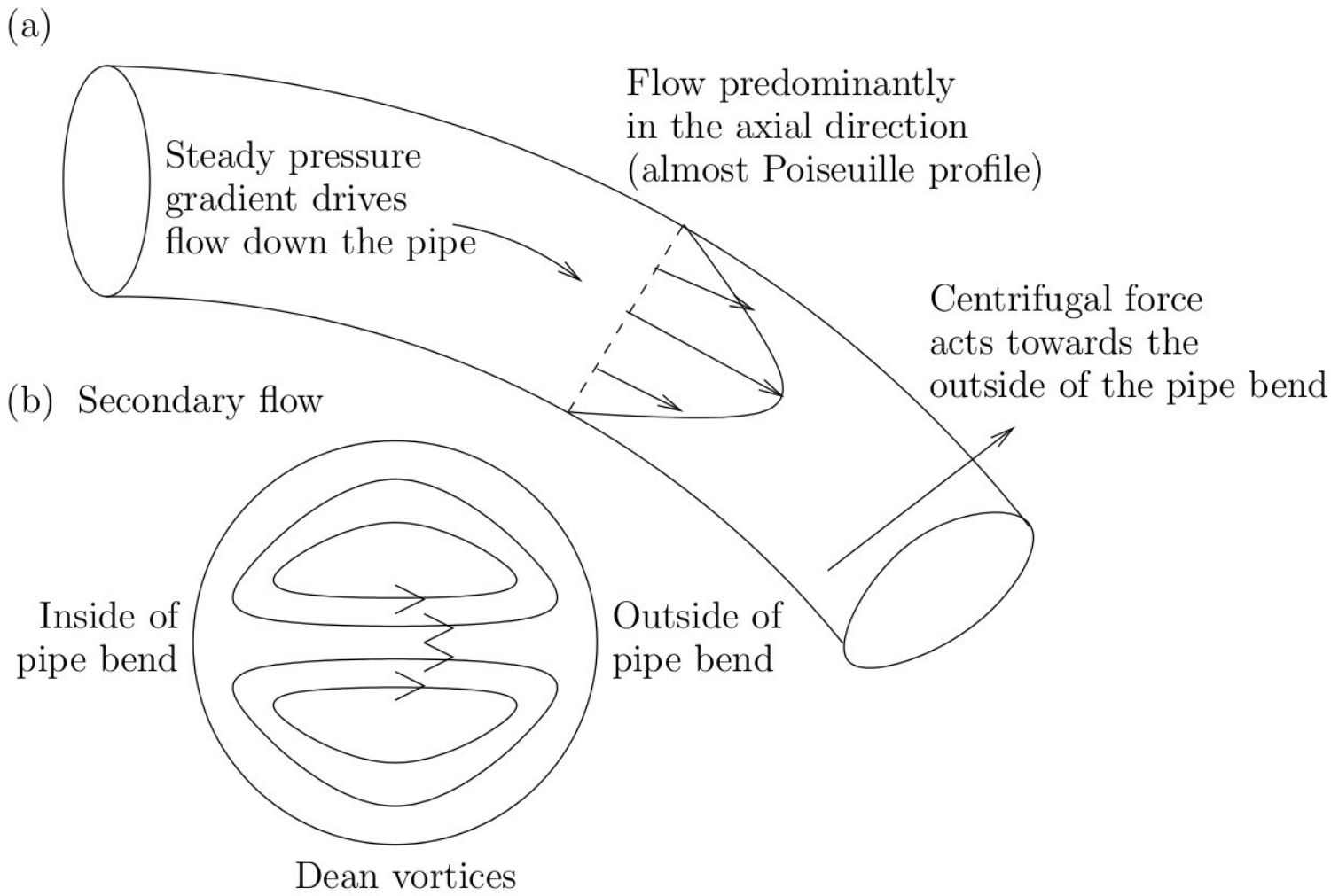

Sketch explaining the formation of Dean vortices in a curved pipe.

The one-dimensional model I

Introduction

In one-dimensional (1D) models the arterial circulation is described as a network of compliant one-dimensional vessels. Along such vessels flux and pressure waves propagate, induced by the cardiac pulse.

One-dimensional models are very powerful tools to study wave propagation in large arteries.

Examples

- Propagation of a pressure wave through a bifurcation
- Propagation of a pressure wave through a network of 55 arteries

Films courtesy of Jordi Alastruey-Arimon from Imperial College London (UK).

The one-dimensional model II

General assumptions

We derive the 1D equations governing the flow in a compliant vessel.

We consider a system of cylindrical coordinates (z, r, φ), with corresponding velocity components (u, v, w) and unit vectors $\mathbf{e}_z$, $\mathbf{e}_r$ and $\mathbf{e}_\varphi$. The main direction of flow is along $\mathbf{e}_z$.

The derivation of the equations presented below is based on the following assumptions.

- **Quasi unidirectional flow.** Due to the shape of the domain the flow is predominantly in the direction of the vessel axis. If R_0 is the characteristic radius of the vessel and L its characteristic length, we have $R_0/L = \epsilon \ll 1$.
- **Axial symmetry.** We assume that all quantities describing the flow are independent of the azimuthal coordinate φ and that the tube has a circular cross-section. The φ component of the velocity (w) is also equal to zero.
- **Fixed axis of the cylinder.** The axis of the cylinder is fixed and straight.
- **Radial displacements of the wall material points.** The wall configuration is characterised by the following equation

$$r = R(z, t) = R_0(z) + \eta(z, t) \tag{90}$$

where $r = R_0$ is a reference configuration of the tube. We assume that each material point of the wall just moves in the radial direction $\mathbf{e}_r$, thus the displacement of a point of the wall can be expressed as $\boldsymbol{\eta} = \eta \mathbf{e}_r$.

The one-dimensional model III

Definitions

We introduce the following definitions:

$$A(z,t) = \int_0^{2\pi} \int_0^{R(z,t)} r dr d\varphi \qquad \textbf{cross-section area,} \tag{91}$$

$$Q(z,t) = \int_0^{2\pi} \int_0^{R(z,t)} u r dr d\varphi \qquad \textbf{volume flux (discharge),} \tag{92}$$

$$U(z,t) = \frac{1}{A} \int_0^{2\pi} \int_0^{R(z,t)} u r dr d\varphi = Q/A \qquad \textbf{cross-sectionally averaged velocity,} \tag{93}$$

$$\alpha = \frac{1}{AU^2} \int_0^{2\pi} \int_0^{R(z,t)} u^2 r dr d\varphi \qquad \textbf{Coriolis coefficient,}$$

where $R(z,t)$ is the radius of the tube, which might depend on z and t.

The one-dimensional model IV

Three-dimensional formulation

In order to derive the one-dimensional governing equations we integrate the three-dimensional equations over the cross-section.

The problem of the flow of a Newtonian fluid in a compliant vessel is governed by the Navier-Stokes equations with suitable boundary conditions.

$$\begin{aligned} &\nabla \cdot \mathbf{u} = 0, \\ &\frac{\partial \mathbf{u}}{\partial t} + (\mathbf{u} \cdot \nabla)\mathbf{u} + \frac{1}{\rho}\nabla P - \nu \nabla^2 \mathbf{u} = 0. \\ &\mathbf{u} = \frac{\partial \boldsymbol{\eta}}{\partial t}, \qquad \text{on } \Gamma^w \end{aligned} \tag{94}$$

where $\Gamma^w \{(z, r, \varphi) : \ r = R(t, z), \ \varphi \in [0, 2\pi), \ z \in (0, L)\}$ and

$$\frac{\partial \boldsymbol{\eta}}{\partial t} = \frac{\partial \eta}{\partial t}\mathbf{e}_r.$$

In the above equations P is the dynamic pressure, defined be equation (14).

The one-dimensional model V

The axisymmetric continuity equation and the z-component of the Navier-Stokes equation in cylindrical coordinates read (see section 7)

$$\frac{\partial u}{\partial z} + \frac{1}{r}\frac{\partial}{\partial r}(rv) = 0, \tag{95}$$

$$\frac{\partial u}{\partial t} + u\frac{\partial u}{\partial z} + v\frac{\partial u}{\partial r} = -\frac{1}{\rho}\frac{\partial P}{\partial z} + 2\nu\frac{\partial^2 u}{\partial z^2} + \frac{\nu}{r}\frac{\partial}{\partial r}\left[r\left(\frac{\partial v}{\partial z} + \frac{\partial u}{\partial r}\right)\right]. \tag{96}$$

Note that this expression for the viscous term can be obtained by summing to $\nabla^2 u$ the derivative with respect to z of the continuity equation.
As the flow is quasi unidirectional the Navier-Stokes equation in the radial direction just states that the pressure is approximately constant on planes orthogonal to z. In the following we will assume that **P is constant on each cross-section**.

The one-dimensional model VI

Leibniz rule

The following rule will be widely employed for the integration of the above equations:

$$\int_{a(z)}^{b(z)} \frac{\partial f(x,z)}{\partial z} dx = \frac{\partial}{\partial z} \int_{a(z)}^{b(z)} f(x,z) dx - f(b,z) \frac{\partial b(z)}{\partial z} + f(a,z) \frac{\partial a(z)}{\partial z}.$$

The one-dimensional model VII

Continuity equation

We integrate first the continuity equation.

$$\int_0^{2\pi}\int_0^{R(z,t)} \frac{\partial u}{\partial z} r dr d\varphi + \int_0^{2\pi}\int_0^{R(z,t)} \frac{\partial (rv)}{\partial r} dr d\varphi =$$

$$= 2\pi \frac{\partial}{\partial z} \int_0^{R(z,t)} urdr - \cancel{2\pi (ur)|_{r=R} \frac{\partial R}{\partial z}} + 2\pi (vr)|_{r=R} - \cancel{2\pi (vr)|_{r=0}} = 0.$$

Using (92) and (94) the above equation can be rewritten as

$$\frac{\partial Q}{\partial z} + 2\pi R \frac{\partial \eta}{\partial t} = 0. \tag{97}$$

Recalling (90) we have

$$A = \pi (R_0 + \eta)^2,$$

from which

$$\frac{\partial A}{\partial t} = 2\pi (R_0 + \eta) \frac{\partial \eta}{\partial t} = 2\pi R \frac{\partial \eta}{\partial t}.$$

The one-dimensional model VIII

Substituting the above expression into (97) we obtain

$$\frac{\partial Q}{\partial z} + \frac{\partial A}{\partial t} = 0. \tag{98}$$

The one-dimensional model IX

Navier-Stokes equation

We now take the average of the Navier-Stokes equation (96). It is first convenient to add to the convective terms the continuity equation (95) multiplied by u. We thus get

$$\frac{\partial u}{\partial t} + u\frac{\partial u}{\partial z} + v\frac{\partial u}{\partial r} + u\frac{\partial u}{\partial z} + \frac{u}{r}\frac{\partial}{\partial r}(rv) = -\frac{1}{\rho}\frac{\partial P}{\partial z} + 2\nu\frac{\partial^2 u}{\partial z^2} + \frac{\nu}{r}\frac{\partial}{\partial r}\left[r\left(\frac{\partial v}{\partial z} + \frac{\partial u}{\partial r}\right)\right].$$

The convective term can now be written as

$$2u\frac{\partial u}{\partial z} + v\frac{\partial u}{\partial r} + \frac{u}{r}\frac{\partial}{\partial r}(rv) = 2u\frac{\partial u}{\partial z} + v\frac{\partial u}{\partial r} + \frac{uv}{r} + u\frac{\partial v}{\partial r} = \frac{\partial u^2}{\partial z} + \frac{\partial uv}{\partial r} + \frac{uv}{r},$$

and we get

$$\underbrace{\frac{\partial u}{\partial t}}_{①} + \underbrace{\frac{\partial u^2}{\partial z}}_{②} + \underbrace{\frac{\partial uv}{\partial r}}_{③} + \underbrace{\frac{uv}{r}}_{④} = \underbrace{-\frac{1}{\rho}\frac{\partial P}{\partial z}}_{⑤} + \underbrace{2\nu\frac{\partial^2 u}{\partial z^2}}_{⑥} + \underbrace{\frac{\nu}{r}\frac{\partial}{\partial r}\left[r\left(\frac{\partial v}{\partial z} + \frac{\partial u}{\partial r}\right)\right]}_{⑦}.$$

We now take the average of each term separately.

$$① : \quad \int_0^{2\pi}\int_0^{R(z,t)} \frac{\partial u}{\partial t} r dr d\varphi = 2\pi\frac{\partial}{\partial t}\int_0^{R(z,t)} u r dr - 2\pi(ur)|_{r=R}\cancel{\frac{\partial R}{\partial t}} = \frac{\partial Q}{\partial t} = \frac{\partial AU}{\partial t}. \qquad (99)$$

The one-dimensional model X

$$\textcircled{2}: \quad \int_0^{2\pi}\int_0^{R(z,t)} \frac{\partial u^2}{\partial z} r dr d\varphi = 2\pi \frac{\partial}{\partial z} \int_0^{R(z,t)} u^2 r dr - \cancel{2\pi (u^2 r)|_{r=R} \frac{\partial R}{\partial z}} = \frac{\partial \alpha U^2 A}{\partial z}. \tag{100}$$

$$\textcircled{3}: \quad \int_0^{2\pi}\int_0^{R(z,t)} \frac{\partial uv}{\partial r} r dr d\varphi = 2\pi \left[\int_0^{R(z,t)} \frac{\partial uvr}{\partial r} dr - \int_0^{R(z,t)} uv dr \right] =$$

$$= \cancel{2\pi (uvr)|_{r=R}} - \cancel{2\pi (uvr)|_{r=0}} - 2\pi \int_0^{R(z,t)} uv dr. \tag{101}$$

$$\textcircled{4}: \quad \int_0^{2\pi}\int_0^{R(z,t)} uv dr d\varphi = 2\pi \int_0^{R(z,t)} uv dr = -\textcircled{3}. \tag{102}$$

The one-dimensional model XI

$$\textcircled{5}: \quad -\frac{1}{\rho}\int_0^{2\pi}\int_0^{R(z,t)}\frac{\partial P}{\partial z}rdrd\varphi = -\frac{2\pi}{\rho}\frac{\partial}{\partial z}\int_0^{R(z,t)}Prdr + \frac{2\pi}{\rho}(Pr)|_{r=R}\frac{\partial R}{\partial z} =$$

$$= -\frac{1}{\rho}\frac{\partial PA}{\partial z} + \frac{2\pi}{\rho}PR\frac{\partial R}{\partial z} =$$

$$= -\frac{P}{\rho}\frac{\partial A}{\partial z} - \frac{A}{\rho}\frac{\partial P}{\partial z} + \frac{P}{\rho}\frac{\partial(\pi R^2)}{\partial z} = -\frac{A}{\rho}\frac{\partial P}{\partial z}. \tag{103}$$

$$\textcircled{6}: \quad 2\nu\int_0^{2\pi}\int_0^{R(z,t)}\frac{\partial^2 u}{\partial z^2}rdrd\varphi = 4\pi\nu\frac{\partial}{\partial z}\int_0^{R(z,t)}\frac{\partial u}{\partial z}rdr - 4\pi\nu R\left(\frac{\partial u}{\partial z}\right)|_{r=R}\frac{\partial R}{\partial z}. \tag{104}$$

$$\textcircled{7}: \quad \nu\int_0^{2\pi}\int_0^{R(z,t)}\frac{\partial}{\partial r}\left(r\frac{\partial v}{\partial z} + r\frac{\partial u}{\partial r}\right)drd\varphi = 2\pi\nu R\left(\frac{\partial v}{\partial z} + \frac{\partial u}{\partial r}\right)|_{r=R}. \tag{105}$$

$$\textcircled{6}+\textcircled{7}: \quad 4\pi\nu\frac{\partial}{\partial z}\int_0^{R(z,t)}\frac{\partial u}{\partial z}rdr + 2\pi\nu R\left(-2\frac{\partial u}{\partial z}\frac{\partial R}{\partial z} + \frac{\partial v}{\partial z} + \frac{\partial u}{\partial r}\right)|_{r=R}. \tag{106}$$

The one-dimensional model XII

In order to understand the meaning of the terms computed at $r = R$ in (106) we evaluate the z component of the viscous stress at the wall. The unit normal to the wall $\mathbf{n} = (n_z, n_r, 0)$ can be written as

$$\mathbf{n} = (-\partial R/\partial z, 1, 0)\,/|\mathbf{n}|.$$

Since $\partial R/\partial z = \mathcal{O}(R_0/L) \ll 1$ we have that $|\mathbf{n}| = 1 + \mathcal{O}(\epsilon^2)$ with $\epsilon = R_0/L$. Neglecting order ϵ^2 or smaller terms, the viscous stress at the wall is given by the vector

$$\mathbf{t}^v = \mathbf{d}\cdot\mathbf{n} = \left(-\frac{\partial R}{\partial z}d_{zz} + d_{zr}, -\frac{\partial R}{\partial z}d_{zr} + d_{rr}, 0\right),$$

with $\mathbf{d}$ the deviatoric part of the stress tensor (see (25)). Thus the component τ in the z direction is given by

$$\tau = \mathbf{t}^v \cdot \mathbf{e}_z = -\frac{\partial R}{\partial z}d_{zz} + d_{zr}.$$

In our cylindrical coordinate system we have

$$d_{zz} = 2\mu\frac{\partial u}{\partial z}, \qquad d_{zr} = \mu\left(\frac{\partial v}{\partial z} + \frac{\partial u}{\partial r}\right).$$

Thus we obtain

$$\tau = -2\mu\frac{\partial R}{\partial z}\frac{\partial u}{\partial z} + \mu\left(\frac{\partial v}{\partial z} + \frac{\partial u}{\partial r}\right),$$

The one-dimensional model XIII

which has to be computed in $r = R$. Note that $2\pi R\tau/\rho$ is the term computed at the wall appearing in (106), and $2\pi R\tau$ is the total viscous stress acting on the boundary of the cross-section.
Note that $u = \mathcal{O}(U_0)$ and $v = \mathcal{O}(\epsilon U_0)$, thus

$$2\frac{\partial R}{\partial z}\frac{\partial u}{\partial z} \approx \frac{\partial v}{\partial z} = \mathcal{O}(R_0 U_0/L^2) = \mathcal{O}(\epsilon^2 U_0/R_0), \qquad \frac{\partial u}{\partial r} = \mathcal{O}(U_0/R_0).$$

Therefore:

$$\tau = \mu\frac{\partial u}{\partial r} + \mathcal{O}(\varepsilon^2).$$

Let us now consider the integral term appearing in (106). It is a cross-sectionally averaged normal viscous stress due to longitudinal variations of u.

$$4\pi\nu\frac{\partial}{\partial z}\int_0^{R(z,t)}\frac{\partial u}{\partial z}r dr \approx \nu\epsilon^2 U_0.$$

This term is also typically very small and is normally disregarded in one-dimensional models.
The one-dimensional momentum equation can therefore be written, using (99), (100), (101), (102), (103), (104), (105), (91), (92) and (93) as

$$\frac{\partial Q}{\partial t} + \frac{\partial}{\partial z}\left(\frac{\alpha Q^2}{A}\right) + \frac{A}{\rho}\frac{\partial P}{\partial z} - \frac{\tau B}{\rho} = 0, \tag{107}$$

The one-dimensional model XIV

where $B = 2\pi R$ is named **wet perimeter**.

The one-dimensional model XV

Velocity distribution in the cross-section

The determination of α and τ in (107) requires the knowledge of the velocity distribution on the cross-section $u(r)$.

- **Poiseuille profile**
  A possible choice for the profile $u(r)$ is the parabolic profile predicted by Poiseuille law.

$$u(r) = 2U\left(1 - \frac{r^2}{R^2}\right).$$

  Such profile corresponds to the steady solution in the circular tube with constant diameter. In this case it is immediate to verify that $\alpha = 4/3$.

- **Power law**
  A profile which is often used for blood flow in arteries is a power law of the following form

$$u(r) = \gamma^{-1}(\gamma + 2)U\left[1 - \left(\frac{r}{R}\right)^{\gamma}\right],$$

  with γ typically equal to 9 (note that the above relationship reduces to the parabolic profile for $\gamma = 2$).
  In this case we have $\alpha = 1.1$.

Note that the choice $\alpha = 1$ implies that the velocity profile is considered flat on the cross-section. This assumption, which is invariably made in turbulent flows is not really justified in the laminar case.

Finally, once the expression for $u(r)$ is known, it is immediate to compute the term $\tau B/\rho$ in (107).

The one-dimensional model XVI

Tube law

The system given by equations (98) and (107) has three unknowns: Q, A and P. A further equations is therefore required to solve the problem.

Such equation has to account for the wall properties by establishing a **relationship between pressure and vessel cross-sectional area**.

A complete mechanical model for the structure of the vessel wall would provide a differential equation linking the wall displacement and its spatial and temporal derivatives to the force applied by the fluid.

Here we adopt a simplified approach which is based on the following assumptions:

- the inertia of the wall is negligible;
- the wall is elastic;
- the tube is cylindrical.

The one-dimensional model XVII

Under the above assumptions the wall mechanics is described by the following simple equation

$$P = \beta_0 \frac{\sqrt{A} - \sqrt{A_0}}{A_0}, \tag{108}$$

with

$$\beta_0 = \frac{\sqrt{\pi} h_0 E}{1 - \zeta^2},$$

where E is the Young modulus, ζ the Poisson coefficient (equal to $1/2$ for an incompressible solid), h_0 the wall thickness and $A_0 = \pi R_0^2$.

One-dimensional linear inviscid model I

The analysis that follows is based on Pedley (2000).

Simplifying assumptions

We now consider the following simplifying assumptions.

- **Inviscid fluid.** Thus we neglect the viscous term $\tau B/\rho$ in (107).
- $\alpha = 1$.
- Infinitely long straight elastic tube with uniform undisturbed cross-section A_0.
- Fluid initially at rest.
- **Small disturbances.**
- Tube law of the form $P = \tilde{P}(A)$, e.g. (108).

The governing equations (98) and (107) can be written in term of A, P and U as

$$\frac{\partial A}{\partial t} + \frac{\partial UA}{\partial z} = 0, \tag{109}$$

$$\frac{\partial U}{\partial t} + U\frac{\partial U}{\partial z} + \frac{1}{\rho}\frac{\partial P}{\partial z} = 0. \tag{110}$$

One-dimensional linear inviscid model II

Linearisation

We consider small disturbances of the pressure and cross-sectional area for which U is small (in a sense specified later). Therefore, we set

$$A = A_0 + A', \qquad P = P_0 + P', \tag{111}$$

where $|A'| \ll A_0$ and $|P'| \ll P_0$. Recalling that the tube law establishes a relationship of the form $P = \tilde{P}(A)$, we can write

$$P = \tilde{P}(A_0) + \left.\frac{d\tilde{P}}{dA}\right|_{A_0} A', \tag{112}$$

from which we obtain

$$P' = \left.\frac{d\tilde{P}}{dA}\right|_{A_0} A'. \tag{113}$$

Substituting (111) and (113) into (109) and (110) and neglecting nonlinear terms in the small quantities we obtain

$$\frac{\partial A'}{\partial t} + A_0 \frac{\partial U}{\partial z} = 0, \tag{114}$$

$$\frac{\partial U}{\partial t} + \frac{1}{\rho} \left.\frac{d\tilde{P}}{dA}\right|_{A_0} \frac{\partial A'}{\partial z} = 0. \tag{115}$$

One-dimensional linear inviscid model III

Subtracting the derivative of (115) with respect to t multiplied by A_0 from the derivative of (114) with respect to z we obtain

$$\frac{\partial^2 A'}{\partial t^2} = c^2(A_0)\frac{\partial^2 A'}{\partial z^2}, \tag{116}$$

where

$$c^2(A) = \frac{A}{\rho}\frac{d\tilde{P}}{dA}.$$

Equation (116) is the well known **D'Alambert equation** or **wave equation**. Note that c has the dimensions of a velocity ($[c] = LT^{-1}$).
Using (113) equation (116) can also be written in terms of the pressure disturbance P' as

$$\frac{\partial^2 P'}{\partial t^2} = c^2(A_0)\frac{\partial^2 P'}{\partial z^2}. \tag{117}$$

Equations (116) and (117) describe the propagation of small-amplitude waves in both directions along the tube with celerity $c_0 = c(A_0)$. The **general solution** of (117) is

$$P'(z,t) = f_+\left(t - \frac{z}{c_0}\right) + f_-\left(t + \frac{z}{c_0}\right).$$

One-dimensional linear inviscid model IV

From equation (108) one immediately derives the following expression for the wave celerity

$$c_0 = \sqrt{\frac{Eh_0}{\rho(1-\zeta^2)d_0}}, \tag{118}$$

with d_0 unperturbed vessel diameter. This is known as **Moens-Korteveg wave speed.**

One-dimensional linear inviscid model V

Example

Data for the **ascending aorta:**

- vessel diameter $d_0 = 1.5 \times 10^{-2}$ m;
- wall thickness $h_0 = 0.065 \times 10^{-2}$ m;
- blood density $\rho = 10^{-3}$ Kg/m^3;
- Young's modulus of the vessel $E = 4.8 \times 10^5$ N/m^2;
- Poisson's coefficient of the vessel $\zeta = 0.5$;
- Measured wave-speed $= 5$ m/s.

From equation (118) we obtain $c_0 = 5.3$ m/s.

One-dimensional linear inviscid model VI

Comments on the validity of the linearised model

The derivation of equation (116) was based on the following assumptions:

- that the pressure wave amplitude be small compared to the mean value;
- that the fluid velocity be small (in some sense).

In humans the mean blood pressure in large arteries (relative to the atmospheric pressure) is about 100 mmHg and varies from ≈ 80 to ≈ 120 mmHg. Therefore, the wave amplitude to mean value ratio is about 0.2, which is reasonably small for the first assumption to be valid.

Let us now consider the second assumption, in order to specify what we mean with "small velocity". If we assume that the solution of the linear wave problem is $U = f(t - z/c)$ and we substitute this expression into the non-linear term in equation (110) we find that the latter is negligible with respect to $\partial U/\partial t$ if $U/c \ll 1$. Since in the ascending aorta $c \approx 5$ m/s and $\max(U) \approx 1$ m/s, it follows that nonlinearity is expected to be weak and the second assumption listed above also approximately holds.

One-dimensional linear inviscid model VII

In conclusion, we can make the following remarks.

- In terms of wave speed the agreement between measured data and theoretical predictions is quite good.
- However, the model predicts that the wave propagate without changing its shape, which is not observed in experiments. In particular the model is unable to predict wave steepening.
- The model predicts a constant wave speed whereas measurements suggest that the wave speed increases with pressure.
- The model predicts a velocity wave with the same shape and speed as the pressure wave. In fact if we assume a pressure wave of the form

$$P' = \overline{P} f\left(t - \frac{z}{c_0}\right),$$

with $\overline{P} \ll \tilde{P}(A_0)$, from the linearised version of (110) we obtain

$$U = \frac{\overline{P}}{\rho c_0} f\left(t - \frac{z}{c_0}\right).$$

One-dimensional linear inviscid model VIII

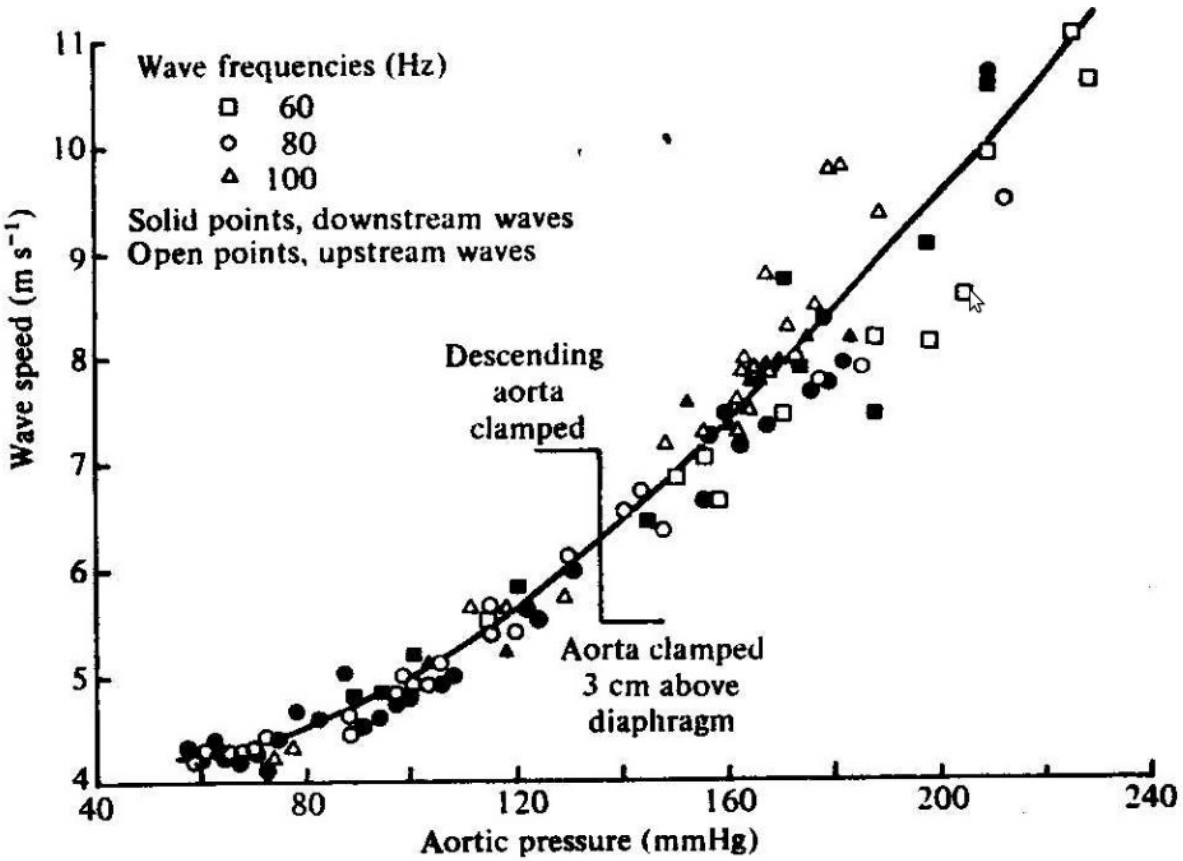

Dependence of the wave speed on the average pressure in the canine aorta (from Pedley, 1980).

One-dimensional linear inviscid model IX

Wave reflection

We now consider a single bifurcation from a parent tube 1 to two daughter tubes 2 and 3 as shown below.

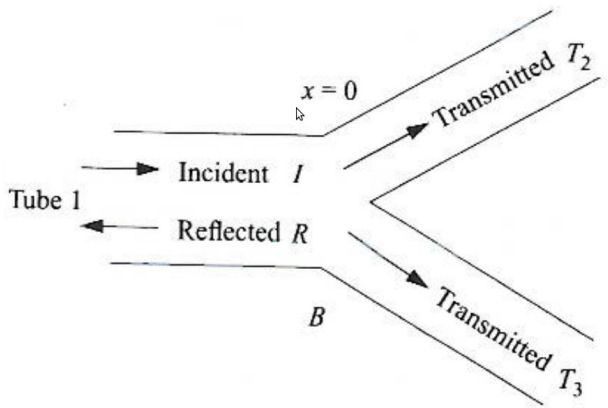

Sketch of an arterial bifurcation.

The undisturbed cross-sections are A_1, A_2 and A_3, and the associated linear wave speeds are c_{01}, c_{02} and c_{03}, respectively.
Let z be the longitudinal coordinate in each tube, with $z = 0$ at the bifurcation point.
An **incident wave I** approaches the bifurcation in tube 1 from $z = -\infty$.
We suppose that the incident pressure wave in tube 1 is

$$P_I' = \overline{P}_I f\left(t - \frac{z}{c_{01}}\right),$$

where $\overline{P}_I$ an amplitude parameter and f is a periodic function the maximum value of which is 1. The corresponding velocity and flux waves are given by

$$U_I = \frac{\overline{P}_I}{\rho c_{01}} f\left(t - \frac{z}{c_{01}}\right), \qquad Q_I = U_I A_1 = \frac{A_1 \overline{P}_I}{\rho c_{01}} f\left(t - \frac{z}{c_{01}}\right) = Y_1 \overline{P}_I f\left(t - \frac{z}{c_{01}}\right),$$

In the above equation we have defined $Y_1 = A_1/(\rho c_{01})$. Y is called **characteristic admittance** of the tube.

One-dimensional linear inviscid model X

At the bifurcation point the incident wave produces a **reflected wave** R in the parent tube and two **transmitted waves** T_2 and T_3 in the daughters.
We define such pressure waves as

$$P'_R = \overline{P}_R g\left(t + \frac{z}{c_{01}}\right), \qquad P'_{Ti} = \overline{P}_{Ti} h_i\left(t - \frac{z}{c_{0i}}\right) \quad (i = 2, 3),$$

and the corresponding flow rate waves are

$$Q_R = -Y_1 \overline{P}_R g\left(t + \frac{z}{c_{01}}\right), \qquad Q_{Ti} = Y_i \overline{P}_{Ti} h_i\left(t - \frac{z}{c_{0i}}\right) \quad (i = 2, 3).$$

We now impose the following **nodal point conditions** (in $z = 0$):

- **continuity of pressure** (required by Newton's law to avoid large local accelerations)

$$P'_1 = P'_2 = P'_3;$$

- **continuity of flow** (required by conservation of mass)

$$Q_1 = Q_2 + Q_3.$$

One-dimensional linear inviscid model XI

Since the above conditions must hold in $z = 0$ for all times it follows that the functions $g(t)$ and $h_j(t)$ are equal to the incident function $f(t)$. Moreover, the following relationships link the wave amplitudes

$$\overline{P}_I + \overline{P}_R = \overline{P}_{T2} = \overline{P}_{T3}, \qquad Y_I \left(\overline{P}_I - \overline{P}_R \right) = \sum_{i=2}^{3} Y_i \overline{P}_{Ti}.$$

It follows that

$$\frac{\overline{P}_R}{\overline{P}_I} = \frac{Y_1 - \sum_{i=2}^{3} Y_i}{Y_1 + \sum_{i=2}^{3} Y_i}, \qquad \frac{\overline{P}_{Ti}}{\overline{P}_I} = \frac{2Y_1}{Y_1 + \sum_{i=2}^{3} Y_i},$$

which allow us to determine the amplitudes of reflected and transmitted waves. We define

$$\beta = \frac{\overline{P}_R}{\overline{P}_I}.$$

The pressure and flow waves in the parent vessel are given by the following expressions

$$P_1' = \overline{P}_I \left[f\left(t - \frac{z}{c_{01}} \right) + \beta f\left(t + \frac{z}{c_{01}} \right) \right], \quad Q_1 = Y_1 \overline{P}_I \left[f\left(t - \frac{z}{c_{01}} \right) - \beta f\left(t + \frac{z}{c_{01}} \right) \right]. \tag{119}$$

One-dimensional linear inviscid model XII

- $\beta > 0$ or $Y_1 > \sum_{i=2}^{3} Y_i$, **closed-end reflection**.

  In this case the overall pressure amplitude has a maximum value equal to $\overline{P}_I(1+\beta)$ at $z = 0$. The amplitude of pressure oscillations decreases with distance upstream, to a minimum value at $z = \pi c_{01}/(2\omega)$, i.e. one-quarter wavelength proximal to the bifurcation.
  The amplitude of the corresponding flow-rate wave increases with distance upstream.

- $\beta < 0$ or $Y_1 < \sum_{i=2}^{3} Y_i$, **open-end reflection**.

  In this case the pressure amplitude is minimum at $z = 0$ and the flow rate is maximum there.

- $\beta = 0$ or $Y_1 = \sum_{i=2}^{3} Y_i$, **no reflection**.

  This case corresponds to a perfect match between upstream and downstream branches, so that there is no reflection. Note that the condition $\beta = 0$ involves both the area of the branches and also the wave celerity in the branches.

Example

Suppose that $f(t)$ is sinusoidal $f(t) = \cos(\omega t)$. Equation (119), after simple manipulation, gives:

$$\frac{P_1'}{\overline{P}_I} = (1-\beta)\cos\omega\left(t - \frac{z}{c_{01}}\right) + 2\beta\cos t\cos\frac{\omega z}{c_{01}}.$$

This represents a **propagating wave** of amplitude $(1-\beta)\overline{P}_I$ and a **standing wave** of amplitude $|2\beta\overline{P}_I\cos(\omega z/c_{01})|$.

One-dimensional linear inviscid model XIII

Implications for flow in the aorta

We know that that the pressure in the aorta increases moving away from the heart. This could be explained with the presence of a reflection coefficient $\beta > 0$ at the **iliac bifurcation** (where the aorta divides to supply the two legs).

This is possible if the length of the aorta (from the aortic valve to the iliac bifurcation) is less than one-quarter wavelength.

A simple calculation shows:

$$c_0 \approx 5 \text{ m/s}, \quad \omega/2\pi \approx 1.25 \text{ Hz} \quad \Rightarrow L/4 \approx 1 \text{ m}.$$

This is typically slightly larger than the length of the aorta.

Moreover, it is required that

$$Y_1 > Y_2 + Y_3.$$

Assuming that wave speed does not vary discontinuously at a bifurcation ($c_{01} \approx c_{02} \approx c_{03}$), this implies

$$A_1 > A_2 + A_3. \tag{120}$$

Measurements show that most bifurcations in the human arterial system are well-matched ($A_2 + A_3 \approx A_1$) but the iliac bifurcation does satisfy (120). Normally, this bifurcation, the ratio between the area of the parent vessel and the daughter vessels is equal to 0.85-0.90.

Perfusion of organs: the liver

The liver: shape, location and main functions I

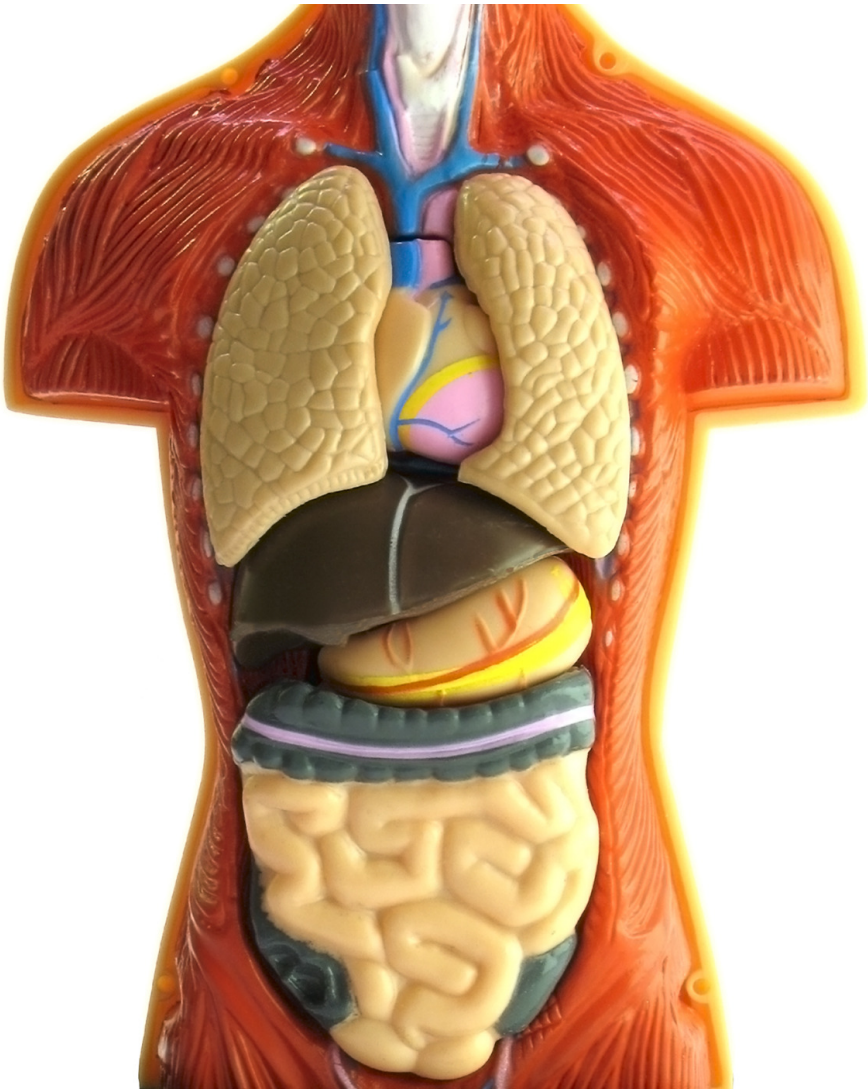

- The adult human liver weighs between 1.4 and 1.6 Kg.
- It measures approximately about 20 cm horizontally (across) and 17 cm vertically and is 12 cm thick.
- It is a brownish-red organ and it is the largest internal organ within the human body.

The liver lies almost completely under the protection of the rib-cage, projecting below it and coming into contact with the anterior abdominal wall only below the right costal margin and the xiphisternum.

The liver consists of two main parts: a larger **right lobe**, a smaller **left lobe** and **two minor lobes**. The upper border of the right lobe is at the level of the top of the 5th rib and the upper border of the left lobe is just below the 5th rib.

The liver: shape, location and main functions II

Photograph of a slice of a normal liver.

Main functions of the liver

The liver is estimated to have over 500 functions. The most important ones are summarised below.

- **Synthesise proteins**, including albumin (to help maintain the volume of blood) and blood clotting factors.
- **Synthesise, store, and process (metabolise) fats**, including fatty acids (used for energy) and cholesterol.
- **Metabolise and store carbohydrates**, which are used as the source for the sugar (glucose) in blood that red blood cells and the brain use.
- **Form and secrete bile** that contains bile acids to aid in the intestinal absorption of fats and the fat-soluble vitamins A, D, E, and K.
- **Eliminate, by metabolising and/or secreting, the potentially harmful biochemical products produced by the body.**

Liver circulation I

The main vessels which constitute the vascular system of the liver are:

- **the portal vein;**
- **the hepatic artery;**
- **and the hepatic veins.**

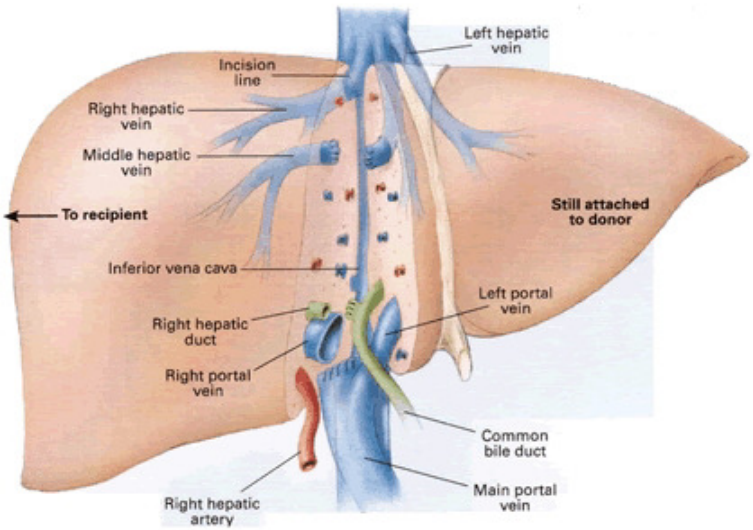

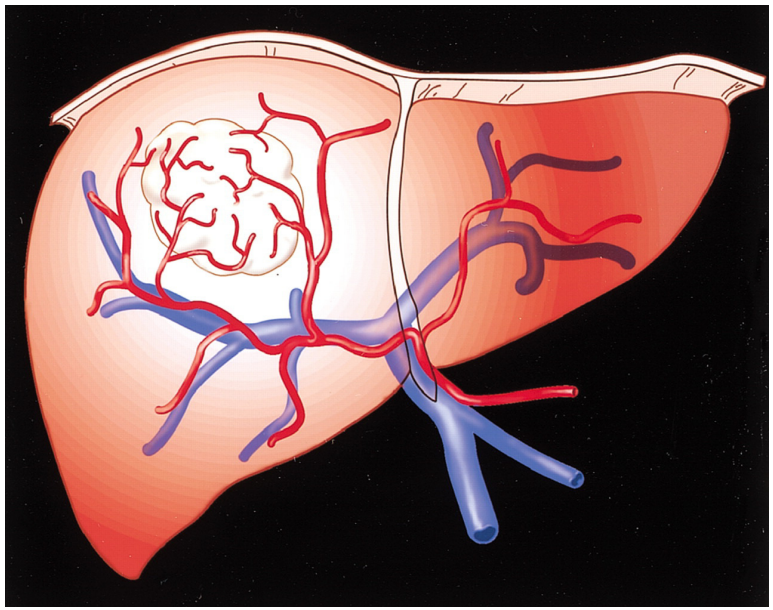

Liver circulation II

The portal vein

The portal vein drains blood from the digestive system and its associated glands. Its main tributaries are the splenic vein and superior mesenteric vein. It divides into a right and a left branch before entering the liver distributing to the liver parenchyma the nutrients absorbed in the small intestine.

The hepatic artery

The hepatic artery is the blood vessel that supplies oxygenated blood to the liver and it arises from the celiac trunk, a branch of the aorta.

The hepatic veins

The hepatic veins are the blood vessels that drain blood from the liver. They drain the blood into the inferior vena cava.

The circulatory system of the liver is different from that of other organs. The most important difference is the fact that the majority of the liver blood supply is venous blood: **75% of the blood entering the liver is venous blood from the portal vein, while the remaining 25% of the blood supply to the liver is arterial blood from the hepatic artery.**

The liver lobule I

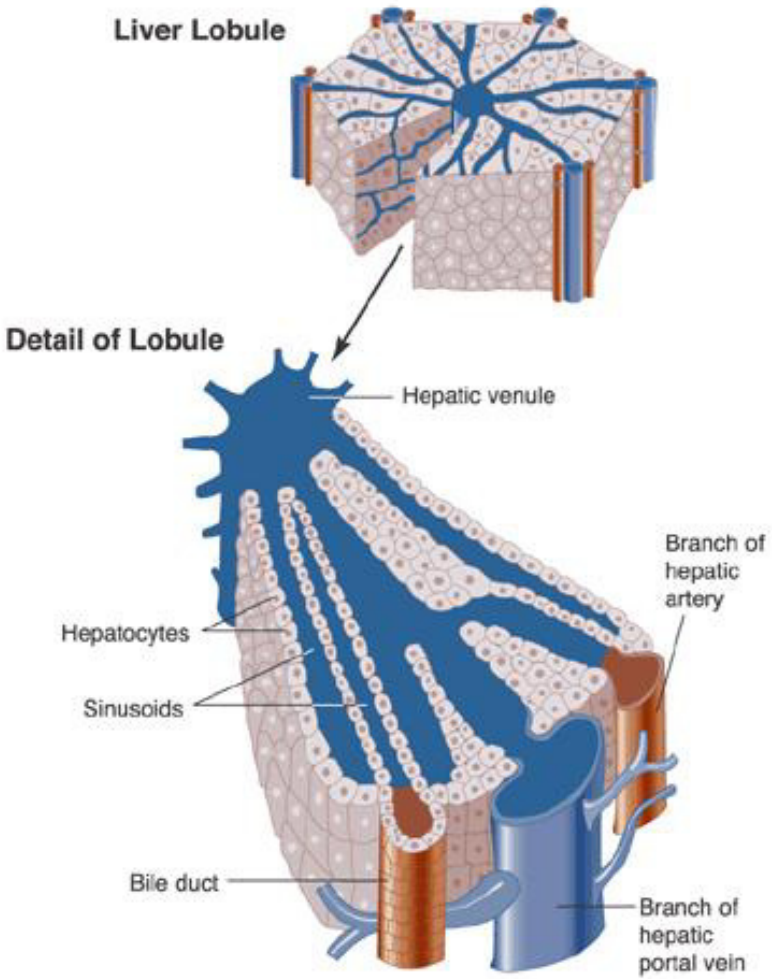

The afferent branches ramify into vessels of ever decreasing calibre. These branches of the portal vein and hepatic artery are present, together with bile ducts, within the so called **portal tracts**.

The basic morphofunctional units of the liver are the **hepatic lobules**. The lobule has approximately a hexagonal shape. The diameter of each lobule is about 1 mm.

At the centre of each lobule is a **centrilobular vein** while the **portal tracts** are at the angles of the hexagon.

Blood flows from the vessels of the portal tracts towards the centrilobular veins within a network of converging tortuous **sinusoids**. These are thin walled, fenestrated capillaries situated between liver cell trabelulae.

The liver lobule II

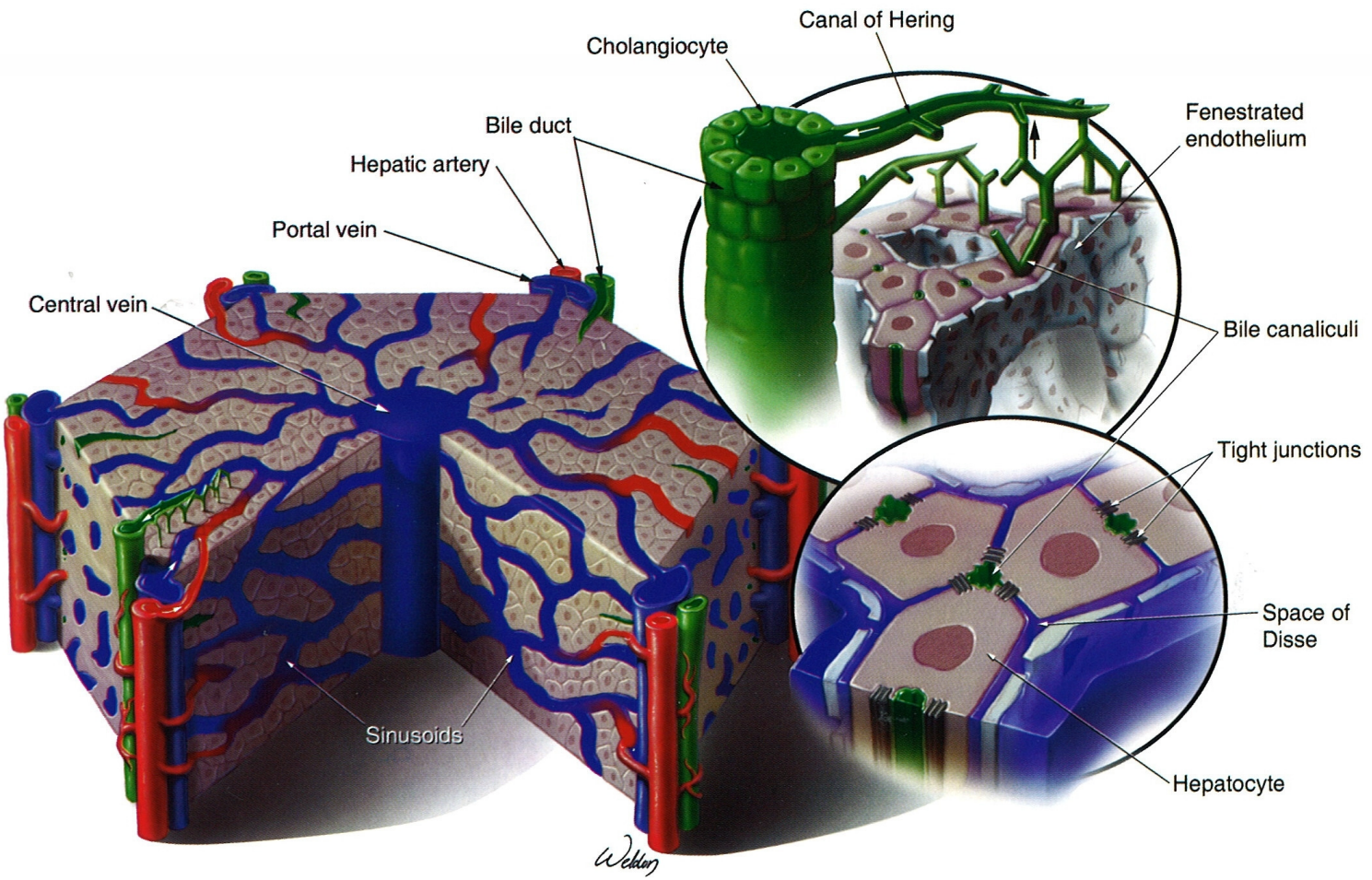

Three-dimensional sketch of a liber lobule.

The liver lobule III

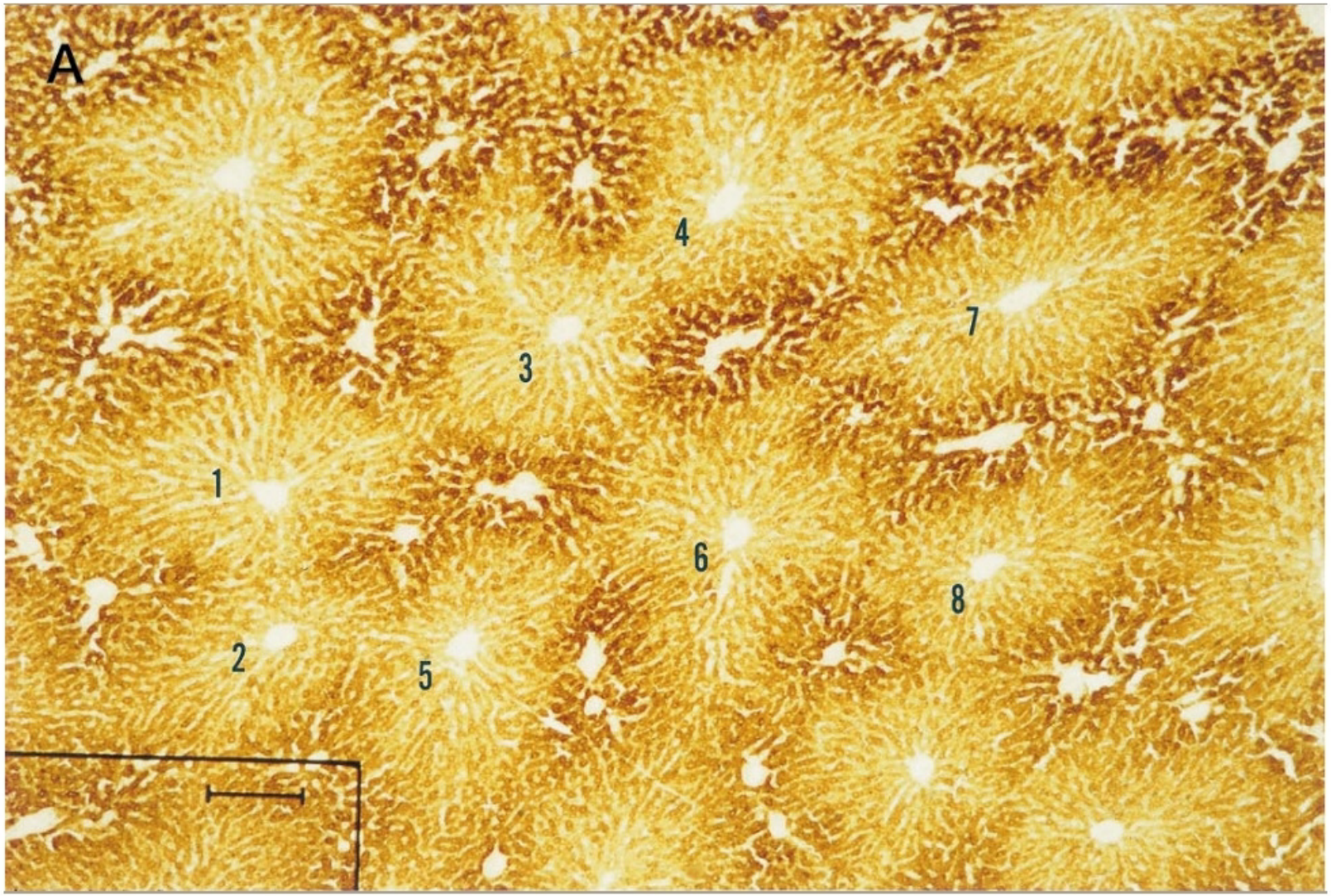

Histological image of the lobular liver structure.

The liver lobule IV

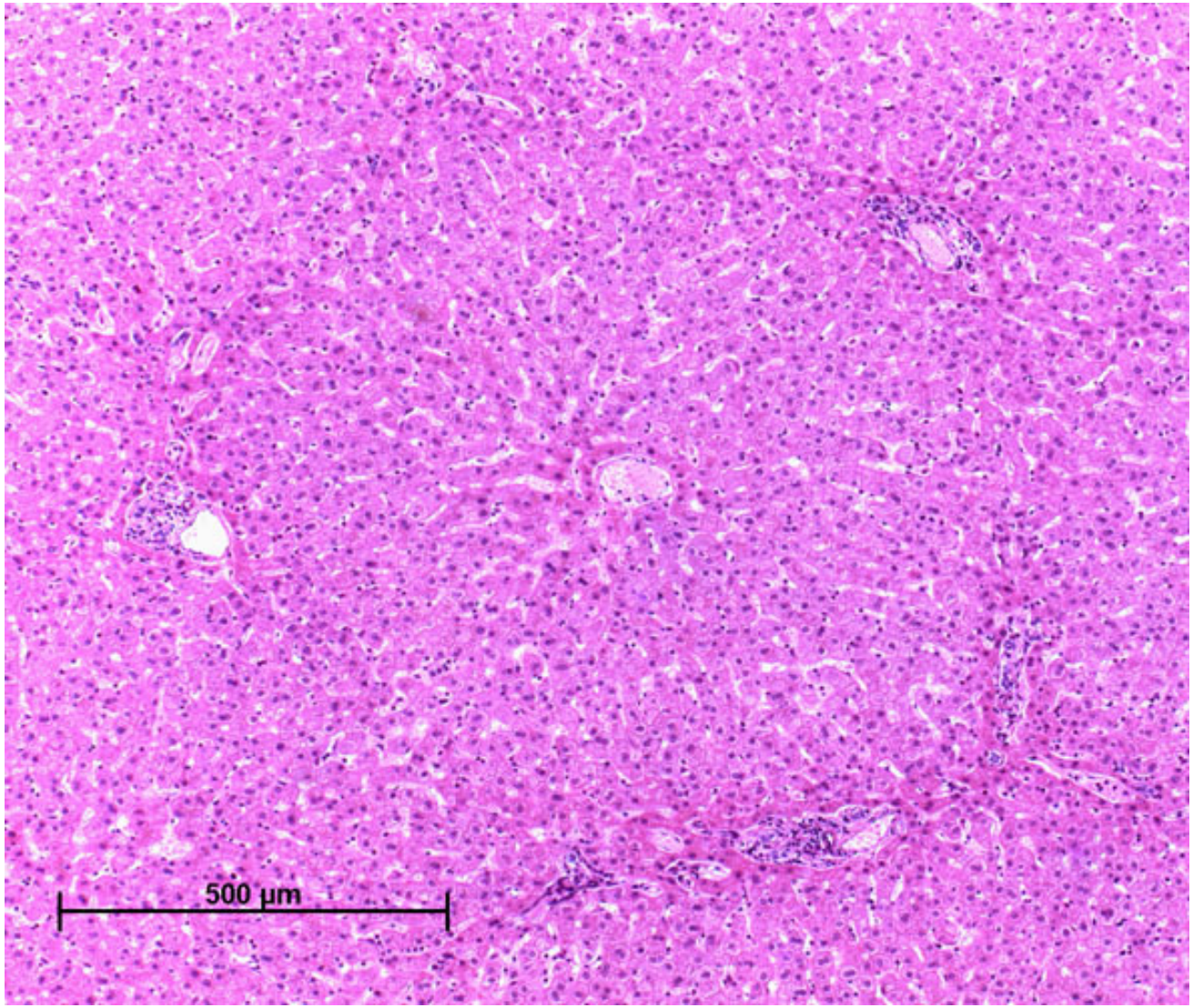

Histological image of the a liver lobule.

The liver lobule V

PT: portal tract;
HV: hepatic venule (centrilobular vein).

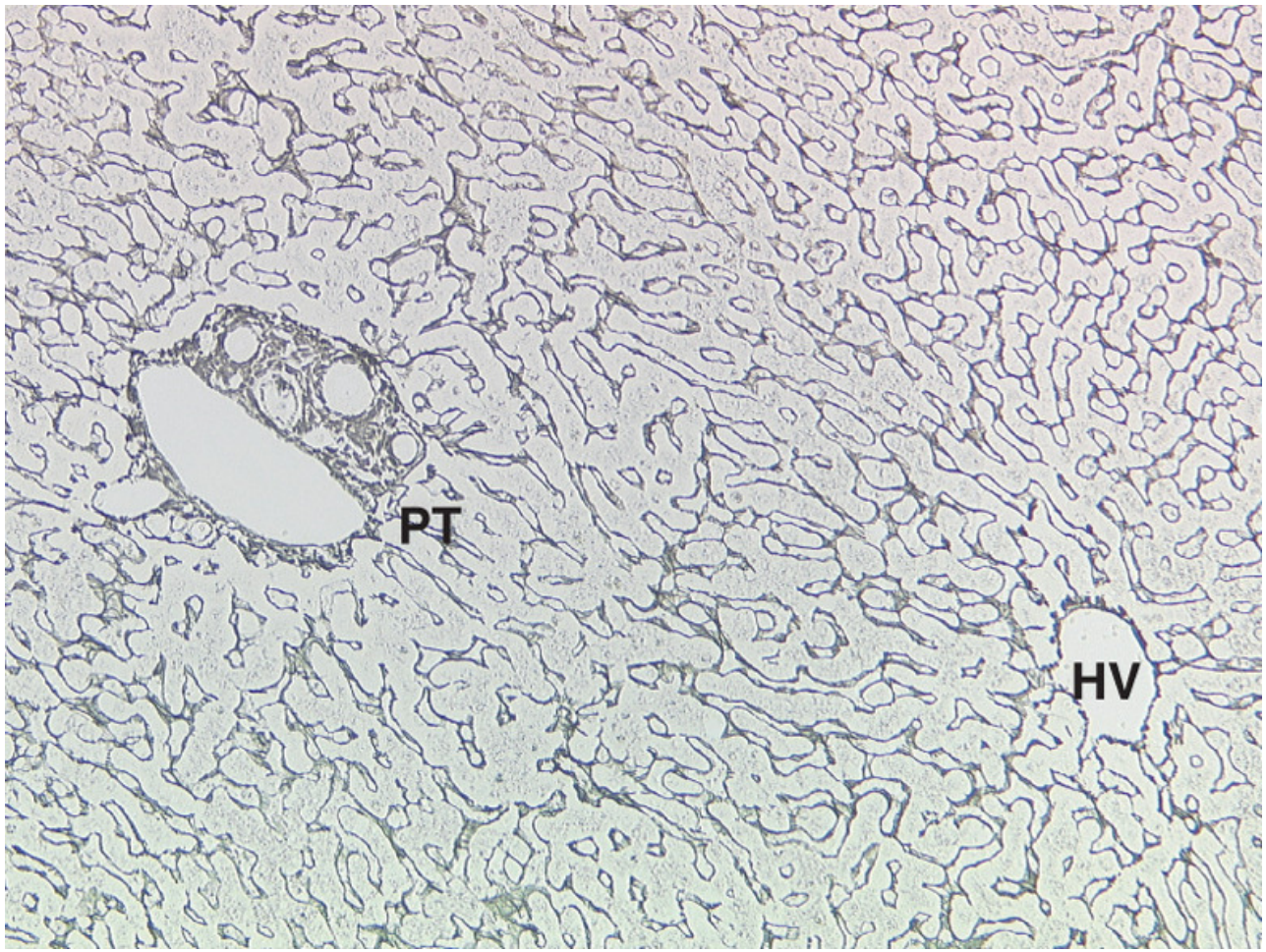

Histological image of the a liver lobule.

The liver lobule VI

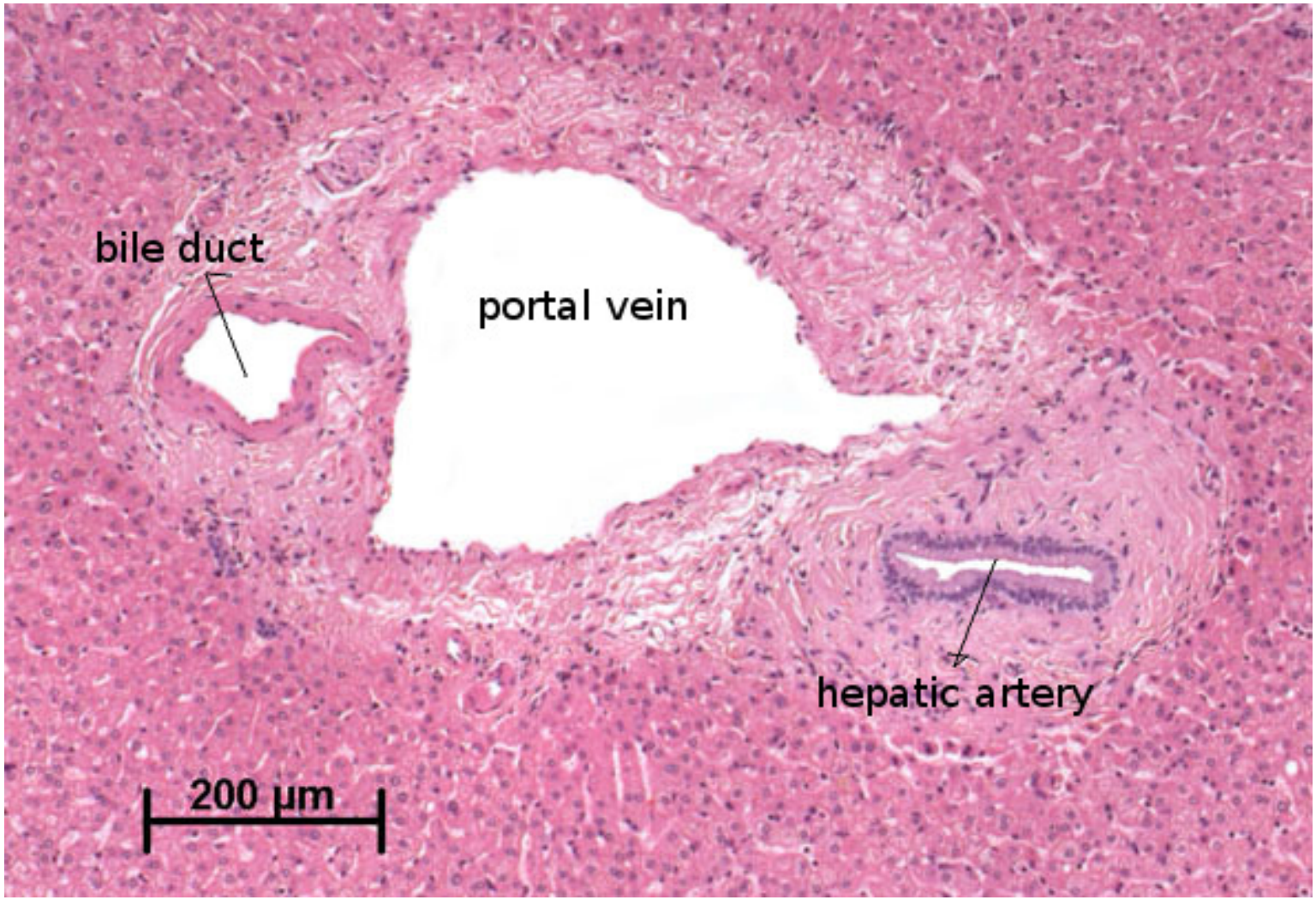

Histological image of a portal tract.

The liver lobule VII

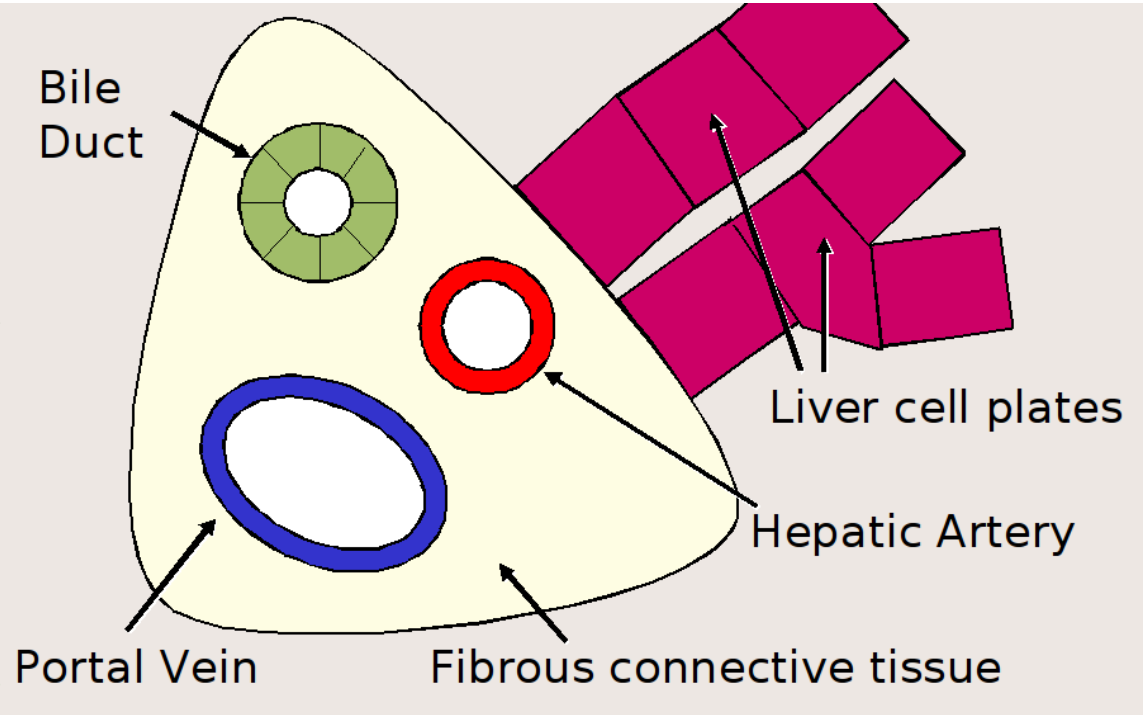

Schematics of a portal tract.

- Bile drains from canaliculi through canals and ductules into progressively larger bile ducts.
- The portal vein brings blood rich in nutrients from the gut.
- The hepatic artery brings oxygenated blood to the liver, which is especially needed by the cells of the bile ducts.

The liver lobule VIII

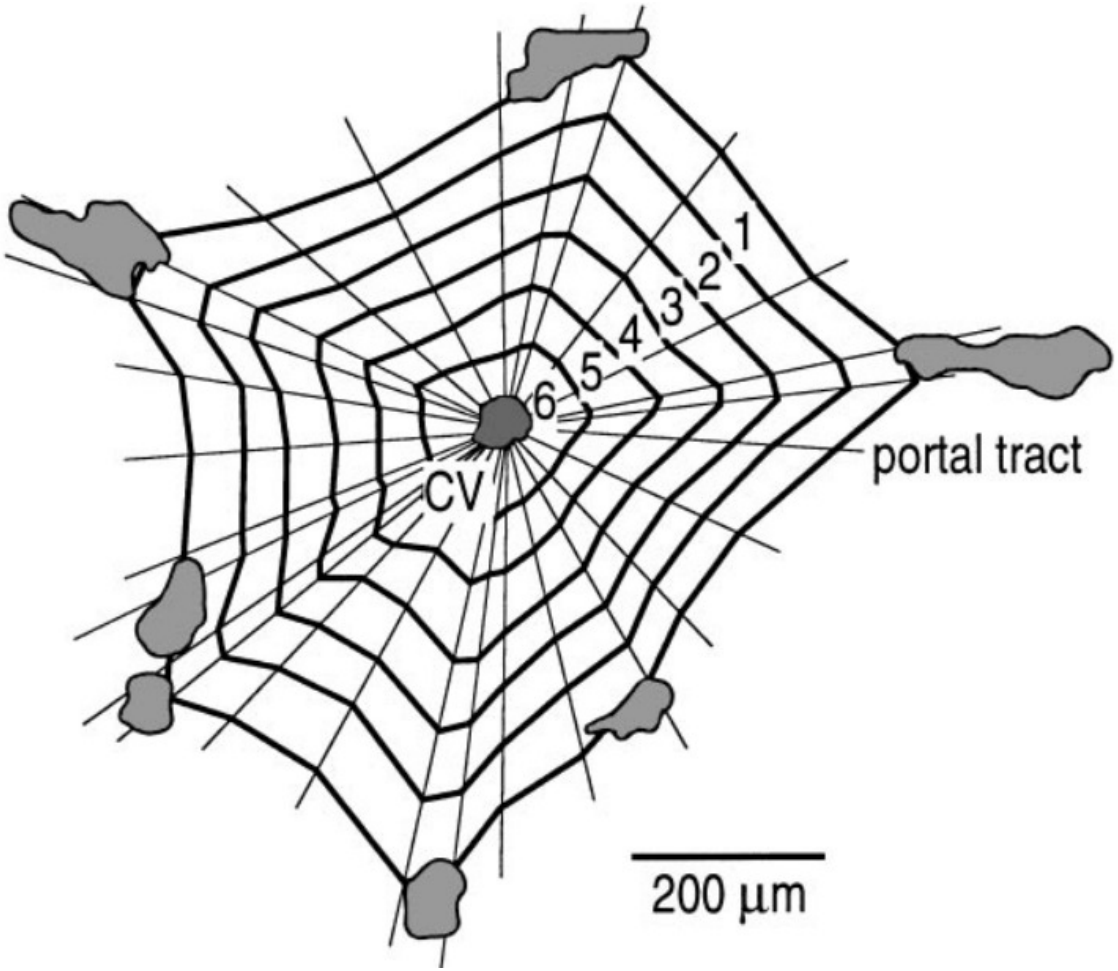

Schematically six different regions characterised by a different enzyme activity (decreasing from 1 to 6) have been identified.

The liver lobule IX

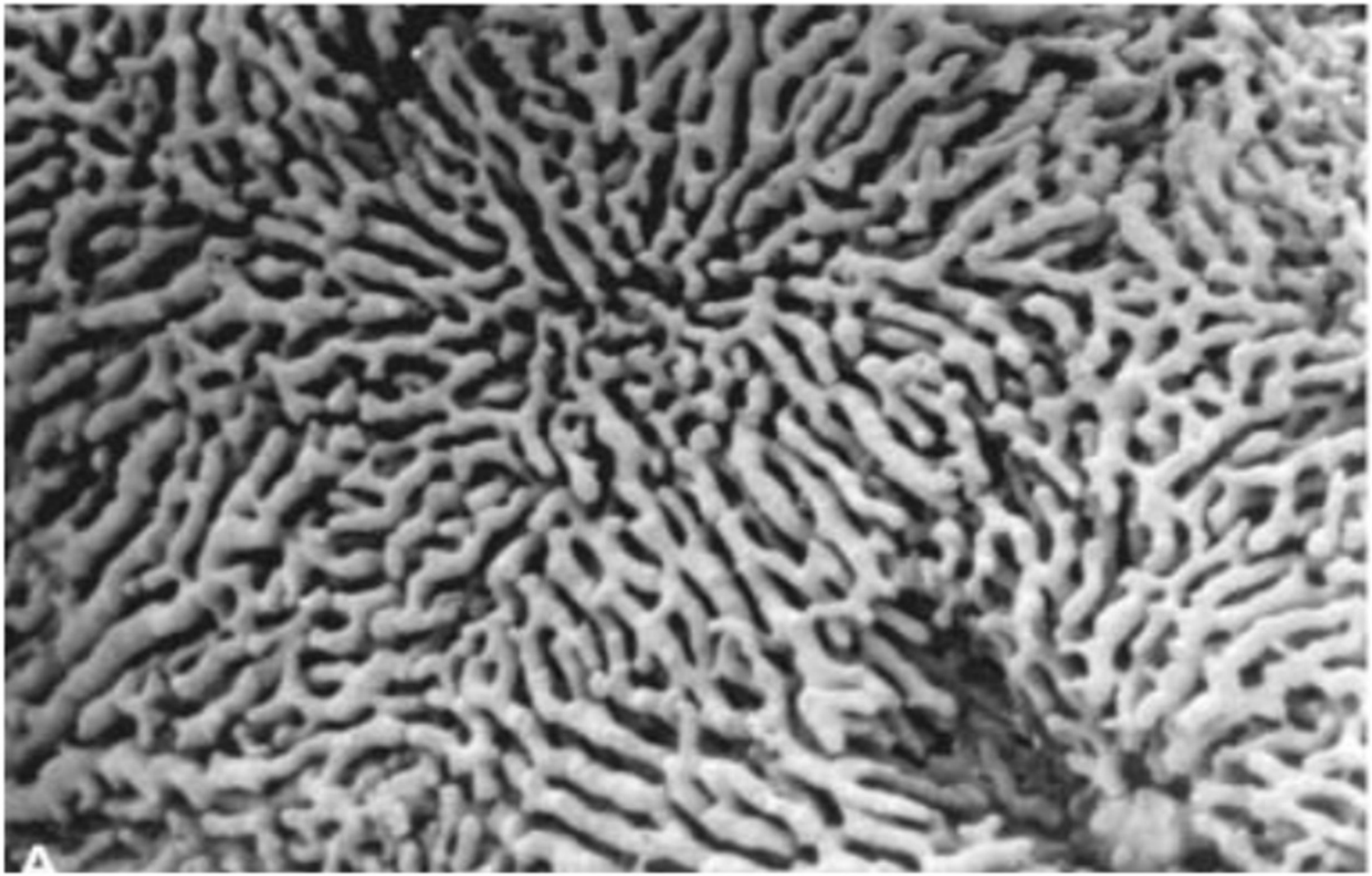

Sinusoids at the electronic microscope.

The liver lobule X

Circulation in the sinusoids

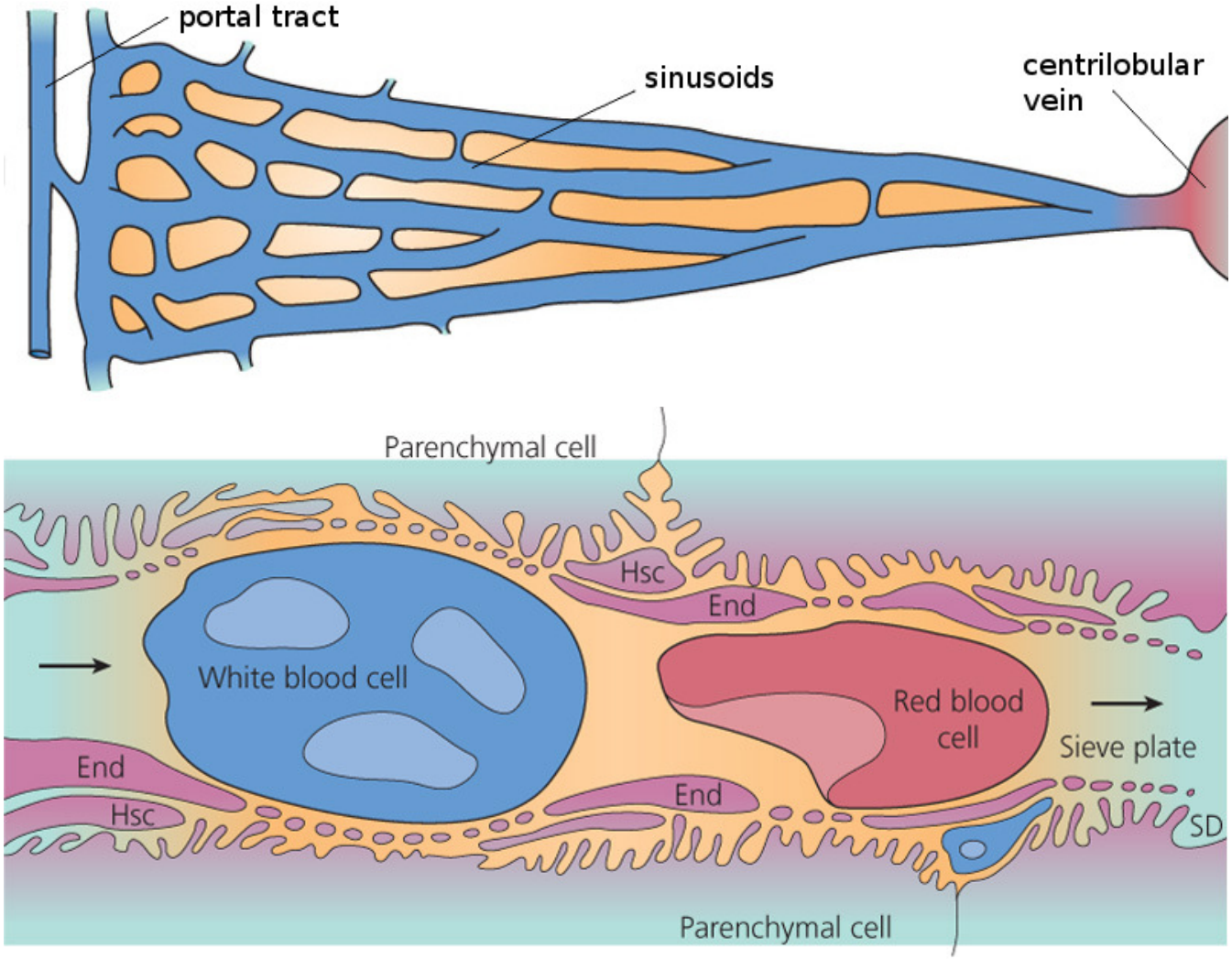

Note that the size of each sinusoid is comparable to the size of red blood cells.

Motivations for studying the mechanics of liver perfusion

- **Small-for-size livers**

  Small-for-size livers can be created after either a small-graft liver transplant or after a partial liver resection.

  The transplanted liver gradually grows to become normal size, but during the process damage can occur due to the high rate of perfusion.

  This results in hypertension in the hepatic portal vein.

  A shunt may be inserted between the portal and hepatic veins to allow some blood to bypass the liver.

  Knowledge of the relationship between the pressure drop across the liver and the blood flow is a prerequisite for a proper shunt design.

- **Oxygen distribution and hepatocyte activity**

  The arrangement of several portal tracts around one central vein may have an important role to improve the oxygen supply to hepatocytes.

  Hepatocytes behave differently in different regions of the lobule and a model of the blood perfusion of the liver lobule might help understanding the heterogeneity of hepatocyte activity.

- **Drug absorption and clearance**

  One of the main functions of the liver is to metabolise substances in the blood.

  Understanding of the spatial drug concentration after administration would help to predict clearance times and determine how much drug is absorbed in different regions of the liver.

Electrical analog approach

Van Der Plaats et al. (2004)

Aims of the work

- Understanding liver circulation characteristics in physiological conditions.
- Investigating the effect of micro-vascular changes due to injury.
- Predicting the effects of temperature, viscosity and perfusion characteristics on the (micro)circulation of the liver to understand optimal characteristics for liver hypothermic machine perfusion.

Characteristics of the model

- The authors performed a simulation the liver circulation in the whole liver based on an **electrical analogue model** (employing de Pater and van den Berg (1964) model).
- They modelled blood flow into various successive generations of vessels, from the hepatic artery and portal vein to the sinusoids and then to the hepatic veins.

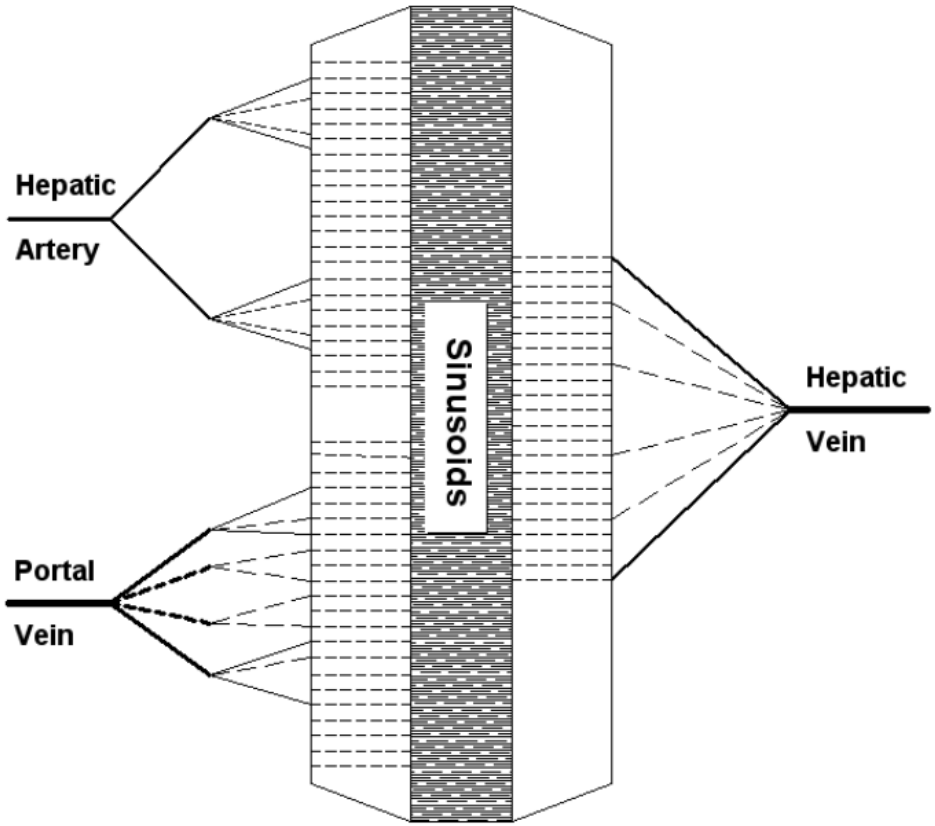

Results of Van Der Plaats et al. (2004)

Pressure distribution along the branching network

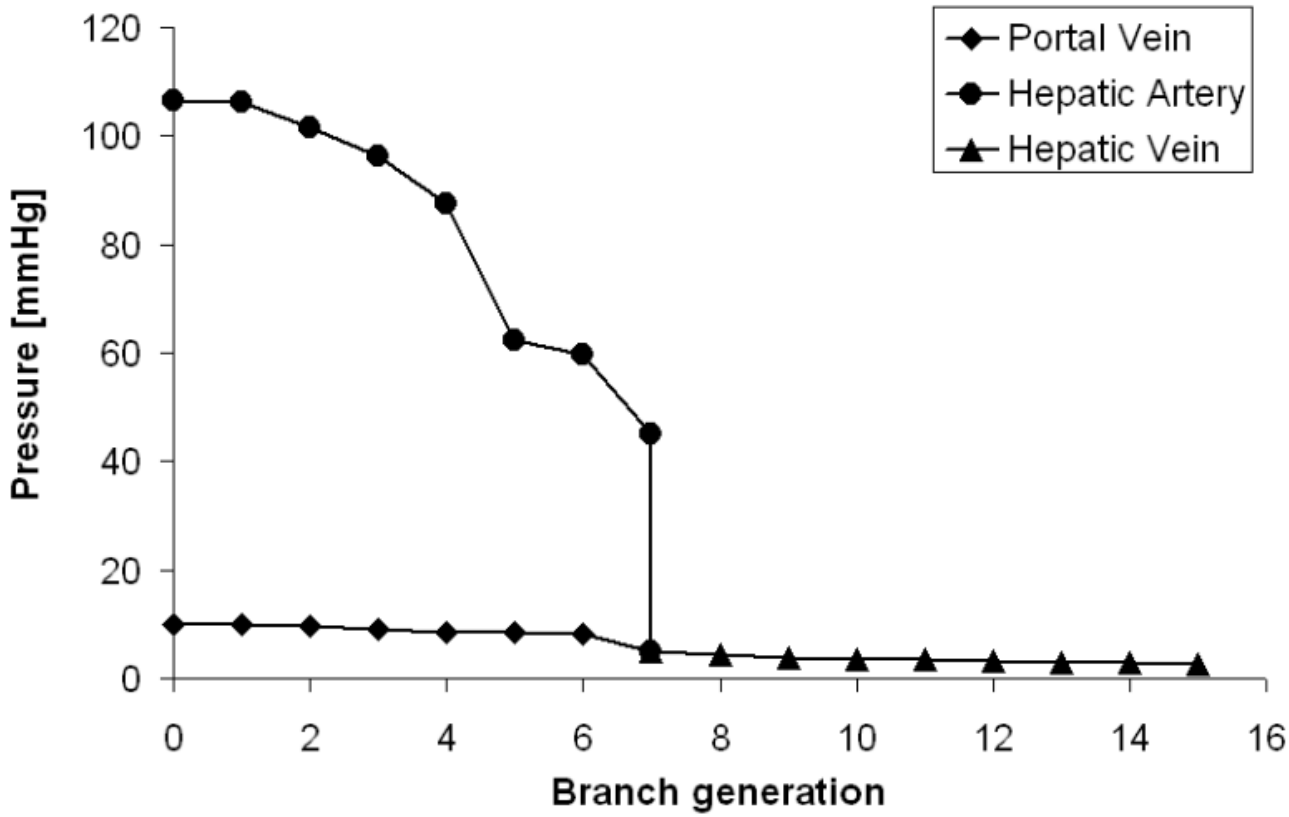

- The model allows to predict the **pressure drop as a function of the flow**.
- Most of the pressure drop occurs at the level of the arterioles and venules and in the sinusoids.
- After some parameter fitting results compare reasonably well with experimental data.

Mathematical model of the flow in the liver lobule

Bonfiglio et al. (2010).

Working assumptions

- The authors study blood flow in the **classic lobule** of the liver.
- The lobules are treated as identical regular hexagonal prisms arranged in a lattice.
- The portal tracts and centrilobular veins are cylindrical with diameters D_p and D_c, respectively.
- The axes of the portal tracts lie along the edges of the prisms, and the centrilobular veins lie along the central axes of the prisms.
- **The sinusoidal space is treated as a porous medium**.
- Portal tracts and centrilobular veins are treated as **point sources and sinks,** respectively.
- The axial length of the lobules is long compared with the length of an edge of the hexagon.
- End effects are neglected and the flow is treated as two-dimensional.

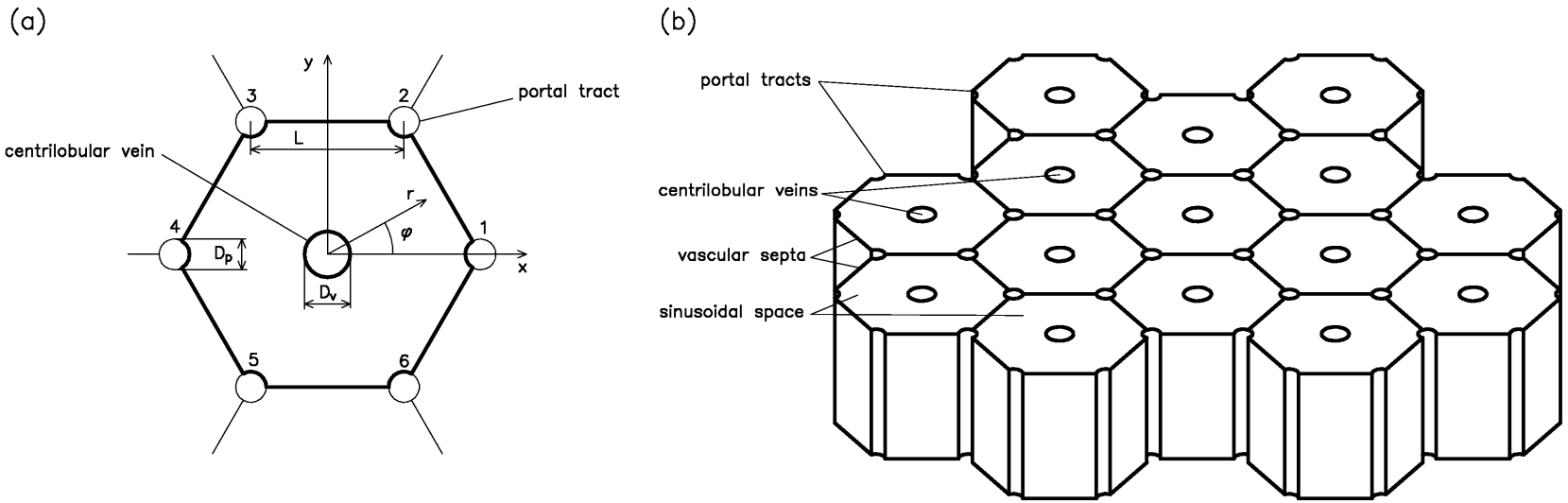

Basic solutions for two-dimensional flows in porous media I

Flow in porous media is governed by the Laplace equation for the pressure (61).

The Laplace equation is linear. This implies that the principle of superimposition of effects holds. In other works if we find many different solutions of the equations their linear combination is still a solution.

Two-dimensional point sources and sinks

Let us consider a two-dimensional point source/sink of strength Q, located in O. Q represents the volume flux per unit length entering/exiting from the source/sink. If $Q > 0$ the point is a source, if $Q < 0$ the point is a sink.
For symmetry reasons the velocity is everywhere radial (with respect to a coordinate system centred in O). Moreover, the flux through any circle l centred in O has to be equal to Q

$$\int_0^{2\pi} r q_r \, d\vartheta = 2\pi r q_r = Q,$$

having set $\mathbf{q} = (q_r, q_\vartheta)$, with $\mathbf{q}$ denoting the **apparent velocity** (see page 78), expressed in polar coordinates and $q_\vartheta = 0$ for symmetry.
From the above expression we have

$$q_r = \frac{Q}{2\pi r}, \qquad q_\vartheta = 0,$$

where r is the distance from the source point.

Basic solutions for two-dimensional flows in porous media II

We can then obtain an expression for the pressure p from Darcy law (60)

$$p = -\frac{Q\mu}{2\pi k} \log r + c,$$

where c is a constant. Note that this pressure distribution satisfies the Laplace equation (61).

Setup of the mathematical model I

We can now assume that

- **portal tracts are modelled as point sources;**
- **centrilobular veins are modelled as point sinks.**

Since we know the solution for the flow induced by a point source and sink, we can now sum up different solutions to obtain the desired flow.

In conclusion the mathematical problem can be formulated as follows:

$$\nabla^2 p = \begin{cases} -\dfrac{\mu Q^+}{k}\Delta & \text{at the hexagon angles (portal tracts),} \\ -\dfrac{\mu Q^-}{k}\Delta & \text{at the hexagon centre (centrilobular vein),} \\ 0 & \text{everywhere else,} \end{cases} \tag{121}$$

$$\nabla p \cdot \mathbf{n} = 0 \qquad \text{along the hexagon sides,} \tag{122}$$

where Q^+ and Q^- denote the intensity of the sources and sinks, respectively and we assume $Q^+ > 0$ and $Q^- < 0$. Moreover, in the above expressions Δ is the Dirac function and $\mathbf{n}$ denotes the unit vector normal to the hexagon side.

Setup of the mathematical model II

Conclusions about the model setup

The following points need careful consideration:

- determination of the relative strength of the sources and the sink;
- verification of the boundary conditions at the hexagon sides;
- if boundary conditions are not satisfied a way to enforce them has to be found.

Note: A possible technique to enforce the no-flux conditions through the hexagon sides is to add additional sources and sinks and look for some symmetry of the system.

- In a lattice of hexagons **there are twice as many sources** (angles of the hexagons) **than sinks** (centres of the hexagons). In order for the mass to be conserved **the intensity of a sink has to be twice that of a source**.
- For the no-flux boundary conditions at the hexagon sides to be satisfied the we can add an infinite number of hexagons which tessellate the whole space.
  The solution for the pressure p in a single point (x, y) within the hexagon can then be expressed as

$$p(x,y) = \lim_{N^- \to \infty} \left[-\sum_{i=1}^{2N^-} \frac{Q^+ \mu}{2\pi k} \log\left(\sqrt{(x - x_i^+)^2 + (y - y_i^+)^2} \right) - \sum_{j=1}^{N^-} \frac{Q^- \mu}{2\pi k} \log\left(\sqrt{(x - x_j^-)^2 + (y - y_j^-)^2} \right) \right], \tag{123}$$

Setup of the mathematical model III

where N^- denotes the number of sinks (and $N^+ = 2N^-$), (x_i^+, y_i^+) denotes the position of the i-th source and, (x_j^-, y_j^-) the position of the j-th sink.

Setup of the mathematical model IV

Scaling

It is covenient to work in terms of dimensionless variables as follows

$$\mathbf{x}^* = \frac{\mathbf{x}}{L}, \qquad \mathbf{q}^* = \frac{\mathbf{q}}{U}, \qquad p^* = \frac{p}{\frac{\mu U L}{k}},$$

where $\mathbf{x}$ denotes lengths, L is the length of the side of the lobule and U is a characteristic blood velocity in the sinusoids. The above pressure scale is suggested by the Darcy law.
Moreover, we assume that the flux per unit length Q^+ coming out of portal tracts can be written as

$$Q^+ = \pi U d,$$

where d is the diamater of a portal tract.

In terms of the above dimensionless variables equation (123) and Darcy law take the form

$$p^*(x^*, y^*) = \lim_{N^- \to \infty} \left[-\sum_{i=1}^{2N^-} \frac{d}{2L} \log\left(\sqrt{(x^* - x_i^{*+})^2 + (y^* - y_i^{*+})^2} \right) + \sum_{j=1}^{N^-} \frac{d}{L} \log\left(\sqrt{(x^* - x_j^{*-})^2 + (y^* - y_j^{*-})^2} \right) \right],$$

$$\mathbf{q}^* = -\nabla^* p^*.$$

Setup of the mathematical model V

Dimensional values

- Length of the side of a lobule L: 500 μm (Burt et al., 2006).
- Diameter of portal tracts d: 50 μm (Burt et al., 2006).
- Characteristic velocity in the sinusoidal space U (for the rat): 4×10^{-3} m/s (Koo et al., 1975).

Results I

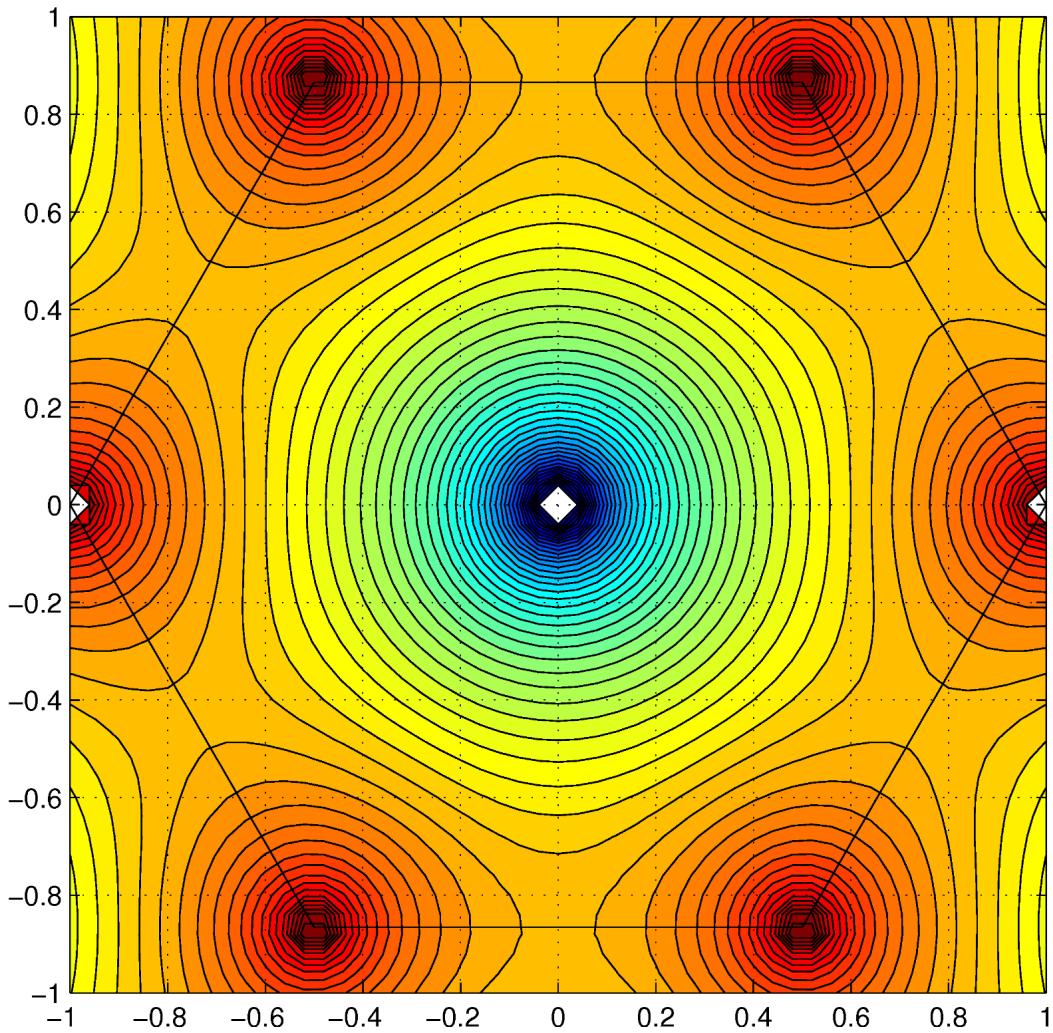

Pressure field.

Results II

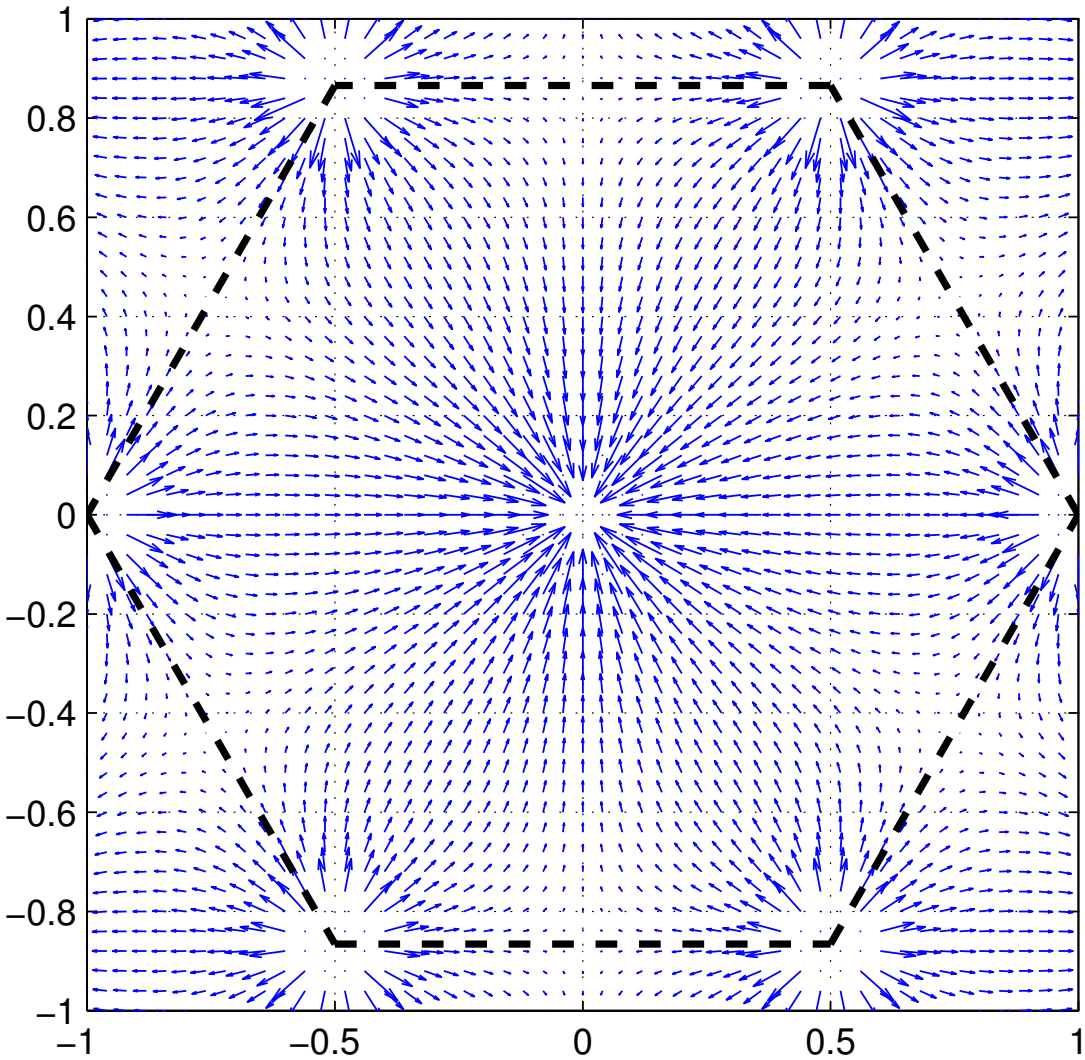

Velocity field.

Ocular Biomechanics: Introduction

Anatomy of the eye

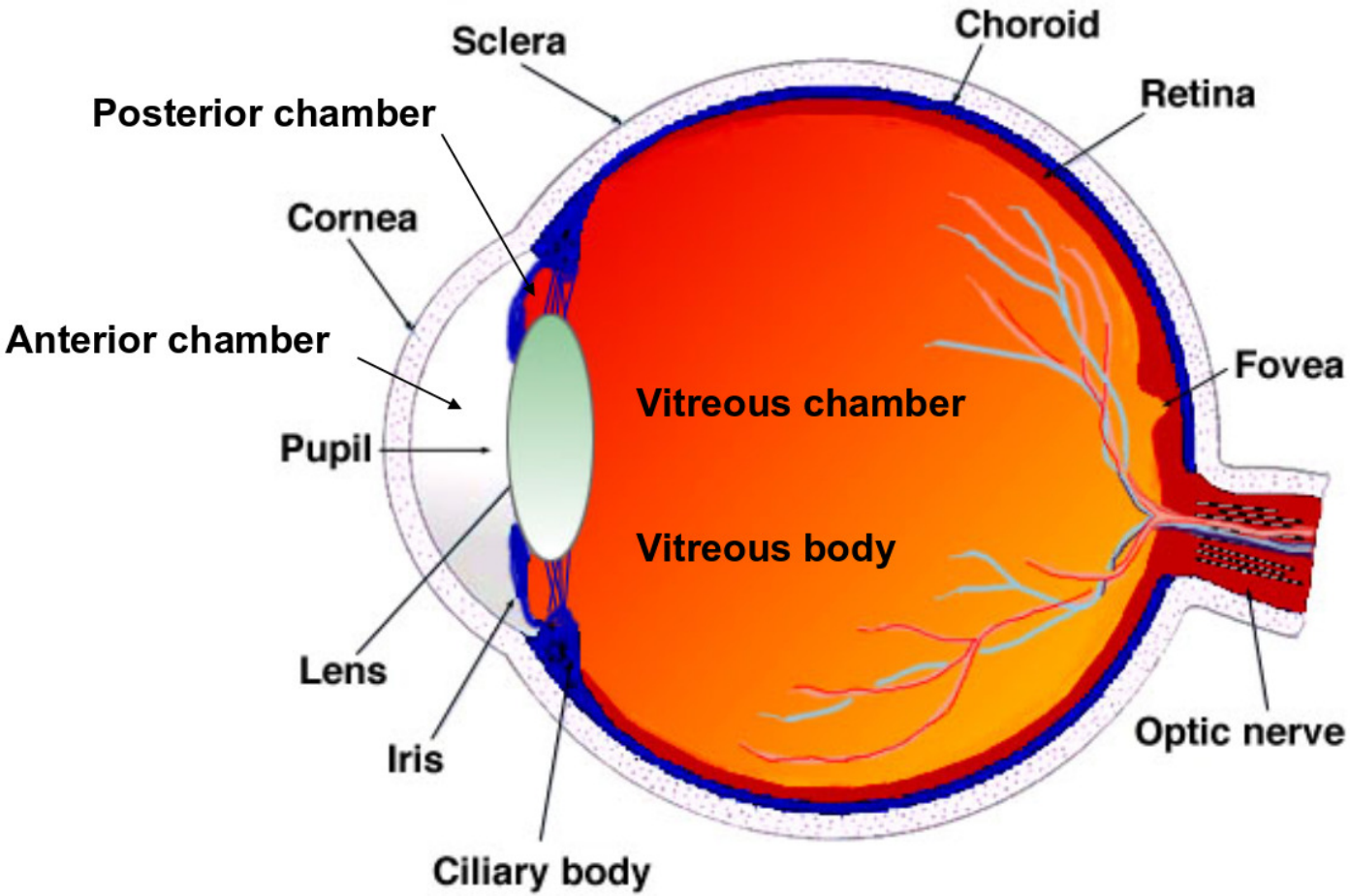

The anterior and posterior chambers

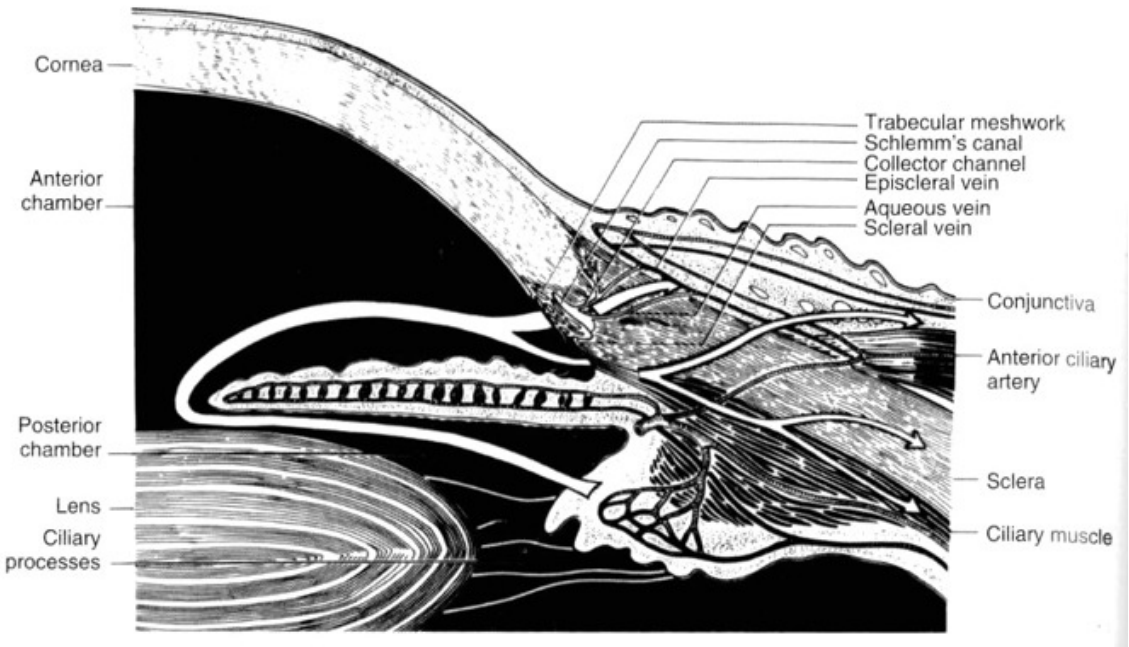

The **anterior chamber** contains the **aqueous humour**, a fluid with approximately the same mechanical characteristics as water

Aqueous humour is produced by the ciliary processes, flows in the **posterior chamber**, through the pupil, in the anterior chamber and is drained out at through the trabecular meshwork and the Schlemm's canal into the venous system.

The aqueous flow has two main roles

- It provides with nutrients the cornea and the lens which are avascular tissues.
- A balance between aqueous production and drainage resistance regulates the intraocular pressure (IOP).

The anterior chamber: drainage system

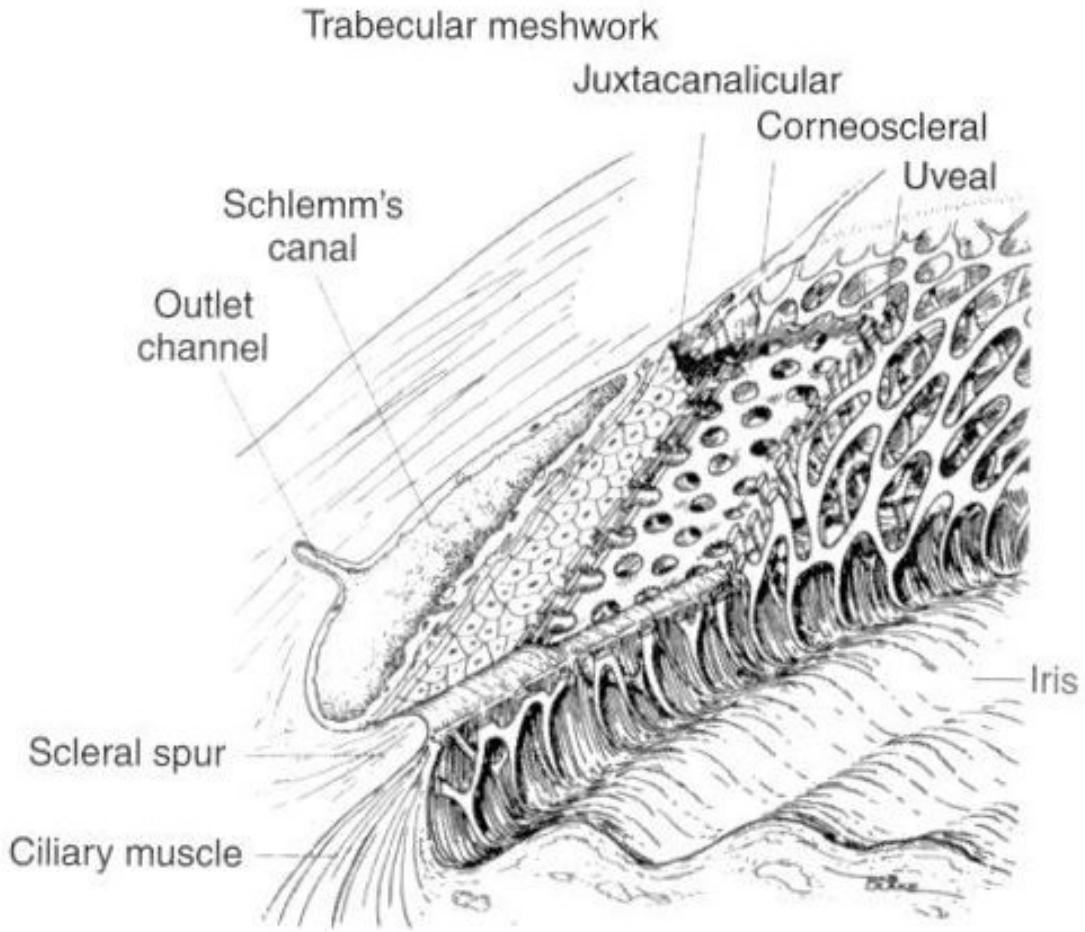

The lens

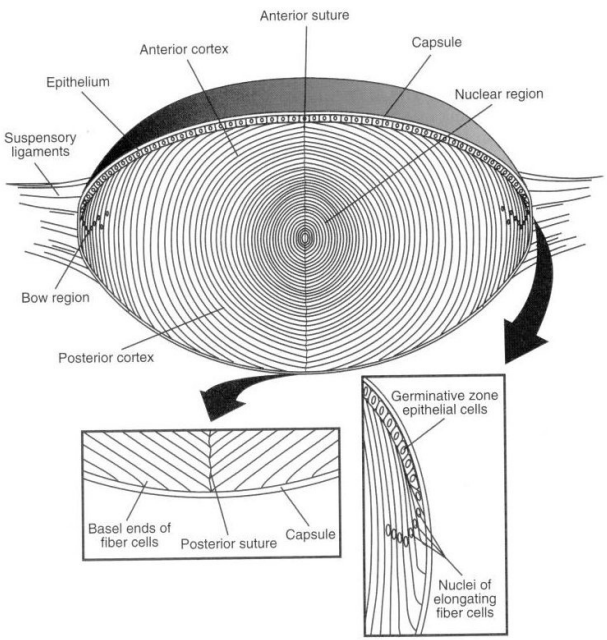

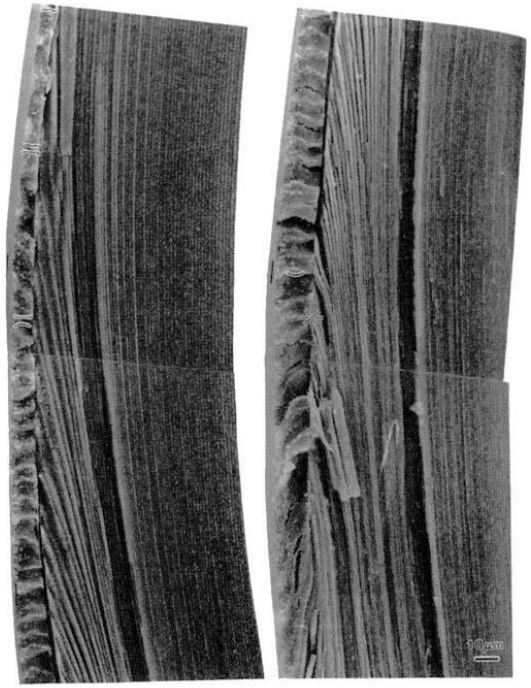

The **lens** is a transparent, biconvex structure in the eye that, along with the cornea, has the role of refracting light rays and to allow focus on the retina. It is responsible for approximately 1/3 of the total eye refractive power. The lens changes the focal distance by changing its shape (**accommodation**).

Structure: The lens is composed by three layers.

- **The capsule** is a smooth, transparent basement membrane that completely surrounds the lens. It is mainly composed of collagen and it is very elastic. Its thickness ranges within 2-28 μm.
- **The lens epithelium** is located in the anterior portion of the lens, between the lens capsule and the lens fibers.
- **The lens fibers** form the bulk of the lens. They are long, thin, transparent and firmly packed to each other. They form an onion-like structure.

The lens accommodation

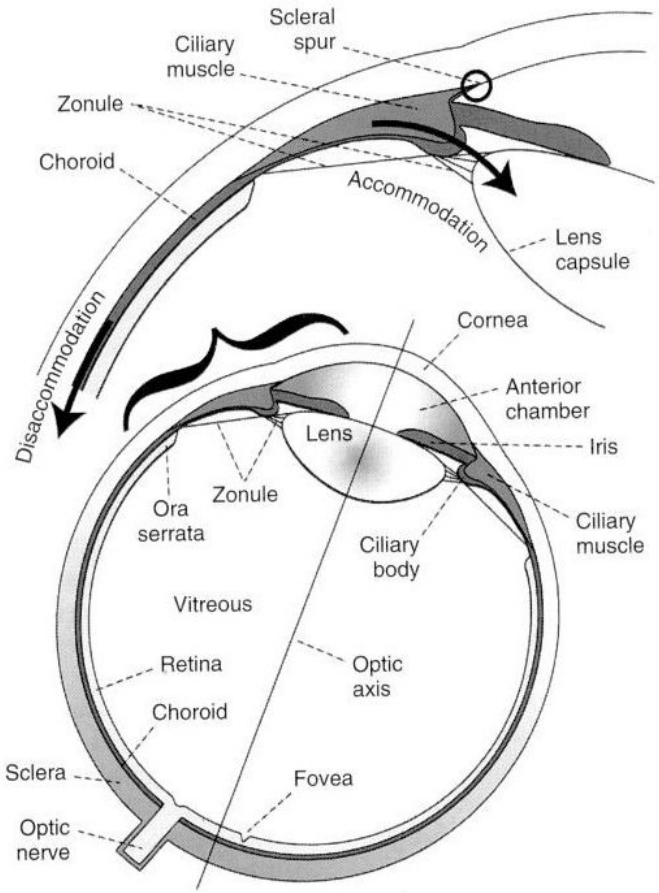

The vitreous chamber

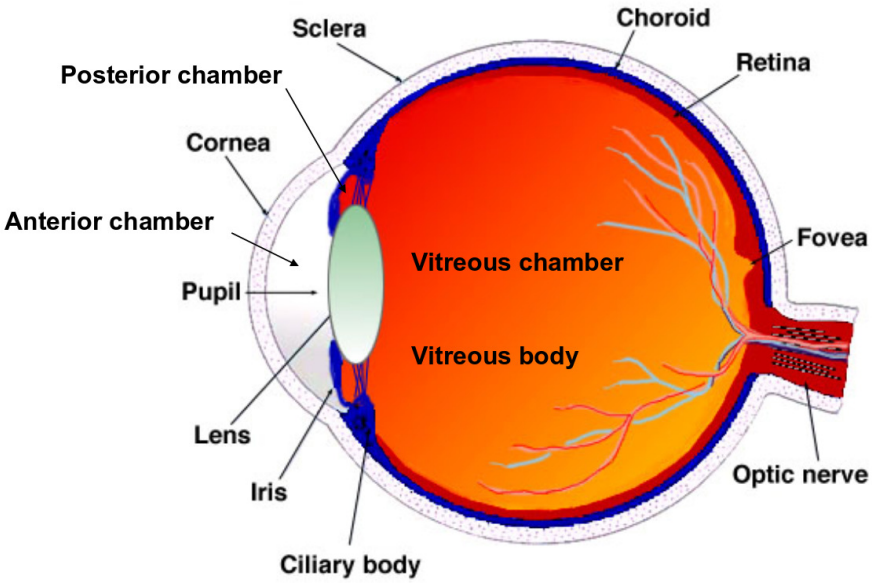

The **vitreous chamber** contains the **vitreous humour**. The vitreous has the following functions:

- **supporting the retina** in contact with the pigment epithelium;
- **filling-up the vitreous cavity**;
- acting as a **diffusion barrier** between the anterior and posterior segments of the eye
- establishing an unhindered path of light from the lens to the retina.

The vitreous goes through considerable physiological changes during life

- disintegration of the gel structure, liquefaction **(synchysis)**;
- approximately linear increase in the volume of liquid vitreous with age;
- possible complete liquefaction;
- **posterior vitreous detachment (PVD)** [film].

Vitreous replacement: After surgery **(vitrectomy)** the vitreous may be completely replaced with tamponade fluids (e.g. silicon oils, aqueous humour, air, . . .).

Optic nerve

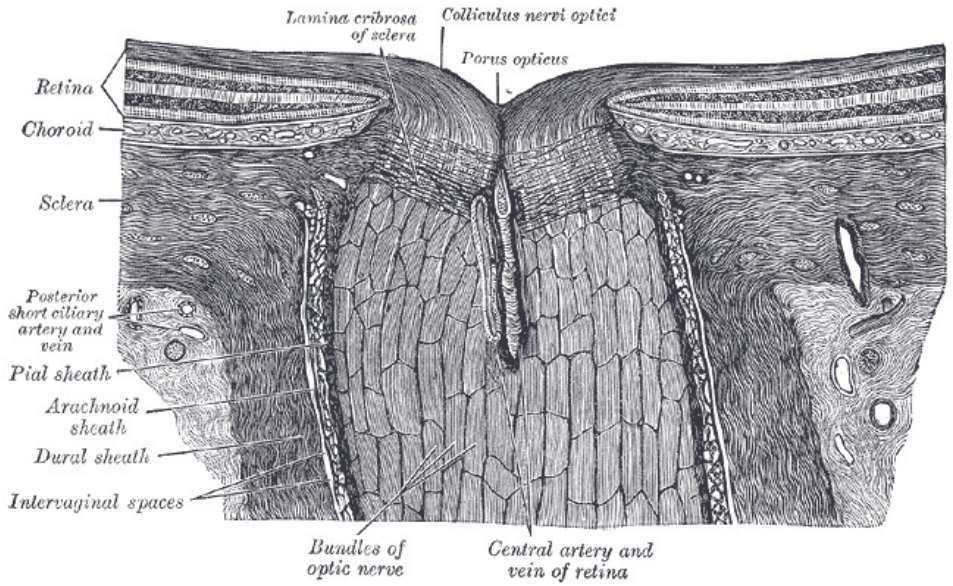
Lamina cribrosa of sclera
Colliculus nervi optici
Porus opticus
Retina
Choroid
Sclera
Posterior short ciliary artery and vein
Pial sheath
Arachnoid sheath
Dural sheath
Intervaginal spaces
Bundles of optic nerve
Central artery and vein of retina

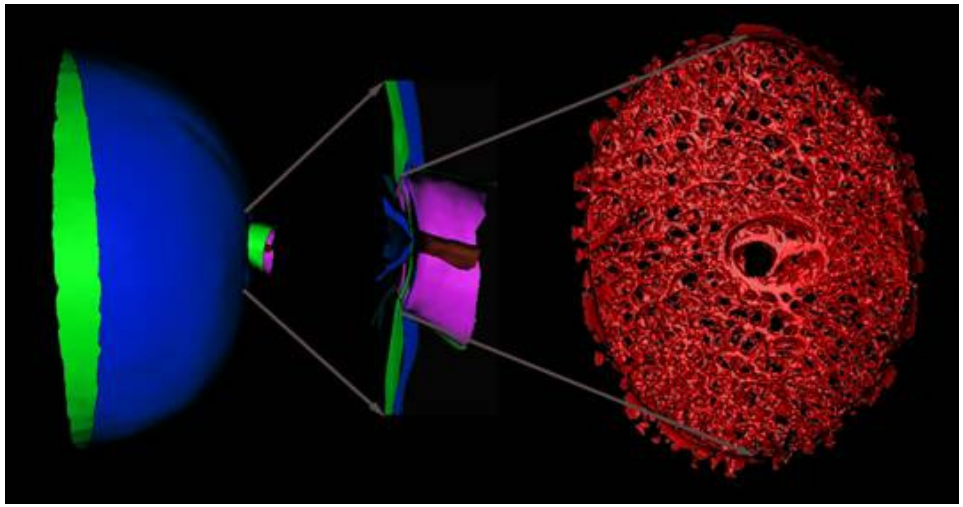

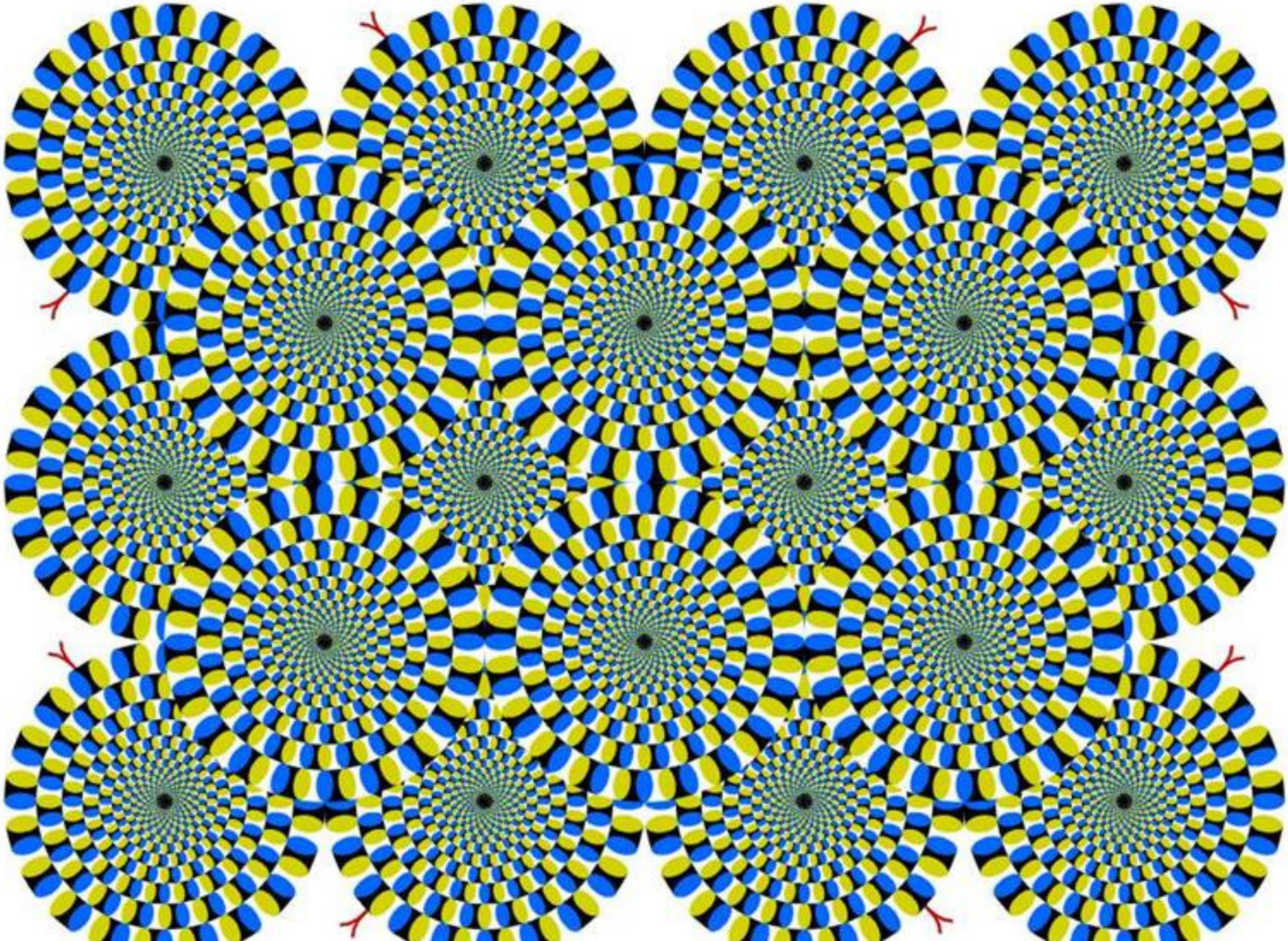

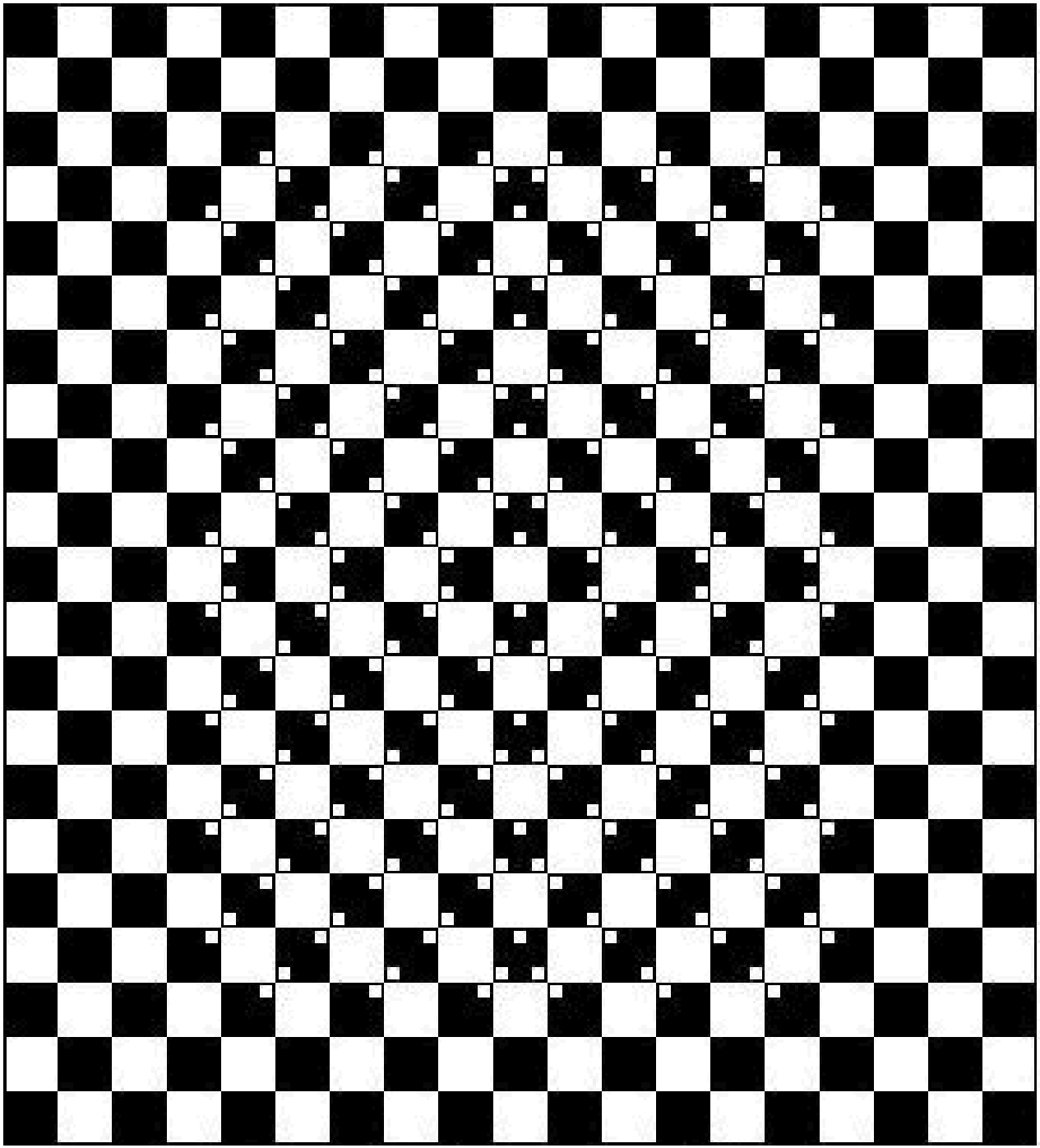

Specific references

- The textbook by Ethier and Simmons (2007) has a section on eye biomechanics.
- Ethier et al. (2004) review biomechanics and biotransport processes in the eye.
- Siggers and Ethier (2012) and Braun (2012) review the fluid mechanics of the eye.

Ocular biomechanics: Flow in the anterior chamber

Flow of aqueous humour: Why is there flow? I

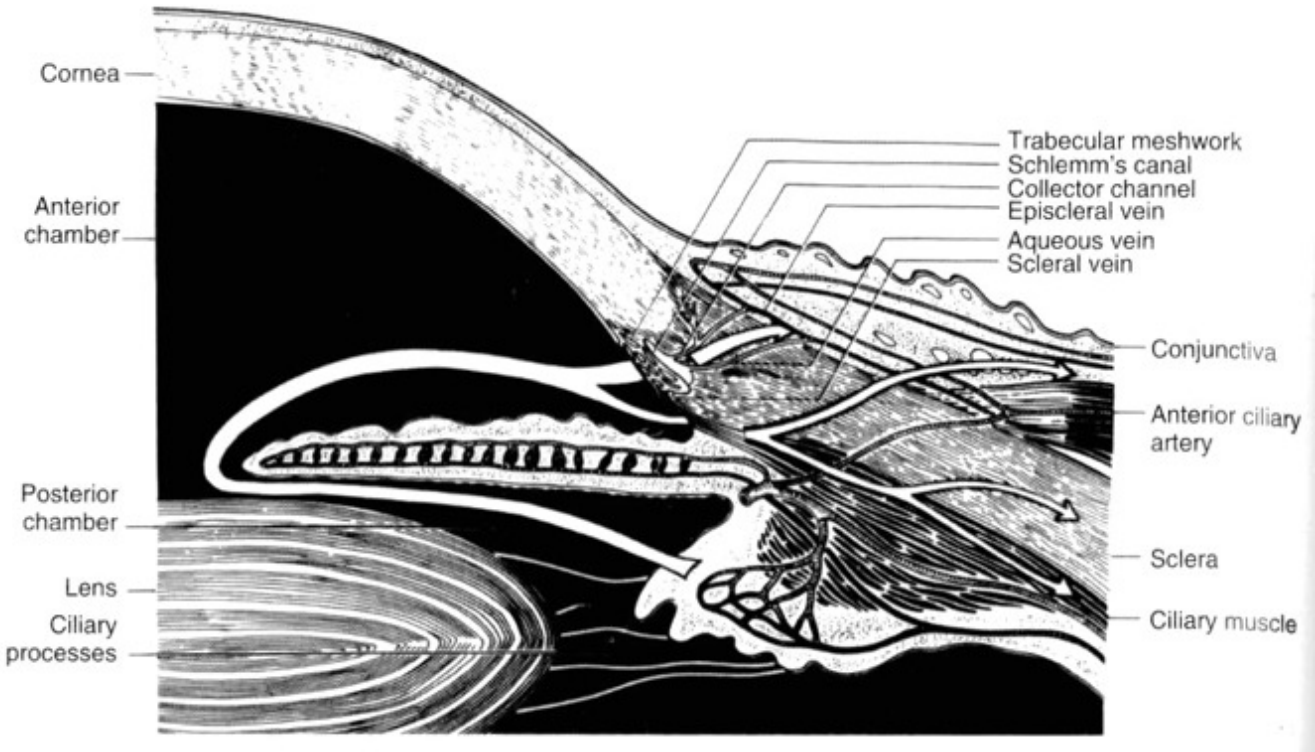

The aqueous flow has two main roles:

- Provides the cornea and the lens (avascular tissues) with nutrients
- Maintains balance between aqueous production and drainage. Outflow resistance regulates the **intraocular pressure (IOP).**
- Nutrition of the cornea and lens is mainly achieved through flow of the aqueous humour.

Flow of aqueous humour: Why is there flow? II

- There is bulk flow from ciliary processes through the pupil (radially inward) and then radially outward to the trabecular meshwork and Schlemm's canal and out of the eye.
- In addition, there is a **temperature gradient across the anterior chamber:**
  - at the back of the anterior chamber the temperature is close to the core body temperature ($\sim 37^\circ$);
  - the outside of the cornea is exposed to ambient conditions (perhaps $\sim 20^\circ$);
  - even though the temperature on the inside wall is close to 37°, there is a significant difference between the temperature at the front and that at the back.

  Therefore **buoyancy effects give rise to an additional flow.**
- The latter flow is particularly relevant when there is particulate matter in the anterior chamber.

Motivation for studying flow of aqueous humour I

Red blood cells

- **Red blood cells** are not normally found in the anterior chamber.
- Occur when there is rupture of blood vessels in the eye.
- Two forms:
  - **fresh cells** (less than 4 months old) can deform substantially and squeeze through the drainage system of the eye;
  - **ghost cells** (older than 4 months) are stiffer and cannot exit the eye. This may cause an increase in intraocular pressure as drainage pathways become blocked. Their density is significantly higher than that of water (~ 1500 kg/m^3). May cause sediment at the bottom of the anterior chamber **(hyphema)**.

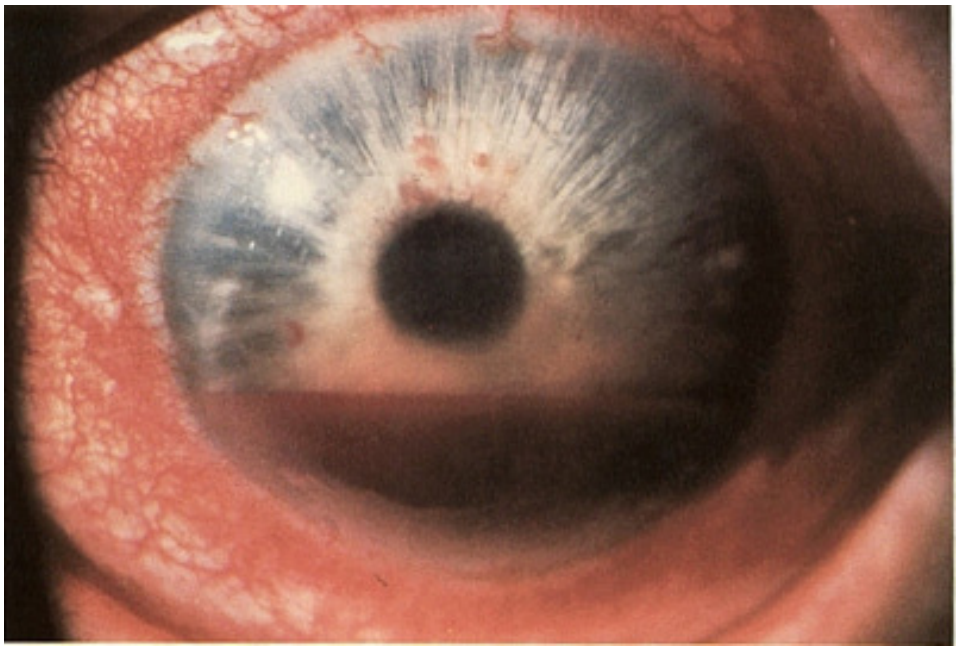

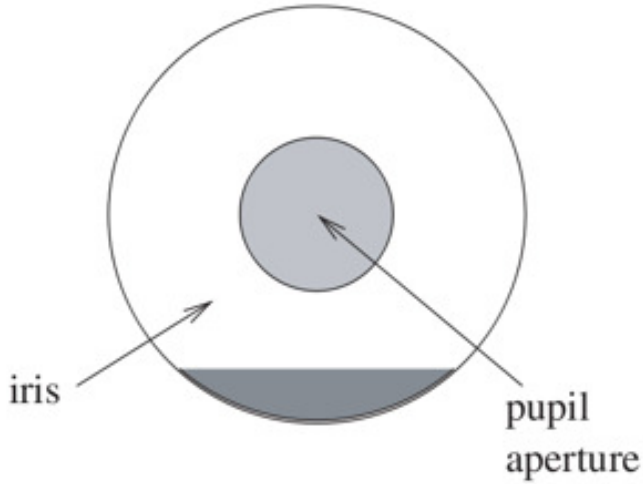

Motivation for studying flow of aqueous humour II

White blood cells

- White blood cells may also be present, typically indicating an inflammatory state of the ciliary body.
- The cells aggregate, forming the so-called **keratic precipitates**, shown below.

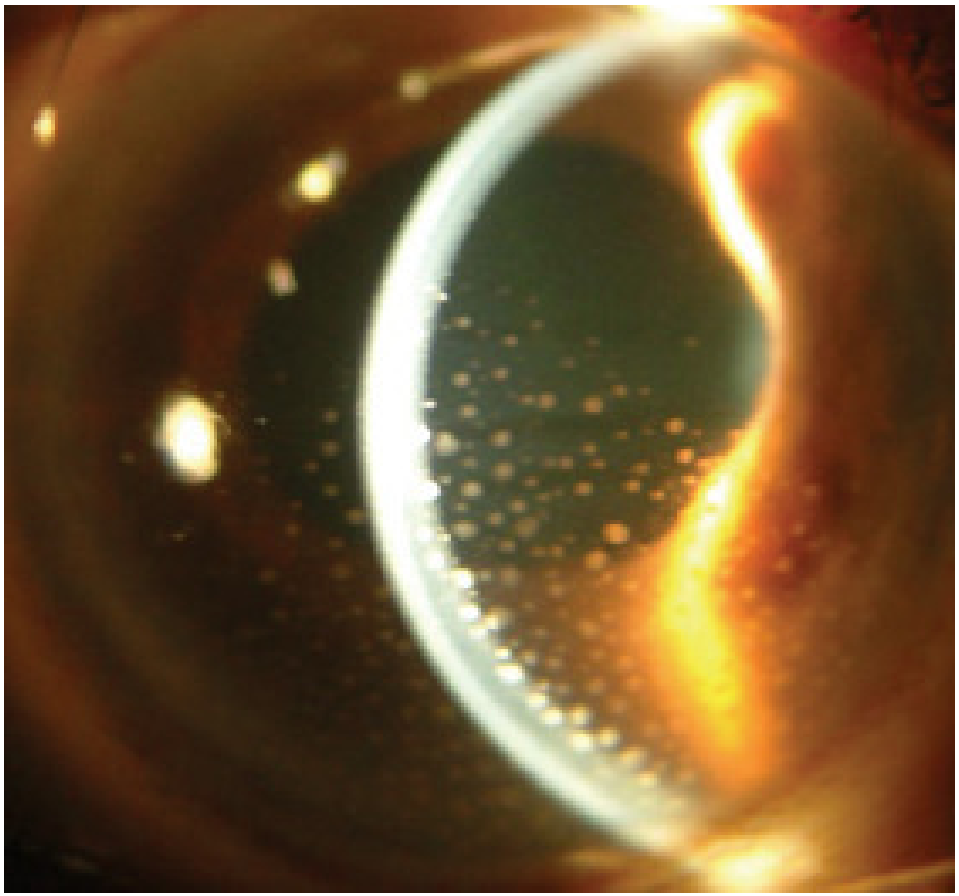

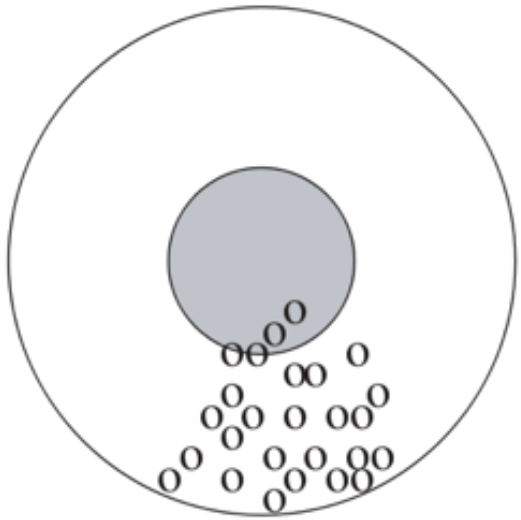

Motivation for studying flow of aqueous humour III

Glaucoma

- **Glaucoma** results in slow **progressive damage to the optic nerve** and subsequent loss of vision.
- Risk factors include:
  - **elevated eye pressure;**
  - increased age;
  - previous ocular injury.

  The only treatable risk factor is elevated eye pressure.

- Characteristics
  - Rate of production of aqueous humour remains constant.
  - The resistance to drainage increases (although the causes of this are not well understood).
  - Result is increase in intraocular pressure.
- Two types:
  - **open-angle glaucoma:** more common, when drainage becomes blocked.
  - **closed-angle glaucoma:** when flow from the posterior to the anterior chambers is blocked.

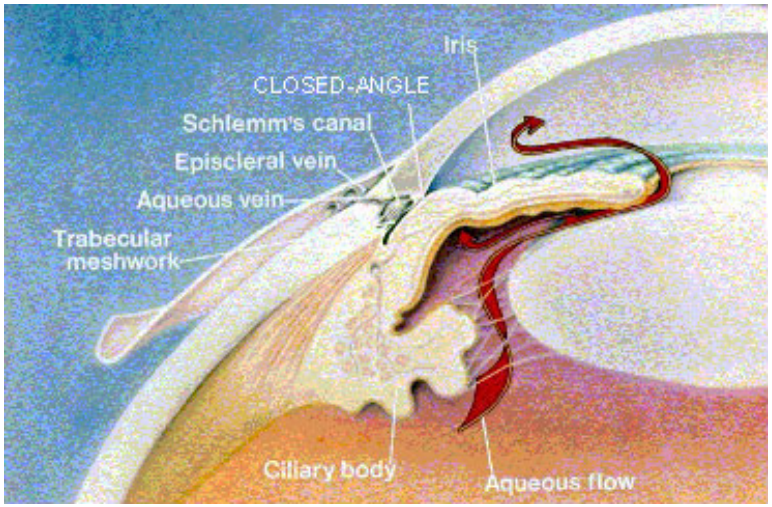

Closed angle glaucoma (Wolfe Eye Clinic)

Thermal flow between infinitely long parallel plates I

As a simple introductory example to understand the flow induced by thermal effects in the anterior chamber of the eye we consider the problem depicted in the figure below. A two-dimensional steady flow is generated in the space between two infinitely long parallel plates, kept at different temperatures (T_0 and T_1, respectively). The two plates are at a distance h between one another. We assume that gravity acts in the positive x-direction.

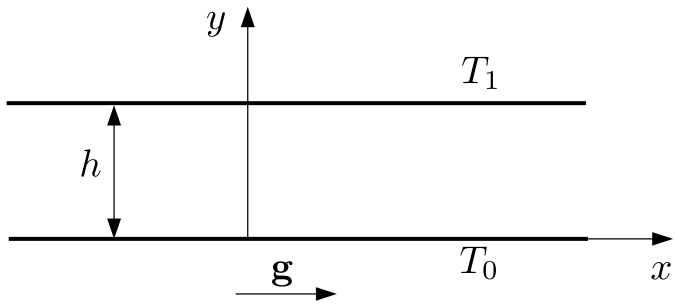

We study the motion of the fluid adopting Boussinesq approximation (see page 45). Owing to the infinite dimension of the domain in the x-direction we seek solutions such that

$$\mathbf{u} = [u(y), 0], \qquad \frac{\partial T}{\partial x} = 0.$$

Under the above assumptions the equations of motion and the corresponding boundary conditions read

$$-\frac{1}{\rho_0}\frac{\partial p}{\partial x} + \nu\frac{\partial^2 u}{\partial y^2} + g\left[1 - \alpha(T - T_0)\right] = 0, \tag{124a}$$

Thermal flow between infinitely long parallel plates II

$$\frac{\partial p}{\partial y} = 0, \tag{124b}$$

$$\frac{\partial^2 T}{\partial y^2} = 0, \tag{124c}$$

$$u = 0 \qquad (y = 0, h), \tag{124d}$$

$$T = T_0 \qquad (y = 0), \tag{124e}$$

$$T = T_1 \qquad (y = h). \tag{124f}$$

Note that the continuity equation is automatically satisfied.
From equation (124c) with boundary conditions (124e) and (124f) we obtain

$$T = T_0 + \eta y, \qquad \eta = \frac{T_1 - T_0}{h}.$$

From equation (124b) we infer that p does not depend on y. We can therefore integrate (124a) with respect to y and, imposing the boundary conditions (124d), we obtain

$$u = \frac{1}{2\nu}\left(\frac{1}{\rho_0}\frac{\partial p}{\partial x} - g\right) y(y-h) + \frac{g\alpha\eta}{6\nu} y\left(y^2 - h^2\right). \tag{125}$$

Since we have assumed $\partial u/\partial x = 0$, (125) implies that $\partial^2 p/\partial x^2 = 0$ and therefore $\partial p/\partial x = \text{const}$.

Thermal flow between infinitely long parallel plates III

In order to determine $\partial p/\partial x$ we note that, for symmetry reasons, the net flux in the x-direction must vanish. Hence, we impose

$$\int_0^h u dy = 0,$$

and finally obtain

$$p = \rho_0 g \left[1 - \frac{\alpha}{2}(T_1 - T_0)\right] x + c,$$

$$u = \frac{g\alpha}{6\nu h}(T_1 - T_0)\, y \left(y - \frac{h}{2}\right)(y - h),$$

where c is an arbitrary constant. As expected for symmetry reasons, the velocity vanishes at $y = 0$, $y = h/2$ and $y = h$.

Thermal flow between infinitely long parallel plates IV

This solution is plotted in terms of normalised variables in the following figure

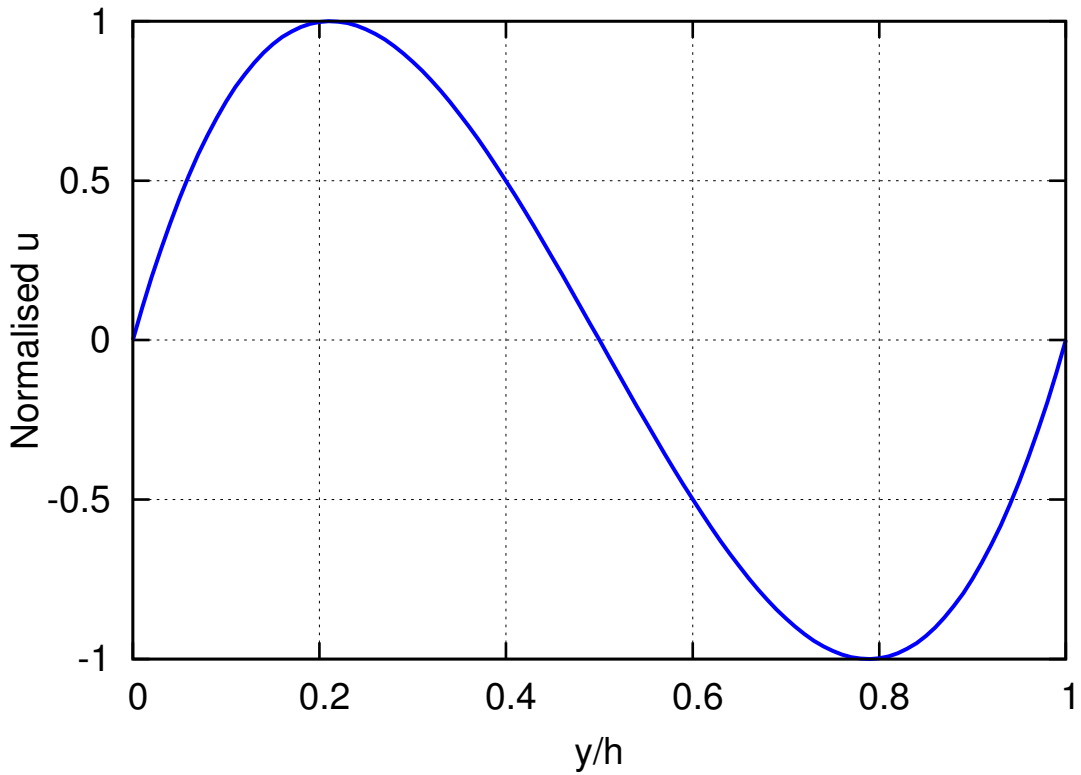

Analytical model of aqueous humour flow I

The generation of thermally riven flows in the anterior chamber has been studied by various authors:

- Canning et al. (2002), Fitt and Gonzalez (2006): **analytical models.**
- Heys et al. (2001), Heys and Barocas (2002) **fully numerical model.**
- ...

In the following we briefly present the models by Canning et al. (2002) and Fitt and Gonzalez (2006).

Geometry

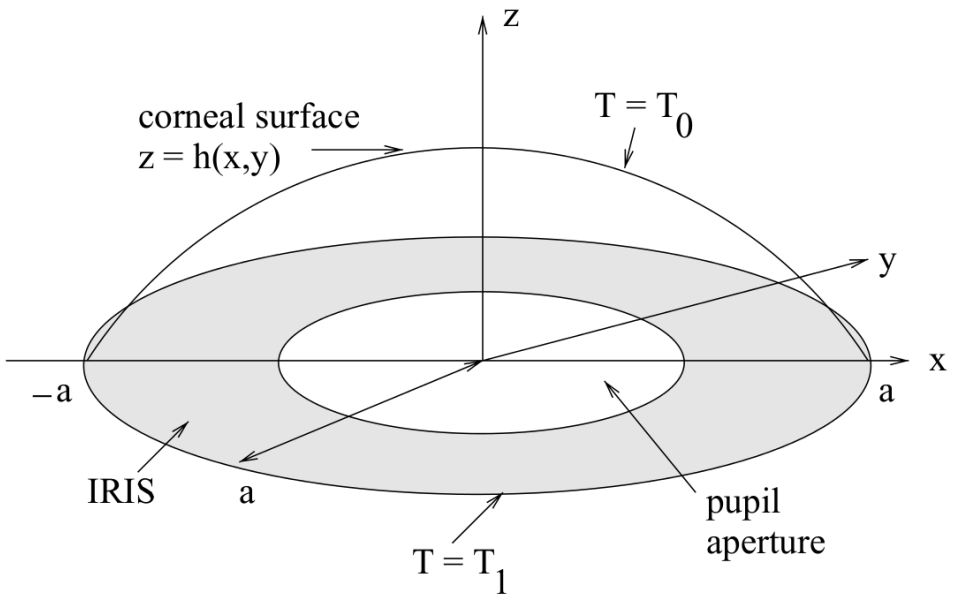

Sketch of the geometry. Note that gravity acts along the positive x-axis.

Analytical model of aqueous humour flow II

Governing equations

We use **Boussinesq approximation** to model density changes due to thermal effects. Thus, according to equation (39), we write

$$\rho = \rho_0 \left(1 - \alpha \left(T - T_0\right)\right).$$

We recall that, according to Boussinesq's approximation (see 45), since density and viscosity changes are small we can replace ρ with ρ_0 in all terms of the Navier-Stokes equation, except the gravitational one, and assume that the kinematic viscosity is constant (ν_0).
We thus need to solve the following system of equations

$$\rho_0 \left(\frac{\partial \mathbf{u}}{\partial t} + (\mathbf{u} \cdot \nabla \mathbf{u})\right) = -\nabla p + \rho_0 \nu_0 \nabla^2 \mathbf{u} + \rho_0 \left(1 - \alpha \left(T - T_0\right)\right) \mathbf{g},$$

$$\nabla \cdot \mathbf{u} = 0,$$

$$\frac{\partial T}{\partial t} + \mathbf{u} \cdot \nabla T = D \nabla^2 T,$$

subjected to the boundary conditions

$$u = v = w = 0, \qquad T = T_1 \qquad (z = 0),$$

$$u = v = w = 0, \qquad T = T_0 \qquad (z = h),$$

with u, v and w the x, y and z components of the velocity, respectively.

Analytical model of aqueous humour flow III

Simplification using lubrication theory

- We define $\epsilon = h_0/a$ (anterior–posterior chamber depth divided by radius).
- Typically $\epsilon^2 \approx 0.06$, motivating the limit of small ϵ.
- We use the lubrication theory to simplify the equations, as described at page 36. In particular we neglect terms of order ϵ^2, $\epsilon^2 Re$ and $\epsilon^2 RePr$ with respect to terms of order 1, where we have defined:

Reynolds number $$Re = \frac{Ua}{\nu_0},$$

Prandtl number $$Pr = \frac{\nu_0}{D},$$

and U is a characteristic scale of the velocity.

Analytical model of aqueous humour flow IV

The reduced system of equations

The simplified equations read:

$$
\begin{aligned}
&x\text{-momentum:} && -\frac{1}{\rho_0}\frac{\partial p}{\partial x} + \nu_0 \frac{\partial^2 u}{\partial z^2} + g\left(1 - \alpha\left(T - T_0\right)\right) = 0, \\
&y\text{-momentum:} && -\frac{1}{\rho_0}\frac{\partial p}{\partial y} + \nu \frac{\partial^2 v}{\partial z^2} = 0, \\
&z\text{-momentum:} && \frac{\partial p}{\partial z} = 0, \\
&\text{Continuity} && \frac{\partial u}{\partial x} + \frac{\partial v}{\partial y} + \frac{\partial w}{\partial z} = 0, \\
&\text{Diffusion} && \frac{\partial^2 T}{\partial z^2} = 0.
\end{aligned}
$$

Analytical model of aqueous humour flow V

This system of equations can be solved analytically (for any domain shape h), following a procedure very similar to that described at page 41. The following solution is obtained

$$u = -\frac{(T_1 - T_0) g \alpha z}{12 \nu h} (2z - h)(z - h)$$

$$v = 0$$

$$w = -\frac{(T_1 - T_0) g \alpha z^2}{24 \nu h^2} \frac{\partial h}{\partial x} (z^2 - h^2)$$

$$p = p_0 + (x + a) g \rho_0 \left(1 - \frac{\alpha (T_1 - T_0)}{2}\right)$$

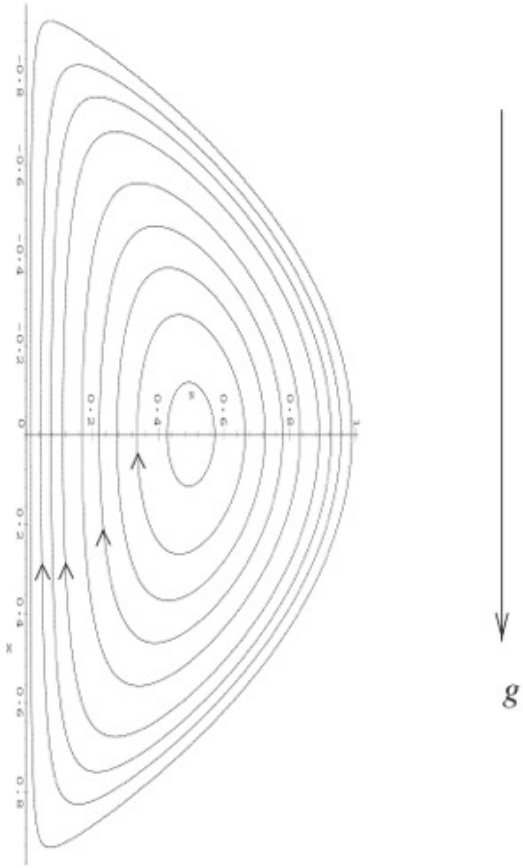

- The **flow is two-dimensional**, as it takes place on planes defined by the equation $y = \text{const}$.
- The **maximum velocity**, computed with realistic values of all parameters, is estimated to be $1.98 \times 10^{-4}(T_1 - T_0)$ m/s/K, which **is consistent with experimental observations**.
- The **solution allows us to compute many other physically meaningful quantities**, *e.g.* the wall shear stress on the surface.

Numerical simulations I

Fully numerical solutions have also been proposed in the literature, e.g. Heys et al. (2001); Heys and Barocas (2002).

Modelling assumptions:

- **Fully numerical approach.**
- The aqueous is modelled as a Newtonian fluid.
- Axisymmetric flow (Heys et al., 2001), fully thee-dimensional flow (Heys and Barocas, 2002).
- Linear elastic behaviour of the iris.

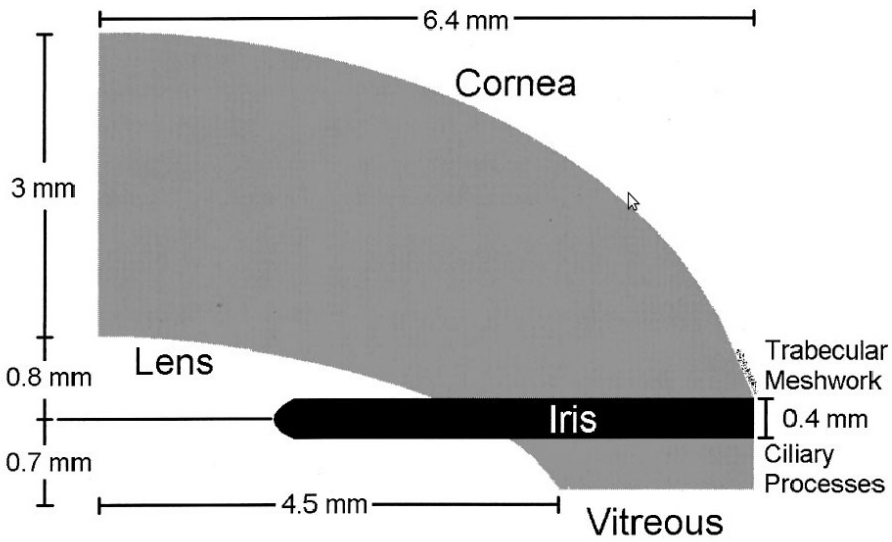

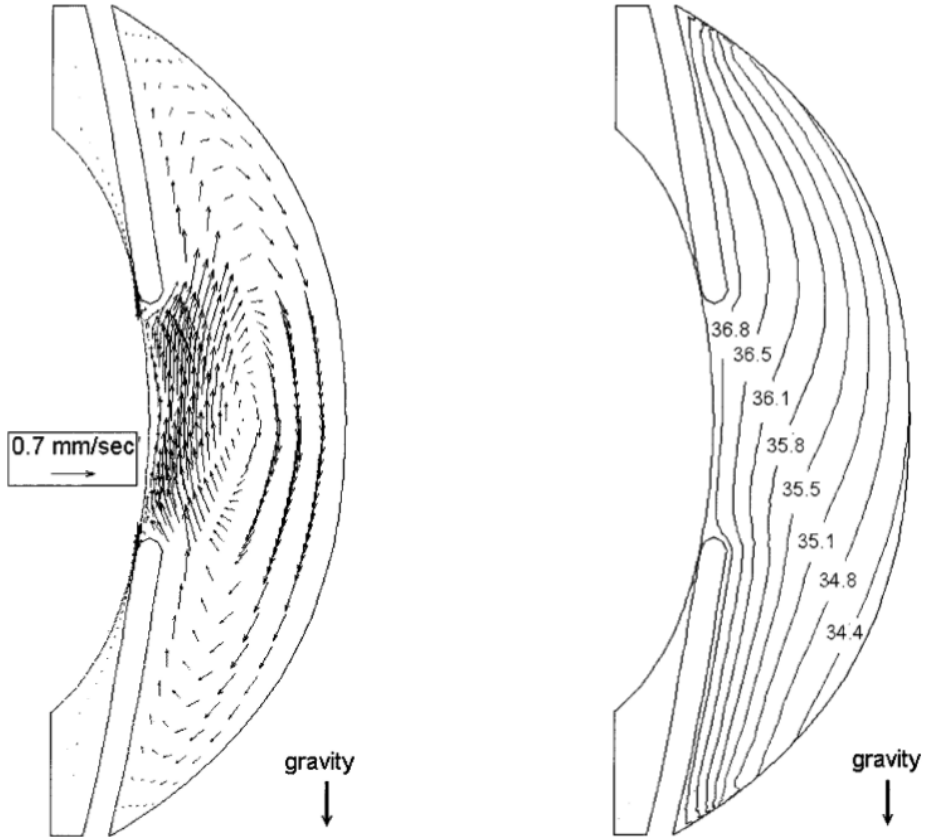

Velocity and temperature fields (from Heys and Barocas, 2002).

Numerical simulations II

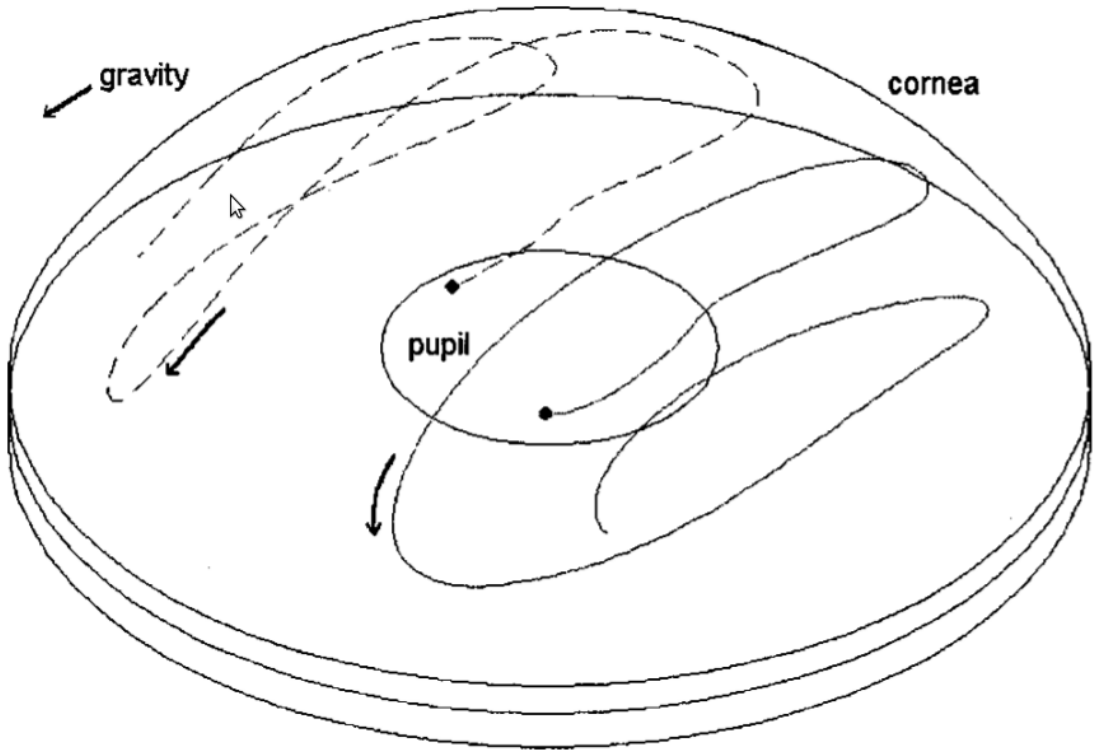

Three-dimensional particle paths (from Heys and Barocas, 2002).

Numerical simulations III

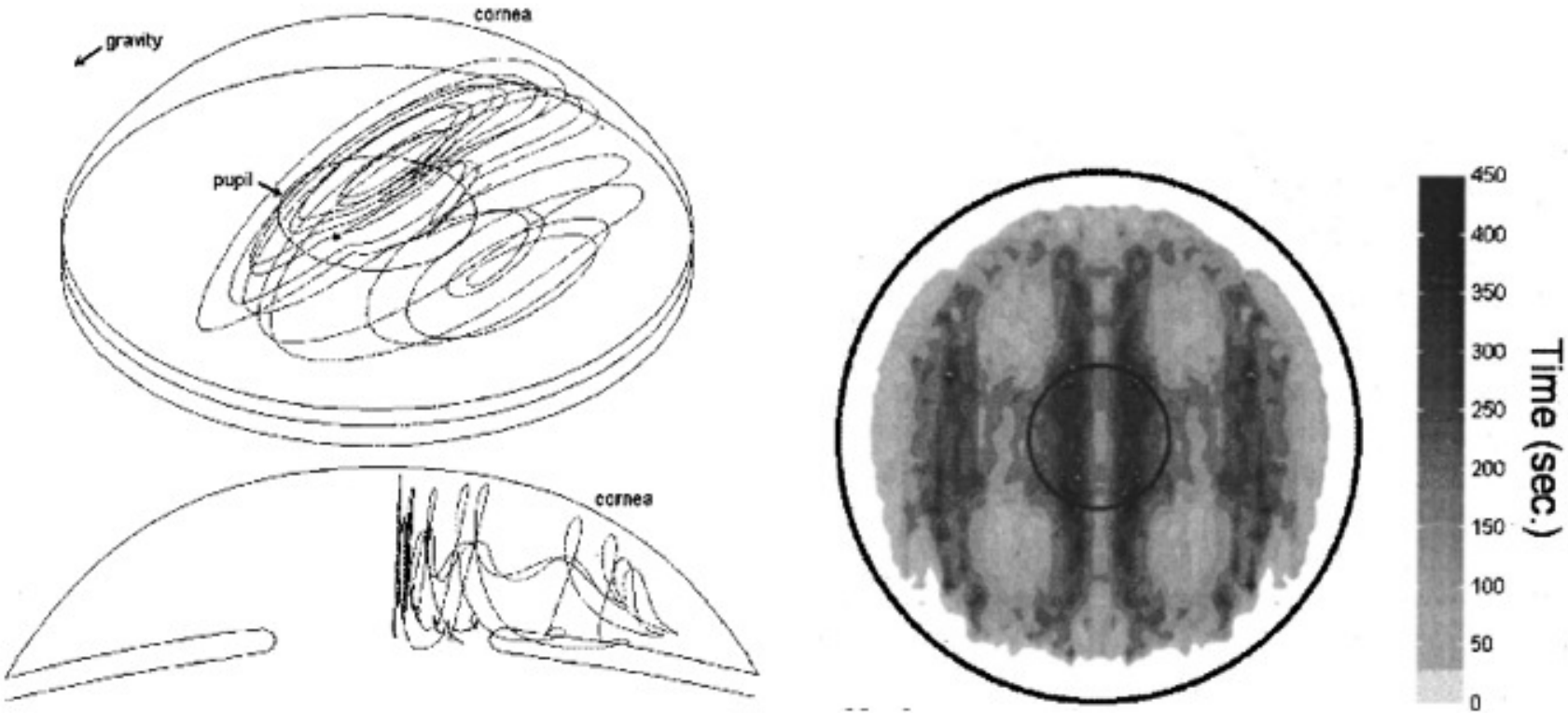

Three-dimensional particle paths and residence times (from Heys and Barocas, 2002).

Ocular Biomechanics: Fluid dynamics of the vitreous chamber

Vitreous characteristics and functions

Vitreous composition

The main constituents are

- Water (99%);
- hyaluronic acid (HA);
- collagen fibrils.

Its structure consists of long, thick, non-branching collagen fibrils suspended in hyaluronic acid.

Normal vitreous characteristics

- The healthy vitreous in youth is a gel-like material with **visco-elastic mechanical properties**, which have been measured by several authors (Lee et al., 1992; Nickerson et al., 2008; Swindle et al., 2008).
- In the outermost part of the vitreous, named **vitreous cortex**, the concentration of collagen fibrils and HA is higher.
- The vitreous cortex is in contact with the **Internal Limiting Membrane (ILM)** of the retina.

Physiological roles of the vitreous

- **Support function for the retina** and filling-up function for the vitreous body cavity;
- **diffusion barrier** between the anterior and posterior segment of the eye;
- establishment of an **unhindered path of light.**

Vitreous ageing

With advancing age the vitreous typically undergoes significant changes in structure.

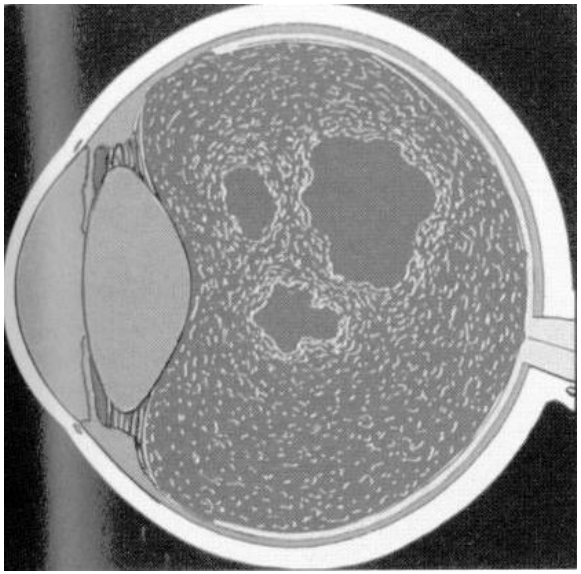

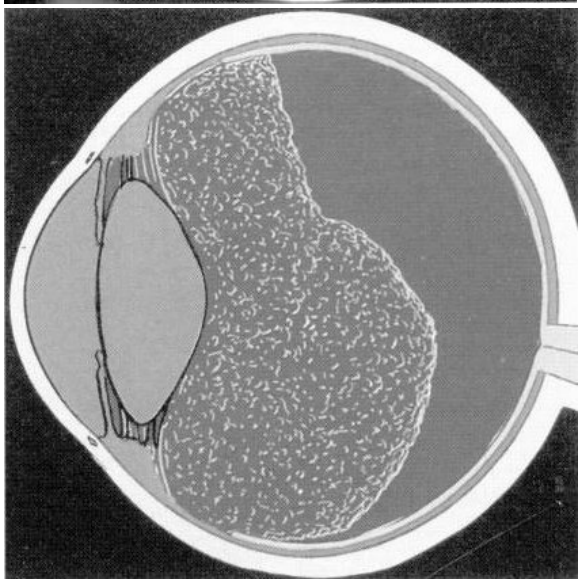

- Disintegration of the gel structure which leads to **vitreous liquefaction (synchisys)**. This leads to an approximately linear increase in the volume of liquid vitreous with time. Liquefaction can be as much extended as to interest the whole vitreous chamber.
- Shrinking of the vitreous gel **(syneresis)** leading to the detachment of the gel vitreous from the retina in certain regions of the vitreous chamber. This process typically occurs in the posterior segment of the eye and is called **posterior vitreous detachment (PVD)**. It is a pathophysiologic condition of the vitreous.

Vitreous replacement

After surgery **(vitrectomy)** the vitreous may be completely replaced with tamponade fluids:

- silicon oils water;
- aqueous humour;
- perfluoropropane gas;
- ...

Partial vitreous liquefaction

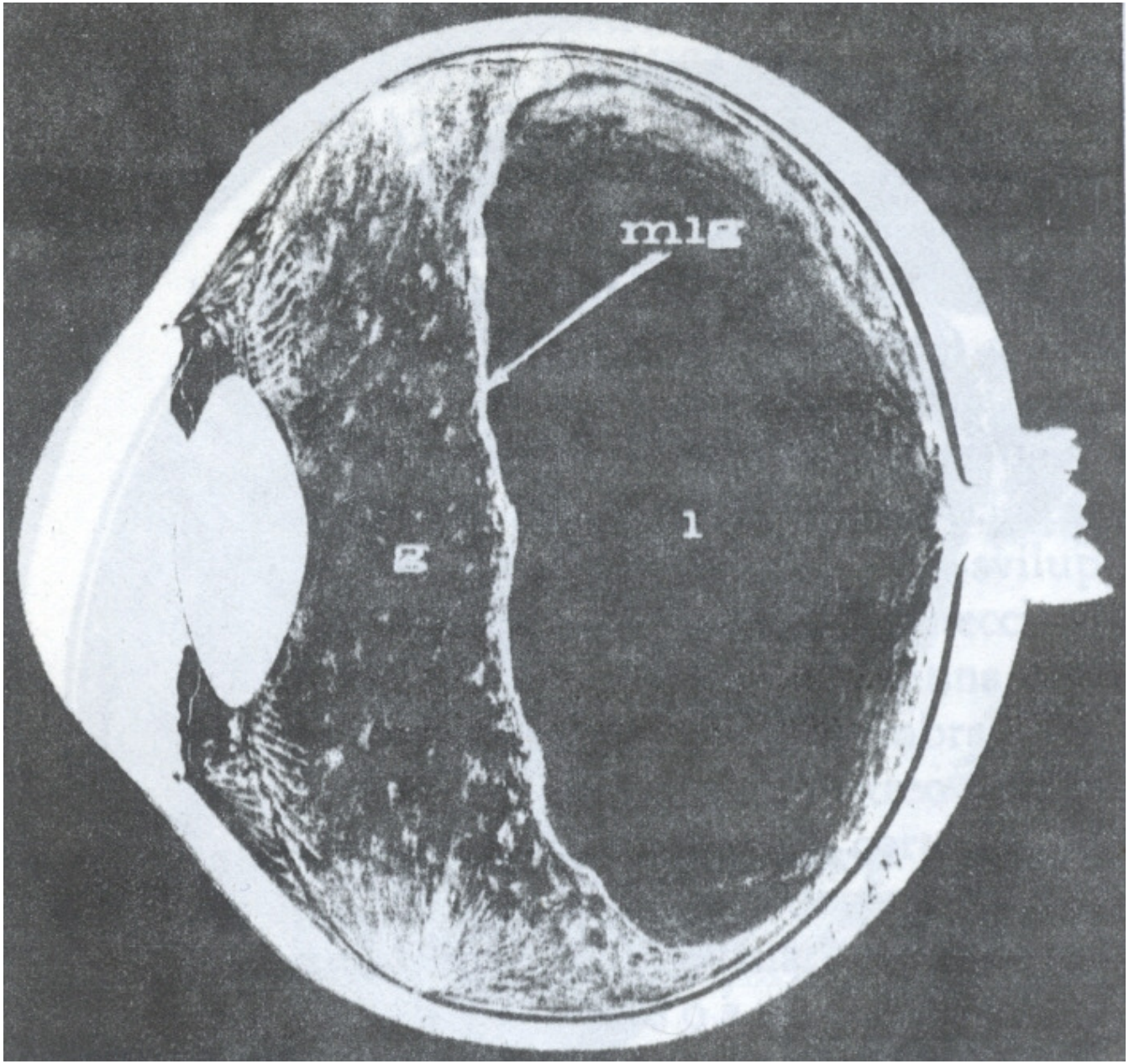

Motivations of the work

Why research on vitreous motion?

- Possible connections between the mechanism of **retinal detachment** and
  - the shear stress on the retina;
  - flow characteristics.
- Especially in the case of liquefied vitreous eye rotations may produce effective **fluid mixing**. In this case **advection may be more important that diffusion** for mass transport within the vitreous chamber.
  Understanding diffusion/dispersion processes in the vitreous chamber is important to predict the behaviour of drugs directly injected into the vitreous.

Retinal detachment

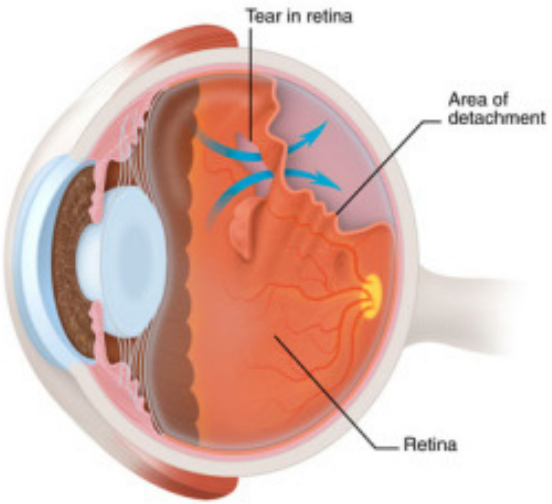

Posterior vitreous detachment and vitreous degeneration:

- more common in myopic eyes;
- preceded by changes in vitreous macromolecular structure and in vitreoretinal interface $\rightarrow$ possibly mechanical reasons.

- If the retina detaches from the underlying layers $\rightarrow$ loss of vision;
- Rhegmatogeneous retinal detachment: fluid enters through a retinal break into the subretinal space and peels off the retina.
- **Risk factors:**
  - **myopia;**
  - posterior vitreous detachment (PVD);
  - lattice degeneration;
  - ...

Scleral buckling

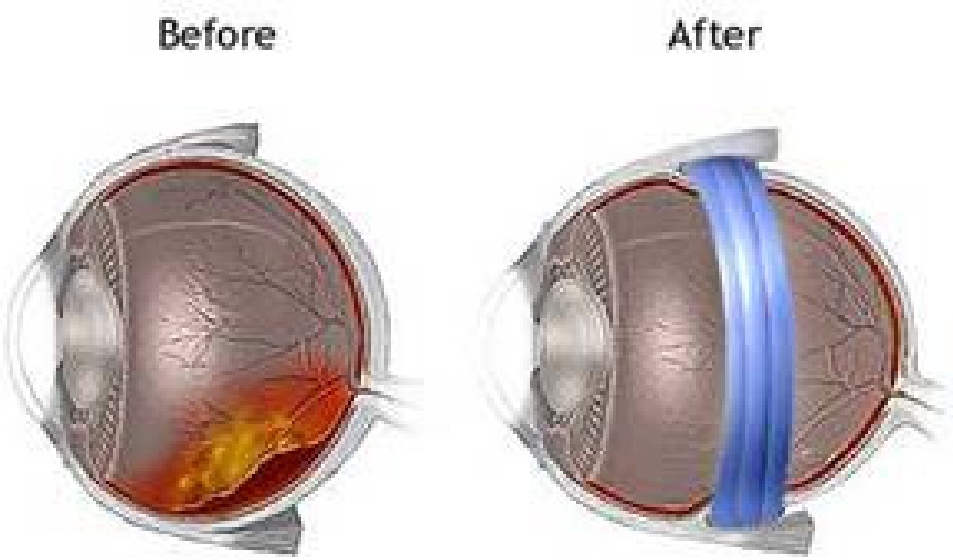

Scleral buckling is the application of a rubber band around the eyeball at the site of a retinal tear in order to promote re-attachment of the retina.

Intravitreal drug delivery

It is difficult to transport drugs to the retina from 'the outside' due to the tight blood-retinal barrier $\rightarrow$ use of **intravitreal drug injections.**

Saccadic eye rotations

Saccades are eye movements that rapidly redirect the eyes from one target to another
The main characteristics of a saccadic eye movement are (Becker, 1989):

- an **extremely intense angular acceleration** (up to 30000 deg/s2);
- a comparatively less intense deceleration which is nevertheless able to induce a very fast arrest of the rotation
- an **angular peak velocity** increasing with the saccade amplitude up to a saturation value **ranging between 400 - 600 deg/s**.

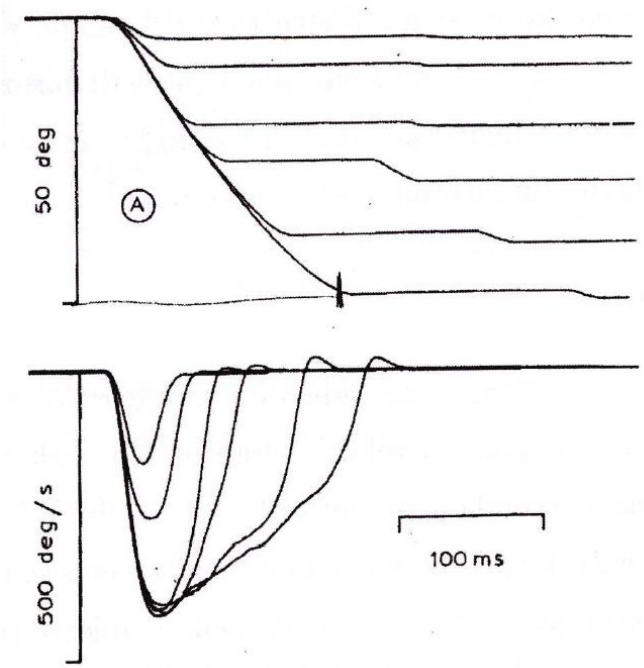

The maximum amplitude of a saccade is about 50° though most eye rotations have amplitudes smaller than 20°. Saccade duration and amplitude are related and the duration is at most of the order of a tenth of a second.

Unidirectional motion of a viscoelastic fluid I

We start by considering a very simple unidirectional flow. Even if the flow in the eye is obviously not unidirectional this analysis allows us to discuss some important characteristics of the flow in the vitreous chamber.
We consider the flow of a homogeneous and viscoelastic fluid within a gap between two parallel walls, located at $y = 0$ and $y = d$.

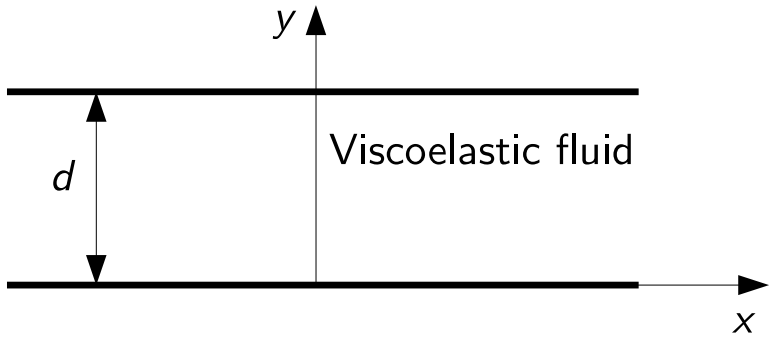

The unidirectional flow under consideration is governed by the following equation

$$\rho \frac{\partial u}{\partial t} + \int_{-\infty}^{t} G(t - t') \frac{\partial^2 u}{\partial y^2} dt' = 0, \tag{126}$$

where the only velocity component, u, is the x-direction, and only depends on y and t.

Unidirectional motion of a viscoelastic fluid II

Eigenvalue problem

We first investigate the **relaxation behaviour of the system,** starting from a prescribed non-zero velocity field at $t = 0$ and assuming the plates remain stationary for $t > 0$. In particular we look for natural frequencies of the system that could be resonantly excited by oscillations of one plate. We seek solutions of the form

$$u(y,t) = u_\lambda(y)e^{\lambda t} + c.c. \tag{127}$$

with $\lambda \in \mathbb{C}$, being an **eigenvalue.** Substituting (127) into (126), and considering stationary plates, we obtain

$$\rho\lambda u_\lambda - \mu^* \frac{d^2 u_\lambda}{dy^2} = 0, \tag{128a}$$

$$u_\lambda = 0 \qquad (y = 0), \tag{128b}$$

$$u_\lambda = 0 \qquad (y = d), \tag{128c}$$

with

$$\mu^* = \int_0^\infty G(s)e^{-\lambda s} ds.$$

being the complex viscosity μ^* (see equation (54)). For simplicity we assume that $\mu^* = \mu' - i\mu''$ is a constant.

Unidirectional motion of a viscoelastic fluid III

We seek a solution in the form

$$u_\lambda = \sum_{m=1}^{\infty} a_m \sin\left(m\pi \frac{y}{d}\right),$$

which satisfies the boundary conditions (128b) and (128c). Substituting into (128a) we find for the m-th mode the following eigenrelationship

$$\lambda = -\frac{m^2\pi^2\mu^*}{\rho d^2}.$$

- The real part of λ is always negative and represents a decay in time of the oscillations.
- If λ is complex the system admits natural frequencies of oscillation.
- The imaginary part of λ represent the **natural frequency of the system.** It obviously depend on m, and different modes (different values of m) are associated with different natural frequencies.

Unidirectional motion of a viscoelastic fluid IV

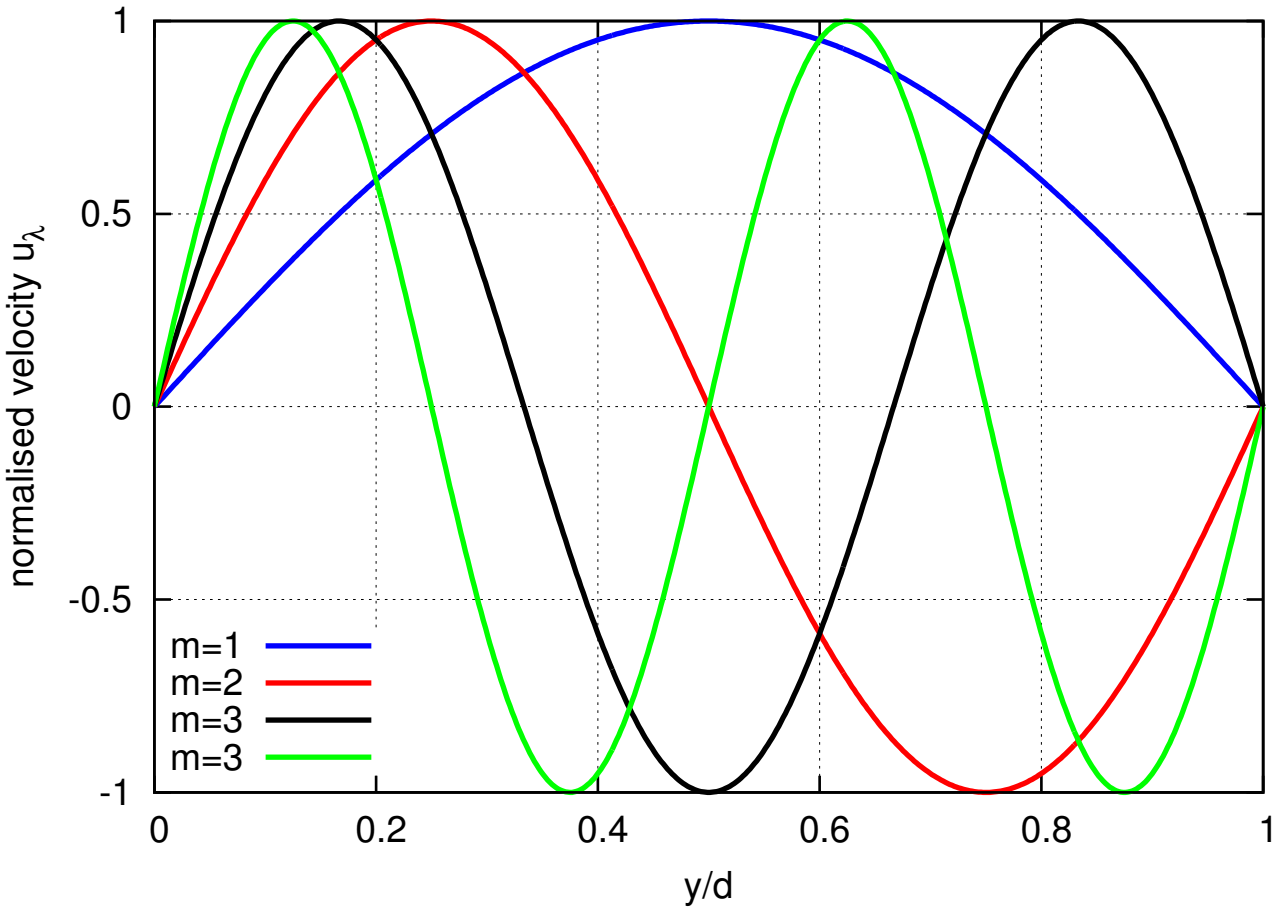

Plot of the first four eigenfunctions.

Unidirectional motion of a viscoelastic fluid V

Forced problem

We now consider the case in which the wall at $y = 0$ oscillates in the x-direction according to the following law

$$u_w = U\cos(\omega t) = \frac{U}{2}\exp(i\omega t) + c.c.,$$

where u_w is the wall velocity, U the maximum wall velocity and $c.c.$ denotes the complex conjugate.
Writing the x-component of the velocity u as $u(y,t) = \hat{u}(y)e^{i\omega t}$ the Navier–Stokes equation in the x-direction and the appropriate boundary conditions read

$$\mu^* \frac{d^2\hat{u}}{dy^2} - \rho i\omega\hat{u} = 0, \tag{129a}$$

$$\hat{u} = \frac{U}{2}, \qquad (y = 0), \tag{129b}$$

$$\hat{u} = 0, \qquad (y = d). \tag{129c}$$

The general solution of equation (129a) is

$$\hat{u} = c_1 \exp\left(\sqrt{\Gamma}y\right) + c_2 \exp\left(-\sqrt{\Gamma}y\right),$$

with $\Gamma = \rho i\omega/\mu^*$, and the constants c_1 and c_2 can be obtained by imposing the boundary conditions (129b) and (129c).

Unidirectional motion of a viscoelastic fluid VI

Velocity profiles - fixed ω and variable μ^*

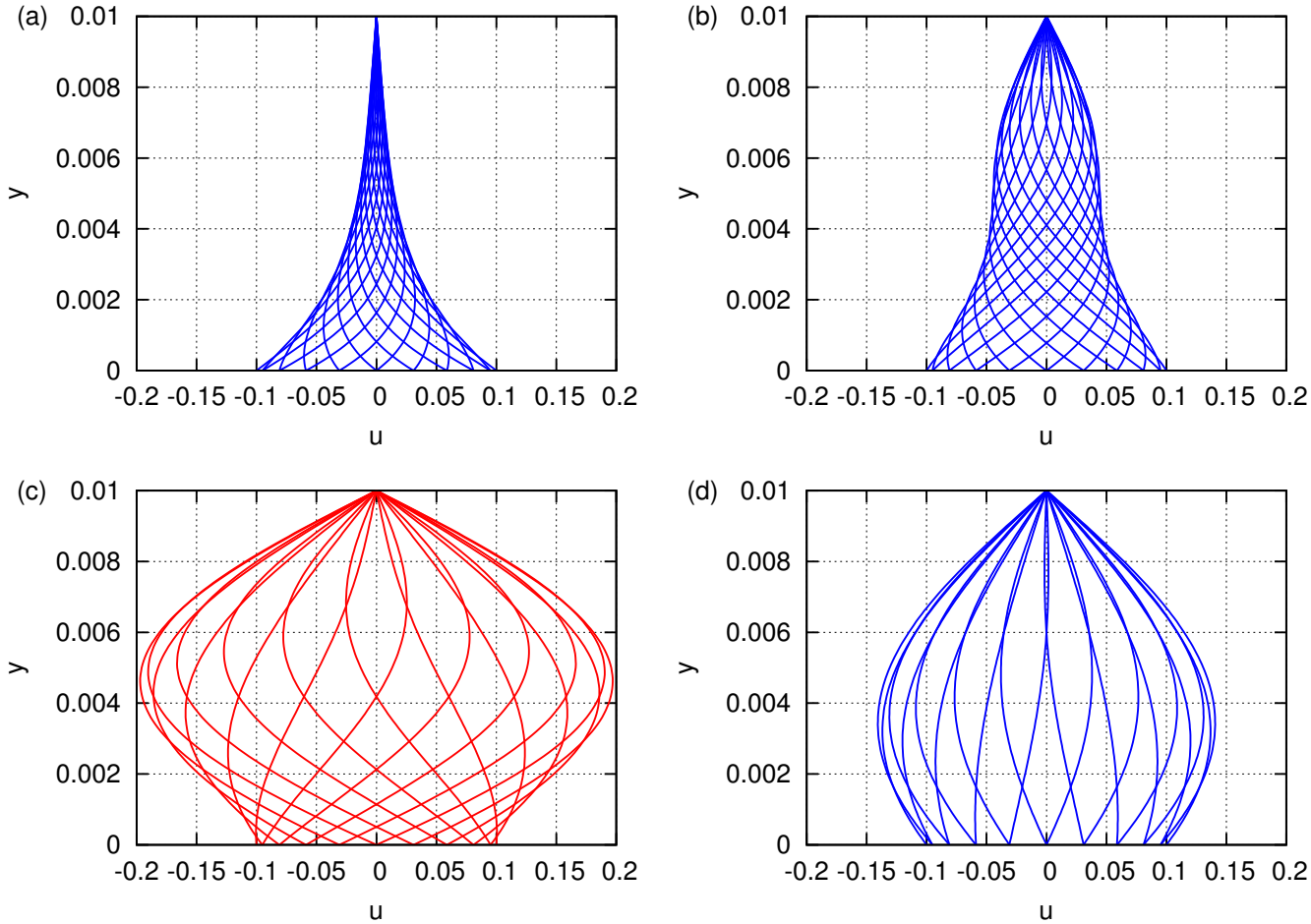

$d = 0.01$ m, $U = 0.1$ m/s, $\omega = 0.3$ rad/s. (a) $\mu^* = 0.001$ Pa·s, (b) $\mu^* = 0.001 + 0.001i$ Pa·s, (c) $\mu^* = 0.001 + 0.003i$ Pa·s **(resonance of mode $m = 1$)**, (d) $\mu^* = 0.001 + 0.005i$ Pa·s.

Unidirectional motion of a viscoelastic fluid VII

Velocity profiles - fixed μ^* and variable ω

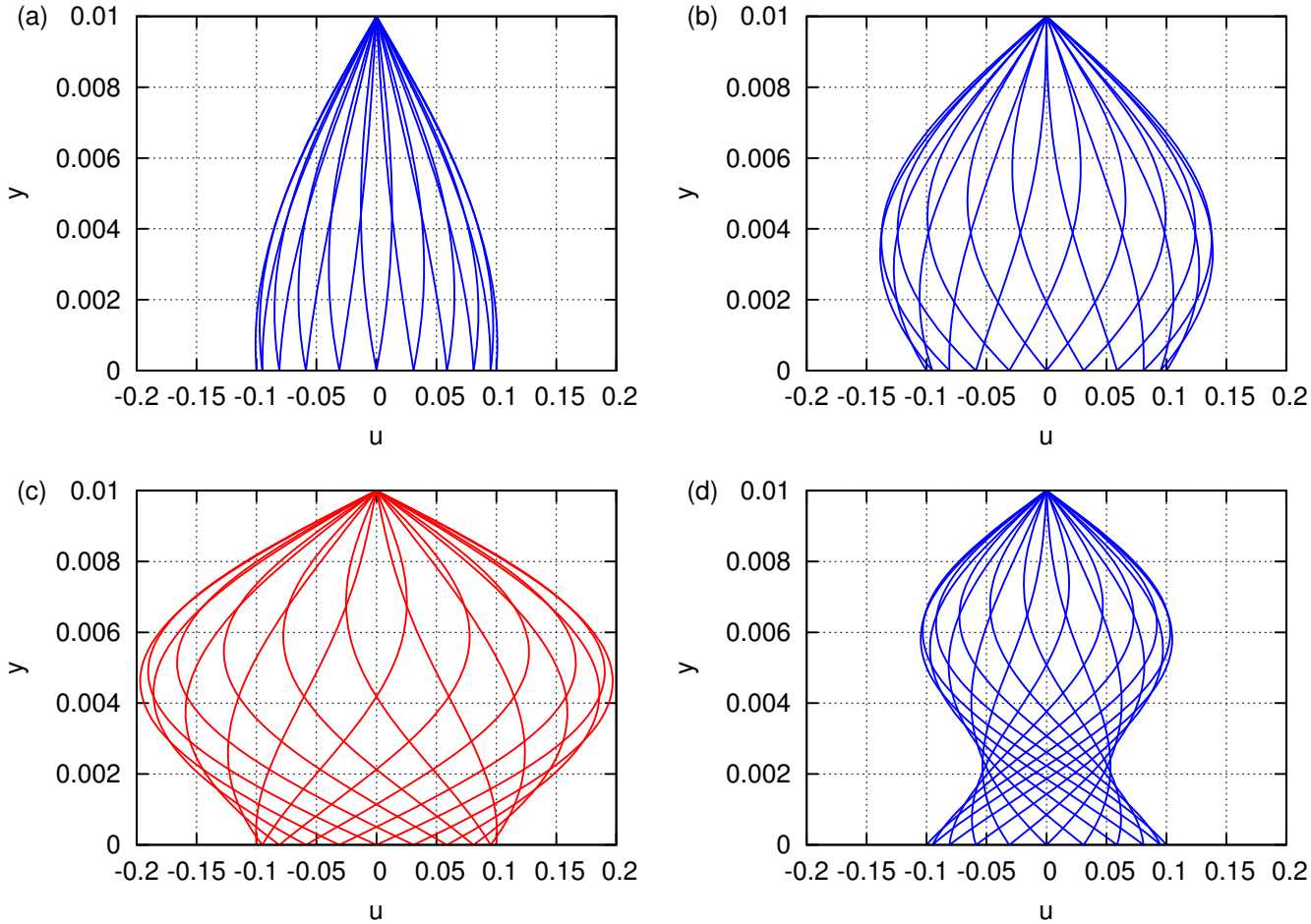

$d = 0.01$ m, $U = 0.1$ m/s, $\mu^* = 0.001 + 0.003i$ Pa·s. (a) $\omega = 0.1$ rad/s, (b) $\omega = 0.2$ rad/s, (c) $\omega = 0.3$ rad/s, **(resonance of mode $m = 1$)**, (d) $\omega = 0.5$ rad/s.

Unidirectional motion of a viscoelastic fluid VIII

Velocity profiles - excitation of different modes

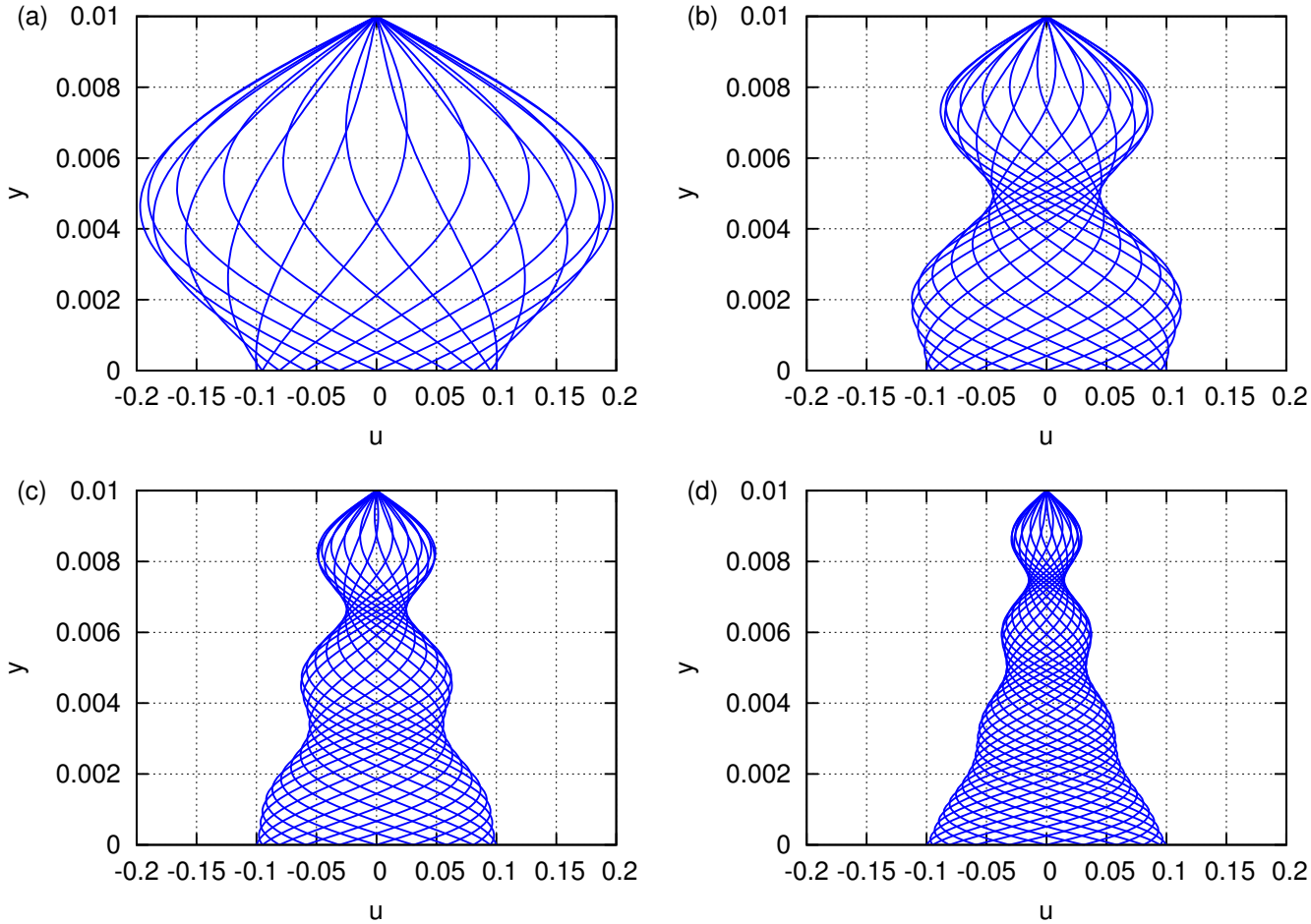

$d = 0.01$ m, $U = 0.1$ m/s, $\mu^* = 0.001 + 0.003i$ Pa·s. (a) $\omega = 0.3$ rad/s (mode $m = 1$), (b) $\omega = 1.18$ rad/s (mode $m = 2$), (c) $\omega = 2.66$ rad/s (mode $m = 3$), (d) $\omega = 4.74$ rad/s (mode $m = 4$).

Motion of a viscous fluid in a periodically rotating sphere

We now consider a more realistic problem. In particular we make the following assumptions (Repetto et al., 2005).

- **Spherical domain**
  As a first approximation we consider that the vitreous chamber has spherical shape, with radius R. The role of departure from sphericity will be discussed in the following.
  We the domain is axisymmetric we will seek **axisymmetric solutions.**
- **Purely viscous fluid**
  We first consider the case of a purely viscous, Newtonian fluid. Therefore, we should not expect the possible occurrence of resonance phenomena.
  This assumption makes sense in the following cases:
  - vitreous liquefaction;
  - substitution of the vitreous with viscous tamponade fluids, such as silicon oils.
- **Small-amplitude harmonic eye rotations**
  We assume that the sphere performs harmonic torsional oscillations with amplitude ε and frequency ω.
  The assumption of small amplitude rotations allows us to **linearise the equations.**

The mathematical details of the following analysis are not reported since they are quite technical. The student is assumed to just follow the reasoning and understand the results.

Theoretical model I

Governing equations

$$\frac{\partial}{\partial t}\mathbf{u} + (\mathbf{u}\cdot\nabla)\mathbf{u} + \frac{1}{\rho}\nabla p - \nu\nabla^2\mathbf{u} = 0,$$
$$\nabla\cdot\mathbf{u} = 0,$$
$$u = v = 0, \quad w = \varepsilon \sin\vartheta \sin t \qquad (r = R),$$

where the equations are written in terms of spherical polar coordinates (r, ϑ, φ), with r being the radial, ϑ the zenithal and φ the azimuthal coordinates. The velocity vector is written as $\mathbf{u} = (u, v, w)^T$ is the velocity vector. Moreover, ε is the amplitude of oscillations.

Solution

At leading order in an expansion in terms of the small parameter ε, it can be shown that $p = u = v = 0$ and the only component of the velocity which is non zero is $w = w(r, \vartheta)$. The solution for w is given by

$$w = -\frac{i\varepsilon\omega R^3\left(\sin\frac{ar}{R} - \frac{kr}{R}\cos\frac{ar}{R}\right)}{2r^2\left(\sin a - a\cos a\right)} e^{i\omega t}\sin\vartheta + c.c., \qquad a = e^{-i\pi/4}\alpha, \tag{130}$$

where we have defined the **Womersley number** as

$$\alpha = \sqrt{\omega R^2/\nu}.$$

Theoretical model II

Velocity profiles on the plane orthogonal to the axis of rotation at different times.

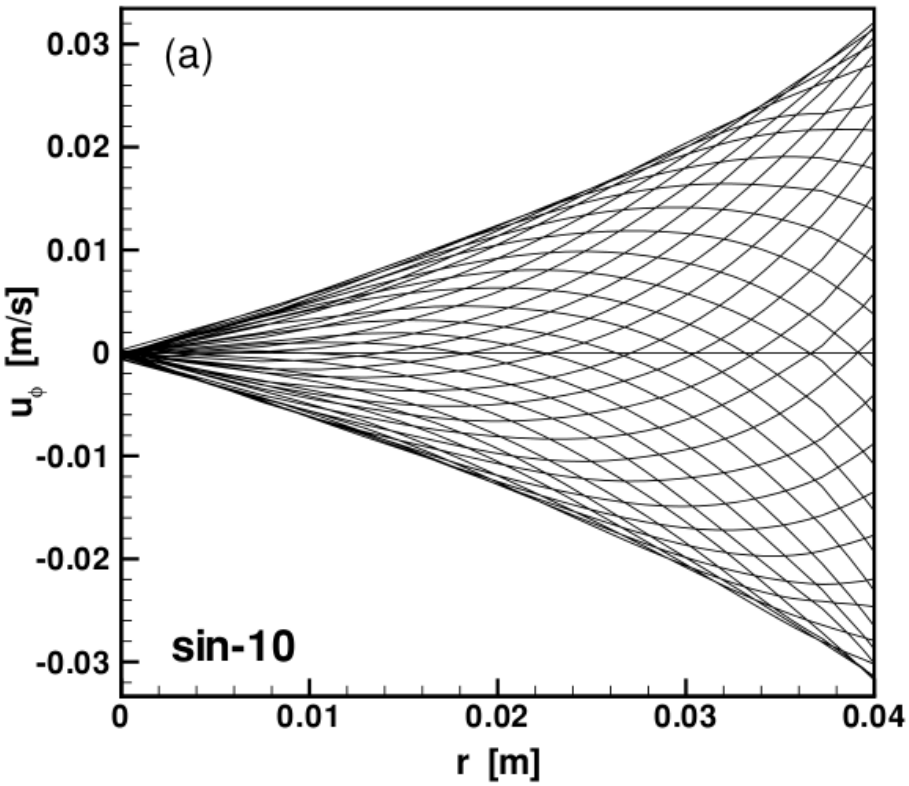

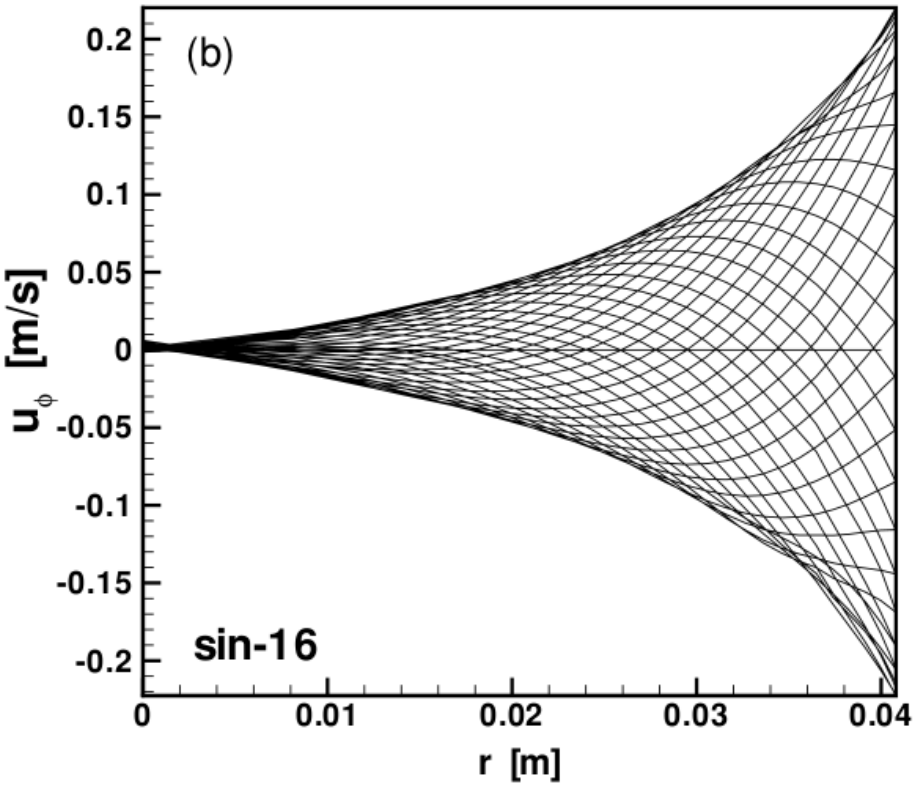

- Limit of small α: **rigid body rotation;**
- Limit of large α: formation of an **oscillatory boundary layer at the wall.**

Experimental apparatus I

- Perspex cylindrical container.
- Spherical cavity with radius $R_0 = 40$ mm.
- Glycerol (highly viscous Newtonian fluid).

Experimental apparatus II

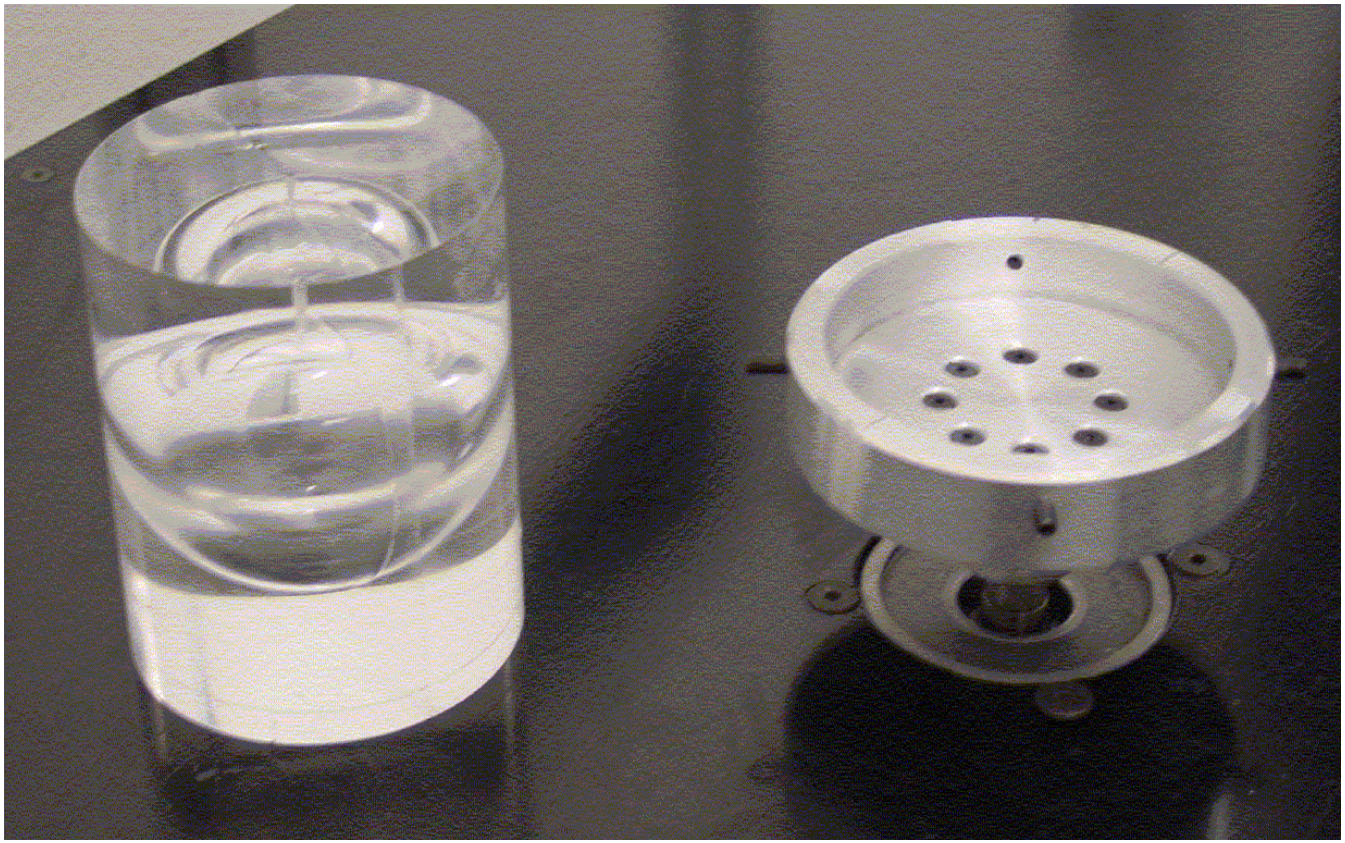

The eye model is mounted on the shaft of a computer controlled motor.

Experimental apparatus III

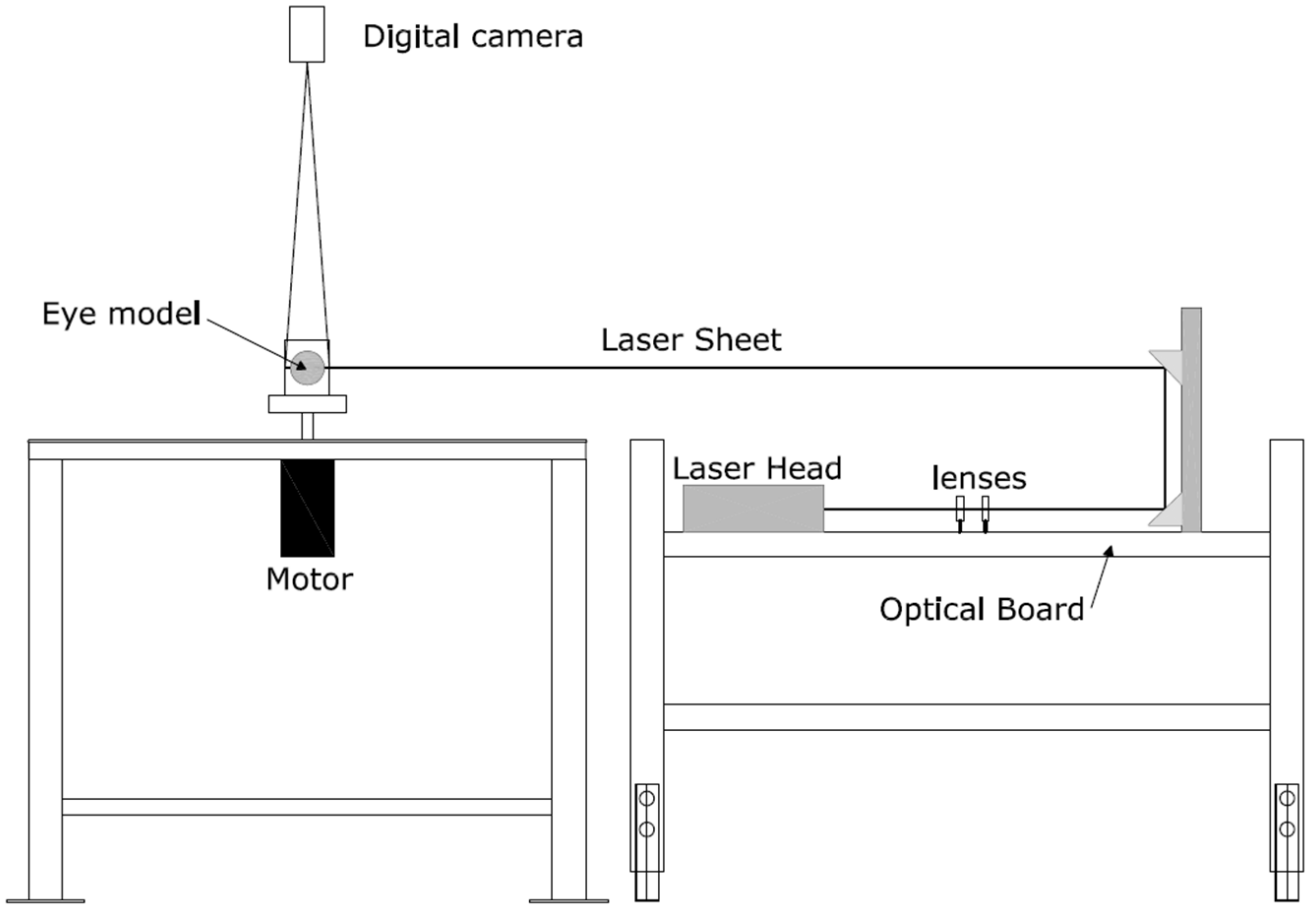

Experimental measurements I

PIV (Particle Image Velocimetry) measurements are taken on the equatorial plane orthogonal to the axis of rotation.

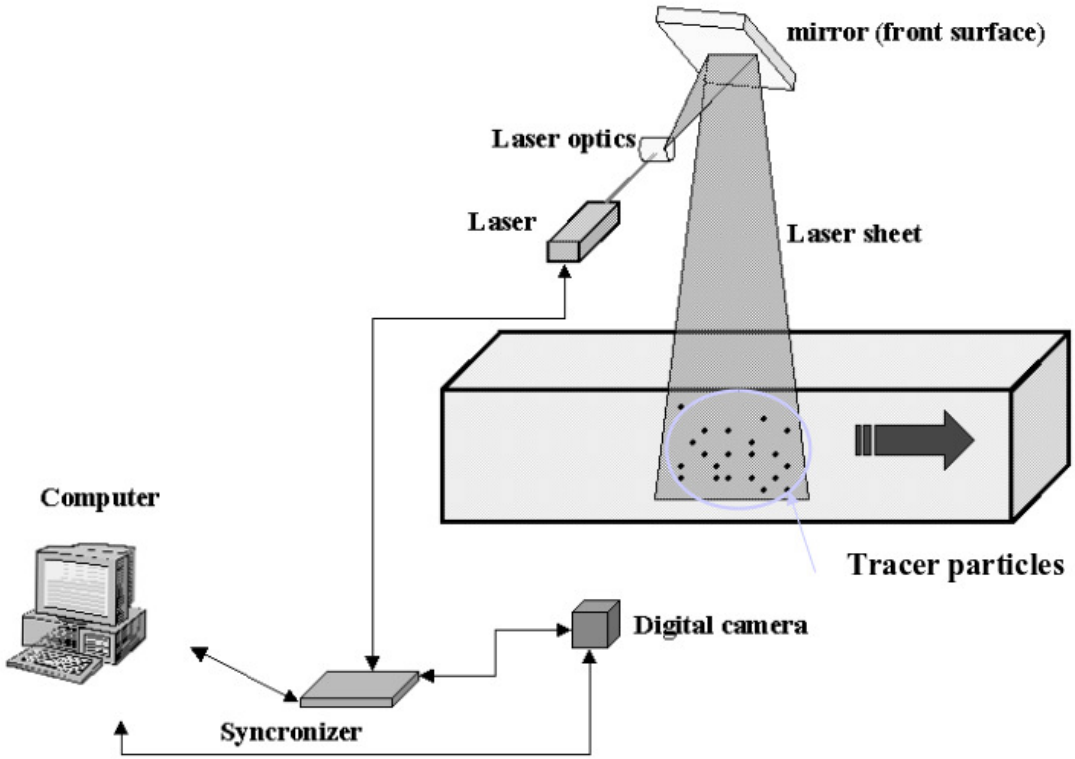

Typical PIV setup

Experimental measurements II

Typical PIV image

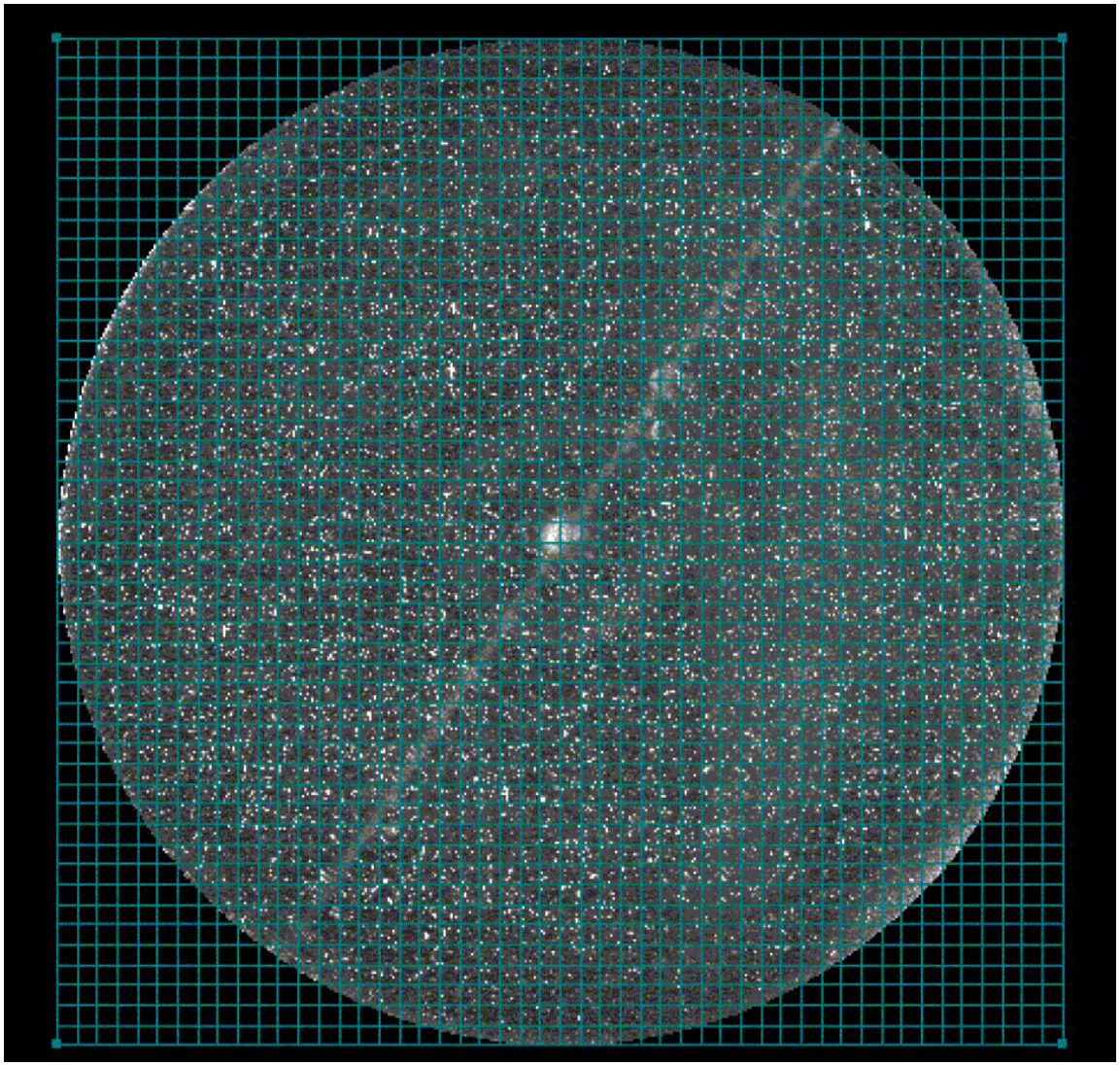

Experimental measurements III

In the PIV technique

- the image is subdivided in small **interrogation windows** (IW);
- **cross-correlation** of the image in each IW at two successive time instants yields the most likely **average displacement** **s** within the IW;
- in each IW the velocity vector is obtained as

$$\mathbf{u} = \frac{\mathbf{s}}{\Delta t},$$

with Δt time step between the two images.

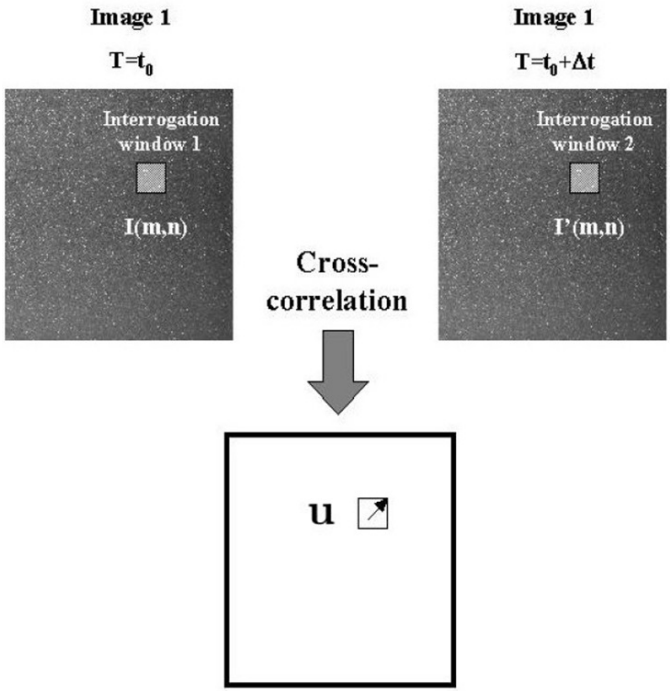

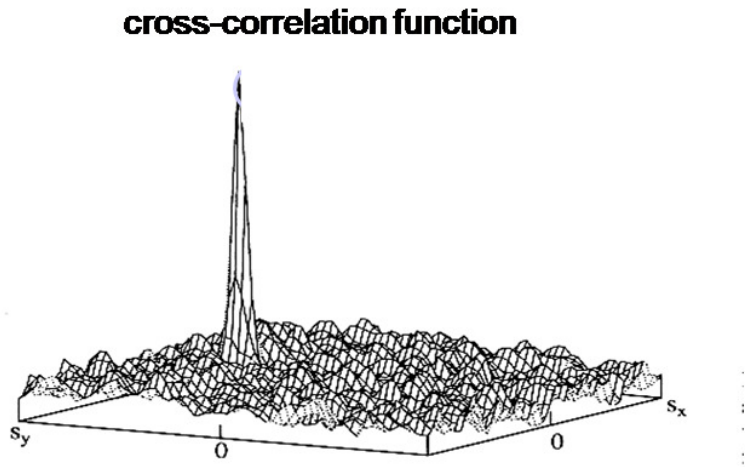

Experimental measurements IV

Typical PIV flow field

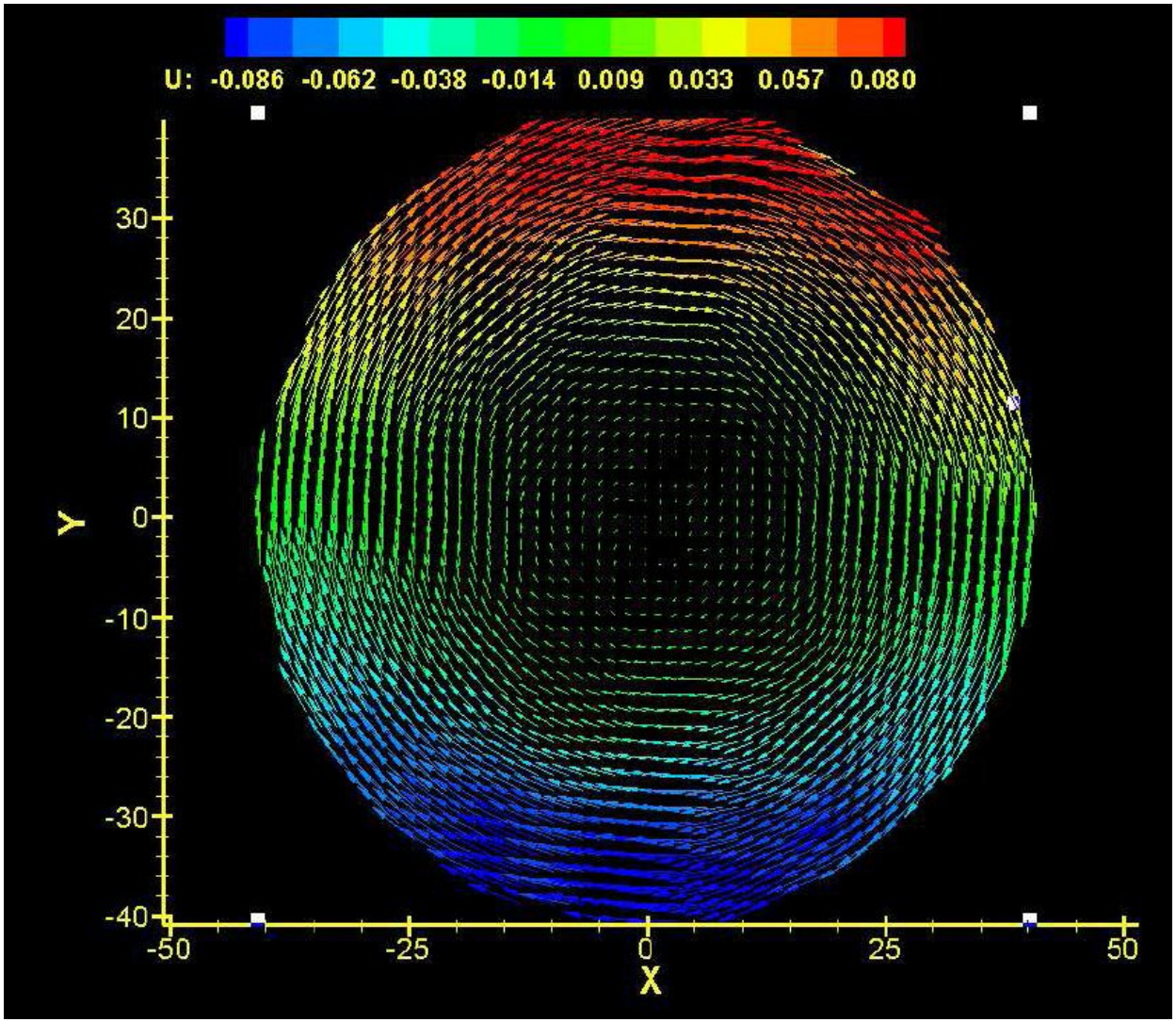

Comparison between experimental and theoretical results

Radial profiles of normalised real and imaginary parts of the velocity (see equation (130)).

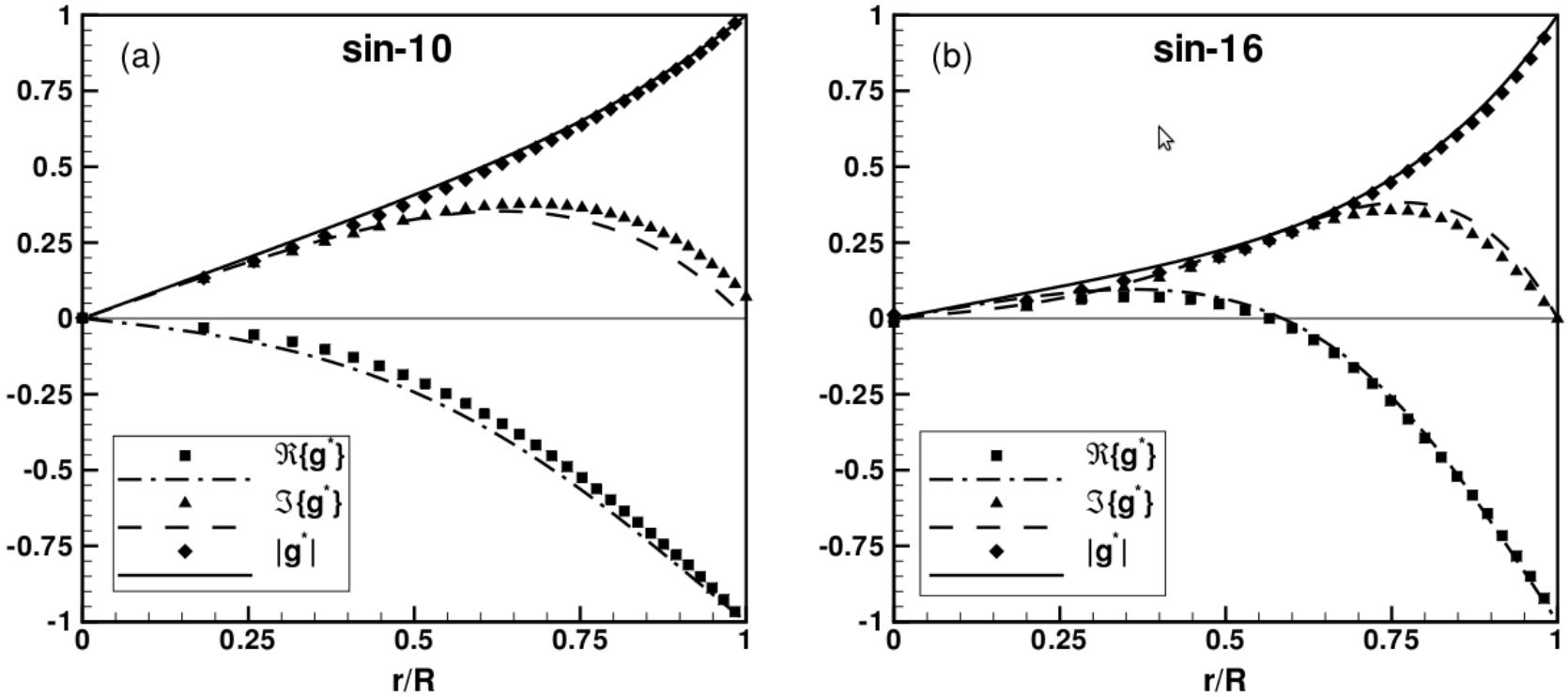

The case of a viscoelastic fluid

We now consider the case of a viscoelastic fluid within a spherical domain (Meskauskas et al., 2011).

- As we deal with an sinusoidally oscillating linear flow we can obtain the solution for the motion of a viscoelastic fluid simply by replacing the real viscosity with the **complex viscosity.**
- Rheological properties of the vitreous (complex viscosity) can be obtained from the works of Lee et al. (1992), Nickerson et al. (2008) and Swindle et al. (2008).
  Note that is this case the complex viscosity μ^* depends on the frequency of oscillations. This dependency is taken either from experimental data (where available) or is based on the use simple rheological models, such as those described at page 69.
- In this case, due to the presence of an elastic component of vitreous behaviour, the system could admit **natural frequencies** that can be excited resonantly by eye rotations.

Relaxation behaviour I

In analogy with what was shown at page 281, we seek solution with the following structure

$$\mathbf{u}(\mathbf{x}, t) = \mathbf{u}_\lambda(\mathbf{x}) e^{\lambda t} + c.c., \qquad p(\mathbf{x}, t) = p_\lambda(\mathbf{x}) e^{\lambda t} + c.c.,$$

where $\mathbf{u}_\lambda, p_\lambda$ do not depend on time and, in general the eigenvalue $\lambda \in \mathbb{C}$.
Substituting into the governing equations we obtain the **eigenvalue problem:**

$$\rho \lambda \mathbf{u}_\lambda = -\nabla p_\lambda + \mu^* \nabla^2 \mathbf{u}_\lambda, \qquad \nabla \cdot \mathbf{u}_\lambda = 0,$$

which has to be solved imposing **stationary no-slip conditions** at the wall and **regularity conditions** at the origin.

Relaxation behaviour II

Solution

- For all existing measurements of the rheological properties of the vitreous we find complex eigenvalues, which implies the **existence of natural frequencies of the system.**
- Such frequencies, for the least decaying modes, are within the range of physiological eye rotations ($\omega = 10 - 30$ rad/s).
- **Natural frequencies could be resonantly excited by eye rotations.**

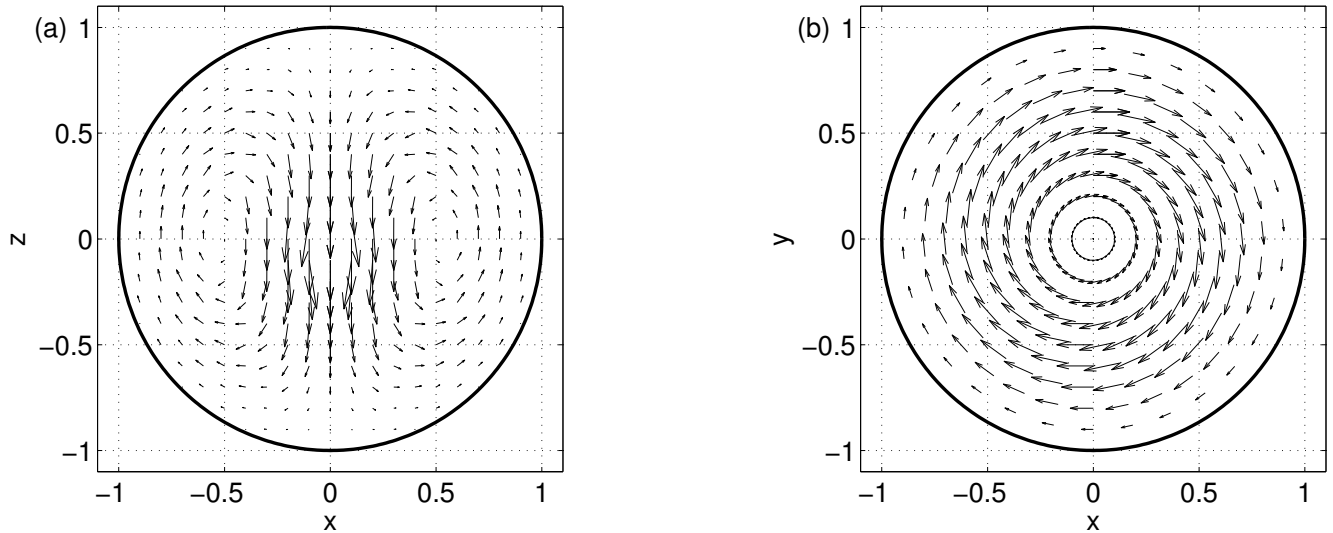

Spatial structure of two different eigenfunctions.

Periodic forcing I

We now consider the case in which the sphere performs small-amplitude harmonic torsional oscillations, with amplitude ε and frequency ω.
As in the case of Newtonian fluids **the velocity is purely azimuthal.**

Velocity profiles

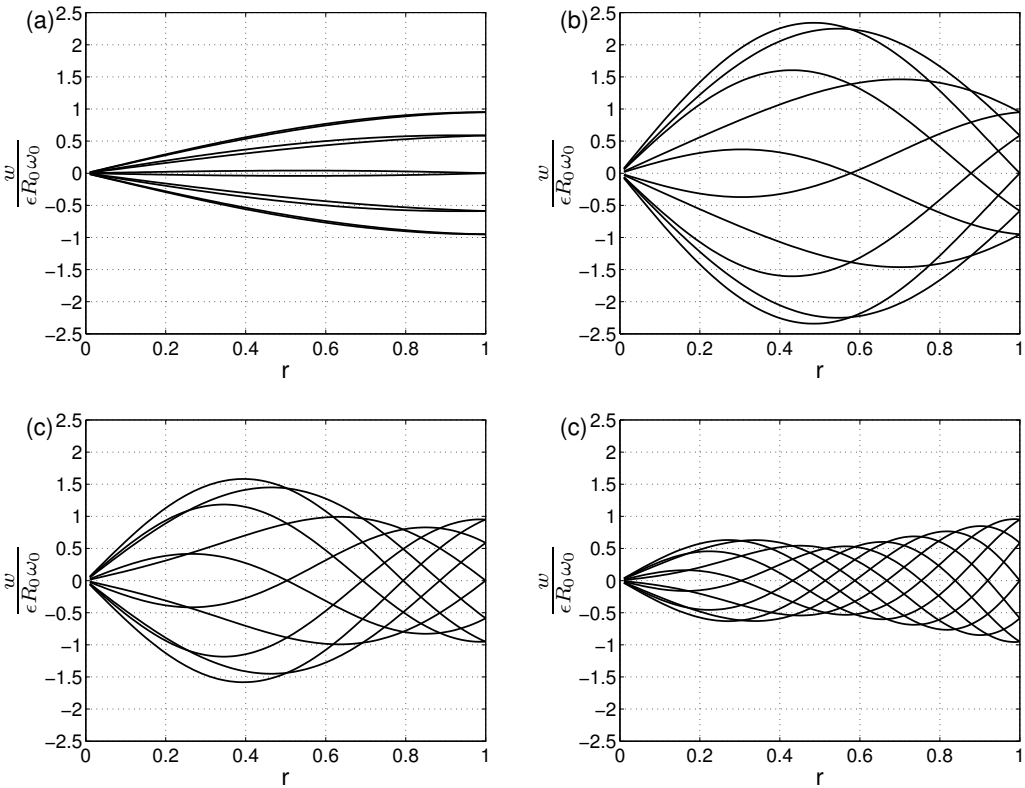

Azimuthal velocity profiles, (a) $\omega = 10$, (b) $\omega = 19.1494$, (c) $\omega = 28$, and (d) $\omega = 45$.

Periodic forcing II

Shear stress at the wall

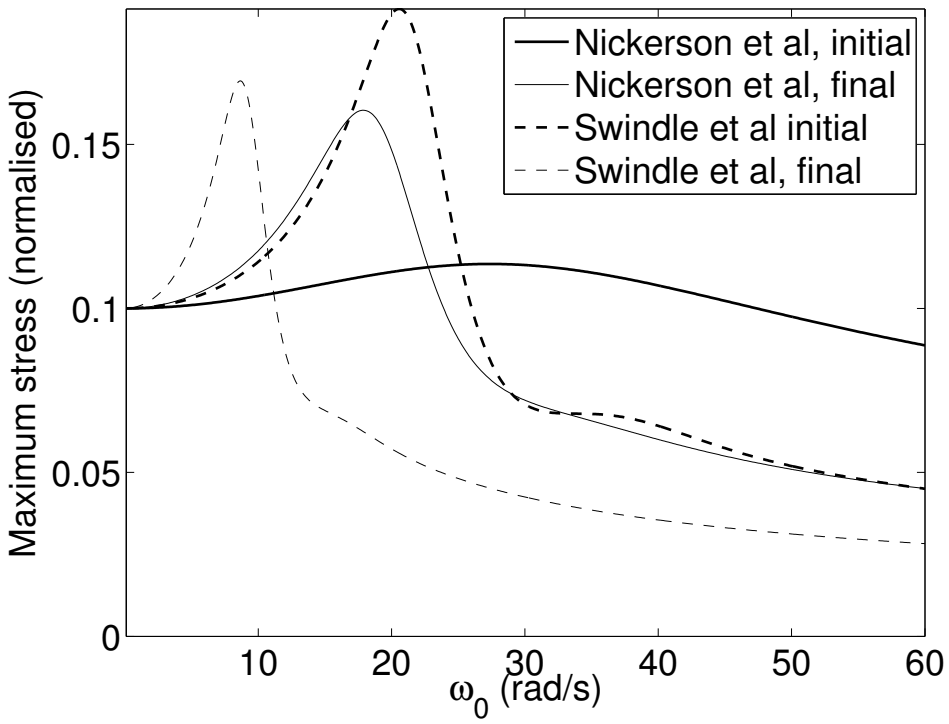

Stress normalised with $\epsilon\rho R^2\omega^2$ vs the oscillation frequency. The different curves correspond to different measurements of the vitreous rheological properties.

Some conclusions

- If the eye rotates at certain frequencies resonant excitation is possible.
- Resonance leads to large values of the stress on the retina.
- Does resonant excitation really occur in-vivo?
  - Need for in-vivo measurements of vitreous velocity (**Ultrasound scan of vitreous motion**).

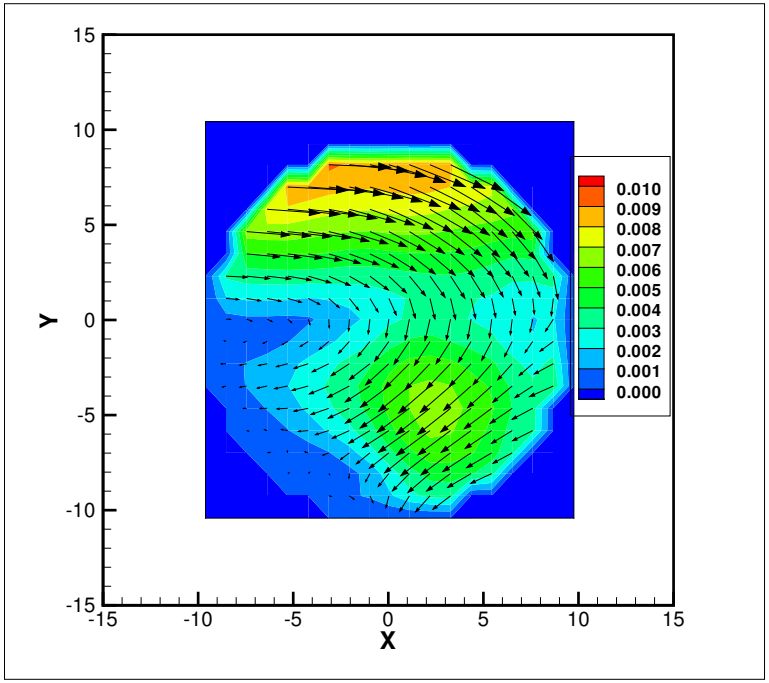

Echo-PIV measurement of vitreous motion (Rossi et al., 2012).

  - Are ex-vivo measurements of vitreous rheological properties reliable?
- The possible occurrence of resonance has implications for the choice of tamponade fluids to be used after vitrectomy.

The effect of the shape of the vitreous chamber

In reality the vitreous chamber is not exactly spherical, mainly because:

- the antero-posterior axis is shorted than the others;
- the lens produces an anterior indentation.

The non-sphericity of the domain may have an important role on the fluid dynamics in the vitreous chamber.
We consider this problem starting with a very simple **two-dimensional irrotational model.** We will then show results from three-dimensional calculations (but will not show the corresponding mathematics, which is quite technical).

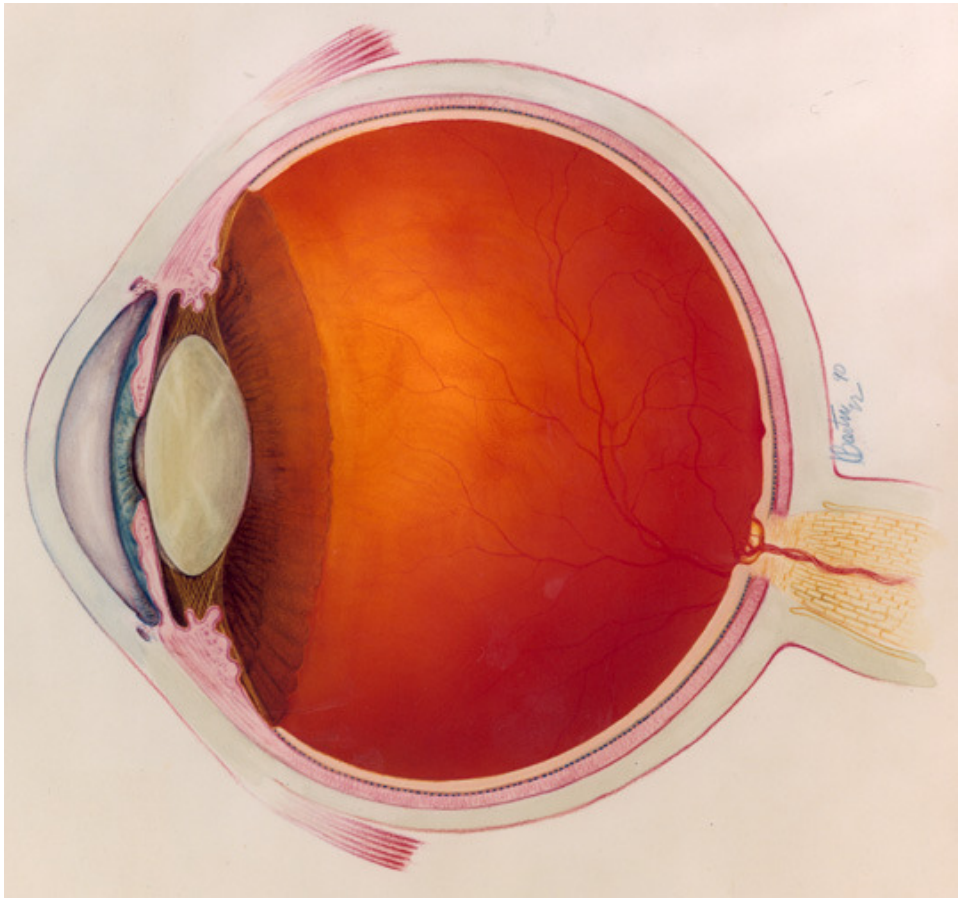

Formulation of the problem I

We consider a two-dimensional irrotational flow within a **weakly deformed, rotating circle.** Recalling the theory of irrotational flows presented at page 50, we can define a **velocity potential** Φ^* as

$$\mathbf{u}^* = \nabla \Phi^*,$$

where $\mathbf{u}^*$ denotes velocity and superscript stars indicate dimensional variables that will be made dimensionless in the following. We work in terms of polar coordinates fixed in space (r^*, ϕ), so that

$$\mathbf{u}^* = (u_r^*, u_\phi^*) = \left(\frac{\partial \Phi^*}{\partial r}, \frac{1}{r^*} \frac{\partial \Phi^*}{\partial \phi} \right). \tag{131}$$

Fluid incompressibility implies that the velocity potential must be a harmonic function, i.e.

$$\nabla^2 \Phi^* = \frac{1}{r^*} \frac{\partial}{\partial r^*} \left(r^* \frac{\partial \Phi^*}{\partial r^*} \right) + \frac{1}{r^{*2}} \frac{\partial^2 \Phi^*}{\partial \phi^2} = 0.$$

We assume that the boundary of the domain be described by the following equation

$$F^* = r^* - R^*(\phi, t^*) = R^*[\phi - \alpha(t^*)] = 0, \tag{132}$$

where $\alpha(t^*)$ denotes the angle of rotation of the domain with respect to a reference position. The boundary conditions impose vanishing flux through the wall. This implies

$$\frac{DF^*}{Dt^*} = \frac{\partial F^*}{\partial t^*} + \mathbf{u}^* \cdot \nabla^* F^* = 0, \qquad (F^* = 0).$$

Formulation of the problem II

Introducing (131) into the above equation and using (132) we get

$$-\frac{\partial R^*}{\partial t^*}+\frac{\partial \Phi^*}{\partial r^*}-\frac{1}{r^{*2}}\frac{\partial \Phi^*}{\partial \phi}\frac{\partial R^*}{\partial \phi}=0 \qquad [r^*=R^*(\phi-\alpha(t^*)].$$

Once the velocity potential is known, one can compute the pressure through the Bernoulli equation (45).
Therefore, the governing equations can be written as

$$\frac{\partial}{\partial r^*}\left(r^*\frac{\partial \Phi^*}{\partial r^*}\right)+\frac{1}{r^*}\frac{\partial^2 \Phi^*}{\partial \phi^2}=0, \tag{133a}$$

$$-\frac{\partial R^*}{\partial t^*}+\frac{\partial \Phi^*}{\partial r^*}-\frac{1}{r^{*2}}\frac{\partial \Phi^*}{\partial \phi}\frac{\partial R^*}{\partial \phi}=0 \qquad [r^*=R^*(\phi-\alpha(t^*)] \tag{133b}$$

$$p^*=-\rho\frac{\partial \Phi^*}{\partial t^*}-\frac{1}{2}\rho\left[\left(\frac{\partial \Phi^*}{\partial r^*}\right)^2+\frac{1}{r^{*2}}\left(\frac{\partial \Phi^*}{\partial \phi}\right)^2\right]. \tag{133c}$$

Change of coordinates I

We now perform the following change of coordinates, so that the equation of the domain becomes time independent

$$(r^*, \phi, t^*) \to (r^*, \varphi, t^*),$$

with $\varphi = \phi - \alpha(t^*)$. This implies

$$\begin{aligned}
&\frac{\partial}{\partial r^*} \to \frac{\partial}{\partial r^*}, \\
&\frac{\partial}{\partial \phi} \to \frac{\partial \varphi}{\partial \phi}\frac{\partial}{\partial \varphi} = \frac{\partial}{\partial \varphi}, \\
&\frac{\partial}{\partial t^*} \to \frac{\partial}{\partial t^*} + \frac{\partial \varphi}{\partial t^*}\frac{\partial}{\partial \varphi} = \frac{\partial}{\partial t} - \dot{\alpha}^*\frac{\partial}{\partial \varphi},
\end{aligned}$$

with $\dot{\alpha}^* = d\alpha/dt^*$, so that equations (133a), (133b) and (133c) become

$$\frac{\partial}{\partial r^*}\left(r^*\frac{\partial \Phi^*}{\partial r^*}\right) + \frac{1}{r^*}\frac{\partial^2 \Phi^*}{\partial \varphi^2} = 0, \tag{134a}$$

$$\dot{\alpha}^*\frac{\partial R^*}{\partial \varphi} + \frac{\partial \Phi^*}{\partial r^*} - \frac{1}{r^{*2}}\frac{\partial \Phi^*}{\partial \phi}\frac{\partial R^*}{\partial \phi} \qquad [r^* = R^*(\varphi)], \tag{134b}$$

$$p^* = \rho\dot{\alpha}^*\frac{\partial \Phi^*}{\partial \varphi} - \rho\frac{\partial \Phi^*}{\partial t^*} - \frac{1}{2}\rho\left[\left(\frac{\partial \Phi^*}{\partial r^*}\right)^2 + \frac{1}{r^{*2}}\left(\frac{\partial \Phi^*}{\partial \varphi}\right)^2\right]. \tag{134c}$$

Scaling

We scale all variables as follows

$$(r, R) = \frac{(r^*, R^*)}{\mathcal{R}}, \quad \Phi = \frac{\Phi^*}{\Omega_p \mathcal{R}^2}, \quad p = \frac{p^*}{\rho \Omega_p^2 \mathcal{R}^4}, \quad t = \Omega_p t^*, \tag{135}$$

where

- $\mathcal{R}$: radius of the circle with the same area as the actual domain;
- Ω_p: peak angular velocity of the saccadic movement.

The governing equations can be written in dimensionless form as

$$\frac{\partial}{\partial r}\left(r \frac{\partial \Phi}{\partial r}\right) + \frac{1}{r}\frac{\partial^2 \Phi}{\partial \varphi^2} = 0, \tag{136a}$$

$$\dot{\alpha}\frac{\partial R}{\partial \varphi} + \frac{\partial \Phi}{\partial r} - \frac{1}{r^2}\frac{\partial \Phi}{\partial \varphi}\frac{\partial R}{\partial \varphi} \qquad [r = R(\varphi)], \tag{136b}$$

$$p = \dot{\alpha}\frac{\partial \Phi}{\partial \varphi} - \frac{\partial \Phi}{\partial t} - \frac{1}{2}\left[\left(\frac{\partial \Phi}{\partial r}\right)^2 + \frac{1}{r^2}\left(\frac{\partial \Phi}{\partial \varphi}\right)^2\right], \tag{136c}$$

where $\dot{\alpha} = d\alpha/dt$.

Expansion

We describe the domain as a weakly deformed circle writing

$$R(\varphi) = 1 + \delta R_1(\varphi),$$

where $\delta \ll 1$ represents the maximum departure of the domain from the unit circle.

The function $R_1(\varphi)$ can be expanded in Fourier series as follows

$$R_1 = \sum_{m=1}^{\infty} a_m \cos(m\varphi) + b_m \sin(m\varphi). \tag{137}$$

Note that with the above expansion we can in principle describe any shape of the domain. Moreover, we assume that the function R_1 is symmetrical with respect to φ, and this implies $b_m = 0 \ \forall m$.

Owing to the assumption $\delta \ll 1$ we can expand Φ and p in powers of δ as follows

$$\Phi = \Phi_0 + \delta\Phi_1 + \mathcal{O}(\delta^2), \tag{138a}$$

$$p = p_0 + \delta p_1 + \mathcal{O}(\delta^2). \tag{138b}$$

Solution I

Leading order problem $\mathcal{O}(\delta^0)$

At leading order we find the trivial solution

$$\Phi_0 = 0, \qquad p_0 = \text{const.}$$

No motion is generated in a fluid within a rotating circle if the no slip condition at the wall is not imposed.

Order δ problem

At order δ the governing equations (136a)-(136c) reduce to

$$\nabla^2 \Phi_1 = 0, \tag{139a}$$

$$\frac{\partial \Phi_1}{\partial r} = -\dot{\alpha} \frac{\partial R_1}{\partial \varphi} \qquad (r = 1), \tag{139b}$$

$$p_1 = -\frac{\partial \Phi_1}{\partial t} + \dot{\alpha} \frac{\partial \Phi_1}{\partial \varphi}. \tag{139c}$$

Equation (137) and the boundary condition (139b) suggest to expand the function Φ_1 as follows

$$\Phi_1 = \sum_{m=0}^{\infty} \Phi_{1m} \sin(m\varphi).$$

Solution II

Substituting the above expansion into the equations (139a) and (139b), we obtain the following ODE

$$r\frac{d^2\Phi_{1m}}{dr^2} + \frac{d\Phi_{1m}}{dr} - \frac{m^2}{r}\Phi_{1m} = 0, \tag{140a}$$

$$\frac{d\Phi_{mn}}{dr} = ma_m\dot{\alpha} \qquad (r = 1), \tag{140b}$$

$$\text{regularity} \qquad (r = 0). \tag{140c}$$

The general solution of equation (140a) is

$$\Phi_{1m} = c_1 r^{-m} + c_2 r^m.$$

The regularity condition at the origin (140c) implies $c_1 = 0$. Imposing condition (140b) we obtain

$$\Phi_{1m} = \dot{\alpha} a_n r^{-m}. \tag{141}$$

Finally, from the linearised Bernoulli equation (139c) we find the pressure, which takes the form

$$p_1 = \sum_{m=1}^{\infty} \left[\ddot{\alpha}\sin(m\varphi) + \dot{\alpha}^2 m\cos(m\varphi)\right] a_m r^m.$$

Results I

We show here results from an analogous but three-dimensional model based on the same approach as described in the previous slides (Repetto, 2006).

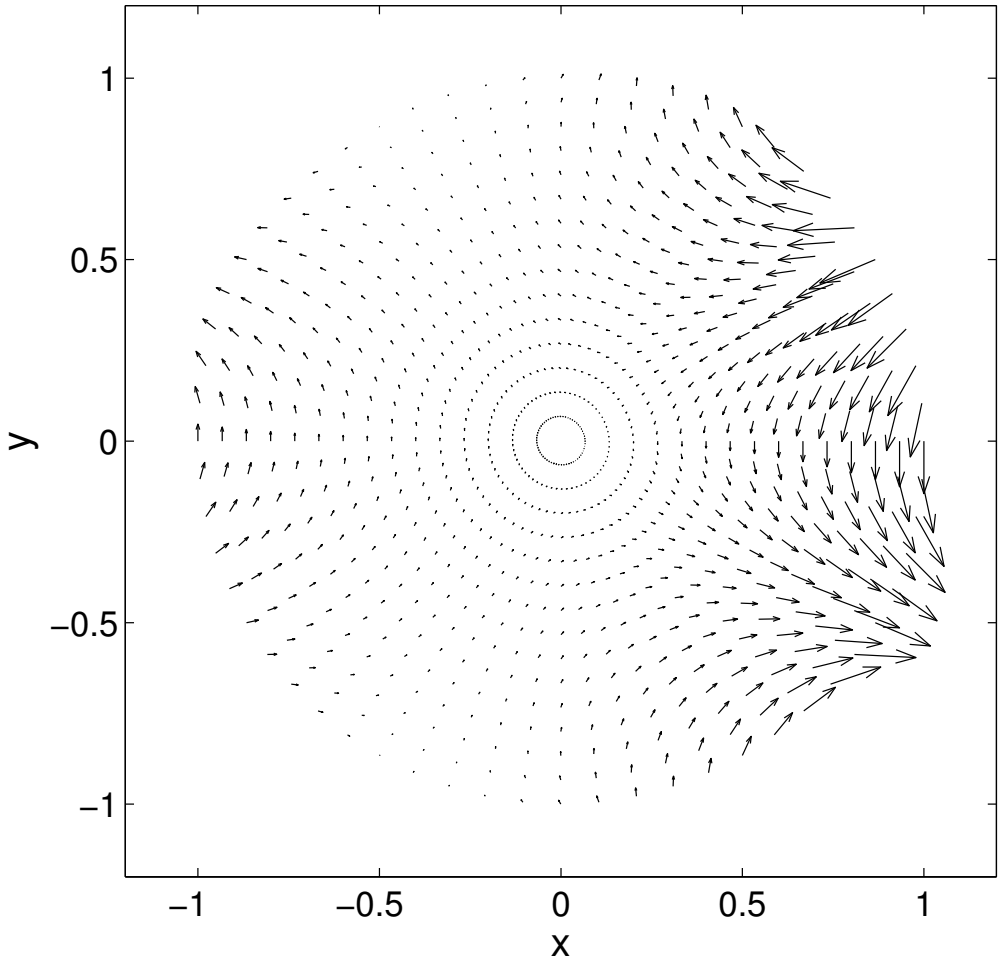

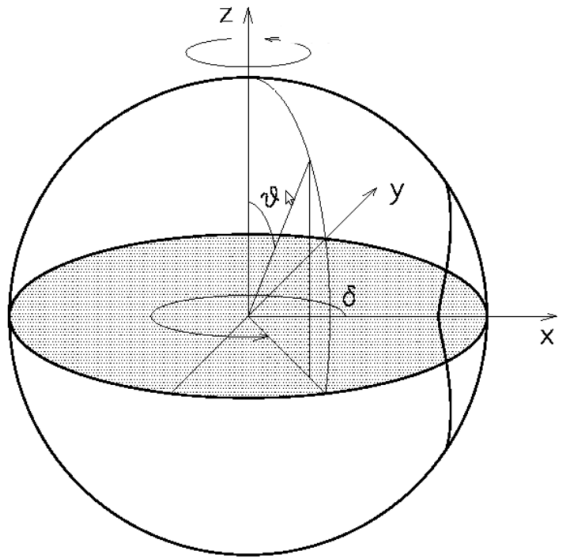

Velocity field on the equatorial plane induced by a counterclockwise rotation.

Results II

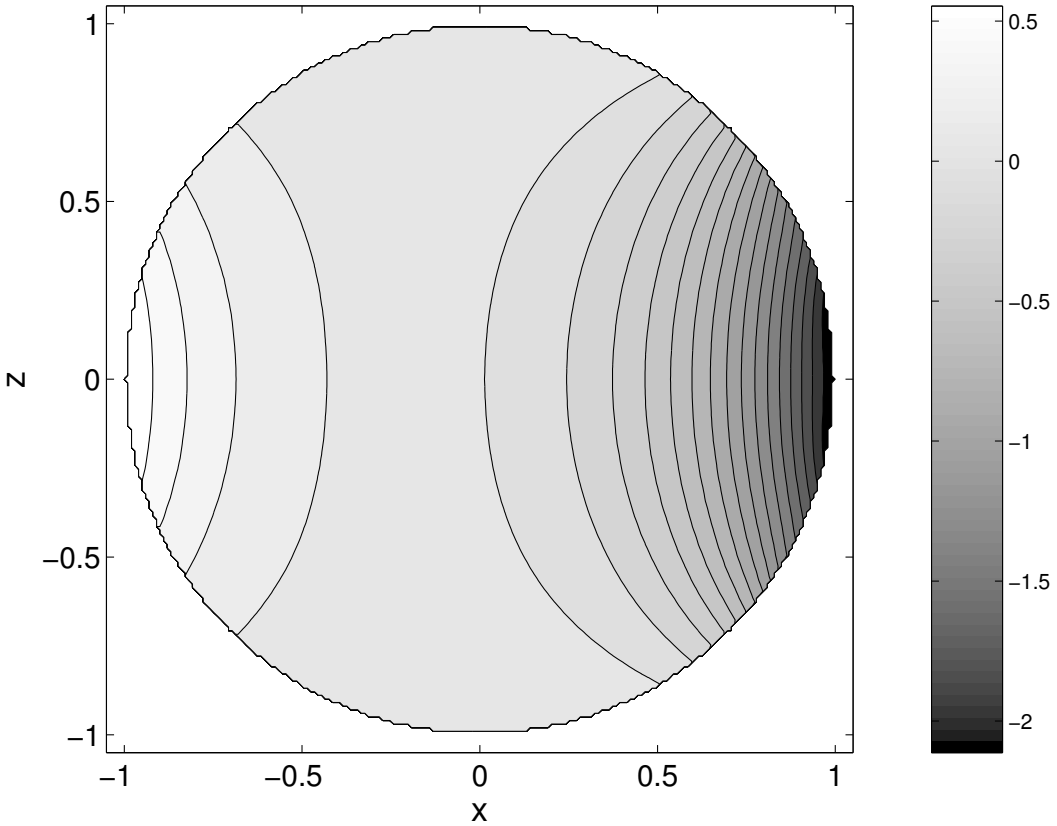

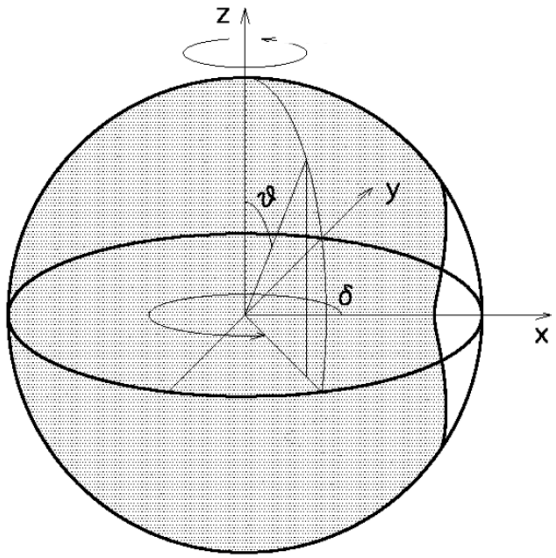

Contours of the out-of-plane velocity magnitude on the vertical plane of symmetry.

Results III

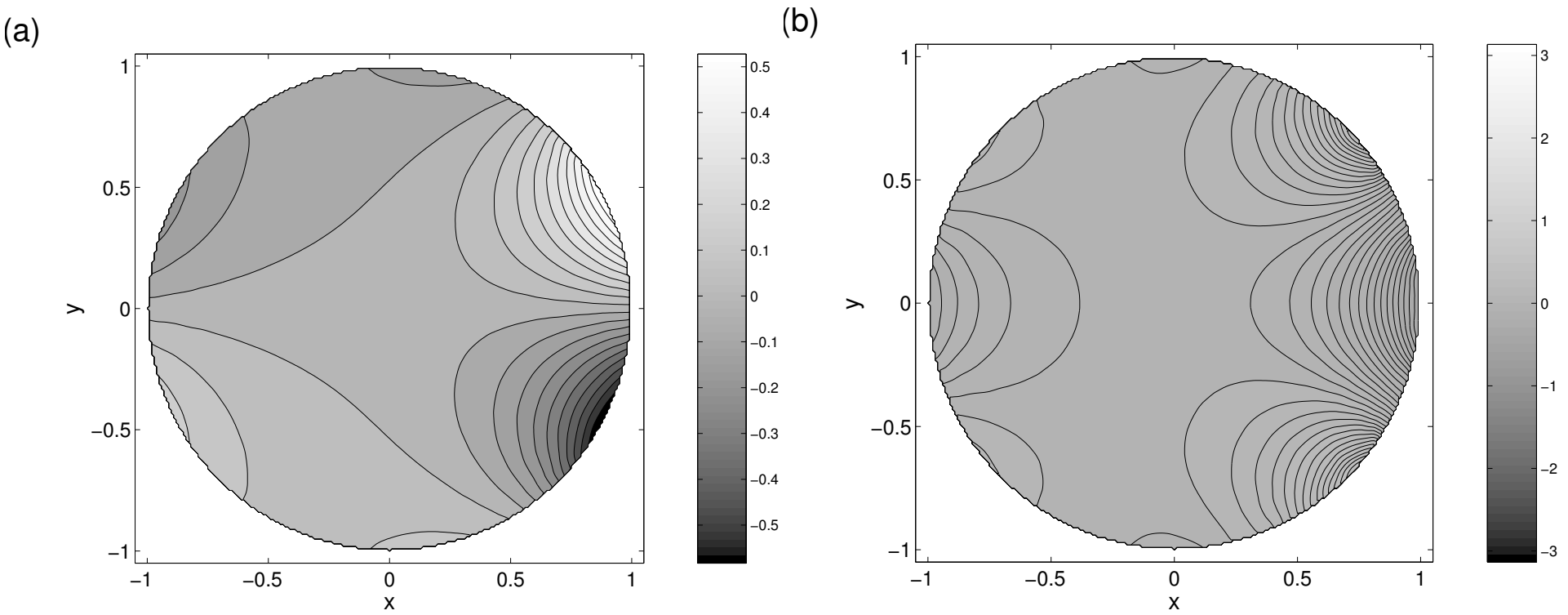

Pressure field on the equatorial plane.

- (a) time of maximum angular acceleration.
- (b) time of maximum angular velocity.

Some conclusions

- This simple model suggests that, especially in the case of low viscosity fluids, **the shape of the vitreous chamber plays a significant role in vitreous motion.**
- The flow field is complex and significantly three-dimensional.
- A circulation is likely to form in the anterior part on the vitreous chamber, close to the lens.

Vitreous motion in myopic eyes

The approach adopted in the previous section to treat the non-sphericity of the domain can also be employed to study the **motion of a viscoelastic fluid in a quasi-spherical domain.**
We describe here the particular case of **myopic eyes** (Meskauskas et al., 2012).
In comparison to emmetropic eyes, myopic eyes are

- larger in all directions;
- particularly so in the antero-posterior direction.

Myopic eyes bear **higher risks of posterior vitreous detachment and vitreous degeneration** and, consequently, an **increased the risk of rhegmatogeneous retinal detachment.**

The shape of the eye ball has been related to the degree of myopia (measured in dioptres D) by Atchison et al. (2005), who approximated the vitreous chamber with an ellipsoid.

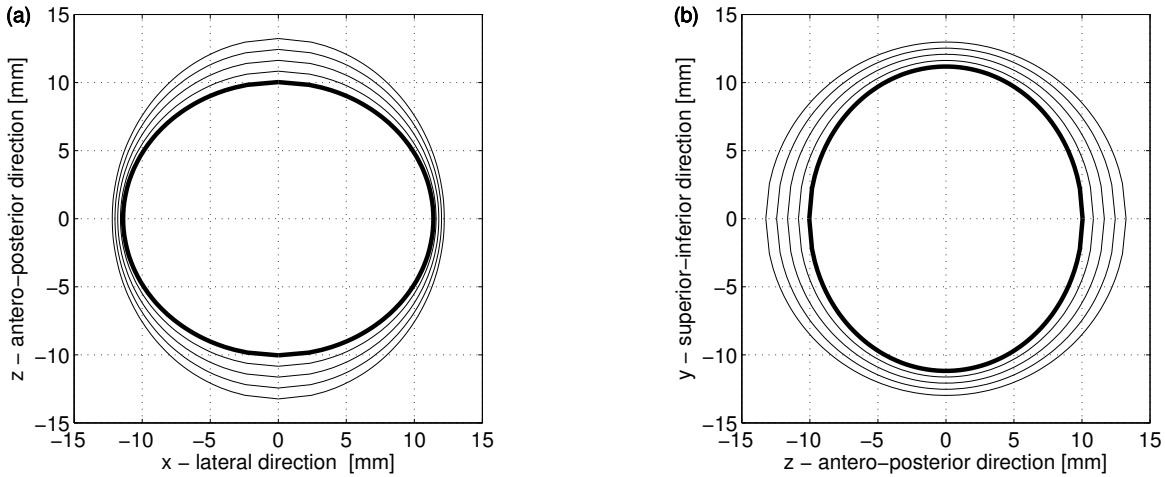

(a) horizontal and (b) vertical cross sections of the domain for different degrees of myopia.

Mathematical problem

Equation of the boundary

We again describe the domain as a weakly deformed sphere, writing

$$R(\vartheta, \varphi) = \mathcal{R}(1 + \delta R_1(\vartheta, \varphi)),$$

where

- $\mathcal{R}$ denotes the radius of the sphere with the same volume as the vitreous chamber;
- δ is a **small parameter** ($\delta \ll 1$);
- the maximum absolute value of R_1 is 1.

Expansion

We expand the velocity and pressure fields in terms of δ as follows

$$\mathbf{u} = \mathbf{u}_0 + \delta \mathbf{u}_1 + \mathcal{O}\left(\delta^2\right), \qquad p = p_0 + \delta p_1 + \mathcal{O}\left(\delta^2\right).$$

Leading order problem $\mathcal{O}(\delta^0)$

At leading order we find the solution in a sphere, discussed at page 305.

Order δ problem

The solution at order δ can be found in the form of a series expansion, similarly to what was done in the case of the irrotational model (see page 299).

Solution I

Stress distribution on the retina

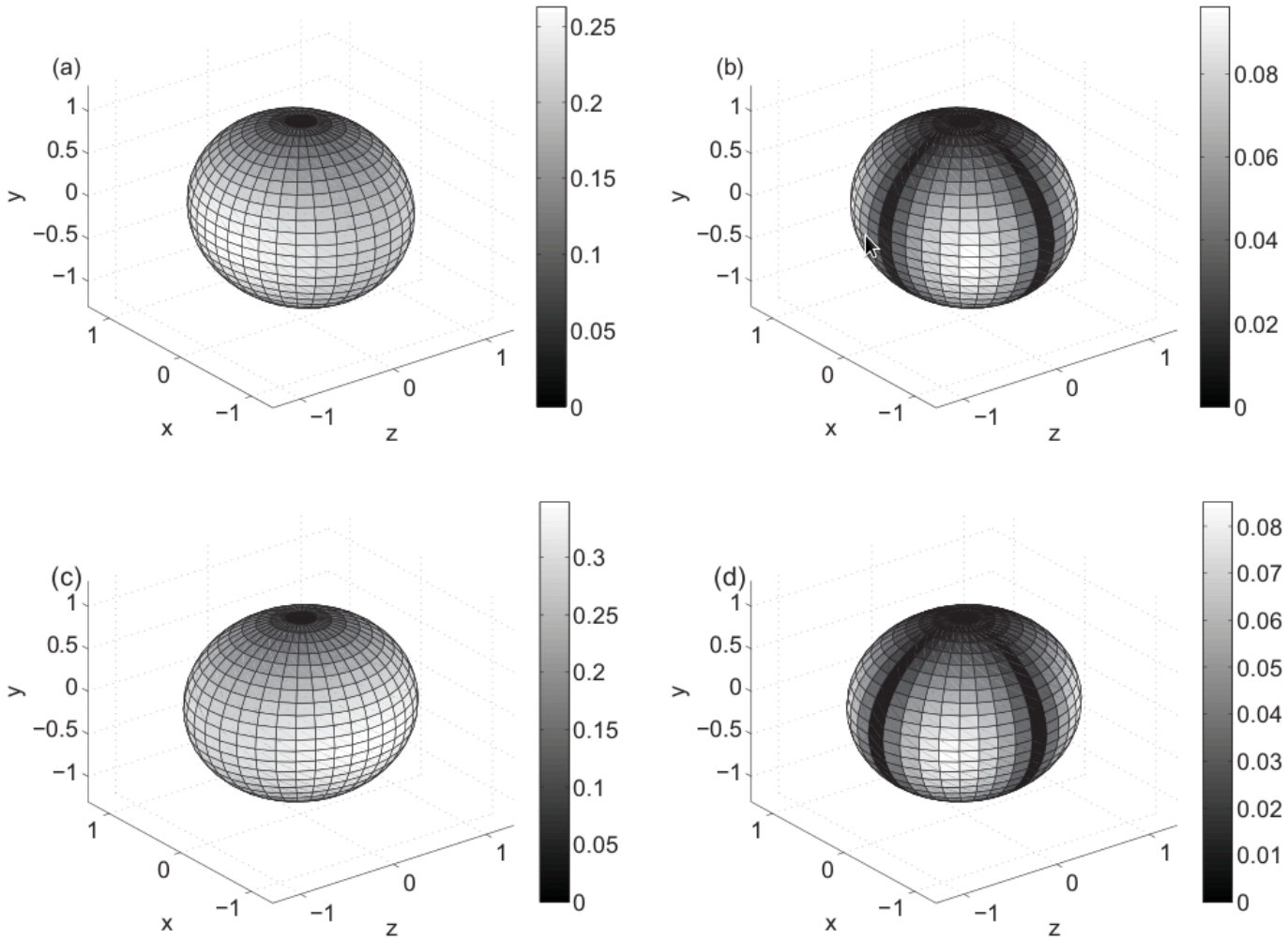

Spatial distribution of (a, c) the maximum dimensionless tangential stress and (b, d) normal stress. (a) and (b): emmetropic eye; (c) and (d): myopic eye with refractive error 20 D.

Solution II

Maximum stress on the retina as a function of the refractive error

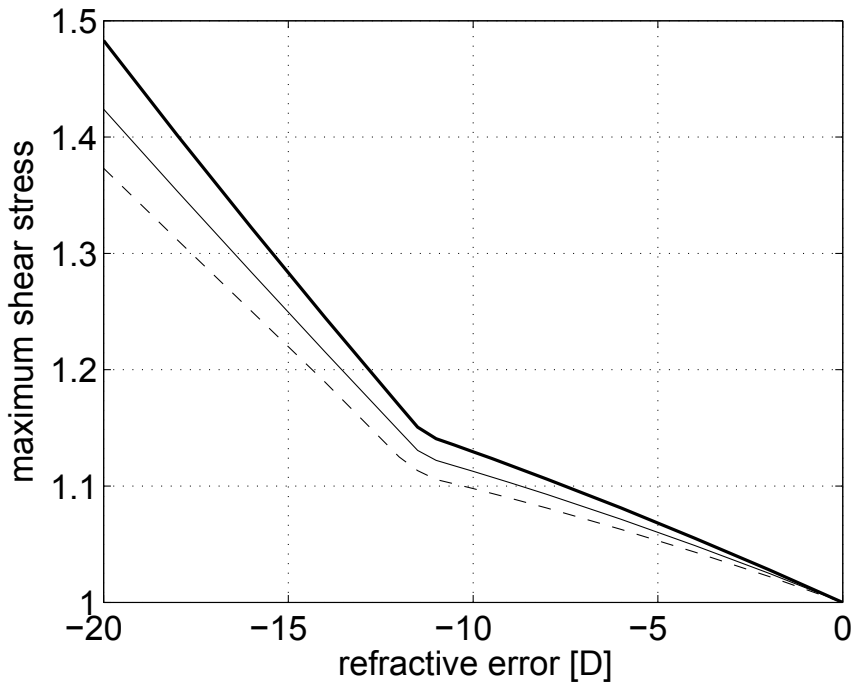

Maximum (over time and space) of the tangential tress on the retina as a function of the refractive error in dioptres. Values are normalised with the corresponding stress in the emmetropic (0 D) eye. The different curves correspond to different values of the rheological properties of the vitreous humour taken from the literature.

Some conclusions

- The vitreous and the retina in myopic eyes are continuously subjected to **significantly higher shear stresses than emmetropic eyes.**
- This provides a feasible explanation for why in myopic eyes vitreous liquefaction, posterior vitreous detachment and retinal detachment are more frequent than in emmetropic eyes.

Appendix A:
the equations of motion in different coordinates systems

Cylindrical coordinates

Let us consider cylindrical coordinates (z, r, φ), with corresponding velocity components (u_z, u_r, u_φ).

Continuity equation

$$\frac{\partial u_z}{\partial z} + \frac{1}{r}\frac{\partial}{\partial r}(r u_r) + \frac{1}{r}\frac{\partial u_\varphi}{\partial \varphi} = 0$$

Navier-Stokes equations

$$\frac{\partial u_z}{\partial t} + u_z\frac{\partial u_z}{\partial z} + u_r\frac{\partial u_z}{\partial r} + \frac{u_\varphi}{r}\frac{\partial u_z}{\partial \varphi} + \frac{1}{\rho}\frac{\partial p}{\partial z} - \nu\left[\frac{\partial^2 u_z}{\partial z^2} + \frac{1}{r}\frac{\partial}{\partial r}\left(r\frac{\partial u_z}{\partial r}\right) + \frac{1}{r^2}\frac{\partial^2 u_z}{\partial \varphi^2}\right] = 0.$$

$$\frac{\partial u_r}{\partial t} + u_z\frac{\partial u_r}{\partial z} + u_r\frac{\partial u_r}{\partial r} + \frac{u_\varphi}{r}\frac{\partial u_r}{\partial \varphi} - \frac{u_\varphi^2}{r} + \frac{1}{\rho}\frac{\partial p}{\partial r} +$$
$$- \nu\left[\frac{\partial^2 u_r}{\partial z^2} + \frac{1}{r}\frac{\partial}{\partial r}\left(r\frac{\partial u_r}{\partial r}\right) + \frac{1}{r^2}\frac{\partial^2 u_r}{\partial \varphi^2} - \frac{u_r}{r^2} - \frac{2}{r^2}\frac{\partial u_\varphi}{\partial \varphi}\right] = 0.$$

$$\frac{\partial u_\varphi}{\partial t} + u_z\frac{\partial u_\varphi}{\partial z} + u_r\frac{\partial u_\varphi}{\partial r} + \frac{u_\varphi}{r}\frac{\partial u_\varphi}{\partial \varphi} + \frac{u_r u_\varphi}{r} + \frac{1}{\rho r}\frac{\partial p}{\partial \varphi} +$$
$$- \nu\left[\frac{\partial^2 u_\varphi}{\partial z^2} + \frac{1}{r}\frac{\partial}{\partial r}\left(r\frac{\partial u_\varphi}{\partial r}\right) + \frac{1}{r^2}\frac{\partial^2 u_\varphi}{\partial \varphi^2} + \frac{2}{r^2}\frac{\partial u_r}{\partial \varphi} - \frac{u_\varphi}{r^2}\right] = 0.$$

Spherical polar coordinates I

Let us consider spherical polar coordinates (r, ϑ, φ) (radial, zenithal and azimuthal), with corresponding velocity components $(u_r, u_\vartheta, u_\varphi)$.

Continuity equation

$$\frac{1}{r^2}\frac{\partial}{\partial r}\left(r^2 u_r\right) + \frac{1}{r\sin\vartheta}\frac{\partial}{\partial \vartheta}\left(\sin\vartheta u_\vartheta\right) + \frac{1}{r\sin\vartheta}\frac{\partial u_\varphi}{\partial \varphi} = 0.$$

Navier-Stokes equations

$$\begin{aligned}
&\frac{\partial u_r}{\partial t} + u_r\frac{\partial u_r}{\partial r} + \frac{u_\vartheta}{r}\frac{\partial u_r}{\partial \vartheta} + \frac{u_\varphi}{r\sin\vartheta}\frac{\partial u_r}{\partial \varphi} - \frac{u_\vartheta^2}{r} - \frac{u_\varphi^2}{r} + \frac{1}{\rho}\frac{\partial p}{\partial r} + \\
&\quad - \nu\left[\frac{1}{r^2}\frac{\partial}{\partial r}\left(r^2\frac{\partial u_r}{\partial r}\right) + \frac{1}{r^2\sin\vartheta}\frac{\partial}{\partial \vartheta}\left(\sin\vartheta\frac{\partial u_r}{\partial \vartheta}\right) + \frac{1}{r^2\sin^2\vartheta}\frac{\partial^2 u_r}{\partial \varphi^2} + \right. \\
&\quad \left. - \frac{2u_r}{r^2} - \frac{2}{r^2\sin\vartheta}\frac{\partial(u_\vartheta\sin\vartheta)}{\partial \vartheta} - \frac{2}{r^2\sin\vartheta}\frac{\partial u_\varphi)}{\partial \varphi}\right] = 0.
\end{aligned}$$

Spherical polar coordinates II

$$\frac{\partial u_\vartheta}{\partial t} + u_r \frac{\partial u_\vartheta}{\partial r} + \frac{u_\vartheta}{r}\frac{\partial u_\vartheta}{\partial \vartheta} + \frac{u_\varphi}{r\sin\vartheta}\frac{\partial u_\vartheta}{\partial \varphi} + \frac{u_r u_\vartheta}{r} - \frac{u_\varphi^2 \cot\vartheta}{r} + \frac{1}{\rho r}\frac{\partial p}{\partial \vartheta} +$$
$$- \nu\left[\frac{1}{r^2}\frac{\partial}{\partial r}\left(r^2\frac{\partial u_\vartheta}{\partial r}\right) + \frac{1}{r^2\sin\vartheta}\frac{\partial}{\partial \vartheta}\left(\sin\vartheta\frac{\partial u_\vartheta}{\partial \vartheta}\right) + \frac{1}{r^2\sin^2\vartheta}\frac{\partial^2 u_\vartheta}{\partial \varphi^2} + \right.$$
$$\left. + \frac{2}{r^2}\frac{\partial u_r}{\partial \vartheta} - \frac{u_\vartheta}{r^2\sin^2\vartheta} - \frac{2\cos\vartheta}{r^2\sin^2\vartheta}\frac{\partial u_\varphi)}{\partial \varphi}\right] = 0.$$
$$\frac{\partial u_\varphi}{\partial t} + u_r \frac{\partial u_\varphi}{\partial r} + \frac{u_\vartheta}{r}\frac{\partial u_\varphi}{\partial \vartheta} + \frac{u_\varphi}{r\sin\vartheta}\frac{\partial u_\varphi}{\partial \varphi} + \frac{u_r u_\varphi}{r} + \frac{u_\vartheta u_\varphi \cot\vartheta}{r} + \frac{1}{\rho r\sin\vartheta}\frac{\partial p}{\partial \varphi} +$$
$$- \nu\left[\frac{1}{r^2}\frac{\partial}{\partial r}\left(r^2\frac{\partial u_\varphi}{\partial r}\right) + \frac{1}{r^2\sin\vartheta}\frac{\partial}{\partial \vartheta}\left(\sin\vartheta\frac{\partial u_\varphi}{\partial \vartheta}\right) + \frac{1}{r^2\sin^2\vartheta}\frac{\partial^2 u_\varphi}{\partial \varphi^2} + \right.$$
$$\left. + \frac{2}{r^2\sin\vartheta}\frac{\partial u_r}{\partial \varphi} + \frac{2\cos\vartheta}{r^2\sin^2\vartheta}\frac{\partial u_\vartheta}{\partial \varphi} - \frac{u_\varphi}{r^2\sin^2\vartheta}\right] = 0.$$

Appendix B: Bessel functions

Bessel functions I

Bessel equation

Bessel functions are the solutions of the following ODE, known as Bessel equation

$$x^2 \frac{d^2y}{dx^2} + x\frac{dy}{dx} + (x^2 - \alpha^2)y = 0, \tag{142}$$

where α is a constant that can be either real or complex.
Bessel's equation is linear and of second order, therefore, there must exist two linearly independent solutions. It is custumary to introduce the **Bessel functions of the first and second kind.**

Bessel functions II

Bessel functions of the first kind : J_α

Bessel functions of the first kind are denoted by J_α, are solutions (142).

- J_α has a finite value in $x = 0$ for integer or positive α;
- J_α diverges as $x \to 0$ for negative non-integer α.

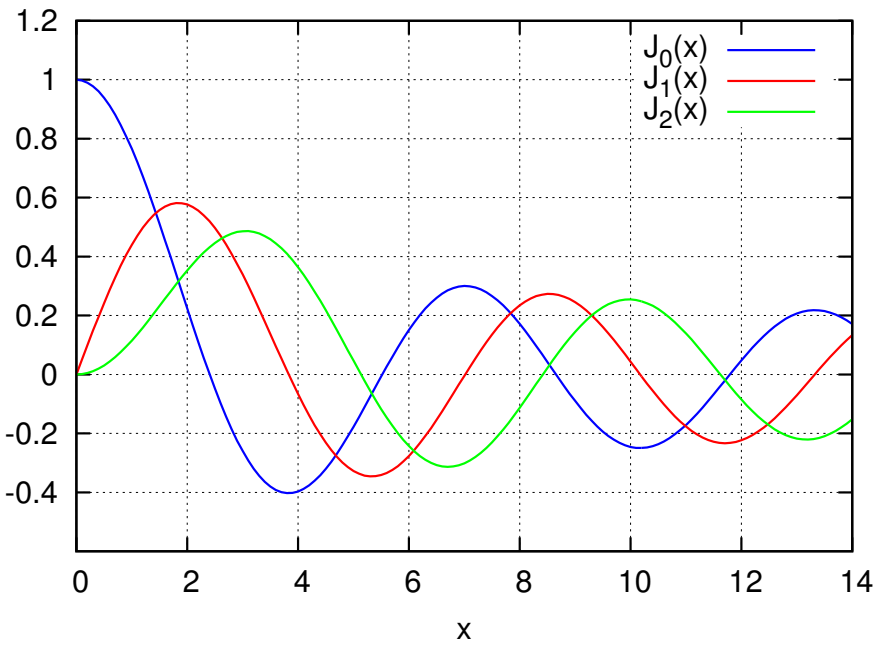

Taylor expansion

The function J_α can be defined by its Taylor expansion about $x = 0$, obtaining follow

$$J_\alpha(x) = \sum_{m=0}^{\infty} \frac{(-1)^m}{m!\,\Gamma(m+\alpha+1)} \left(\frac{x}{2}\right)^{2m+\alpha},$$

where Γ is the gamma function that, for positive integer numbers, is defined as

$$\Gamma(n) = (n-1)!$$

Bessel functions III

Bessel functions of the second kind : Y_α

Bessel functions of the second kind are denoted by Y_α, are solutions (142). They are divergent for $x \to 0$.

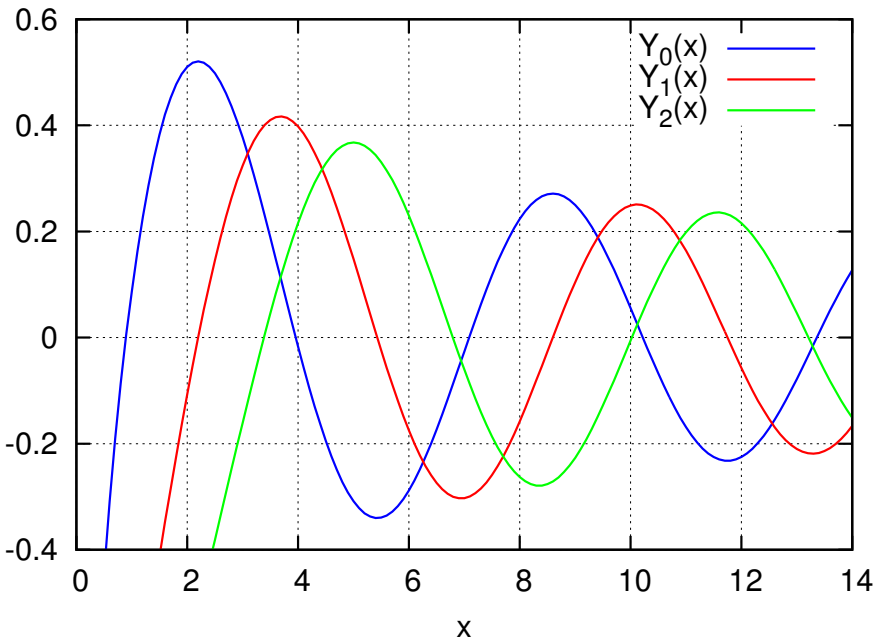

- For non-integer α, $Y_\alpha(x)$ is related to $J_\alpha(x)$ by

$$Y_\alpha(x) = \frac{J_\alpha(x)\cos(\alpha\pi) - J_{-\alpha}(x)}{\sin(\alpha\pi)}.$$

- In the case of integer α, say $\alpha = n$, the function is defined by taking the limit as a non-integer α tends to n

$$Y_n(x) = \lim_{\alpha \to n} Y_\alpha(x).$$

Bessel functions IV

Orthogonality conditions

Let α_i and α_j be defined so that

$$J_n(\alpha_i) = J_n(\alpha_j) = 0.$$

The following orthogonality condition holds

$$\int_0^1 x J_n(\alpha_i x) J_n(\alpha_j x) dx = \begin{cases} \frac{1}{2} J_{n+1}^2(\alpha_i) & \text{if } (i = j), \\ 0 & \text{if } (i \neq j). \end{cases} \tag{143}$$

References I

D. J. Acheson. *Elementary Fluid Dynamics*. Oxford University Press, 1990.

R. Aris. *Vectors, tensors, and the basic equations of fluid mechanics*. Dover Publications INC., New York, 1962.

D. A. Atchison, N. Pritchard, K. L. Schmid, D. H. Scott, C. E. Jones, and J. M. Pope. Shape of the retinal surface in emmetropia and myopia. *Investigative Ophthalmology & Visual Science*, 46(8):2698–2707, 2005. doi: 10.1167/iovs.04-1506.

G. K. Batchelor. *An Introduction to Fluid Dynamics*. Cambridge University Press, 1967.

J. Bear. *Dynamics of Fluids in Porous Media*. Dover Publications, Sept. 1988. ISBN 0486656756.

W. Becker. Metrics. In R. Wurtz and M. Goldberg, editors, *The neurobiology of saccadic eye movements*. Elsevier Science Publisher BV (Biomedical Division), 1989.

B. J. Bellhouse. Fluid mechanics of a model mitral valve and left ventricle. *Cardiovascular Research*, 6(2):199–210, Mar. 1972. ISSN 0008-6363. doi: 10.1093/cvr/6.2.199.

A. Bonfiglio, K. Leungchavaphongse, R. Repetto, and J. H. Siggers. Mathematical modeling of the circulation in the liver lobule. *Journal of Biomechanical Engineering*, 132(11):111011, Nov. 2010. ISSN 1528-8951. doi: 10.1115/1.4002563. PMID: 21034152.

R. J. Braun. Dynamics of the tear film. *Annual Review of Fluid Mechanics*, 44(1):267–297, 2012. doi: 10.1146/annurev-fluid-120710-101042.

Brooks, Goodwin, and Seaman. Interactions among erythrocytes under shear. *J. Appl. Physiol.*, 28(174), 1970.

References II

A. D. Burt, B. C. Portmann, and L. D. Ferrell. *MacSween's Pathology of the Liver*. Churchill Livingstone, 5 edition, Nov. 2006. ISBN 0443100128.

C. R. Canning, M. J. Greaney, J. N. Dewynne, and A. Fitt. Fluid flow in the anterior chamber of a human eye. *IMA Journal of Mathematics Applied in Medicine and Biology*, 19:31–60, 2002.

C. G. Caro, T. J. Pedley, R. C. Schroter, and W. A. Seed. *The Mechanics of the Circulation*. Oxford University Press, 1978.

Cokelet. *Biomechanics, its foundations and objectives*, chapter The rheology of human blood. Prentice-Hall, New Jersey, 1972.

L. de Pater and J. van den Berg. An electrical analogue of the entire human circulatory system. *Medical and Biological Engineering and Computing*, 2(2):161–166, Apr. 1964. doi: {10.1007/BF02484215}.

W. R. Dean. The stream-line motion of fluid in a curved pipe. *Philos. Mag.*, 5:673, 1928.

C. R. Ethier and C. A. Simmons. *Introductory Biomechanics - From Cells to Organisms*. (Cambridge Texts in Biomedical Engineering) Cambridge University Press, 2007.

C. R. Ethier, M. Johnson, and J. Ruberti. Ocular biomechanics and biotransport. *Annu. Rev. Biomed. Eng*, 6:249–273, 2004.

A. D. Fitt and G. Gonzalez. Fluid mechanics of the human eye: Aqueous humour flow in the anterior chamber. *Bulletin of Mathematical Biology*, 68(1):53–71, 2006.

J. J. Heys and V. H. Barocas. A Boussinesq model of natural convection in the human eye and formation of krunberg's spindle. *Annals of Biomedical Engineering*, 30:392–401, 2002.

References III

J. J. Heys, V. H. Barocas, and M. J. Taravella. Modeling passive mechanical interaction between aqueous humor and iris. *Transactions of the ASME*, 123:540–547, December 2001.

J. P. Keener and J. Sneyd. *Mathematical physiology*, volume 1. Springer, 1998.

A. Koo, I. Y. S. Liang, and K. K. Cheng. The terminal hepatic microcirculation in the rat. *Quarterly Journal of Experimental Physiology*, 60:261–266, 1975.

B. Lee, M. Litt, and G. Buchsbaum. Rheology of the vitreous body. Part I: viscoelasticity of human vitreous. *Biorheology*, 29:521–533, 1992.

C. C. Mei and B. Vernescu. *Homogenization Methods for Multiscale Mechanics*. World Scientific, May 2010. ISBN 9789814282444.

J. Meskauskas, R. Repetto, and J. H. Siggers. Oscillatory motion of a viscoelastic fluid within a spherical cavity. *Journal of Fluid Mechanics*, 685:1–22, 2011. doi: 10.1017/jfm.2011.263.

J. Meskauskas, R. Repetto, and J. H. Siggers. Shape change of the vitreous chamber influences retinal detachment and reattachment processes: Is mechanical stress during eye rotations a factor? *Investigative ophthalmology & visual science*, 53(10):6271–6281, Oct. 2012. ISSN 1552-5783. doi: 10.1167/iovs.11-9390. PMID: 22899755.

C. S. Nickerson, J. Park, J. A. Kornfield, and H. Karageozian. Rheological properties of the vitreous and the role of hyaluronic acid. *Journal of biomechanics*, 41(9):1840–1846, 2008.

H. Ockendon and J. R. Ockendon. *Viscous Flow*. Cambridge University Press, 1995. ISBN 0521458811.

References IV

J. T. Ottesen, M. S. Olufsen, and J. K. Larsen. *Applied Mathematical Models in Human Physiology*. SIAM Monographs on Mathematical Modelling and Computation, 2004.

T. J. Pedley. *The Fluid Mechanics of Large Blood Vessels*. Cambridge University Press, 1980.

T. J. Pedley. Perspectives in fluid mechanics, a collective introduction to current research. In G. Batchelor, M. H. K., and W. M. G., editors, *Perspectives in Fluid Mechanics, A Collective Introduction to Current Research*. Cambridge University Press, 2000.

G. Pedrizzetti and F. Domenichini. Nature optimizes the swirling flow in the human left ventricle. *Physical Review Letters*, 95(10):108101, 2005. doi: 10.1103/PhysRevLett.95.108101.

C. Pozrikidis. *Fluid Dynamics: Theory, Computation, and Numerical Simulation*. Springer, softcover reprint of hardcover 2nd ed. 2009 edition, Nov. 2010. ISBN 1441947191.

R. Repetto. An analytical model of the dynamics of the liquefied vitreous induced by saccadic eye movements. *Meccanica*, 41:101–117, 2006. doi: 10.1007/s11012-005-0782-5.

R. Repetto, A. Stocchino, and C. Cafferata. Experimental investigation of vitreous humour motion within a human eye model. *Phys. Med. Biol.*, 50:4729–4743, 2005. doi: 10.1088/0031-9155/50/19/021.

T. Rossi, G. Querzoli, G. Pasqualitto, M. Iossa, L. Placentino, R. Repetto, A. Stocchino, and G. Ripandelli. Ultrasound imaging velocimetry of the human vitreous. *Experimental eye research*, 99(1):98–104, June 2012. ISSN 1096-0007. doi: 10.1016/j.exer.2012.03.014. PMID: 22516112.

References V

T. W. Secomb. *Modeling and Simulation of Capsules and Biological Cells*, chapter 4. Mechanics of red blood cells and blood flow in narrow tubes. Chapman and Hall/CRC, 1 edition, May 2003. ISBN 1584883596.

J. H. Siggers and C. R. Ethier. Fluid mechanics of the eye. *Annual Review of Fluid Mechanics*, 44 (1):347–372, 2012. doi: 10.1146/annurev-fluid-120710-101058.

K. Swindle, P. Hamilton, and N. Ravi. In situ formation of hydrogels as vitreous substitutes: Viscoelastic comparison to porcine vitreous. *Journal of Biomedical Materials Research - Part A*, 87A(3):656–665, Dec. 2008. ISSN 1549-3296.

R. I. Tanner. *Engineering Rheology*. Oxford University Press, USA, 2 edition, May 2000. ISBN 0198564732.

A. Van Der Plaats, N. A. Hart, G. J. Verkerke, H. G. D. Leuvenink, P. Verdonk, R. J. Ploeg, and G. Rakhorst. Numerical simulation of the hepatic circulation. *Int. J. Artif. Organs*, 27(3): 222–230, 2004.

W. White and J. Fine. *Applied Biofluid Mechanics*. Mc Graw Hill, 2007.

Whitmore. *Rheology of the circulation*. Pergamon Press, Oxford University Press, 1968.